



OpenAIR@RGU

The Open Access Institutional Repository at Robert Gordon University

<http://openair.rgu.ac.uk>

Citation Details

Citation for the version of the work held in 'OpenAIR@RGU':

SARTAWI, Z., 2015. A novel polyelectrolyte complex between amphiphilic poly (allyl amine) and sodium alginate. Available from *OpenAIR@RGU*. [online]. Available from: <http://openair.rgu.ac.uk>

Copyright

Items in 'OpenAIR@RGU', Robert Gordon University Open Access Institutional Repository, are protected by copyright and intellectual property law. If you believe that any material held in 'OpenAIR@RGU' infringes copyright, please contact openair-help@rgu.ac.uk with details. The item will be removed from the repository while the claim is investigated.

A novel polyelectrolyte complex between
amphiphilic poly (allyl amine) and
sodium alginate.

Ziad Sartawi

A novel polyelectrolyte complex between
amphiphilic poly (allyl amine) and sodium
alginate

Ziad Sartawi

A thesis submitted in partial fulfilment of the requirements
of the Robert Gordon University for the degree of Master of
research

June 2015

Contents.....	i
Abstract.....	iv
1. Introduction.....	1
1.1 Insulin and barriers of oral delivery.....	1
1.2 Alternative protein and peptide delivery.....	2
1.3 Polyelectrolyte complexes.....	8
1.3.1 Hydrophilic polyelectrolytes.....	11
1.3.1.1 Chitosan.....	11
1.3.1.2 Alginate.....	22
1.3.2 Amphiphilic polyelectrolytes.....	28
1.3.2.1 Hydrophobically Modified Chitosan.....	29
1.3.2.2 Lactide-Polyvinyl Alcohol Copolymers.....	30
1.3.2.3 Hydrophobically Modified Poly (allyl amine).....	31
1.4 Aims and objectives.....	34
References.....	35
2. Polymer synthesis and characterisation.....	45
2.1. Materials.....	45
2.2. Method of polymer synthesis.....	45
2.2.1. Conversion of poly(allylamine hydrochloride) to poly (allylamine) free base.....	45
2.2.2. Synthesis of amphiphilic polymers.....	46
2.2.3. Synthesis of quaternised amphiphilic polymers.....	46
2.3. Polymer characterisation.....	47
2.3.1. Elemental analysis and proton nuclear magnetic resonance.....	47
2.3.2. Infra-red analysis.....	47
2.3.3. Thermal analysis.....	47
2.4. Results and discussion.....	49
2.4.1. Elemental analysis and NMR for synthesis validation.....	49
2.4.2. IR analysis.....	56
2.4.3. Thermal analysis.....	60
2.5. Conclusion.....	69
References.....	70
3. Polyelectrolyte complex formation.....	72

3.1 Materials	72
3.2 Polyelectrolyte complex formation	72
3.3 Polyelectrolyte complex characterisation	73
3.3.1 Dynamic light scattering	73
3.3.2 Transmittance studies	74
3.3.3 Zeta potential	74
3.3.4 Infra-red analysis	74
3.3.5 Thermal analysis	74
3.3.6 Transmission electron microscopy	75
3.4 Results and Discussion.....	76
3.4.1 Dynamic light scattering	76
3.4.2 Transmittance studies	93
3.4.3 Zeta potential	97
3.4.4 Infra-red analysis	98
3.4.5 Thermal analysis	104
3.4.6 Transmission electron microscopy.....	115
3.5 Conclusion	118
References	119
4. Polyelectrolyte interaction with Insulin.....	121
4.1 Materials	122
4.2 Insulin polyelectrolyte complex formation	122
4.3 Insulin polyelectrolyte complex characterisation.....	123
4.3.1 Dynamic light scattering	123
4.3.2 Transmittance studies	123
4.3.3 Zeta potential	123
4.3.4 Thermal analysis	123
4.3.5 Infra-red analysis	124
4.3.6 Determination of insulin complexation.....	124
4.3.7 α -Chymotrypsin enzyme study	124
4.3.8 Transmission electron microscopy.....	125
4.4 Results and discussion	126
4.4.1 Dynamic light scattering	126
4.4.2 Transmittance studies	128
4.4.3 Zeta potential	129

4.4.4 Transmission electron microscopy	130
4.4.5 Thermal analysis	131
4.4.6 Infra-red analysis.....	136
4.4.7 Determination of insulin complexation	138
4.4.8 α -Chymotrypsin enzyme study.....	141
4.5 Conclusion	144
References	145
5. General conclusion	147
6. Future work.....	148
Bibliography	149

Abstract

Polyelectrolytes are charge carrying polymers, when two oppositely charged polyelectrolytes are combined in a solution favouring charge expression, a polyelectrolyte complex can result. These complexes have been shown to be useful in the field of drug delivery in general. Amphiphilic polyelectrolytes contain both hydrophilic and hydrophobic groups as part of their structure; these amphiphilic polymers have shown interesting results in the field of protein and peptide delivery.

Peptides and proteins are natural polyelectrolytes, and have been used in combination with other charged polymers in the delivery of peptide drugs. The oral route of delivery for peptides and proteins has many barriers, but is of great interest, due to its potential to improve patients' adherence to medications.

In this study poly (allyl amine) and sodium alginate were used to produce a polyelectrolyte complex with the peptide insulin, with a view to investigating one of a number of barriers preventing the peptides oral delivery, namely its enzymatic cleavage by α -chymotrypsin.

Poly (allyl amine) was prepared from poly (allyl amine) hydrochloride, amphiphilic derivatives were prepared using palmitic acid-N-hydroxy succinamide and resulted in 3.7% and 5.1% palmitoyl grafted poly (allyl amine) based on elemental analysis. Furthermore samples were quaternised using methyl iodide and resulted in samples with degrees of quaternisation of 18% and 35% based on elemental analysis.

alginate/poly (allyl amine) complexes were analysed at a number of mass ratios and using a number of techniques including dynamic light scattering, differential scanning calorimetry with hot-stage microscopy, zeta potential, and infra-red analysis.

Results showed that alginate and the different derivatives of poly (allyl amine) resulted in nano-sized aggregates with estimated hydrodynamic diameters ranging from 130-400nm. Thermal analysis showed that complexation appeared to have resulted in changes in the thermal decomposition temperatures of polymers. Variations in the vibrational frequencies of infra-red results for analysed samples were used as evidence of polyelectrolyte interactions. Zeta potential of select samples resulted in values $>50\text{mV}$, indicating good colloidal stability of nano-

aggregates. Transmission electron microscopy showed the formation of distinct spherical particles, and agglomerations of spherical and needle shaped particles.

Polyelectrolyte complexes of poly (allyl amine), sodium alginate, and insulin were prepared at a different pH, but were investigated using similar methods as complexes of poly (allyl amine) and sodium alginate without insulin. Dynamic light scattering results showed the formation of complexes with estimated hydrodynamic diameters of 150-200nm. Thermal analysis showed changes in the thermal decomposition temperatures of complexes compared to individual polyelectrolytes. Infra-red analysis showed small variations in vibrational frequencies which were seen as signs of electrostatic interaction. Reverse phase high performance liquid chromatography was used in enzymatic studies to ascertain whether prepared polyelectrolyte complexes were capable of protecting insulin from the enzymatic activity of α -chymotrypsin, results showed that complexes appeared to increase the susceptibility of insulin to enzymatic cleavage, with results after 2 hours incubation with α -chymotrypsin showing <5% remaining insulin for complexes, whereas insulin control show approximately 35% remaining peptide after 2 hours in the presence of the enzyme.

The polyelectrolytes used appeared to result in stable complexes maintained by a combination of electrostatic and hydrophobic interactions, however these interaction also appeared to lead to increased degradation of insulin by α -chymotrypsin.

Keywords: Polyelectrolytes, poly (allyl amine), insulin, α -chymotrypsin, dynamic light scattering.

1. Introduction

1.1 Insulin and barriers of oral delivery

Insulin is a 51 amino acid endogenous protein that controls blood sugar (figure 1.1). Therapeutically it can be used in the management of type-1 diabetes, as well as advanced cases of type-2 diabetes. Lifelong treatment with insulin is often required, involving multiple daily subcutaneous injections in order to maintain control over glucose levels in the blood. Otherwise, uncontrolled hyperglycaemia may eventually lead to a number of debilitating, and possibly fatal endpoints, including: neuropathy, retinopathy, and nephropathy as well as the more acute complications, hyperosmolar hyperglycaemic state in type-2 diabetes, and diabetic ketoacidosis in type-1 diabetes. An oral delivery agent for insulin has been a target of research since the isolation and purification of insulin in 1922, with a number of different delivery systems being investigated by companies around the world (1). In general, most delivery systems to date have met with limited success.

The barriers towards insulin and peptide oral delivery have been thoroughly covered in the literature; therefore this section will be concise.

One of the first barriers encountered by the insulin molecule would be the acidic environment of the stomach. Brange et al. suggested that the rapid deterioration of insulin in acidic conditions was due to the deamidation of asparagine, the 21st amino acid of the insulin A chain (2). The stomach also contains the enzyme pepsin, the team of Lee and Ryle showed the probable cleavage sites of the insulin B chain by pepsin to be as follows:

Phenylalanine¹/Valine, glutamine⁴/histidine, glutamic acid¹³/alanine, alanine¹⁴/leucine, leucine¹⁵/tyrosine, tyrosine¹⁶/leucine, glycine²³/phenyl alanine, phenyl alanine²⁴/phenyl alanine, phenyl alanine²⁵/tyrosine (3).

The intestine also contains a variety of proteases (which are the enzymes responsible for the digestion of proteins and peptides in food) whose purpose is to further digest material coming from the stomach. Examples of proteases include trypsin, α -chymotrypsin and the carboxypeptidases. Zhang et al. show the enzymatic cleavage sites of insulin by trypsin and chymotrypsin as follows:

Trypsin was shown to cleave insulin at glutamic acid²¹/arginine, and proline²⁷/lysine on the B chain.

Chymotrypsin was shown to cleave insulin at leucine¹³/tyrosine, and asparagine¹⁸/tyrosine on the A chain. While on the B chain it was found to cleave at leucine¹⁵/tyrosine, phenyl alanine²⁴/phenyl alanine, and phenyl alanine²⁵/tyrosine (4). The cleavage sites of the proteases can be seen in Figure 1.1.

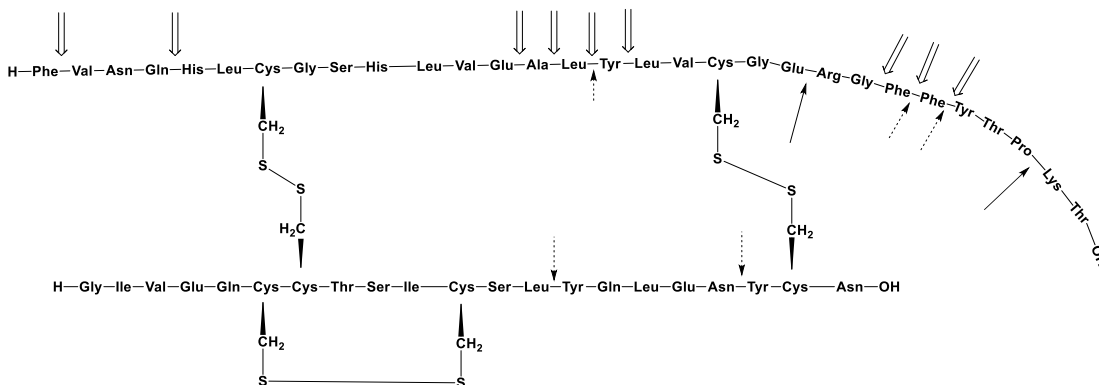


Figure 1.1 Primary amino acid structure of insulin. Arrows indicate the cleavage sites of proteases. Hollow arrow: pepsin, solid arrow: trypsin, dashed arrow: α -chymotrypsin.

The small intestine is responsible for the absorption of digested nutrients, while acting as a barrier against the infiltration of harmful microorganisms. This is also the case for large molecules such as undigested protein. The natural process would be for protein to be digested, with consequent di/tri peptides absorbed by a group of transport proteins termed the proton-dependant oligopeptide transporters (5). Other barriers to protein delivery in general include the mucous membrane lining the intestinal epithelia, cellular efflux pumps, and cellular enzymes. Together these barriers limit the intestinal absorption of complete proteins to less than 1% (6). The combination of these barriers shows the complexity of the problem facing oral delivery of insulin and other peptides.

1.2 Alternative protein and peptide delivery

Invasive injections are currently the most effective way to deliver protein and peptide drugs, and with the rapid growth of protein therapeutics, it is essential that the science of protein and peptide delivery keeps pace with developments. The delivery of peptides and protein by any route other than the parenteral is

complicated by the relative fragility of proteins, which require specific conditions of temperature, pH, and the surrounding environment in order to be fully effective. The difficulties of protein delivery and the steps taken to overcome them have been widely covered in the literature (7). Therefore the focus of this section will be on recent developments in non-injectable delivery systems for proteins and peptides.

Ocular

Ocular delivery of any therapeutic agent is challenging due to the natural physiology of the eye which includes barriers such as low corneal permeability and nasolacrimal drainage. Peptide delivery by the ocular route would be further hindered by the large size of peptides, their susceptibility to metabolism, and hydrophilicity leading to poor membrane permeability (8). However Pillion et al. were able to reduce the blood glucose of streptozotocin diabetic rats using eye drop solutions of insulin and saponin, a plant based surfactant (9).

Yamamoto et al. used a number of absorption enhancers including polyoxyethylene-9-lauryl ether, sodium deoxycholate, sodium glycocholate, and sodium taurocholate in a study of the ocular delivery of insulin. The group were able to achieve systemic bioavailability values of 3-8% of administered insulin dose. Furthermore the groups showed that 80% of the bioavailability was in fact due to absorption through the nasal mucosa (following nasolacrimal drainage) rather than conjunctival epithelia (10).

Nasal

Nasal delivery of peptides has usually involved the use of permeability enhancers and/or mucoadhesive agents.

Wang et al. used gelatin and aminated gelatin in the place of surfactants and bile salts, as absorption enhancers in investigations towards the nasal delivery of insulin. The group prepared microspheres of gelatin and insulin, they then analysed whether dry microspheres or microsphere suspensions were able to improve insulin bioavailability. The suspensions were not found to result in any significant

reduction in blood glucose of male Wistar rats. However, the powder forms of gelatin/insulin and aminated gelatin/insulin microspheres resulted in reductions in plasma glucose levels of 9.3% and 13.8%, respectively (11).

Cho et al. prepared spray dried particles of salmon calcitonin with absorption enhancers: chitosan, sodium taurocholate, and beta-cyclodextrin. The group performed an *in vivo* test using Sprague-Dawley rats by administering their powder to the nasal cavity. Their results showed a four-fold increase in serum calcitonin compared to an unprocessed control (12).

The nasal pathway can also be used in the delivery of peptides to provide a local effect in the brain. Kamei and Takeda-Morishita used a solution of insulin and the cell penetrating peptide, penetratin, in an attempt to deliver insulin via the nasal route to the brain, with a view to investigating its effect in the treatment of Alzheimer's disease. The group were able to transport insulin to the cerebral cortex, cerebellum, and brain stem of mice while avoiding excessive systemic insulin delivery (13).

Transdermal

Transdermal delivery of proteins and peptides has been investigated using a number of methods including liposomes, permeation enhancer, microporation, iontophoresis, and sonophoresis; with some more successful than others due to the inherent difficulty of delivering relatively large molecules across the body's first line of defence (14).

Yin et al. prepared a liposomal dry powder for the transdermal delivery of human epithelial growth factor, and studied the ability of the liposomes to penetrate *ex vivo* mouse skin using fluorescent microscopy. The group suggested that the transdermal hydration gradient forces liposomal vesicles through the stratum corneum towards the epidermis (15).

Yerramsetty et al. investigated 22 chemical permeation enhancers for the transdermal delivery of an insulin analogue, as well as testing for toxicity. Solutions of permeation enhancers were added to insulin solutions and analysed using Franz permeation cells. The group found 8 non-toxic chemical permeation enhancers that had a four-fold higher permeability coefficient than control (16).

Bai et al. combined iontophoresis and microporation in a study investigating the transdermal delivery of bovine serum albumin using both *in vitro* and *in vivo* models. The group showed that the combination of the two techniques led to improved transdermal penetration of albumin (300µm) compared to microporation alone (150µm) based on images from confocal microscopy, while the fluorescent intensity of labelled albumin was 23.7 times higher *in vitro* and 8.2 times greater *in vivo*. Furthermore, using Franz permeation cells it was shown that the combined techniques led to the rate of permeation being increased 5 fold (17).

Pulmonary

The pulmonary route provides interesting possibilities for the delivery of proteins and peptides due to large surface area, and abundance of vasculature. However, just as with other routes, there are barriers towards optimal delivery, such as mucocilliary clearance, macrophage activity in the alveoli, and a number of pulmonary enzymes including elastase, collagenase, chymotrypsin, aminopeptidase, among others (18).

A variety of techniques have been used in investigations towards successful pulmonary protein delivery. The team of Huang and Wang developed a cholesterol based liposomal pulmonary delivery system for insulin, whereby mice were exposed to aerosolised solution of nano sized liposomes. A fluorescent probe showed that the liposomes were well distributed in the alveoli. Furthermore, the results of *in vivo* administration of liposomes showed that the liposome encapsulated insulin caused a reduction in blood glucose level over at least 6 hours. The group suggested that the liposomes encouraged a process of surfactant recycling, and subsequent uptake of liposomes containing insulin (19).

Dong et al. investigated the pulmonary absorption enhancing effect of polyamidoamine dendrimers for model peptides insulin and calcitonin; the group used an *in vivo* study on rats, where a solution of dendrimers and peptide were administered directly to the lungs of anaesthetised rats. Results showed a 2.8 fold reduction in serum glucose and 3.1 fold increase in the bioavailability of insulin. Results for calcitonin showed a 2.8 fold reduction in serum calcium and 2.8 fold increase in the bioavailability of calcitonin (20).

Attempts to deliver insulin by inhalation have led to some interesting results with a number of candidates emerging, only to be withdrawn from the market. Including dry powder inhaler Exubera (Nektar Therapeutics (San Carlos, California)/Pfizer Inc. (New York, New York)), which was famously withdrawn from the market 1 year after its release. Afrezza (MannKind Corporation, Valencia, California), AIR Insulin (Alkermes Inc. (Dublin, Ireland)/Eli Lilly and company (Indianapolis, Indiana)), and Technosphere insulin (TI; MannKind) were some of the other powder based inhaled insulin devices investigated. Of those devices mentioned above, the only candidate still under investigation is the next generation of devices from MannKind based on a combination of the technologies used for Afrezza and Technosphere insulin. Aerosolised liquid inhalers for insulin, such as AERx insulin diabetes management system (iDMS) (Aradigm corporation clinical therapeutics (Hayward, California)/Novo Nordisk (Bagsvaerd, Denmark)) were also investigated, however they suffered from a number of drawbacks including the need for refrigeration as well as being more complicated to use than powder based systems (21).

Oral

The oral route of delivery is generally the most accepted route among patients. However proteins cannot be delivered via this route in their native state. This is due to the many challenges encountered by the relatively large (difficult absorption), and fragile (high enzymatic susceptibility) proteins and peptides. Some of the techniques used to improve oral protein and peptide delivery are similar to those used for other routes, such as liposomes, permeation enhancers, and protease inhibitors, among others. A small section will be exhibited here while more comprehensive reviews of all the different methods can be found in the literature (22).

Liposomes, as mentioned above, are a well-known technique in oral peptide delivery. Parmentier et al. prepared liposomes containing human growth hormone with a number of permeation enhancers, including cetylpyridinium chloride, phenyl piperazine, and sodium caprate. The group used glycerylaldityl tetraether to stabilise the liposomes and slow the release contents. Results showed the formation of nano-sized vesicles, which were able to provide a measure of

improvement in bioavailability. In the case of cetylpyridinium chloride, the bioavailability was estimated at 3.4% compared to 0.01% for protein control. It is important to mention that the dose of human growth hormone used was approximately 26 times higher than the subcutaneous dose given as standard (23).

Huang et al. prepared liposomes for the oral delivery of salmon calcitonin by a multifunctional approach, incorporating the following permeation enhancers with the liposome carrier: trimethyl chitosan, which is thought to widen the paracellular pathway, and oligoarginine, a cell penetrating peptide whose activity is attributed to the induction of micropinocytosis. The two positively charged permeation enhancers were adsorbed onto the negatively charged liposomal surface by electrostatic interaction. Results of an *in vivo* test on Sprague-Dawley rats showed that the trimethyl chitosan/arginine modified liposomes resulted in a 16.6 fold reduction in blood calcium levels compared to non-modified calcitonin liposomes (24).

The use of stimuli responsive hydrogels have shown interesting results in the field of protein and peptide delivery. Gao et al. prepared hydrogels for the oral delivery of insulin. They use a carboxymethyl cellulose/poly(acrylic acid) hydrogel hybrid which swells and releases its contents at intestinal pH. Using streptozotocin induced diabetic Wistar rats, the group were able to reduce serum glucose to 72.4% of baseline 6 hours after intragastric administration of the insulin 60IU/kg hydrogel oral dose, this was calculated as a bioavailability of 6.35% compared to an insulin 3IU/kg subcutaneous standard (25).

Another option in protein and peptide delivery is to make use of the polyelectrolyte nature of proteins and peptides and their ability to interact electrostatically with other materials of polyelectrolyte nature. Ibie et al. used derivatives of the polymer, poly(allyl amine), to prepare a polymer/insulin complex based on electrostatic interaction. The group investigated the cellular uptake of fluorescent polymer/insulin complexes by Caco-2 cells. Results of fluorescent microscopy showed that some of the polymer/insulin samples, notably those employing quaternised and thiolated polymer derivatives, appeared to have been internalised by the cells, the mechanism of internalisation was unclear but appeared to be

unaffected by calcium dependant mechanisms or the down-regulation of insulin receptors (26).

The use of polymers and polyelectrolytes in combination with insulin for the oral delivery of the peptide will be the focus of this work.

1.3 Polyelectrolyte complexes

A polyelectrolyte (PE) is defined by the international union of pure and applied chemistry (IUPAC) as a "Polymer composed of macromolecules in which a substantial portion of the constitutional units contains ionic or ionizable groups, or both" (27).

PEs can be natural, such as proteins and nucleic acids, or synthetic such as derivatives of polystyrene and polyacrylic acid, as well as chemically modified natural biopolymers such as pectin and chitosan (from the deacetylation of chitin).

PEs can be hydrophilic, hydrophobic, or amphiphilic. They are classified electrochemically as polyanions and polycations, the complexation of two or more of which can produce polyelectrolyte complexes (PECs).

PECs are formed by oppositely charged PEs, their association is dependent on the electrostatic interaction between the opposite charges, with varying influence from hydrogen bonding and hydrophobic interactions depending on the polymers used (28, 29).

Salt concentration of the reaction medium, the degree of charge on the polymers, as well as the molecular weight and mixing ratio used will influence the form the complexes take. Changing these variables has led to aqueous PECs being developed either as small, homogenous, soluble complexes, colloidal PEC solutions, or as two phase systems of large precipitated aggregates and supernatant (30).

The major factor in the formation of PECs is the release of low molecular mass ions (counter ions) from PEC components, which leads to increased entropy; making complex formation thermodynamically favourable (31).

Structurally, PECs have been divided into stoichiometric and non-stoichiometric complexes (Figure 1.2). The non-stoichiometric or "sequential" model is when PEs

with large differences in molecular mass are mixed non-stoichiometrically, with regard to charge bearing functional groups.

The stoichiometric model is where PEs of similar molecular masses are mixed at stoichiometric charge ratios and lead to either an ordered "Ladder" model or the disordered "Scrambled egg" model, depending on the balance between attractive and repulsive forces of opposing charges (30).

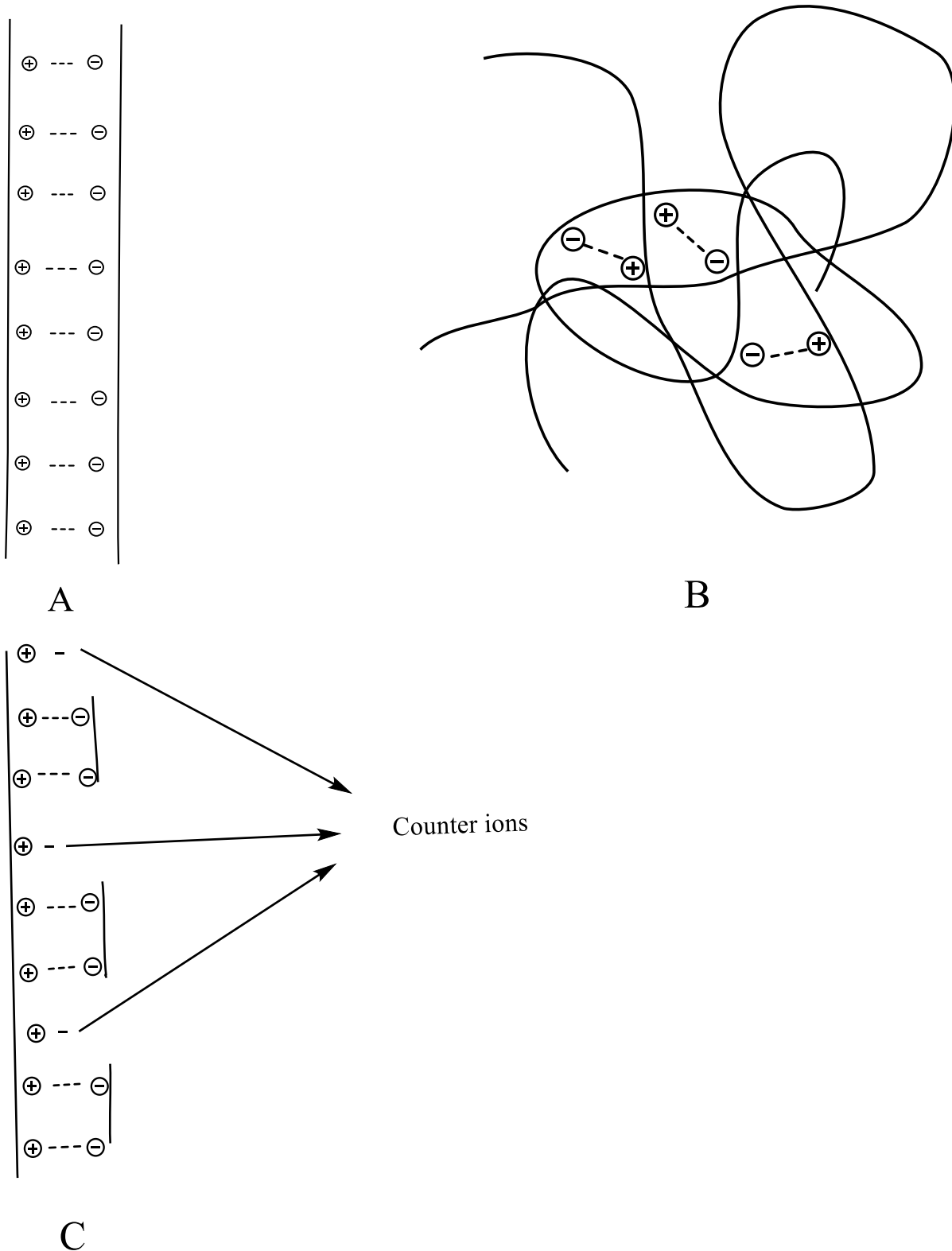


Figure 1.2 Illustrations of assumed structural conformations of polyelectrolytes. (A) Ladder model (B) Scrambled egg model (C) Sequential model.

The most commonly used PEs are generally safe to handle, non-toxic, biocompatible and biodegradable. Furthermore, non-toxicity is maintained even

after PEC formation (32-34). Such qualities, among others, have led to the application of PECs in a wide variety of studies, spanning the pharmaceutical, biomedical, and engineering fields of research (35).

PECs have been incorporated in the synthesis of a number of different formulations, and a large variety of medicinal products. Tsao et al. synthesised a hydrogel based PEC, composed of positively charged chitosan and negatively charged polyglutamic acid, and investigated their antibacterial activity (36). Fukui et al. studied microcapsules formed of oppositely charged chitosan and alginate, they then proceeded to examine their ability to encapsulate albumin (a protein) and dextran (a polysaccharide) (37).

Basmanav et al. synthesised PEC microspheres of polyvinyl pyridine and alginic acid, with a view to delivering growth factors in bone tissue engineering (38).

Shelly et al. prepared PE nanoparticles from anionic ghatti gum and cationic chitosan, the antibacterial ofloxacin was then incorporated, and the group were able to produce a slow, sustained release of the drug while maintaining activity (39).

Nanoparticle PEC formulations have been shown to have a number of advantages over microparticle formulations. Desai et al. showed that the uptake of PECs of polylactic and polyglycolic acid, by a gastrointestinal model, was dependent on particle size; with 0.1 μ m diameter particles showing a 2.5 fold better uptake than 1 μ m diameter particles, as well as a 6 fold improvement when compared against 10 μ m diameter particles (40). Nano-sized PEC's may be able to improve oral protein delivery by a combination of enzymatic protection, intestinal adhesion, and cellular permeability enhancement.

1.3.1 Hydrophilic polyelectrolytes

1.3.1.1 Chitosan

One of the most commonly used polycationic PEs, chitosan has been the subject of numerous research papers due to its natural abundance and wealth of favourable attributes (41, 42), some of which will be discussed in more detail.

Chitosan is prepared by the N-deacetylation of natural chitin (Figure 1.3), a common biopolymer derived from the shells of shrimp and crab (43). There is also a technique that provides access to natural low molecular weight chitosan found

in certain fungi that bypasses the deacetylation step of the standard procedure (44).

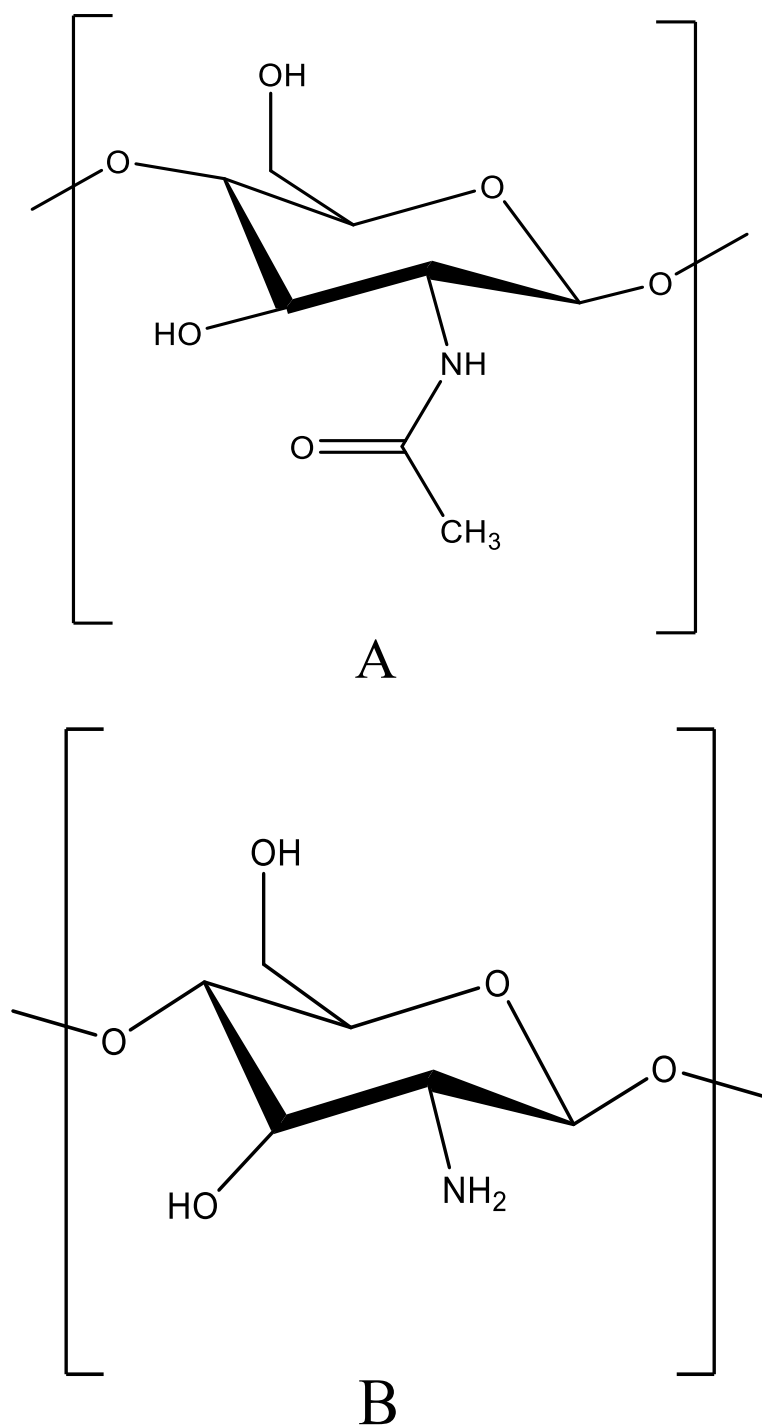


Figure 1.3 Chemical structure of (A) Chitin (B) Chitosan.

Chitosan has been shown to be biocompatible (45), biodegradable (33), generally safe and lacking in toxicity. Chitin and chitosan are commonly used in a number of applications throughout the food industry as reviewed by Shahidi et al. (46).

Rampino et al. studied the biocompatibility of chitosan by using a chorioallantoic membrane assay (a test that used the live embryos of fertilised chicken eggs) to investigate any vascular changes that may arise, this was achieved by placing the chitosan, in solid form, in direct contact with the embryo and monitoring events using a microscope and camera system, the authors found no negative changes after 24 hours (45).

Onishi and Macheda investigated the biodegradability of chitosan, by measuring the change in viscosity and molecular weight after mixing chitosan in solution with lysozyme, a natural enzyme found in saliva and tears. A viscometer was used and showed a 60% drop in viscosity after 4 hours versus a 20% drop for the control after 40 hours, the group attributed the change in viscosity to degradation. The change in molecular weight was determined by gel permeation chromatography after incubation of chitosan in murine plasma and urine, the results showed a ten-fold drop in molecular weight, compared to control, indicating degradation (33).

Chitin, chitosan, and their derivatives have been subjected to other safety studies, one such study investigated the effect of various chitosan solutions on the mucociliary transport rate *in vitro* and *in vivo*, this was done by applying chitosan solution to surgically removed human nasal tissue (from a procedure to correct deviated septa) and monitoring any changes in the mucociliary transport of graphite particles. The *in vivo* test involved placing a portion of saccharine tablet in direct contact with the nasal tissue of volunteers (who were to undergo the aforementioned procedure), the time taken to sense a sweet taste in the throat was interpreted as successful mucociliary transport and was measured. Results were compared with the time taken to sense the same taste after the administration of a chitosan solution nasal spray; this test was repeated for 7 days prior to the volunteers' surgery. Afterwards the removed tissue was studied by light microscopy to assess for inflammation. Results of the *in vitro* test showed that the chitosan solutions caused a slowing of the mucociliary transport, with higher molecular weight samples causing a longer duration of effect (47).

The *in vivo/in vitro* test showed no negative effect on clearance or histology of nasal tissue.

Mao et al. looked at the properties of depolymerised chitosan and the effect of molecular weight on a number of aspects, including a cytotoxicity test using a

mouse connective tissue fibroblast cell line MTT assay; where cultivated cells were placed in direct contact with various dilutions of chitosan solution and incubated for 24 hours. The results showed that the cytotoxicity of chitosan is concentration dependant, although with an half maximal inhibitory concentration (IC_{50}) of 4200mg/ml is relatively non-toxic, the study also found no connection between molecular weight and toxicity (48). These studies, a sample of many, show the safety profile of chitosan is robust and well documented.

Chitosan and many of its derivatives have been and continue to be studied in the fields of textiles, membranes and wound dressings, flocculating agents, metal ion chelators, and molecular sieves in water treatment (49).

The application of chitosan in drug delivery by forming PECs with medicinal compounds has been investigated in some cases. Liu et al. investigated a chitosan/DNA PEC produced through a simple process at a number of charge ratios. Using highly deacetylated chitosan (99%), they were able to produce stable complexes in the nanoscale range, the shape of which was assessed by atomic force microscopy and found to be dependent on the ratio used; with higher positive ratios producing more consistently regular complexes, the group also used FT-IR and ^{31}P NMR to show that the incorporated DNA maintained its structure post complexation (50).

Mei-chin et al. produced a nanoparticle PEC of chitosan and heparin, a glycosaminoglycan with a high negative charge density, its primary indication is as an anticoagulant in the initial treatment and prevention of deep vein thrombosis. The PEC was prepared by mixing heparin into a chitosan solution using various concentrations of each component. The authors were able to produce spherical nanoparticles in the range of 150nm in diameter, confirmed by transmission electron microscopy (TEM) and dynamic light scattering (DLS). The release and activity of the complexed heparin was tested both *in vitro* and *in vivo*, the *in vitro* test involved a simulated GI environment with a gradient pH media complete with enzymes (pepsin, pancreatin). Results were a pH dependant release of heparin, with very low release in the gastric simulation, as the electrostatic interaction at gastric pH was sufficiently robust to maintain the integrity of the complex. Heparin release gradually increased as the pH of the simulation was increased towards intestinal conditions. The *in vivo* test involved the oral

administration of the PEC nanoparticle to Sprague-Drawley rats and comparing bioavailability and efficacy (through measuring anti-factor Xa activity) against a standard heparin IV administration. Results showed an oral bioavailability of 20.5% and plasma levels within the therapeutic range for 12 hours (51).

Although results were promising, it should be kept in mind that the amount of heparin required to achieve these results was 30 times greater than that required in the IV administration.

Joung-Pyo et al produced PEC nanoparticles of insulin and chitosan using different ratios by a simple mixing technique, resulting in particles with sizes of 150-300nm. The group used FT-IR and ¹H-NMR to show the interaction of the two PE, as well as fluorescence spectrophotometry to show how the intensity peaks of insulin remained the same before nanoparticle formulation and after nanoparticle dissociation with hydrochloric acid. The release of insulin from the complex was analysed using a dialysis membrane and a bicinchoninic assay to assess protein content. Results showed insulin release over at least 120 hours for all ratios used, with complexes containing greater amounts of insulin showing slower release patterns, presumably due to greater electrostatic interaction (52).

One of the most important properties possessed by chitosan, when discussing drug delivery, is mucoadhesion, which is defined as the adhesive interaction between the mucous membrane, and a mucoadhesive agent. Lehr et al. measured the mucoadhesion of a number of chitosan products of various molecular weights; this was achieved by measuring the force of detachment of chitosan coated cover glasses from pig intestinal mucosa (53).

Abdel mouez et al. produced microspheres of chitosan and verapamil, which is an anti-hypertensive/anginal/arrhythmic calcium channel blocker, with a view to improving the drug's poor bioavailability. These mucoadhesive microspheres, when administered nasally, showed 58.6% bioavailability compared to 47.8% for a nasal solution of verapamil alone at the same dosage (54). Indicating that mucoadhesion may be effective in increasing bioavailability by the nasal pathway. With regard to the oral pathway, studies have shown mixed results. Lueßen et al. were able to enhance the intestinal bioavailability of buserelin using a chitosan hydrochloride preparation (55), while Sakkinen et al. investigated the ability of chitosan/furosemide granules to increase the bioavailability of orally delivered

furosemide (a diuretic compound), this test was performed to assess whether the promising mucoadhesive results seen with *in vitro* chitosan tests might also be seen *in vivo*. In this case, the bioavailability was found to be no better than standard tablets (56). The authors followed up this study with a gamma scintigraphic evaluation of radio labelled chitosan granules on human volunteers, with results showing that adhesion occurred in 6 cases out of 10, with only 2 of the cases being in the small intestine (57).

These results are less promising, although further studies using different formulations, perhaps micro or nano particles with greater surface area may show improved results.

Mucoadhesion can be seen as something of a requirement to another of chitosan's properties, namely its permeability enhancing effect.

In oral drug delivery, the small intestine is a major site of absorption and at the same time a major barrier against the infiltration of foreign material, this is achieved through a combination of the mucous membrane, efflux pumps, tight junctions and the presence of digestive enzymes. The effect of chitosan on permeability and enzymatic activity has been investigated with regard to the oral administration of proteins, which are usually too complex to be absorbed in their active form. Proteins must be digested and broken down into single amino acids or di/tri peptides in order to be absorbed by normal intestinal mechanisms (5).

Chitosan may improve protein permeability by providing the option of paracellular transport through tight junctions. These junctions are close contacts between the plasma membranes of adjacent cells and are made up of at least 40 proteins, including the claudin, adherin, and occludin families of proteins.

Tight junctions allow the passage of small molecules, with the claudin proteins known to form a system of 4 angstrom radius pores. However, molecules larger than 4 angstrom have been found to pass through tight junctions, and an upper limit has not been ascertained (58).

A commonly used tool to measure permeability is transepithelial electrical resistance (TEER). Fromter and diamond have shown in studies using gall bladder epithelium, that a low TEER reading is suggestive of higher permeability or "leaky"

epithelia as termed by the authors, whereas high TEER readings suggest “tight” epithelia or low permeability (59).

Dodane et al. provided evidence of a general mechanism of action for chitosan’s permeability enhancing effect at tight junctions. The authors investigated the effect using confocal microscopy and measuring the change in the fluorescent intensity for stained tight junction proteins, with only subtle decreases in intensity for tight junction proteins, clearer results show the redistribution of F-actin; a protein known to be involved in paracellular transport when using intestinal epithelia monolayers. Within the same study, the reversibility of the tight junction opening was evaluated, with TEER values returning to normal after 24 hours. The recovery was also tested in the presence of a protein synthesis inhibitor, which when present resulted in the prevention of complete recovery of TEER values (60).

Kotze et al. studied the effect of chitosan hydrochloride on the permeability of Caco-2 (human colorectal carcinoma) cell monolayers, using TEER measurements. Results showed an 80% reduction in TEER after 20 minutes of exposure, the study also showed that chitosan increased the transport of radio labelled mannitol (usually practically impermeable) by approximately 30 fold compared to a mannitol control.

Using a similar method, the same group investigated the permeability enhancing effect of chitosan for a group of peptide drugs, including buserelin and insulin. Both cases resulted in increases in transport; buserelin transport was increased from 0.04% to 4.3% of the dose. Insulin transport was increased from undetectable levels to 1.2% of the dose.

Another aspect covered in the study was whether chitosan could inhibit the enzymatic activity of α -chymotrypsin, thereby providing a measure of protection to the peptides or proteins. In the presence of the enzyme, the transport of buserelin was found to decrease from 4.3% to 1.3%, showing that chitosan was unable to protect against enzymatic degradation (32).

In a test of two other enzymes, trypsin and carboxypeptidase B; chitosan was found to actually hasten the degradative process, as evidenced by the increased breakdown of the enzymes’ respective test substrates, benzoyl arginine ethylester and hippuryl-L-arginine (61).

This lack of enzymatic inhibition or protection, is one of the limitations of chitosan in the delivery of proteins, but the most obvious limitation is that, as a weak base with a pK_a of ≈ 6.1 (62) the ionisation and solubility of chitosan in the acidic environment of the stomach is high, meaning that any chitosan/drug (or protein) complex would be subject to a rapid release or burst effect in the stomach. Conversely, in the intestine chitosan will lack or have reduced ionisation and solubility, and will be unable to interact with the mucous membrane, this would severely hinder attempts to deliver highly sensitive compounds, such as proteins. These limitations led to research into modified versions of chitosan via thiolation, carboxymethylation and quaternisation (63).

Thiolated chitosan was developed to produce a stronger source of adhesion between chitosan and the mucous membrane; stronger than the ionic interaction seen as the source of unmodified chitosan's mucoadhesive properties. The thiolated derivatives are believed to form covalent disulphide bonds through thiol/disulphide exchange reactions with the cysteine rich mucous membrane glycoproteins. Furthermore, crosslinking within the polymer itself leads to further entanglement and adhesion to the mucous membrane. There have been a number of derivatives synthesised, including chitosan thiobutylamide, chitosan thioglycolic acid (Figure 1.4), and chitosan glutathione (64).

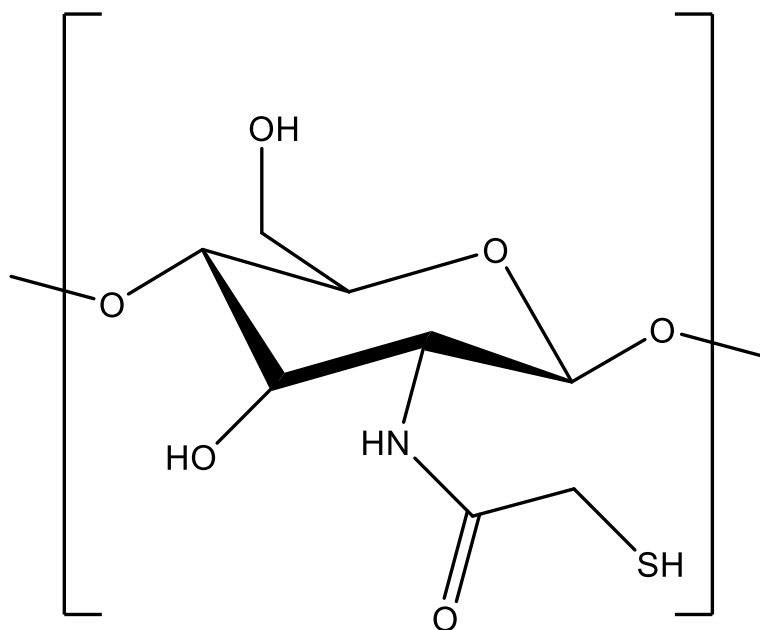


Figure 1.4 Chemical structure of chitosan thioglycolic acid.

Schnürch et al. examined the difference in mucoadhesion between unmodified chitosan, chitosan thiobutylamidine, and chitosan thioglycolic acid, by attaching flat tablets of each sample to a section of intestinal porcine mucosa which was then agitated in a dissolution apparatus at specific pH and revolutions per minute. The samples, which were then observed for a period of one week showed a 140-fold improvement in mucoadhesion for the thiobutylamidine derivative, and a 5-fold increase for the thioglycolic acid derivative when compared to the unmodified control (65). This study shows that thiolation can be an effective option in increasing the mucoadhesive properties of chitosan.

Dongwon et al. produced nanocomplexes of chitosan thioglycolic acid (as well as unmodified chitosan) with a DNA plasmid, by a simple mixing procedure. The goal of this study was to investigate the ability of the thiolated polymer to introduce plasmids to cells (transfection), but the study also included a cytotoxicity MTT assay using human embryonic kidney cells that showed that the thiolated derivative produced no cytotoxicity, in a result similar to the unmodified chitosan nanocomplexes.

The mucoadhesion of the nanocomplexes were investigated using a technique involving mucin in solution, mixed with the nanocomplexes, and measuring the amount adsorbed over 8 hours. Results showed a small improvement in mucoadhesion. The ability of the complexes to protect the plasmid from the enzyme DNase-1 was investigated and found able to provide some protection to the plasmid, although not as effectively as the unmodified sample (66).

A number of carboxymethyl chitosan derivatives have been developed through the modification of the amine and/or hydroxyl units of the chitosan structure (Figure 1.5).

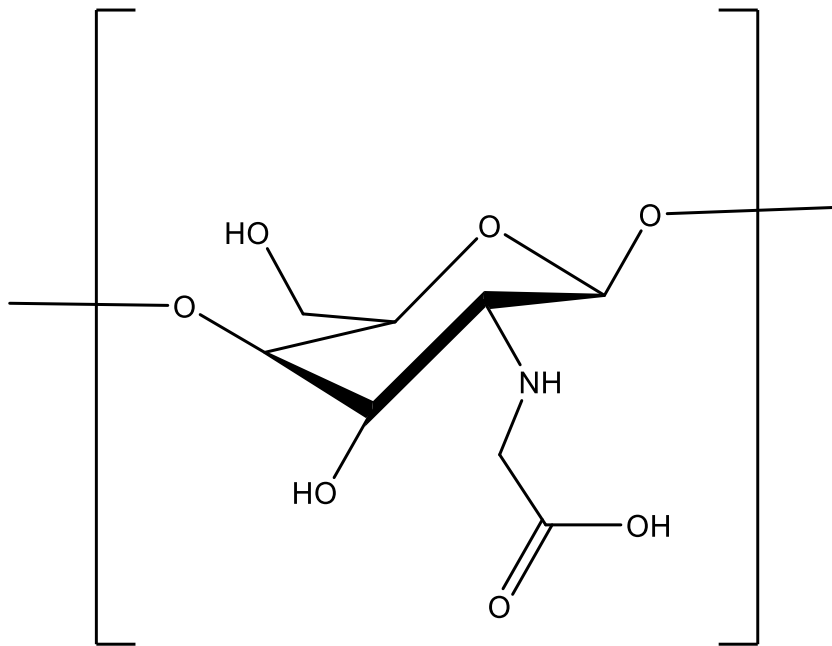


Figure 1.5 Chemical structure of N-Carboxymethyl chitosan.

de Abreu et al. synthesised samples of N,O-carboxymethylchitosan by reacting unmodified starting material with excesses of monochloroacetic acid and sodium hydroxide in 2-propanol, with higher excess leading to greater degrees of carboxymethyl substitutions. The solubility of the samples was compared to unmodified chitosan using UV/Vis spectroscopy transmittance readings. Results showed that the greater the number of substitutions, the greater the solubility. All samples showed better solubility than unmodified chitosan at higher pH (>7.2), this was attributed to the carboxymethyl substitutions imparting a negative charge along the polymer chain at pH >4 (67), this work shows that carboxymethylation is a valid technique to increase the solubility of chitosan in conditions of increased pH (ex: the duodenum).

Thanou et al. synthesised N-carboxymethylchitosan by the addition of glyoxylic acid followed by sodium borohydride to produce a mono substituted derivative. The group tested the safety of the polymer by incubation with Caco-2 cells and microscopically assessing any change in cellular integrity, results showed no cytotoxic evidence. The samples were tested *in vitro* (using Caco-2 cells) to determine their ability to reduce TEER; as a measure of permeability enhancement. It was observed that the samples were able to reversibly reduce TEER. The group followed this with both *in vitro* and *in vivo* tests for the intestinal delivery of heparin, using Caco-2 cell line and Wister rats respectively.

In both cases, heparin transport across epithelia was increased compared to controls, with the *in vivo* test showing a 7-fold increase in bioavailability and concentrations achieving, and being maintained, within the therapeutic range for up to 3 hours (68).

Quaternisation of chitosan involves the introduction of a permanent positive charge to the amine groups of the backbone; with a view to increasing the solubility of chitosan in neutral and basic pH. The most common example of quaternisation is trimethylchitosan (TMC) (Figure 1.6). The degree of quaternisation can be manipulated to a certain extent.

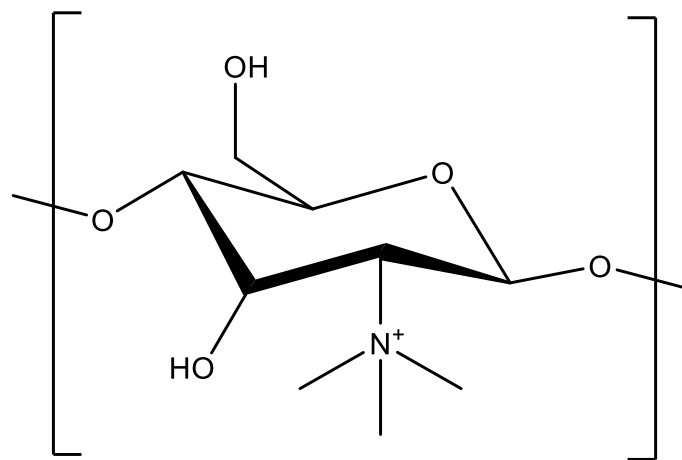


Figure 1.6 Chemical structure of N-trimethyl chitosan.

Sieval et al. was able to produce TMC using a number of techniques, achieving up to 80% quaternisation of amine groups (69). Although, the steps required to achieve this level of quaternisation, actually led to a reduction in solubility due to concomitant methylation of the hydroxyl group at the position 6 carbon in the chitosan structure.

Thanou et al. investigated the effect of TMC on TEER, as well as its ability to enhance the transport of mannitol across Caco-2 intestinal cell lines. Results showed a concentration dependant reduction in TEER (reversibility was not measured in this paper), as well as an almost 20-fold increase in mannitol transport compared to control. The cytotoxicity was tested by incubating Caco-2 cells with polymer samples for 4 hours and measuring their ability to exclude propidium iodide, with results showing no signs of toxicity. Despite there being no reversibility data, the cell lines used for the TEER test were washed and assessed

for their ability to exclude trypan blue dye as a sign of maintained cellular integrity. Results showed no uptake of the dye, signifying no cellular damage (70).

The degree of quaternisation appears to have an effect on TEER reduction and permeability, as shown by Kotze et al. the group compared TMC with a degree of quaternisation of 12.6% with a sample at 19.9% quaternisation. Results showed greater reductions in TEER and improved transport of mannitol and polyethylene glycol 4000 across Caco-2 cell monolayer (71).

Hamman et al. used an *in vivo* test of rat nasal epithelia with a wide range of quaternisation (12-59%), it was found that the ability of TMC to enhance the permeability of mannitol increased with greater degrees of quaternisation up to a point, 48%, above which no additional improvement in permeability was detected, this was attributed to a steric effect due to added methyl groups (72).

Jintapattanakit et al. produced a PEC of TMC and insulin by mixing equal volumes of the two components at different ratios under gentle stirring. The stability of the PEC in different temperature environments was tested, the PEC being found to protect insulin for at least 6 hours, even at 50°C, compared to control. Investigations of enzymatic protection were carried out using a solution containing trypsin, with the PEC providing a measure of protection compared to insulin alone. Enzyme inhibition was investigated as the method of TMC protection of insulin, but the polymer was found to have no effect on the trypsin substrate benzoylarginine, this led the authors to assume a shielding effect on insulin being the most likely source (73).

Currently, the use of chitosan in drug delivery especially as part of a PEC, is still far from efficient, often requiring many-fold the dose of standard treatment, to result in minute increases in bioavailability.

1.3.1.2 Alginate

Alginate is a natural anionic PE, its low cost and abundance have led to its mass production and wide use in a variety of enterprises, including the pharmaceutical, medical, industrial and food industries (74).

Alginate is mainly obtained from brown algae (seaweed) by a process of alkaline extraction and filtration (75), although there is also a bacterial biosynthetic

pathway which may produce more precise chemical forms of alginate as its applications expand (76).

The chemical structure of alginate is that of a polysaccharide made up of blocks of two different units, α -L-guluronate (G) and β -D-mannuronate (M) linked by (1, 4) glycosidic linkages. The alginate polymer is randomly made up of continuous blocks of G units, continuous blocks of M units, as well as sections of alternating blocks of G and M units (74, 75) (Figure 1.7). The content of different alginate formulations regarding the G and M units varies depending on the source of raw material, the stipe (stem or stalk) of the algae *Laminaria hyperborea* is a source of high G unit alginate, compared to *Laminaria japonica* which has a greater percentage of M unit blocks in its product. The relative amounts of G or M units in a sample of alginate can greatly affect its properties; this is demonstrated in alginate's characteristic gelling property. Alginate is known to form a gel when exposed to certain stimuli, with a low pH environment or the introduction of divalent cations, such as calcium or zinc causing cross-linking of the alginate polymer. The G unit is thought to be of considerable importance in the cross-linking process, Haug (1959) was able to determine that the guluronate residue possessed greater affinity than mannuronate for calcium in a calcium-potassium ion exchange procedure. This has been attributed to the different stereochemistry of the two units (74, 77).

The physical properties of the gels are also affected, with G unit rich alginates forming stronger more rigid gels compared to softer, slurry-like gels produced when M units predominate (78).

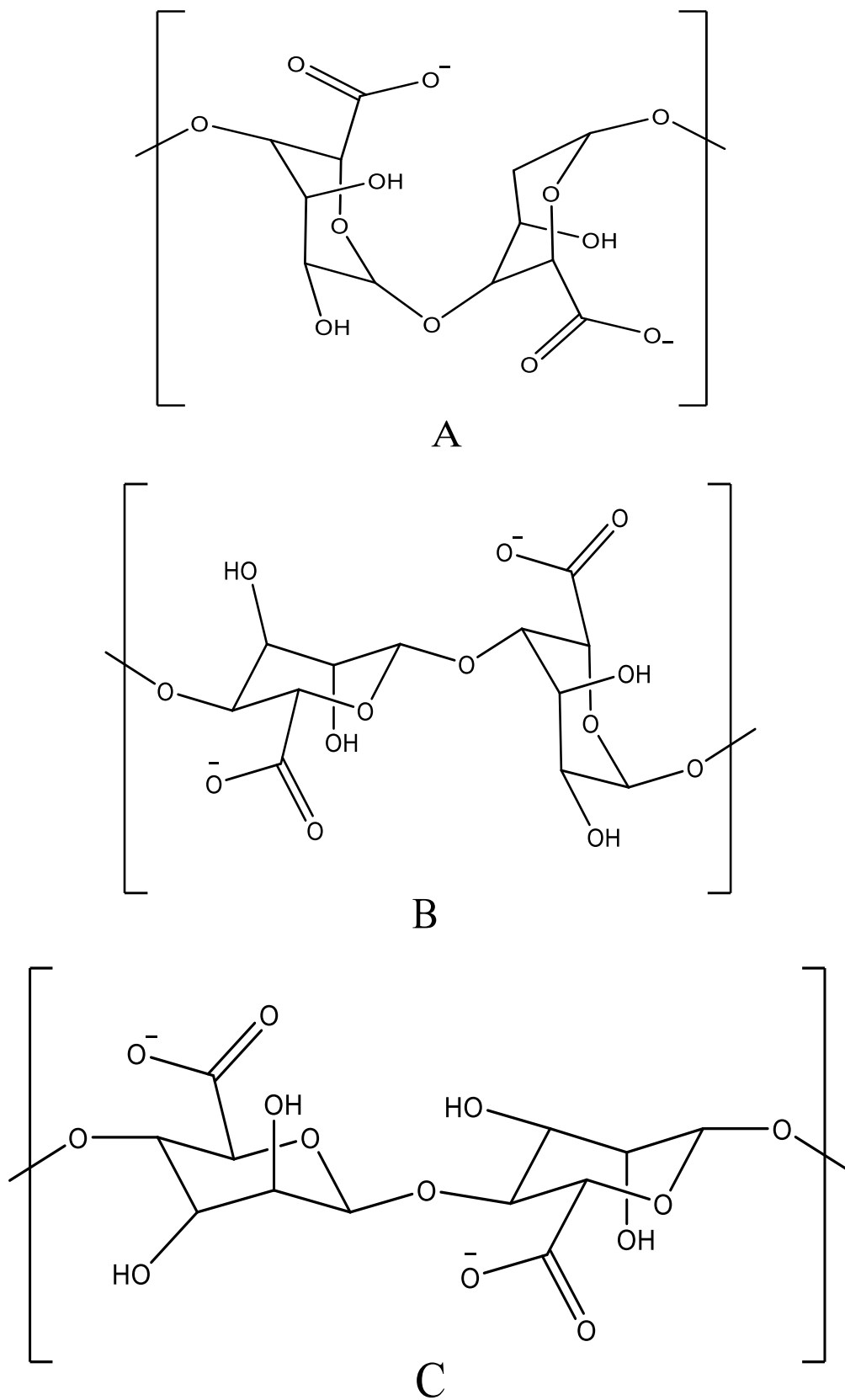


Figure 1.7 Chemical structure of alginate blocks. (A) G-G block (B) G-M block (C) M-M block.

Alginate is soluble in water at room temperature and has pK_a values of 3.65 for the G unit and 3.38 for the M unit (79).

Alginate presents a number of interesting properties with regard to drug delivery; such as biocompatibility and low toxicity (34), as shown by Orive et al. who compared alginate solutions of varying compositions (regarding G and M units) and viscosities and purities, and monitored their effect on murine splenocytes. As well as investigating whether alginate led to the release of pro-inflammatory tumour necrosis factor (TNF- α) from murine peritoneal macrophages. In the cases where biomedical grade alginates were used, results showed no adverse effects or inflammation irrespective of composition (80).

Bernkop-schnürch et al. analysed the mucoadhesion of alginate in tensile studies by compressing alginate into tablets and fixing the tablets to glass tissue mounted porcine mucosa, they were then pulled apart at a set rate, with results of maximum detachment force and total work of adhesion collected and interpreted by software, providing a quantitative measurement of adhesion for alginate (81).

Although alginate cannot be digested enzymatically by mammals, it undergoes chemical degradation quite readily. Alginate undergoes a process of degradation at any $pH < 5$ or > 10 by proton catalysed hydrolysis and beta-alkoxy elimination respectively, as well as being prone to oxidative-reductive depolymerisation in the presence of free radicals (82).

Alginate gel beads as well as micro and nanoparticles for the delivery of drug molecules and proteins, have been widely covered in the literature (83). However the use of alginate, without gelation, in forming electrostatic complexes with medicinal compounds is less common. Klemmer et al. produced a pea protein/alginate complex through simple coacervation with a view to investigating the effects of pH and mixing ratios on complex formation, as well as looking at any changes in the secondary structure of the protein. Using Raman spectroscopy the group found no significant changes in composition with regard to α -helix and β -sheet content before and after complexation with alginate (84). This provides some evidence in support of further investigation into the PEC forming properties of alginate.

A more common practice is to combine alginate with a cationic PE such as chitosan. Douglas and Tabrizian prepared complexes of chitosan and alginate and studied the effect of pH, molecular weight, and component ratios on particle formation. Results showed the smallest particle sizes at ratios of 1.5:1 and 1:1.5 with any increase in either component leading to greater particle sizes, increasing the molecular weight of starting material (especially chitosan) also led to greater particle size, although the effect was less significant than changing ratios. The authors showed that a pH of 5.1-5.7 was the optimal range for interaction between ionisable groups that produced samples with the smallest particle sizes.

The effect of the absence of calcium ions (used in the pregelation of alginate) was investigated and found to result in slightly larger particle sizes, with broader size distributions (85).

Sarmiento et al. produced PECs of alginate and chitosan using two methods, chitosan added drop wise to calcium chloride pre-gelled alginate, and simple coacervation by the addition of chitosan solution to alginate solution, the resultant particles underwent size analysis using photon correlation spectroscopy, with the coacervation PEC resulting in average particle sizes of around 500nm compared to 850nm for the gelation method, the morphology of the particles was studied by electron microscopy and showed smooth spherical particles in the gelation method whereas coacervation led to amorphous, porous particles. The same study investigated the incorporation of insulin into both types of nanoparticle, with similar loading results in both cases. The release of the protein was evaluated *in vitro* in simulated gastric and intestinal pH environments. Results showed that the coacervation nanoparticles released all incorporated insulin in a burst effect within the first 5 minutes regardless of the environment. The pregelation nanoparticles also produced a burst effect, but to a lesser degree, that was followed by a slow release of the protein over two hours (86). The same group investigated the secondary structure of insulin post incorporation into nanoparticles produced by the pregelation method. The protein was analysed by FTIR and circular dichroism (CD) following incorporation into the nanoparticles, as well as after release from the particles. Results showed no structural changes with regard to α -helices and β -sheets, which may be a sign of maintenance of biological function (87).

The bioactivity of insulin was confirmed to a degree when the group studied the effect of intra-gastric administration of alginate/chitosan insulin loaded nanoparticles. Streptozotocin induced diabetic male Wister rats were used to test for hypoglycaemic efficacy. Plasma glucose levels after administration of various nanoparticle/insulin doses were compared with standard subcutaneous insulin control, the PEC nanoparticles were shown to reduce glycaemia by up to 40% and maintained a hypoglycaemic effect for over 18 hours, the nanoparticles were able to increase the bioavailability of insulin from 1.6% to 6.8% (88). While a promising result, the dose required to achieve these results was 20 times greater than the subcutaneous dose, suggesting changes may be needed in order to improve efficacy.

Li et al. synthesised PEC nanoparticles of alginate and quaternised chitosan, and studied their ability to encapsulate the protein albumin. The potential for electrostatic interaction between the two components was shown using Fourier transform-infra-red spectroscopy (FT-IR), with changes in the frequency and intensity of charge carrying groups in the spectra of alginate, Quaternised chitosan, and alginate/Quaternised chitosan nanoparticles.

The group showed that increasing the molecular weight of chitosan used, led to greater nanoparticle size, whereas increasing the degree of substitution of the charge bearing N-propyltrimethyl ammonium, showed no significant effect on particle size.

The effect of molecular weight and the degree of substitution on the entrapment of albumin in the complex was investigated, and showed a trend of increasing encapsulation efficiency of albumin with increasing molecular weight and degree of substitution. Increasing the initial concentration of albumin or that of chitosan improved encapsulation efficiency, but only to a point, above which no additional improvement was measured. In the case of increasing molecular weight, improved encapsulation was attributed to increased particle size, while the improvement seen with increased substitution was associated with the increased abundance of positive charges, leading to more interactions with the negative functional groups of albumin.

The release of albumin from nanoparticles was studied *in vitro* using different pH environments. In the simulated gastric pH, results showed a slow release of

albumin (20% over 100 hours), whereas at pH 7.4, a burst effect was evident with 60% release after 12 hours followed by slower release. The burst effect was attributed to the disintegration of the alginate component of the nanocomplex.

In the acidic pH environment, lower molecular weight chitosan showed slower release patterns, which was, according to the authors, due to the low molecular weight chitosan diffusing more easily in the pre-gelled alginate, leading to the formation of thicker complexes that slowed the release of albumin.

The effect of degrees of substitution on release showed clear results, with increasing substitution leading to decreased protein release in both pH environments. Increased electrostatic interaction between PEC components was seen as the cause of the slower release pattern (89).

1.3.2 Amphiphilic polyelectrolytes

Amphiphilic PEs contain hydrophilic and hydrophobic groups in their structure, these PE were developed to make use of the potential benefits of the addition of hydrophobicity to drug delivery agents, including a possible increase in hydrophobic interaction with epithelial cells of gastrointestinal or nasal tissue, which may increase the likelihood of absorption, as well as increased interaction between components of a PEC, to complement the pre-existing electrostatic interaction.

The effect of increasing hydrophobicity was investigated by Mende et al. who synthesised sets of oppositely charged maleic anhydride polymers; the hydrophobicity of the PEs was controlled through the addition of increasingly hydrophobic grafts, ethylene, isobutylene, or styrene.

The group studied the effect on colloidal stability, size, and morphology of the resultant PEC. The samples with the greatest hydrophobicity, the styrene grafted PE, showed the broadest particle size distribution, with size and structure studies indicating the formation of large aggregates as well as small, distinct, dense particles. The increase in hydrophobicity also led to lower colloidal stability, with styrene samples precipitating after 5 hours (90).

Broderick et al. synthesised an amphiphilic derivative of alginate by covalently linking butanol to alginate via esterification. The resulting polymer was found to have maintained the gelling property of alginate, as well as the low toxicity of

unmodified alginate (91). Liqun et al. synthesised a cholesteryl grafted alginate polymer, using dicyclohexylcarbodiimide as a coupling agent, the resulting amphiphilic PE was investigated and found to self-assemble into particles in aqueous solution. The particle size and morphology were analysed; with results showing the consistent formation of spherical particles in the range of 100-200nm (92).

1.3.2.1 Hydrophobically Modified Chitosan

Wang et al. synthesised hydrophobically modified chitosan to investigate its effect on the oral absorption of enoxaparin, a low molecular weight heparin used in the prophylaxis and treatment of deep vein thrombosis, enoxaparin carries a strong negative charge and has poor oral bioavailability. Glyceryl monostearate, the fatty acid components of which had previously been shown to display a degree of interaction with rat intestinal sections, was grafted onto the chitosan backbone with varying degrees of substitution. Following the addition of enoxaparin, the polymer and drug self-assembled into nanocomplexes.

The effect of the degree of substitution of glyceryl monostearate on particle size was found to be minimal when low percentages of grafted substituent are used. Particle sizes showed similar results to unmodified chitosan based nanoparticles, although an increase in particle size was seen as the percentage graft increased; this was attributed to a reduction in positive charge density leading to weaker electrostatic interaction with enoxaparin.

In vitro release studies of amphiphilic PEC in simulated gastric and intestinal conditions showed limited release at gastric pH, while at intestinal pH the release results were similar for all samples tested, including unmodified chitosan control, indicating no significant effect on release by the addition of hydrophobic moieties.

The *in vivo* absorption of amphiphilic chitosan was studied in rats, by administering nanocomplexes directly into the stomach. The bioavailability of administered doses was then measured against an intravenous injection of enoxaparin. Results showed that bioavailability increased with increasing graft percentage, up to a certain point above which no additional increase was seen. In total the group was able to increase the bioavailability of oral enoxaparin from 1.34% to 12.96% (93). This shows that the addition of hydrophobic elements to some PECs may be extremely

useful in increasing the interaction with gastrointestinal epithelia and possibly enhancing absorption of typically poorly absorbable compounds.

1.3.2.2 Lactide-Polyvinyl Alcohol Copolymers

Simon et al. synthesised PECs using lactide and diethylaminopropylamine grafted polyvinyl alcohol backbone with insulin. The resulting self assembled particles were measured for size and found to be in the range of 200-400nm. Morphology studies showed smooth spherical particles. A higher degree of grafting of either component was found to result in decreased particle size, and increased binding and loading of insulin, the influence of electrostatic interactions appeared to be greater than that of increasing hydrophobicity, the authors, using turbidimetric studies, found that turbidity decreased with increasing diethylaminopropylamine concentration, this decrease was attributed to the formation of more compact structures, the observed effect was significantly less in tests of increasing lactide grafts. The group also used isothermal micro-titration calorimetry to show the degree of interaction between different PE compositions and insulin. Using this technique, results showed a similar increase in binding constants of both graft components as the degree of substitution was increased, despite this, the gained entropy from the liberation of counter ions was deemed the most important factor in complex formation (94).

The same group investigated the effectiveness of their PEC in delivering insulin nasally and orally; the bioavailability of nasally administered nanoparticles was tested *in vivo*, using streptozotocin induced diabetic rats, nanoparticle suspensions were delivered directly to the nostrils of anaesthetised rats, with blood samples taken and compared to subcutaneous injections of insulin and free insulin solution.

PECs with greater hydrophobic grafting provided greater hypoglycaemic effect, with plasma glucose reductions of over 20%, which corresponded to a bioavailability of 7.7%, compared to less than 1% for free insulin solution (95).

In studies towards oral delivery, the group studied the effect of the nanocomplexes on enzyme degradation, cytotoxicity, and transport across Caco-2 cells. Nanoparticles were analysed in solutions of the enzyme trypsin, and found to provide protection for complexed insulin. The level of protection was found to be greater with increased lactide grafting.

In vitro cytotoxicity was assessed by incubating Caco-2 cells with the PEC and monitoring the release of lactate dehydrogenase (LDH), a cytosolic enzyme used as a marker for cellular damage, the results showed increased LDH concentrations with higher lactide grafting.

Cellular uptake and transport was investigated using Caco-2 monolayers, with results showing that less than 1% of the initial insulin dose in the PEC was transported across the monolayer, whereas cellular uptake, whether of released insulin or the complexes as a whole, increased the amount of internalised insulin from less than 1% (control) to 25% of initial insulin dose, the percentage was found to increase with increasing hydrophobic grafting (96).

Highly lactide grafted samples also showed the highest reductions in TEER during cellular transport studies but the reduction was found to be completely reversible by 17 hours after removal of the sample, and by 26 hours TEER was recorded as >200% of initial readings. The authors attributed this to the reorganisation of tight junction proteins following cellular damage.

This shows that further research is required to improve levels of paracellular, and transcellular transport if they are to be relied upon to achieve therapeutic levels, as well as economic and efficient doses. It would seem that the addition of hydrophobic groups resulted in increased interaction between nanocomplexes and the cell membrane of epithelial cells.

1.3.2.3 Hydrophobically Modified Poly (allyl amine)

Thompson et al. showed the effect of hydrophobicity on the self-assembly products of the PE poly (allyl amine). The group synthesised cetyl, palmitoyl (Figure 1.8) and cholesteryl derivatives of poly (allylamine) and studied a number of characteristics, including the critical aggregation concentration (CAC), particle sizing, and morphology.

The same group followed up their work by incorporating amphiphilic PEs, as well as the quaternised polyallylamine version of each, in the formation of PECs with insulin, these complexes were studied for size, stability, and morphology. It was shown that as the ratio of polymer to insulin was increased, the average size of complexes decreased from over 1 micron with lower concentrations of polymer, to around 150nm when the ratio of the amphiphile was greater. Electron microscopy showed that morphology was dependant on polymer/insulin ratio, with higher polymer ratios leading to dense nanoparticles, while vesicular structures were the result of lower polymer ratios.

In order to measure the stability of the PEC, samples underwent centrifugation; the subsequent supernatant was measured for zeta-potential, which showed that the amphiphilic polymer and the insulin remained in complex, as the pre and post centrifugation readings were similar.

Studies on enzymatic degradation of insulin *in vitro* showed that the palmitoyl based PEC was able to provide the protein with a degree of protection from trypsin and pepsin, but led to a more rapid degradation in the presence of α -chymotrypsin. Furthermore, the cetyl and cholesteryl based PEC provided protection against trypsin and α -chymotrypsin, but not pepsin. Indicating that perhaps a combination of polymers may be able to provide the necessary range of enzymatic protection required to overcome this particular barrier to oral delivery of proteins and peptides.

In cytotoxicity studies using an MTT assay of Caco-2 cells incubated with samples, the amphiphilic samples were found to have greater IC_{50} values than the unmodified polyallylamine, showing the reduced toxicity of the amphiphilic derivatives, especially the palmitoylated derivative which exhibited a 3 fold decrease in cytotoxicity compared to the original compound (97).

Uptake of palmitoylated amphiphilic PE/insulin nanocomplexes by Caco-2 cells was performed either in the presence of the metabolic inhibitor sodium azide, or the endocytosis inhibitors cytochalasin D and nocodazole.

The effect of the presence of calcium on uptake was also evaluated. Results showed that the palmitoylated PEC became localised around the cell membrane without internalisation, but with a degree of interaction that was found to be calcium dependent.

The quaternised palmitoyl PEC was found to be localised in the cytoplasm regardless of the presence of calcium or the endocytosis inhibitors, with only sodium azide showing a small negative effect on uptake, indicating the involvement of a metabolically active process of uptake with the quaternised PEC.

The transport of palmitoyl PECs across Caco-2 cells was studied using Transwell plates, and measuring samples of the basal compartment media for the presence of insulin. The TEER of the Caco-2 cells was also measured.

Results showed TEER reductions of 15% from baseline for the palmitoyl PEC, and 25% for the quaternised PEC, indicating paracellular transport. Complementing this was the data from the concentration of insulin in the basal compartment; which showed higher concentrations than control (insulin alone), with quaternised palmitoyl nanocomplexes showing the highest percentage of transported insulin. Although the percentage transported amounts to less than 1% of the insulin dose used (98). A significant increase in the percentage of transported insulin would be necessary, if PECs were to be seen as a possible option for oral protein delivery.

1.4 Aims and objectives

The aim of this work was the investigation of the electrostatic complexation of palmitoyl grafted poly(allyl amine) amphiphilic polymers, and the oppositely charged hydrophilic polymer sodium alginate. This was followed by the incorporation of insulin into the complex and analysis of the effect of the combination on the enzymatic activity of α -chymotrypsin towards the insulin molecule.

The objectives of this work included:

- Synthesis and characterisation of amphiphilic and quaternised poly(allyl amine).
- Preparation and characterisation of polyelectrolyte complexes using synthesised poly(allyl amine) derivatives and sodium alginate.
- Incorporation of insulin into alginate/poly(allyl amine)/insulin complexes, and investigating any changes in the enzymatic activity of α -chymotrypsin towards insulin.

References

1. L. Heinemann, Y. Jacques. Oral Insulin and Buccal Insulin: A Critical Reappraisal. *Journal of Diabetes Science and Technology* 3 (2009) 568-584.
2. J. Brange, L. Langkjaer, S. Havelund, A. Vølund. Chemical stability of insulin. 1. Hydrolytic degradation during storage of pharmaceutical preparations. *Pharmaceutical Research* 9 (1992) 715-726.
3. D. Lee, A. Ryle. Pepsin D a minor component of commercial pepsin preparations. *Biochemical Journal* 104 (1967) 742-748.
4. L. Zhang, H. Jiang, W. Zhu, L. Wu, L. Song, Q. Wu, Y. Ren. Improving the stability of insulin in solutions containing intestinal proteases in vitro. *International Journal of Molecular Sciences* 9 (2008) 2376-2387.
5. B. Brodin, C. Nielsen, B. Steffansen, S. Frøkjær. Transport of Peptidomimetic Drugs by the Intestinal Di/Tri-peptide Transporter, PepT1. *Pharmacology & Toxicology* 90 (2002) 285-296.
6. M. Rekha, C. Sharma. 2010. Nanoparticle Mediated Oral Delivery of Peptides and Proteins: Challenges and Perspectives. In: C. Van der Walle. Ed. *Peptide and Protein Delivery*. Elsevier, pp. 165-195.
7. C. van der Walle. 2011. *Peptide and protein delivery*. London, UK: Elsevier.
8. S. Wadhwa, R. Paliwal, S. Paliwal, S. Vyas. Nanocarriers in ocular drug delivery: an update review. *Current Pharmaceutical Design* 15 (2009) 2724-2750.
9. D. Pillion, J. Bartlett, E. Meezan, M. Yang, R. Crain, W. Grizzle. Systemic absorption of insulin delivered topically to the rat eye. *Investigative Ophthalmology & Visual Science* 32 (1991) 3021-3027.
10. A. Yamamoto, A. Luo, S. Dodda-Kashi, V. Lee. The ocular route for systemic insulin delivery in the albino rabbit. *The Journal of Pharmacology and Experimental Therapeutics* 249 (1989) 249-255.
11. J. Wang, Y. Tabata, K. Morimoto. Aminated gelatin microspheres as a nasal delivery system for peptide drugs: Evaluation of in vitro release and in vivo insulin absorption in rats. *Journal of Controlled Release* 113 (2006) 31-37.

12. W. Cho, M. Kim, M. Jung, J. Park, K. Cha, J. Kim, H. Park, A. Alhalaweh, S. Velaga, S. Hwang. Design of salmon calcitonin particles for nasal delivery using spray-drying and novel supercritical fluid-assisted spray-drying processes. *International Journal of Pharmaceutics* 478 (2015) 288-296.
13. N. Kamei, M. Takeda-Morishita. Brain delivery of insulin boosted by intranasal coadministration with cell-penetrating peptides. *Journal of Controlled Release* 197 (2015) 105-110.
14. A. Herwadkar, A. Banga. 2011. Transdermal Delivery of Peptides and Proteins. In: C. Van der Walle. Ed. *Peptide and Protein Delivery*. London, UK: Elsevier, pp. 69-86.
15. F. Yin, S. Guo, Y. Gan, X. Zhang. Preparation of redispersible liposomal dry powder using an ultrasonic spray freeze-drying technique for transdermal delivery of human epithelial growth factor.
16. K. Yerramsetty, V. Rachakonda, B. Neely, S. Madihally, K. Gasem. Effect of different enhancers on the transdermal permeation of insulin analog. *International Journal of Pharmaceutics* 398 (2010) 83-92.
17. Y. Bai, V. Sachdeva, H. Kim, P. Friden, A. Banga. Transdermal delivery of proteins using a combination of iontophoresis and microporation. *Therapeutic Delivery* 5 (2014) 525-536.
18. P. Kwok, H. Chan. 2011. Pulmonary Delivery of Peptides and Proteins. In: C. Van der Walle. Ed. *Peptide and Protein Delivery*. London, UK: Elsevier, pp. 23-46.
19. Y. Huang, C. Wang. Pulmonary delivery of insulin by liposomal carriers. *Journal of Controlled Release* 113 (2006) 9-14.
20. Z. Dong, K. Abdul Hamid, Y. Gao, Y. Lin, H. Katsumi, T. Sakane, A. Yamamoto. Polyamidoamine Dendrimers Can Improve the Pulmonary Absorption of Insulin and Calcitonin in Rats. *Journal of Pharmaceutical Sciences* 100 (2011) 1866-1878.
21. T. Cavaiola, S. Edelman. Inhaled insulin: A breath of fresh air? a review of inhaled insulin. *Clinical Therapeutics* 36 (2014) 1275-1289.
22. B. Choonara, Y. Choonara, P. Kumar, D. Bijukumar, L. du Troit, V. Pillay. A review of advanced oral drug delivery technologies facilitating the protection and absorption of protein and peptide molecules. *Biotechnology advances* 32 (2014) 1269-1282.

23. J. Parmentier, G. Hofhaus, S. Thomas, L. Cuesta, F. Gropp, R. Schröder, K. Hartmann, G. Fricker. Improved oral bioavailability of human growth hormone by a combination of liposomes containing bio-enhancers and tetraether lipids and omeprazole. *Journal of Pharmaceutical Sciences* 103 (2014) 3985-3993.
24. A. Huang, Z. Su, M. Sun, Y. Xiao, Q. Ping, Y. Deng. Oral absorption enhancement of salmon calcitonin by using both N-trimethyl chitosan chloride and oligoarginine-modified liposomes as the carriers. *Drug Delivery* 21 (2014) 388-396.
25. X. Gao, Y. Cao, X. Song, Z. Zhang, X. Zhuang, C. He, X. Chen. Biodegradable, pH-responsive carboxymethyl cellulose/poly(acrylic acid) hydrogels for oral insulin delivery. *Macromolecular Bioscience* 14 (2014) 565-575.
26. C. Ibie, R. Knott, C. Thompson. In-vitro evaluation of the effect of polymer structure on the uptake of novel polymer-insulin polyelectrolyte complexes by human epithelial cells. *International Journal of Pharmaceutics* 479 (2015) 103-117.
27. M. Hess, R. Jones, J. Kahovec, T. Kitayama, P. Kratochvil, P. Kubisa, W. Mormann, R. Stepto, D. Tabak, J. Vohlidal, E. Wilks. Terminology of polymers containing ionizable or ionic groups and of polymers containing ions (IUPAC Recommendations 2006). *Pure and Applied Chemistry* 78 (2006) 2067-2074.
28. S. Lankalapalli, V. R. M. Kolapalli. Polyelectrolyte Complexes: A Review of their Applicability in Drug Delivery Technology. *Indian Journal of Pharmaceutical Sciences* 71 (5) (2009) 481-487.
29. Thompson CJ, Ding C, Qu X et al. The effect of polymer architecture on the nano self-assemblies based on novel comb-shaped amphiphilic poly(allyl amine). *Colloid and Polymer Science* 286 (2008) 1511-1526.
30. S. M. Hartig, R. R. Greene, M. M. Dikov, A. Prokop, J. M. Davidson. Multifunctional Nanoparticulate Polyelectrolyte Complexes. *Pharmaceutical Research* 24 (2007) 2353-2369.
31. J. van der Gucht, E. Spruijt, M. Lemmers, M. Cohen Stuart. Polyelectrolyte complexes: Bulk phases and colloidal systems. *Journal of Colloid and Interface Science* 361 (2011) 407-422.

32. A.F. Kotze, B.J. de Leeuw, H.L. Lueßen, A.G. de Boer, J.C. Verhoef, H.E. Junginger. Chitosans for enhanced delivery of therapeutic peptides across intestinal epithelia: in vitro evaluation in Caco-2 cell monolayers. *International Journal of Pharmaceutics* 159 (1997) 243–253.
33. H. Onishi, Y. Machida. Biodegradation and distribution of water-soluble chitosan in mice. *Biomaterials* 20 (1999) 175-182.
34. U.S Food and Drug Administration. Database of Select Committee on GRAS Substances Reviews. 1973 (24 CFR 184.1724).
35. M. Muller. 2014. *Polyelectrolyte Complexes in the Dispersed and Solid State II Application Aspects*. Heidelberg, Germany: Springer.
36. C. Tsao, C. Chang, Y. Lin, M. Wu, J. Wang, J. Han, K. Hsieh. Antibacterial activity and biocompatibility of a chitosan–*c*-poly(glutamic acid) polyelectrolyte complex hydrogel. *Carbohydrate Research* 345 (2010) 1774-1780.
37. Y. Fukui, T. Maruyama, Y. Iwamatsu, A. Fujii, T. Tanaka, Y. Ohmukai, H. Matsuyama. Preparation of monodispersed polyelectrolyte microcapsules with high encapsulation efficiency by an electrospray technique. *Colloids and Surfaces A: Physicochemical and Engineering Aspects* 370 (2010) 28–34.
38. F. Basmanav, G. Kose, V. Hasirci. Sequential growth factor delivery from complexed microspheres for bone tissue engineering. *Biomaterials* 29 (2008) 4195–4204.
39. Shelly, M. Ahuja, A. Kumar. Gum ghatti–chitosan polyelectrolyte nanoparticles: Preparation and characterization. *International Journal of Biological Macromolecules* 61 (2013) 411– 415.
40. M. Desai, V. Labhassetwar, E. Walter, R. Levy, G. Amidon. The Mechanism of Uptake of Biodegradable Microparticles in Caco-2 Cells is Size Dependent. *Pharmaceutical Research* 14 (1997) 1568-1573.
41. K. Bowman, K. W. Leong. Chitosan nanoparticles for oral drug and gene delivery. *International Journal of Nanomedicine* 1 (2006) 117–128.
42. M. Amidi, E. Mastrobattista, W. Jiskoot, W. E. Hennink. Chitosan-based delivery systems for protein therapeutics and antigens. *Advanced Drug Delivery Reviews* 62 (2010) 59–82.

43. J. Doczi. Process for purification of chitosan by means of the salicylic acid salt thereof. US patent: US2795579 A (1953).
44. W. Wang, Y. Dua, Y. Qiu, X. Wang, Y. Hu, J. Yang, J. Cai, J. F. Kennedy. A new green technology for direct production of low molecular weight chitosan. *Carbohydrate Polymers* 74 (2008) 127–132.
45. A. Rampino, M. Borgogna, P. Blasi, B. Bellich, A. Cesàro. Chitosan nanoparticles: Preparation, size evolution and stability. *International Journal of Pharmaceutics* 455 (2013) 219– 228.
46. F. Shahidi, J. Kamil, V. Arachchi, Y. Jeon. Food applications of chitin and chitosans. *Trends in Food Science & Technology* 10 (1999) 37-51.
47. T. Aspden, J. Mason, N. Jones, J. Lowe, Ø. Skaugrud, L. Illum. Chitosan as a Nasal Delivery System: The Effect of Chitosan Solutions on in Vitro and in Vivo Mucociliary Transport Rates in Human Turbinates and Volunteers. *Journal of Pharmaceutical Sciences* 86 (1997) 509-513.
48. S. Mao, X. Shuai, F. Unger, M. Simona, D. Bi, T. Kissel. The depolymerization of chitosan: effects on physicochemical and biological properties. *International Journal of Pharmaceutics* 281 (2004) 45–54.
49. M. Kumar. A review of chitin and chitosan applications. *Reactive & Functional Polymers* 46 (2000) 1–27.
50. W. Liu, S. Sun, Z. Cao, X. Zhang, K. Yao, W. Lu, K. Luk. An investigation on the physicochemical properties of chitosan/DNA polyelectrolyte complexes. *Biomaterials* 26 (2005) 2705–2711.
51. C. Mei-Chin, W. Hen-Sheng, L. Kun-Ju, C. Hsin-Lung, W. Shiaw-Pyng, K. Sonaje, L. Yu-Hsin, C. Che-Yi, S. Hsing-Wen. The characteristics, biodistribution and bioavailability of a chitosan-based nanoparticulate system for the oral delivery of heparin. *Biomaterials* 30 (2009) 6629–6637.
52. J. Nam, C. Choi, M. Jang, Y. Jeong, J. Nah. Insulin-incorporated Chitosan Nanoparticles Based on Polyelectrolyte Complex Formation. *Macromolecular Research* 18 (7) (2010) 630-635.

53. C. Lehr, J. Bouwstra, E. Schacht, H. Junginger. In vitro evaluation of mucoadhesive properties of chitosan and some other natural polymers. *International Journal of Pharmaceutics* 78 (1992) 43-48.
54. M. Abdel Mouez, N. Zaki, S. Mansour, A. Geneidi. Bioavailability enhancement of verapamil HCl via intranasal chitosan microspheres. *European Journal of Pharmaceutical Sciences* 51 (2014) 59–66.
55. H. Lueßen, B. de Leeuw, M. Langmeyer, A. De Boer, J. Verhoef, H. Junginger. Mucoadhesive Polymers in Peroral Peptide Drug Delivery. VI. Carbomer and Chitosan Improve the Intestinal Absorption of the Peptide Drug Buserelin In Vivo. *Pharmaceutical Research* 13 (11) (1996) 1668-1672.
56. M. Sakkinen, T. Tuononen, H. Jurjenson, P. Veski, M. Marvola. Evaluation of microcrystalline chitosans for gastro-retentive drug delivery. *European Journal of Pharmaceutical Sciences* 19 (2003) 345–353.
57. M. Sakkinen, J. Marvola, H. Kanerva, K. Lindevall, A. Ahonen, M. Marvola. Are chitosan formulations mucoadhesive in the human small intestine? An evaluation based on gamma scintigraphy. *International Journal of Pharmaceutics* 307 (2006) 285–291.
58. J. Anderson, C. Van Itallie. Physiology and Function of the Tight Junction. *Cold Spring Harbor Perspectives in Biology* (2009); 1:a002584.
59. E. Frömter, J. Diamond. Route of Passive Ion Permeation in Epithelia. *Nature new biology* 235 (1972) 9-13.
60. V. Dodane, M. A. Khan, J. R. Merwin. Effect of chitosan on epithelial permeability and structure. *International Journal of Pharmaceutics* 182 (1999) 21–32.
61. H. Lueßen, C. Rentel, A. Kotze, C. Lehr, A. De Boer, J. Verhoef, H. Junginger. Mucoadhesive polymers in peroral peptide drug delivery: IV. Polycarbophil and chitosan are potent enhancers of peptide transport across intestinal mucosae in vitro. *Journal of Controlled Release* 45 (1997) 15-23.
62. M. Rinaudo, G. Pavlov, J. Desbrières. Influence of acetic acid concentration on the solubilisation of chitosan. *Polymer* 40 (1999) 7029-7032.

63. M. Werle, H. Takeuchi, A. Bernkop-schnurch. Modified Chitosans for Oral Drug Delivery. *Journal of Pharmaceutical Sciences* 98 (2009) 1643–1656.
64. F. Sarti, A. Bernkop-Schnürch. Chitosan and Thiolated Chitosan. *Advances in Polymer Science* 243 (2011) 93–110.
65. A. Bernkop-Schnürch, M. Hornof, T. Zoidl. Thiolated polymers—thiomers: synthesis and in vitro evaluation of chitosan–2-iminothiolane conjugates. *International Journal of Pharmaceutics* 260 (2003) 229–237.
66. L. Dongwon, Z. Weidong, S. Shirley, K. Xiaoyuan, G. Hellermann, R. Lockey, S. Mohapatra. Thiolated Chitosan/DNA Nanocomplexes Exhibit Enhanced and Sustained Gene Delivery. *Pharmaceutical Research* 24 (2007) 157-167.
67. F. de Abreu, S. Campana-Filho. Characteristics and properties of carboxymethylchitosan. *Carbohydrate Polymers* 75 (2009) 214–221.
68. M. Thanou, M. Nihot, M. Jansen, J. Verhoef, H. Junginger. Mono-N-Carboxymethyl Chitosan (MCC), a Polyampholytic Chitosan Derivative, Enhances the Intestinal Absorption of Low Molecular Weight Heparin Across Intestinal Epithelia In Vitro and In Vivo. *Journal of pharmaceutical sciences* 90 (2001) 38-46.
69. A. Sieval, M. Thanou, A. Kotze, J. Verhoef, J. Brussee, H. Junginger. Preparation and NMR characterization of highly substituted IV-trimethyl chitosan chloride. *Carbohydrate Polymers* 36 (1998) 157-165.
70. M. Thanou, A. Kotze, T. Scharringhausen, H. Lueßen, A. de Boer, J. Verhoef, H. Junginger. Effect of degree of quaternization of N-trimethyl chitosan chloride for enhanced transport of hydrophilic compounds across intestinal Caco-2 cell monolayers. *Journal of Controlled Release* 64 (2000) 15–25.
71. A. Kotze, M. Thanou, H. Lueßen, B. de Boer, J. Verhoef, H. Junginger. Effect of the degree of quaternization of N-trimethyl chitosan chloride on the permeability of intestinal epithelial cells (Caco-2). *European Journal of Pharmaceutics and Biopharmaceutics* 47 (1999) 269–274.
72. J. Hamman, M. Stander, A. Kotze. Effect of the degree of quaternisation of N-trimethyl chitosan chloride on absorption enhancement: in vivo evaluation in rat nasal epithelia. *International Journal of Pharmaceutics* 232 (2002) 235–242.

73. A. Jintapattanakit, V. Junyaprasert, S. Maob, J. Sitterberg, U. Bakowsky, T. Kissel. Peroral delivery of insulin using chitosan derivatives: A comparative study of polyelectrolyte nanocomplexes and nanoparticles. *International Journal of Pharmaceutics* 342 (2007) 240–249.
74. K. I. Draget, O. Smidsrød, G. Skjåk-Bræk. 2005. Alginates from Algae. In: A. Steinbüchel, S. Rhee. Eds. *Polysaccharides and polyamides in the food industry. Properties, production and patents*. Weinheim, Germany: Wiley, pp. 1-30.
75. D. McHugh. A guide to the seaweed industry FAO Fisheries technical paper No. 441, 2003. Chapter 5, Alginate, 39-49.
76. B. H. A. Rehm, S. Valla. Bacterial alginates: biosynthesis and applications. *Applied Microbiology and Biotechnology* 48 (1997) 281-288.
77. A. Haug. Ion exchange properties of alginate fractions. *Acta Chemica Scandinavica* 13 (1959) 601-603.
78. O. Smidsrød, A. Haug. Properties of poly (1,4-heuronates) in the gel state, comparison of gels of different chemical composition. *Acta Chemica Scandinavica* 26 (1972) 79-88.
79. A. Haug. Dissociation of alginic acid. *Acta Chemica Scandinavica* 15 (1961) 950-952.
80. G. Orive, A. M. Carcaboso, R. M. Hernandez, A. R. Gascon, J. L. Pedraz. Biocompatibility Evaluation of Different Alginates and Alginate-Based Microcapsules. *Biomacromolecules* 6 (2005) 927-931.
81. A. Bernkop-Schnürch, C. Kast, M. Richter. Improvement in the mucoadhesive properties of alginate by the covalent attachment of cysteine. *Journal of Controlled Release* 71 (2001) 277–285.
82. A. Haug, B. Larsen, O. Smidsrød. The degradation of Alginates at different pH values. *Acta Chemica Scandinavica* 17 (1963) 1466-1468.
83. K. Y. Lee, D. J. Mooney. Alginate: Properties and biomedical applications. *Progress in Polymer Science* 37 (2012) 106–126.

84. K. Klemmer, L. Waldner, A. Stone, N. Low, M. Nickerson. Complex coacervation of pea protein isolate and alginate polysaccharides. *Food Chemistry* 130 (2012) 710–715.
85. K. Douglas, M. Tabrizian. Effect of experimental parameters on the formation of alginate–chitosan nanoparticles and evaluation of their potential application as DNA carrier. *Journal of Biomaterials Science, Polymer Edition* 16 (2005) 43–56.
86. B. Sarmiento, S. Martins, A. Ribeiro, F. Veiga, R. Neufeld, D. Ferreira. Development and Comparison of Different Nanoparticulate Polyelectrolyte Complexes as Insulin Carriers. *International Journal of Peptide Research and Therapeutics* 12 (2006) 131–138.
87. B. Sarmiento, D. Ferreira, L. Jorgensen, M. van de Weert. Probing insulin's secondary structure after entrapment into alginate/chitosan nanoparticles. *European Journal of Pharmaceutics and Biopharmaceutics* 65 (2007) 10–17.
88. B. Sarmiento, A. Ribeiro, F. Veiga, P. Sampaio, R. Neufeld, D. Ferreira. Alginate/Chitosan Nanoparticles are Effective for Oral Insulin Delivery. *Pharmaceutical Research* 24 (2007) 2198-2206.
89. T. Li, X. Shi, Y. Du, Y. Tang. Quaternized chitosan/alginate nanoparticles for protein delivery. *Journal of biomedical materials research Part A*. 83 (2007) 383-390.
90. M. Mende, S. Schwarz, S. Zschoche, G. Petzold, A. Janke. Influence of the Hydrophobicity of Polyelectrolytes on Polyelectrolyte Complex Formation and Complex Particle Structure and Shape. *Polymers* 3 (2011) 1363-1376.
91. E. Broderick, H. Lyons, T. Pembroke, H. Byrne, B. Murray, M. Hall. The characterisation of a novel, covalently modified, amphiphilic alginate derivative, which retains gelling and non-toxic properties. *Journal of Colloid and Interface Science* 298 (2006) 154–161.
92. Y. Liqun, Z. Bifang, W. Liqun, L. Qiuyi, Z. Li-Ming. Amphiphilic cholesteryl grafted sodium alginate derivative: Synthesis and self-assembly in aqueous solution. *Carbohydrate Polymers* 68 (2007) 218-225.
93. L. Wang, L. Li, Y. Sun, Y. Tian, Y. Li, C. Li, V. Junyaprasert, S. Mao. Exploration of hydrophobic modification degree of chitosan-based nanocomplexes on the oral

delivery of enoxaparin. *European Journal of Pharmaceutical Sciences* 50 (2013) 263–271.

94. M. Simon, M. Wittmar, U. Bakowsky, T. Kissel. Self-Assembling Nanocomplexes from Insulin and Water-Soluble Branched Polyesters, Poly[(vinyl-3-(diethylamino)-propylcarbamate-co-(vinyl acetate)-co-(vinyl alcohol)]-graftpoly(L-lactic acid): A Novel Carrier for Transmucosal Delivery of Peptides. *Bioconjugate Chemistry* 15 (2004) 841-849.

95. M. Simon, M. Wittmar, T. Kissel, T. Linn. Insulin Containing Nanocomplexes Formed by Self-Assembly from Biodegradable Amine-Modified Poly(Vinyl Alcohol)-Graft-Poly(L-Lactide): Bioavailability and Nasal Tolerability in Rats. *Pharmaceutical Research* 22 (2005) 1879-1886.

96. M. Simon, I. Behrens, L. Dailey, M. Wittmar, T. Kissel. Nanosized insulin-complexes based on biodegradable amine-modified graft polyesters poly[vinyl-3-(diethylamino)-propylcarbamate-co-(vinyl acetate)-co-(vinyl alcohol)]-graft-poly(L-lactic acid): Protection against enzymatic degradation, interaction with Caco-2 cell monolayers, peptide transport and cytotoxicity. *European Journal of Pharmaceutics and Biopharmaceutics* 66 (2007) 165–172.

97. C. Thompson, L. Tetley, I. Uchegbu, W. Cheng. The complexation between novel comb shaped amphiphilic polyallylamine and insulin—Towards oral insulin delivery. *International Journal of Pharmaceutics* 376 (2009) 46–55.

98. C. Thompson, W. Cheng, P. Gadad, K. Skene, M. Smith, G. Smith, A. McKinnon, R. Knott. Uptake and Transport of Novel Amphiphilic Polyelectrolyte-Insulin Nanocomplexes by Caco-2 Cells—Towards Oral Insulin. *Pharmaceutical Research* 28 (2011) 886–896.

2. Polymer synthesis and characterisation

This chapter focuses on the synthesis of amphiphilic and quaternised derivatives of poly(allylamine) with a view to investigating their ability to interact with sodium alginate (chapter 3), and towards formulating an amphiphilic polyelectrolyte complex with insulin (chapter 4).

The synthesis of amphiphilic polymers involved the reaction of palmitic acid-N-hydroxysuccinamide with primary amines of poly(allylamine). The 16 carbon palmitic acid chains provided an increased hydrophobic character to the polymer. The addition of hydrophobic groups to poly(allylamine) is known to produce an amphiphilic polymer with the ability to self-assemble into particles in the nano size range.

Quaternisation involved the use of methyl iodide to produce methylation of free amines of the poly(allyl amine) backbone, the resulting permanent positive charge was expected to provide electrostatic interaction with sodium alginate regardless of pH environment, this will be discussed in more detail in chapter 3.

Characterisation of synthesised polymers was performed in order to help confirm synthesis, as well as examine any clear changes in polymer properties. Techniques used include infra-red, thermal, and elemental analysis as well as nuclear magnetic resonance.

2.1. Materials

Poly(allylamine hydrochloride) (Mw =15000Da) (Sigma-Aldrich, UK), sodium hydroxide pellets, sodium hydrogen carbonate, palmitic acid-N-hydroxysuccinamide (Sigma-Aldrich, UK), sodium iodide (Sigma-Aldrich, UK), methyl iodide (Sigma-Aldrich, UK), amberlite 93 resin (Sigma-Aldrich, UK), all other chemicals were of analytical grade and sourced from fisher scientific, UK.

2.2. Method of polymer synthesis

The methods of polymer synthesis are based on the work of Thompson et al (1).

2.2.1. Conversion of poly(allylamine hydrochloride) to poly (allylamine) free base.

Poly(allylamine hydrochloride) (10g) was dissolved in (100mL) of distilled water. The pH of the solution was then adjusted to approximately 13, this was followed by dialysing the solution against (5L) of distilled water using 7kDa molecular

weight cut-off dialysis bags; water was changed 6 times over 24 hours. Dialysate was then lyophilised over 72 hours using a freeze drier (VirTis advantage, Biopharma Process Systems, UK) to obtain a dry, white solid.

2.2.2. Synthesis of amphiphilic polymers

The objective of palmitoyl (PA) grafting was to synthesise 2.5% and 5% substituted poly(allylamine) (pa2.5 and pa5), the method of synthesis is identical except for the molar feed ratio of palmitic acid-N-hydroxy succinamide.

Poly(allylamine) free base (1000mg) and sodium bicarbonate (1176mg) were dissolved in 100mL distilled water. Palmitic acid-N-hydroxy succinamide ester (304mg for pa2.5 or 608mg for pa5) was dissolved in 100mL ethanol.

The palmitic acid ester solution was added drop-wise to the round bottomed flask containing poly(allylamine), the flask was then stoppered and the reaction left under magnetic stirring for 72 hours at room temperature.

Solution was dialysed against 5L distilled water, using 12-14kDa molecular weight cut-off dialysis bags. Water was changed 6 times over 24 hours. Dialysate was lyophilised over 72 hours to obtain dry, white solid.

2.2.3. Synthesis of quaternised amphiphilic polymers

Quaternisation was performed on pa2.5 and pa5, leading to the synthesis of quaternised pa2.5 (Qpa2.5) and quaternised pa5 (Qpa5).

Amphiphilic polymer (600mg), sodium hydroxide (557mg), and sodium iodide (250mg) were dissolved in 100mL methanol. Methyl iodide 3.51mL was added to the solution. The reaction was carried out under nitrogen environment at 36°C for 3 hours.

The resulting precipitate was separated from the solution. Diethyl ether 400mL was added to the precipitate, while a further 200mL diethyl ether was added to the separated solution to enhance precipitation of any leftover product. Both suspensions were then left to dry overnight under a fume hood.

An ethanol and water (1:1) stock was prepared and used to dissolve the dried precipitate. Solutions were dialysed against 5L distilled water using 12-14 kDa molecular weight cut-off dialysis bags. Water was changed 6 times over 24 hours.

Dialysate was then passed through an amberlite ion exchange column. The column was prepared by washing with 2M hydrochloric acid (100mL) followed by regular washing with distilled water until neutral pH was recorded.

Ion exchanged dialysate was then lyophilised over 72 hours to produce dry, white/off white solid.

2.3. Polymer characterisation

2.3.1. Elemental analysis and proton nuclear magnetic resonance

Elemental analysis of synthesised polymers pa2.5, pa5, Qpa2.5 and Qpa5 (20mg of each) was carried out to determine the relative abundance of carbon, nitrogen, and hydrogen, as well as chlorine in the case of quaternised samples. Data was obtained using a Perkin Elmer 2400 Series II CHNS analyser (Perkin Elmer, UK)

Polymer structure was investigated using ¹H-NMR. PAA, pa2.5, pa5, Qpa2.5 and Qpa5 (15mg of each) were sonicated in deuterated methanol (1-2mL) and inserted into a BRUKER 400MHz ultrashield spectrometer (Bruker, USA); TOPSPIN 1.3 software was used to acquire and annotate sample spectra.

2.3.2. Infra-red analysis

Infra-red analysis (IR) was carried out on samples of PAA, pa2.5, pa5, Qpa2.5 and Qpa5 using a Thermo Nicolet IR spectrophotometer (Thermo Fisher Scientific, USA) using diamond tip accessory. Measurements were performed at 32 scans per spectrum between 4000-500cm⁻¹. Data was analysed using OMNIC software.

2.3.3. Thermal analysis

Differential scanning calorimetry (DSC) was used to investigate the thermal properties of the polymers to be used in complex formation. Data was acquired using a Q100 differential scanning calorimeter (TA instruments, UK). Samples of PAA, pa2.5, pa5, Qpa2.5, and Qpa5 (1-5mg) were run over a temperature range of 0-300°C at 20°C/minute under nitrogen atmosphere. The instrument was calibrated with an indium standard.

LEICA DFC 420 digital microscope (LEIKA, Germany) coupled to a LINKAM LTS 350 hot-stage (Linkam scientific instruments, UK) was used to capture images of PAA, pa2.5, pa5, Qpa2.5, and Qpa5 at temperature points from room temperature to 300°C at 20x magnification.

Thermogravimetric analysis (TGA) was carried out on PAA, pa2.5 and pa5 using a Q500 thermogravimetric analyser (TA instruments, UK) in order to study the amount of weight change as a function of increasing temperature. This data was used in conjunction with DSC and hot-stage images in order to assist in the assessment of detected thermal events.

2.4. Results and discussion

2.4.1. Elemental analysis and NMR for synthesis validation

The NMR spectrum of PAA (Figure 2.1) shows two groups of peaks; the first at 1.0-1.7ppm designated (A) corresponds to the protons of the polymer backbone. The second set of peaks at 2.4-2.8ppm, designated (B) corresponds to the protons adjacent to the electron withdrawing amine.

The NMR of pa2.5 (Figure 2.2) and pa5 (Figure 2.3) are very similar, and will be discussed together. The signal at 0.8ppm, signal (A), is attributed to the terminal methyl group of palmitic acid chains. The peaks from 1.0-1.5ppm (B) are due to overlapping signals from polymer and palmitic acid backbone protons. The signal at 2.2ppm designated (C) was attributed to protons next to the carbonyl of palmitic acid graft. The peak at 2.5ppm (D) was attributed to the protons adjacent to amine groups of the polymer backbone (2).

The degree of palmitic acid substitution along the PAA backbone was estimated using NMR data. The terminal methyl was used to estimate the percentage graft of palmitic acid, by comparing the integral at point (A) with the integral at point (D) (Equation 2.1).

$$\%Grafting = \left(\left(\frac{Integral\ of\ A}{Number\ of\ protons\ (CH_3)} \right) \div \left(\frac{Integral\ of\ C}{Number\ of\ protons\ (CH_2)} \right) \right) \times 100\%$$

Equation 2.1 Estimating %graft of palmitic acid-N-hydroxysuccinamide using ¹H-NMR.

The NMR spectra of Qpa2.5 (Figure 2.4) and Qpa5 (Figure 2.5) were not used in the estimation of quaternisation, due to the overlapping signals of protons adjacent to amines and quaternary ammonium, shown in the figures as (C) and (D) respectively, in both cases falling within the region of 2.5-3.0ppm. Signals (A) and (B) were equivalent to those found for pa2.5 and pa5.

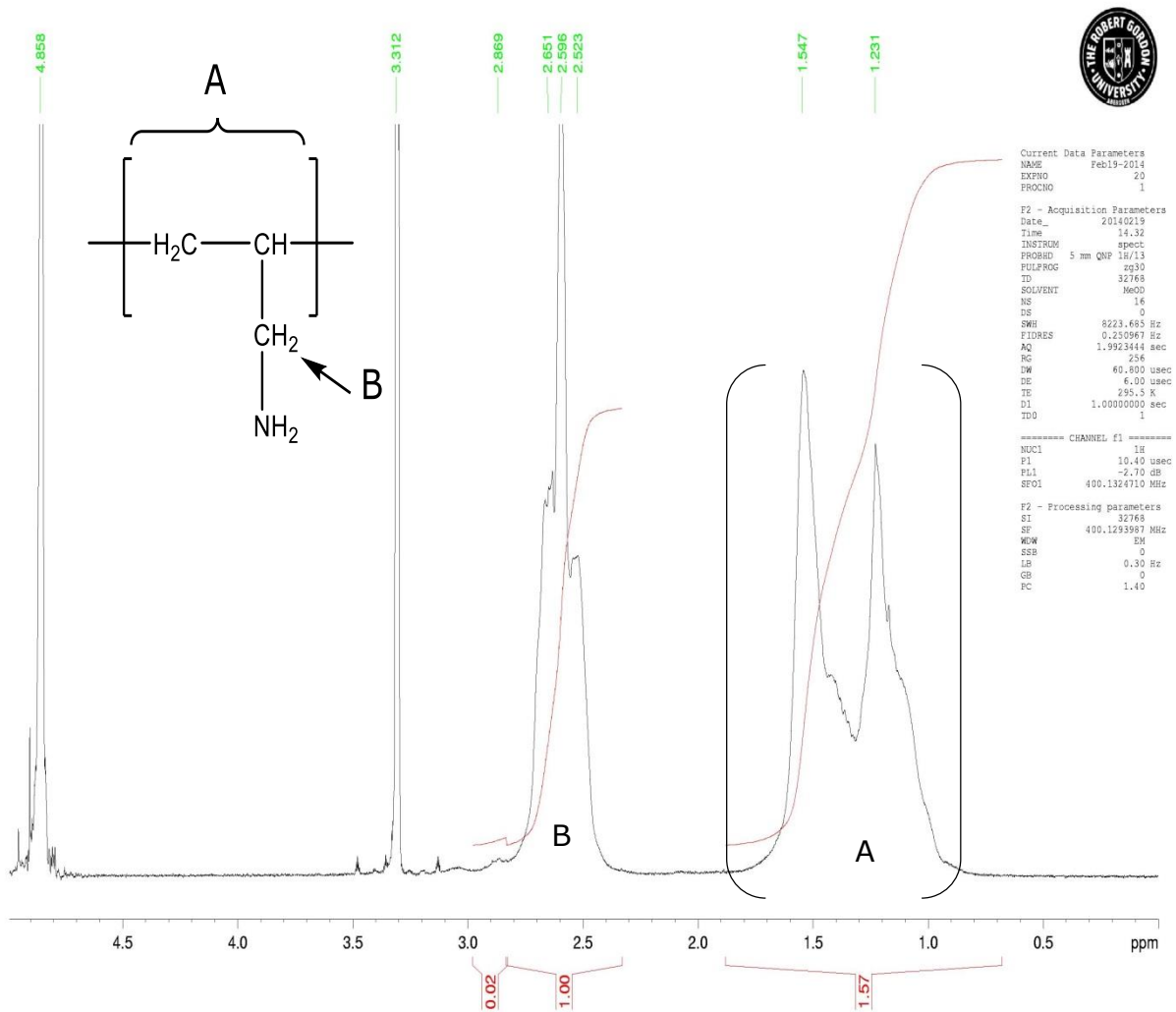


Figure 2.1 ^1H -NMR of poly(allylamine) in deuterated methanol

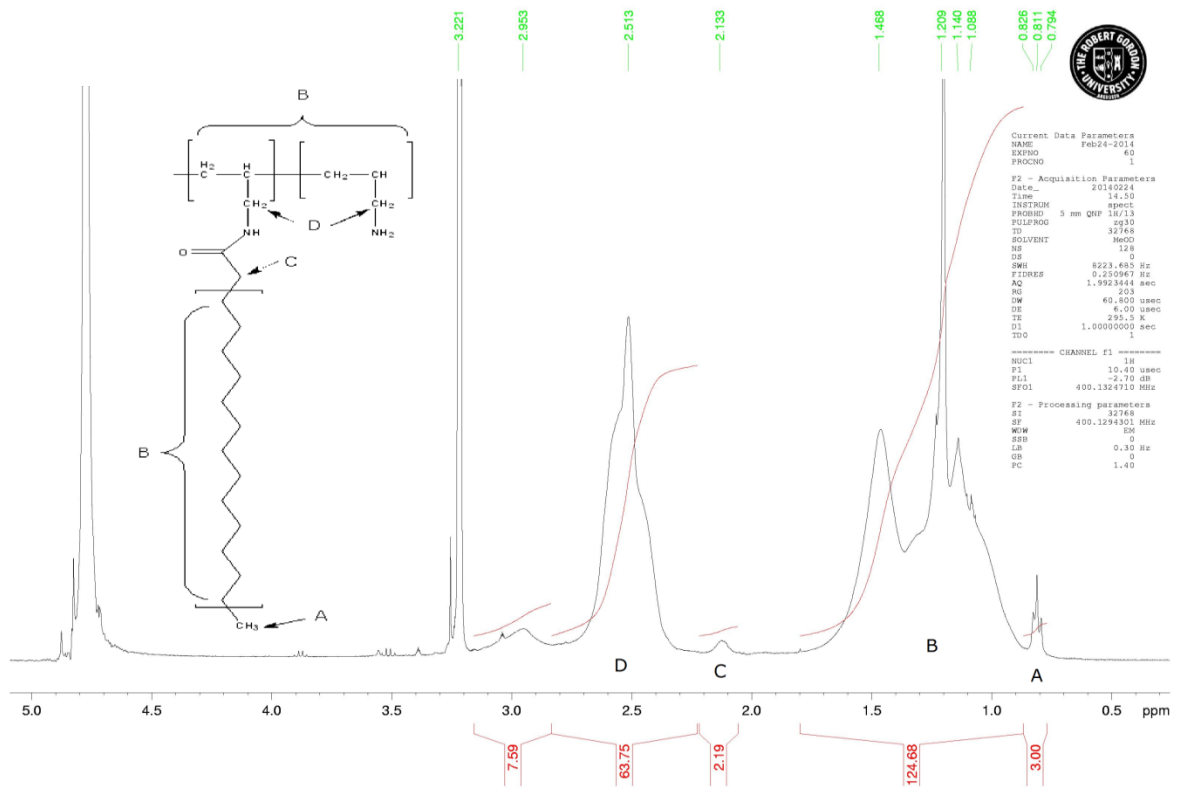


Figure 2.2 $^1\text{H-NMR}$ of 2.5% pa-poly(allylamine) in deuterated methanol.

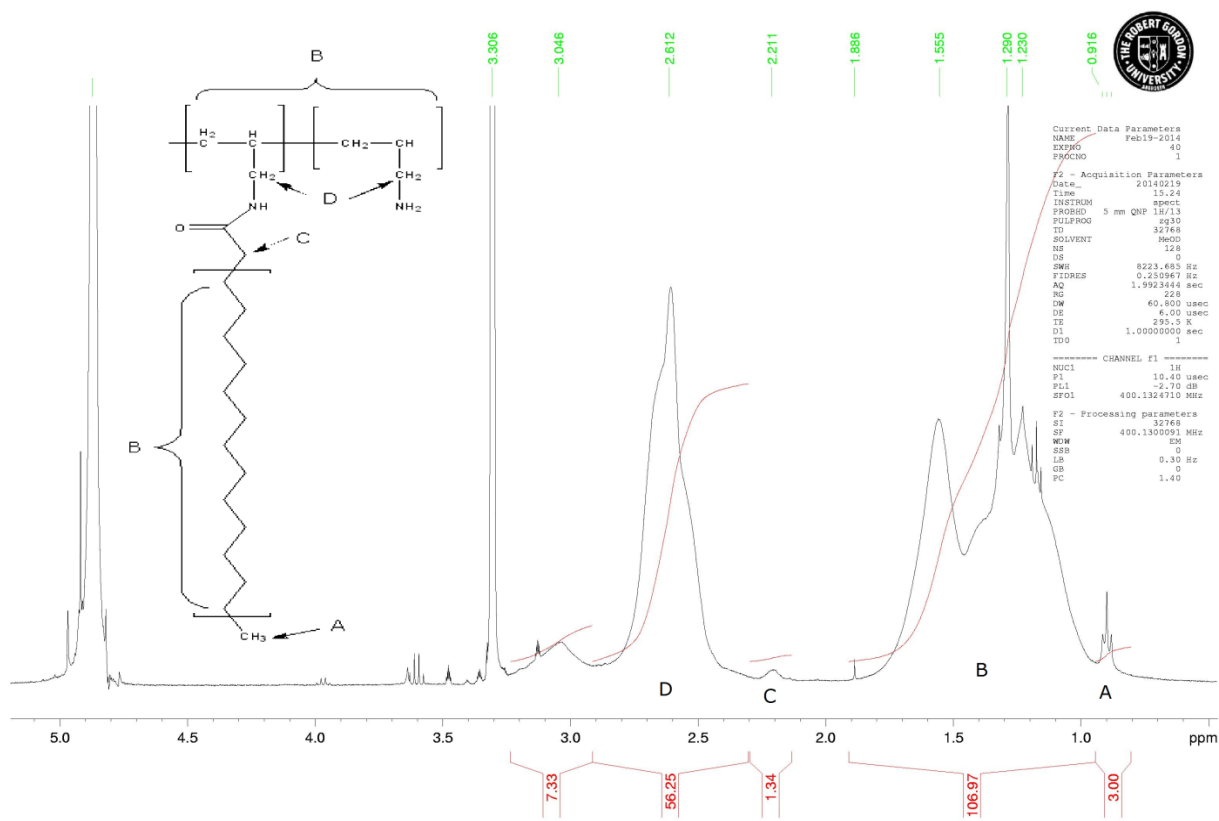


Figure 2.3 $^1\text{H-NMR}$ of 5% pa-poly(allylamine) in deuterated methanol.

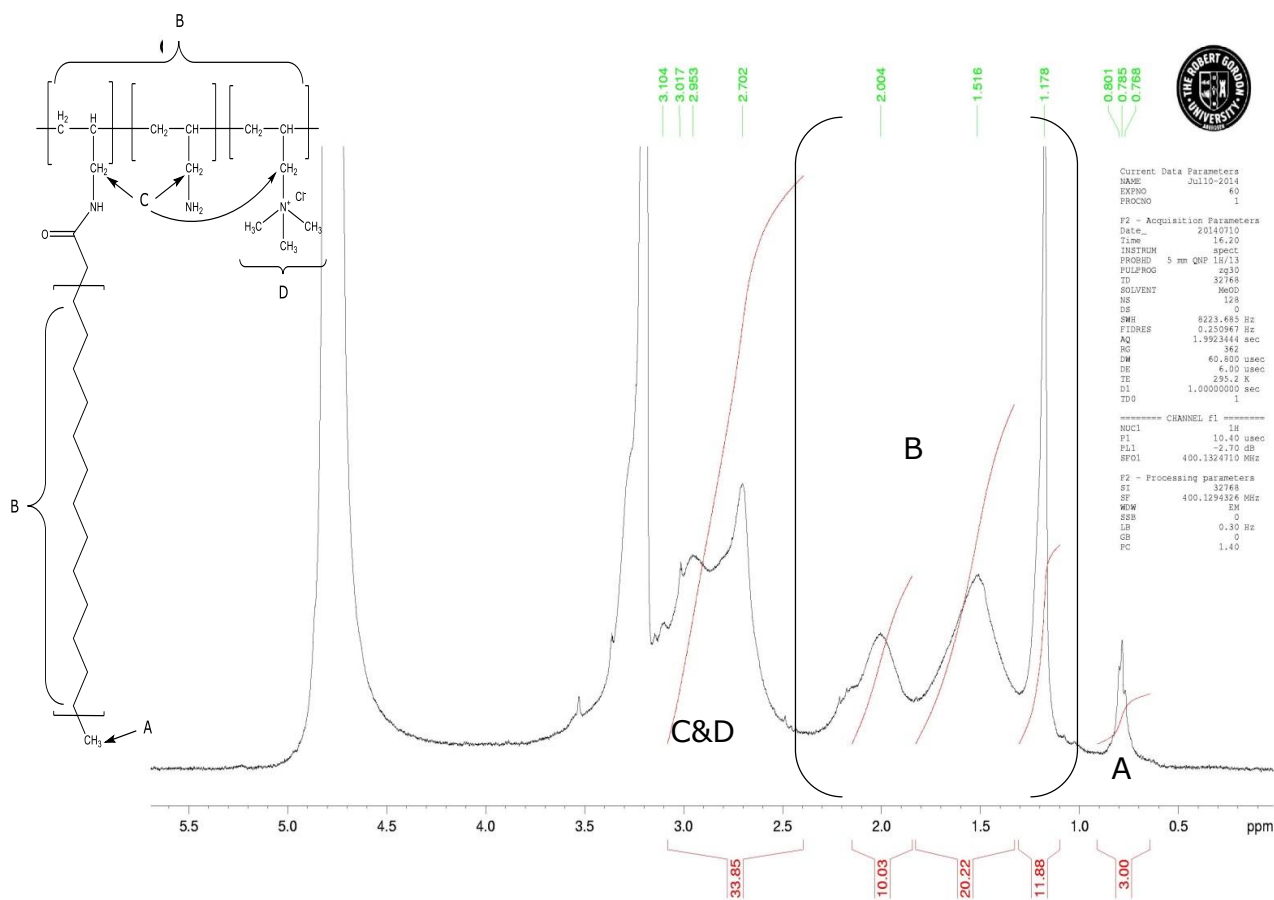


Figure 2.4 $^1\text{H-NMR}$ of quaternised 2.5% pa-poly(allylamine) in deuterated methanol.

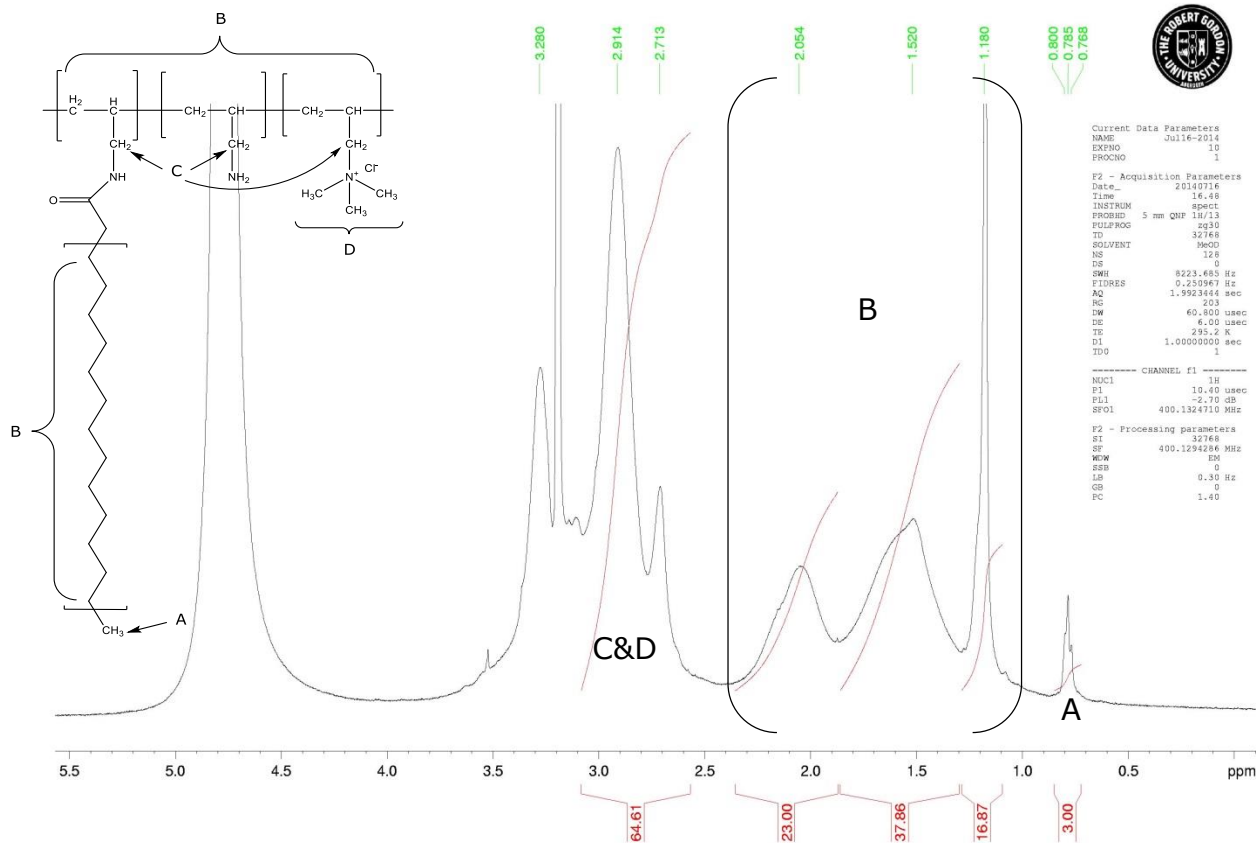


Figure 2.5 ^1H -NMR of quaternised 5% pa-poly(allylamine) in deuterated methanol.

Elemental analysis of the amphiphilic polymers was also used in the estimation of hydrophobic grafting by measuring the relative increase of carbon, in comparison to poly(allyl amine), in the amphiphilic polymer samples; it was assumed that the source of additional carbon must be from added palmitic acid groups. This assumption was seen as reasonable, due to a lack of other possible sources of carbon. By then approximating the number of palmitic acid units accounting for the carbon excess, a percentage graft can be estimated (equation 2.2). This method was used by Thompson et al. to estimate palmitoyl substitution of PAA (1). Wang et al. used elemental analysis to estimate the degree of cetylation of poly(ethylenimine) (3).

$$\text{Carbon excess} = \left(\frac{\text{Abundance of carbon in amphiphilic polymer}}{\text{Abundance of nitrogen in amphiphilic polymer}} \right) - \left(\frac{\text{Abundance of carbon in PAA}}{\text{Abundance of nitrogen in PAA}} \right)$$

$$\% \text{graft} = \left(\frac{\text{carbon excess}}{16} \right) \times 100\%$$

Equation 2.2 Estimating %graft of palmitic acid using elemental analysis.

Table 2.1 shows the results of NMR and elemental analysis calculations for the amphiphilic polymers. Although results did not produce exact 2.5 and 5 percent grafts, the two techniques used appeared to be in agreement that pa5 did possess higher grafting values than pa2.5.

Table 2.1 Estimation of palmitic acid-N-hydroxysuccinamide grafting.

PAA derivative	Estimation based on NMR (n=1)	Estimation based on elemental analysis (n=2)
Pa2.5	3.1%	3.7%
Pa5	3.5%	5.1%

Elemental analysis was used to estimate the degree of quaternisation by comparing the relative elemental abundance in quaternised samples to those of the non-quaternised samples. Elemental analysis has previously been used in the estimation of quaternisation of poly(allyl amine) (1), as well as a number of other polymers, such as chitosan (4), pectin (5), and poly(vinyl alcohol) (6).

Quaternised samples presented with an increase in carbon abundance, which was attributed to methylation of amine groups along the Pa-PAA backbone. By assuming tri-methylation of primary amines (The estimation does not take into account the possible formation of secondary and tertiary amines), an estimated level of quaternisation can be calculated according to equation 2.3.

$$\text{Carbon excess} = \left(\frac{\text{Abundance of carbon in quaternised polymer}}{\text{Abundance of nitrogen in quaternised polymer}} \right) - \left(\frac{\text{Abundance of carbon in amphiphilic polymer}}{\text{Abundance of nitrogen in amphiphilic polymer}} \right)$$

$$\% \text{Quaternisation} = \left(\frac{\text{carbon excess}}{3} \right) \times 100\%$$

Equation 2.3 Estimating %quaternisation of amphiphilic polymers.

Results of the quaternisation process are shown in table 2.2

Table 2.2 Estimation of quaternisation of amphiphilic polymers (n=1).

Polymer	Estimated degree of quaternisation
Qpa2.5	18%
Qpa5	35%

It would be expected that pa2.5, which was estimated to have had a greater number of free amines, would undergo quaternisation more readily than pa5, as the addition of large hydrophobic groups may interfere with the accessibility of free amines (7). However, the result was the opposite. It may simply be a matter of errors during the synthesis process leading to incomplete quaternisation.

2.4.2. IR analysis

The IR spectra for PAA (Figure 2.6) exhibited primary amine stretch vibrations at 3354cm^{-1} , 3279cm^{-1} , and 3181cm^{-1} and N-H bending vibrations at 1591cm^{-1} . C-N stretching vibrations were visible at 1120cm^{-1} . C-H stretching vibrations were visible at 2908cm^{-1} and 2848cm^{-1} , with bending vibrations at 1448cm^{-1} .

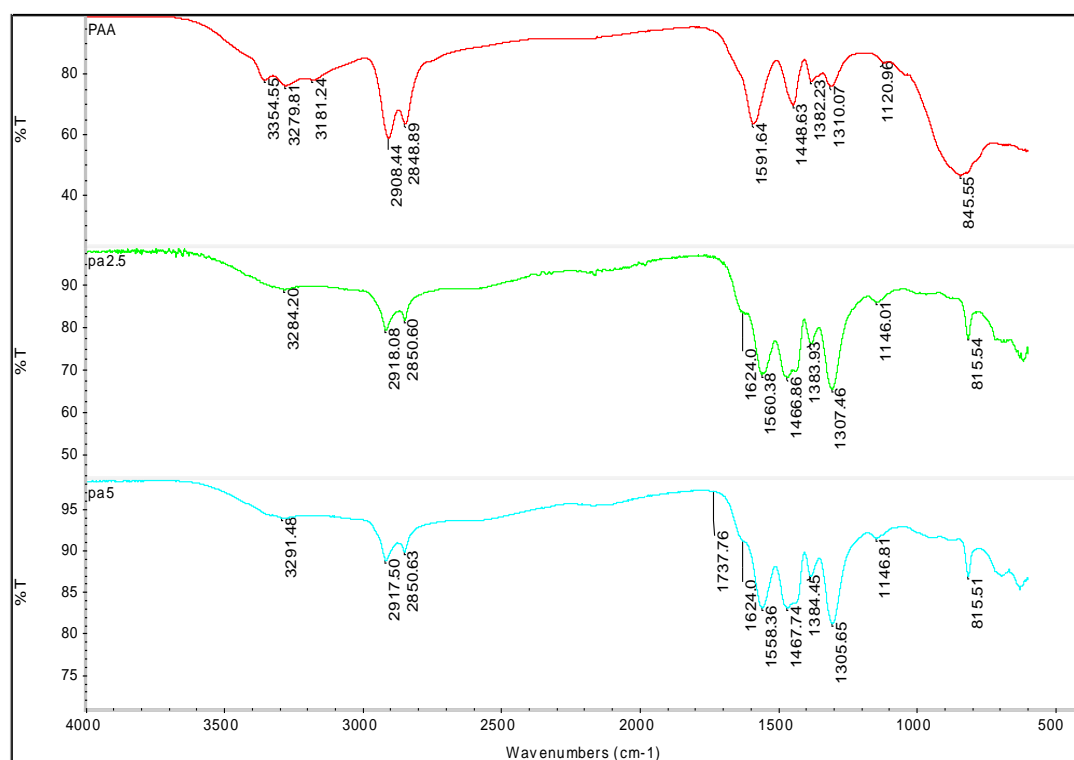


Figure 2.6 IR spectra of PAA, pa2.5 and pa5.

The addition of palmitic acid led to some changes to the spectrum of PAA. The three peaks attributed to primary amine stretching were replaced by single, shallow signals at 3284cm^{-1} and 3291cm^{-1} for pa2.5 and pa5, respectively; this may be due to palmitic acid substitution of primary amines leading to lower absorption. This trend was repeated at the other end of the spectrum, where primary N-H bending vibrations of PAA at 1591cm^{-1} was replaced by what appeared to be two amide bands at 1624cm^{-1} and 1560cm^{-1} in pa2.5, as well as 1624cm^{-1} and 1558cm^{-1} in pa5. A similar finding was obtained by Jiang et al. who synthesised palmitic acid grafted chitosan, and found that the primary amine peak of chitosan was replaced by amide bands; this was reported even at 0.9% palmitic acid substitution (8).

Table 2.3 summarises the detected vibrations for synthesised polymers.

Table 2.3 IR bands of PAA and amphiphilic polymers.

Polymer	Vibration (cm^{-1})	Chemical assignment
PAA	3354, 3279, 3181	N-H stretch
	1591	N-H bend
	1120	C-N stretch
	2908, 2848	C-H stretch
	1448	C-H bend
pa2.5	3284	N-H stretch
	1624, 1560	Amide I & II
	1146	C-N stretch
	2917, 2850	C-H stretch
	1466	C-H bend
pa5	3291	N-H stretch
	1624, 1558	Amide I & II
	1146	C-N stretch
	2917, 2850	C-H stretch
	1737	C=O stretch

	1467	C-H bend
Qpa2.5	3372	N-H stretch
	1613	N-H bend
	1177	C-N stretch
	2919, 2851	C-H stretch
	1464	C-H bend
Qpa5	3378	N-H stretch
	1617	N-H bend
	1176	C-N stretch
	2919, 2851	C-H stretch
	1466	C-H bend

Upon closer inspection of the pa5 spectrum (Figure 2.7), a signal at 1737cm^{-1} may indicate the presence of carbonyl groups of palmitic acid graft.

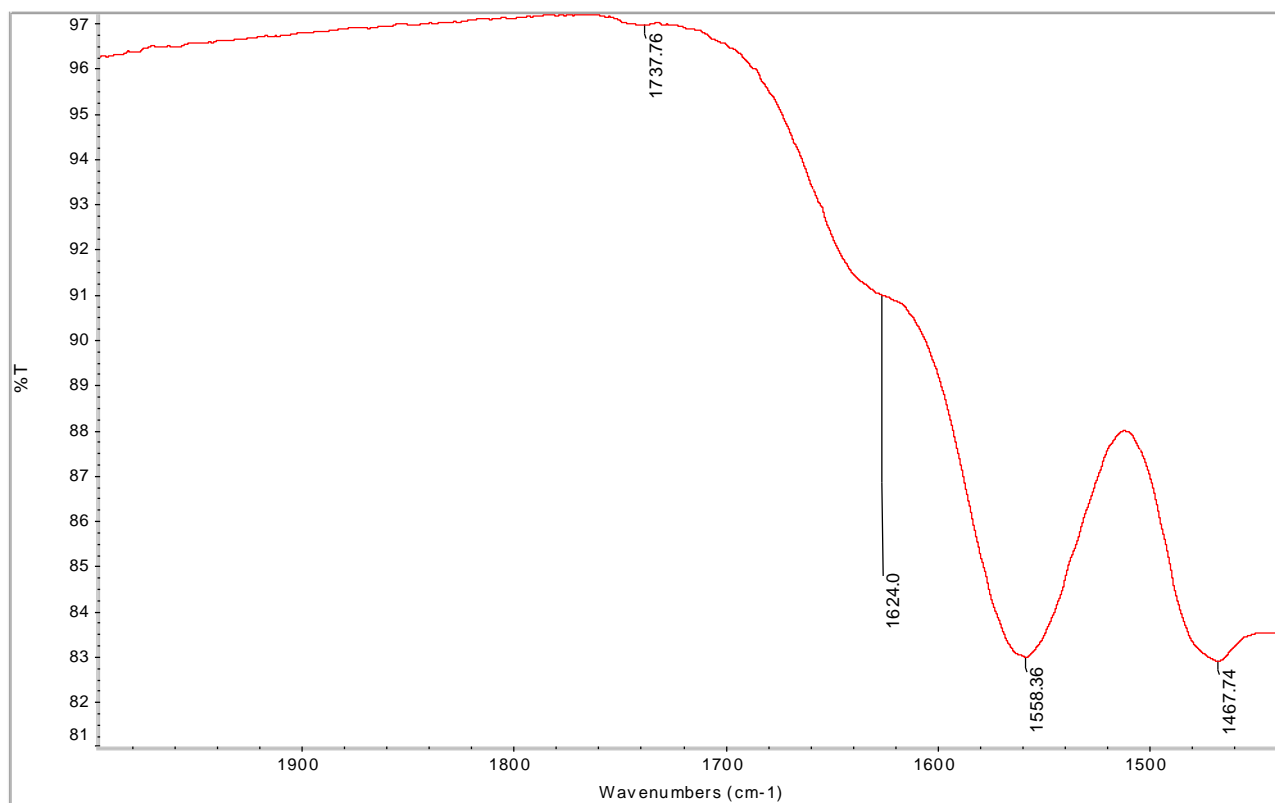


Figure 2.7 Magnification of IR spectrum of pa5 from $2000\text{--}1400\text{cm}^{-1}$.

Quaternised polymers showed similar spectra to their amphiphilic precursors (Figure 2.8). Qpa2.5 showed amine stretching vibrations at 3372cm^{-1} , N-H bending peak appeared at 1613cm^{-1} . C-H peaks at 2919cm^{-1} , 2851cm^{-1} and 1464cm^{-1} .

Qpa5 exhibited amine stretching at 3378cm^{-1} , with amine bending at 1617cm^{-1} . C-H peaks were recorded at 2919cm^{-1} , 2851cm^{-1} and 1466cm^{-1} .

increased absorbance of C-N stretch vibrations at 1177cm^{-1} and 1176cm^{-1} for Qpa2.5 and Qpa5 respectively may be due to methylation of nitrogen and increased abundance of C-N bonds, Snyman et al found a similar increase in absorption when working with quaternised chitosan (9).

The new peaks around 960 cm^{-1} in the quaternised polymers were attributed to the quaternary nitrogen, similar peaks have been recorded in the literature, in the case of quaternised derivatives of methacrylate co-polymers (10), poly(vinyl alcohol) (11), and poly(ethyleneimine) (12, 13).

Another new signal at 1518cm^{-1} in both quaternised polymers may also have some association with quaternary ammonium and electrostatic interaction, and will therefore be discussed further in chapter 3. Quaternisation also led to the disappearance of amide bands and the return of amine bending vibrations (1591cm^{-1} in PAA) at 1615cm^{-1} , the cause of this is unknown.

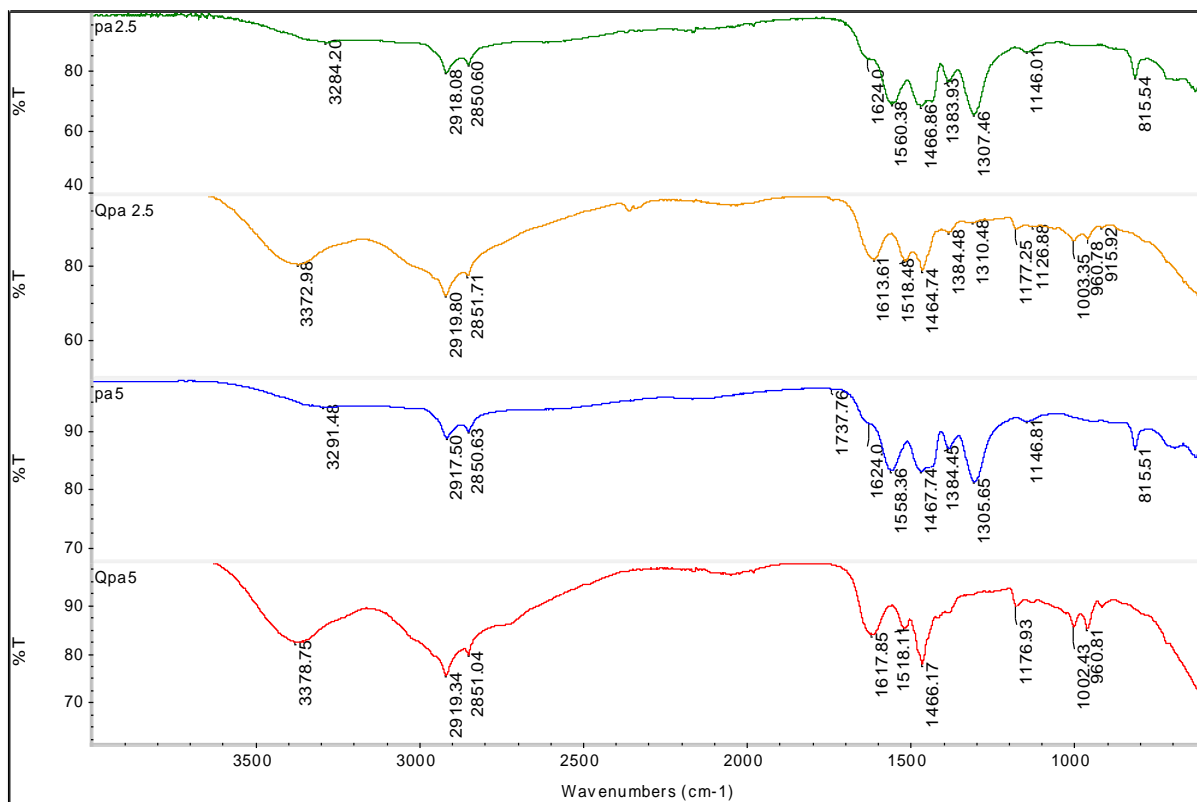


Figure 2.8 IR spectra of pa2.5, pa5, Qpa2.5 and Qpa5.

2.4.3. Thermal analysis

PAA showed a series of endotherms beginning at 141°C (Figure 2.9). This differs from results obtained by Thompson et al who found a sharp peak at 220°C that was attributed to melting (1). This may be caused by differences in molecular weight of synthesised polymers, arising from the dialysis process. Lower molecular weights result in lower melting points (14), therefore if the dialysis process resulted in a large population of low molecular weight fractions, it may explain the variation between these results and those of Thompson et al.

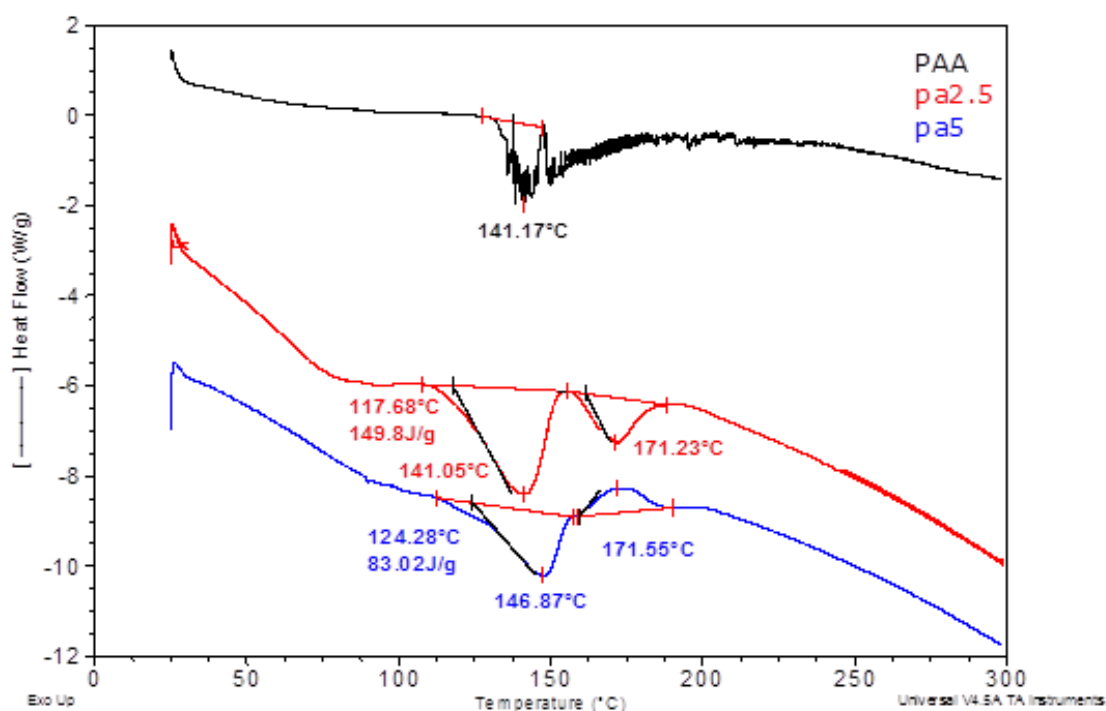


Figure 2.9 DSC thermograms of PAA and amphiphilic derivatives.

According to hot stage microscopy (Figure 2.10), melting appeared to begin at 90°C, while 245°C was the point at which sample discolouration began. Discolouration was expected to represent polymer decomposition, but data from TGA shows only a small reduction in weight from baseline to 300°C (Figure 2.11). This could represent sample dehydration, although when coupled with hot-stage images and the failure of PAA samples to return to baseline state on cooling, or exhibit the same DSC peaks on reheating (Figure 2.11), it appears that some type of irreversible degradation may have taken place.

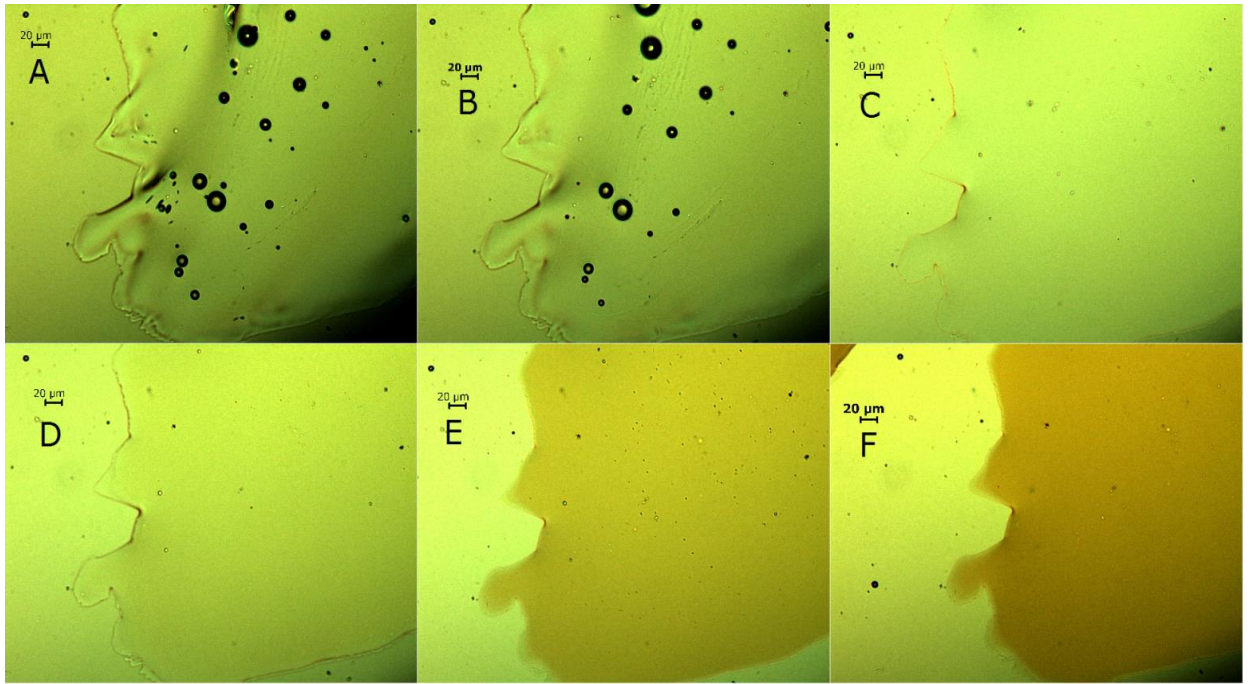


Figure 2.10 Hot-stage images of PAA at magnification x20. (A) Room temperature (B) 90°C (C) 155°C (D) 245°C (E) 300°C (F) Cooled to room temperature.

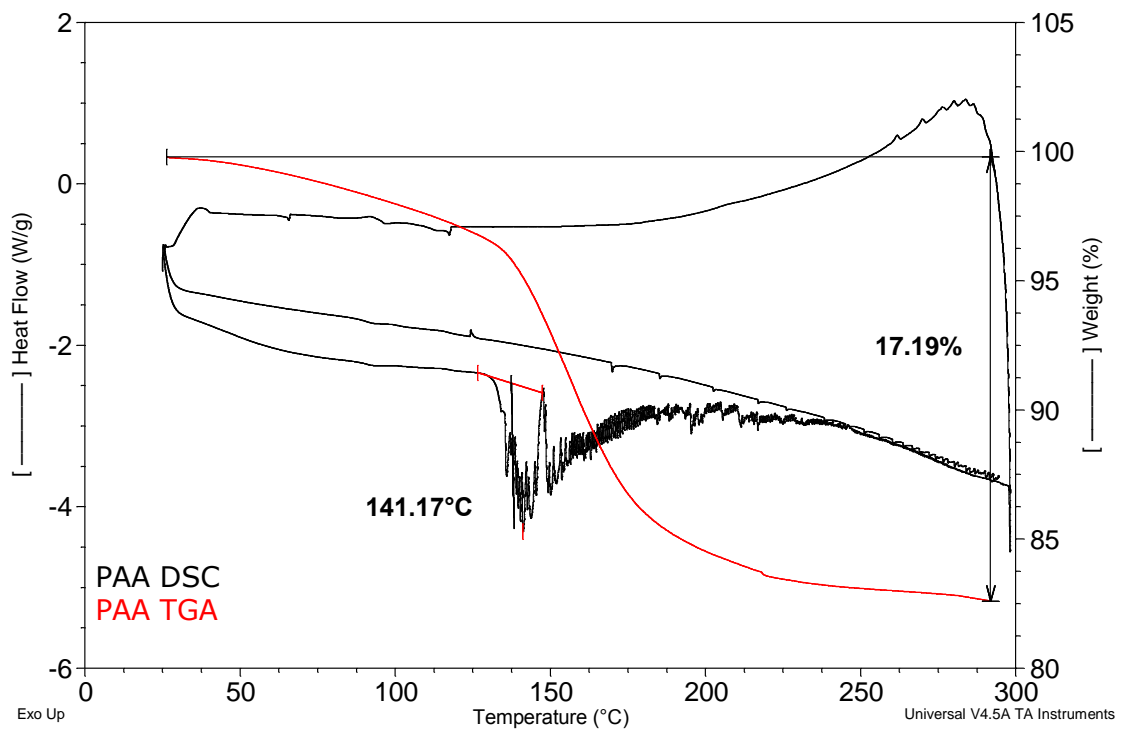


Figure 2.11 Heat/cool/reheat DSC thermogram and TGA for PAA.

The thermogram of pa2.5 showed an endothermic event at 141°C, followed by another endotherm at 171°C. When coupled with hot-stage images (Figure 2.12), a measure of correlation can be seen. Images appeared to show the polymer melting at approximately 100°C, by 155°C the thermal process appeared to be complete, this is in agreement with the wide DSC endotherm at 141°C. The widening of endotherms in comparison to PAA could be due to a less ordered crystalline structure with the addition of hydrophobic grafts, leading to a softening or melting over a relatively wide temperature range. This can be expected, as the addition of palmitic acid carbon chains will have hindered the ability of PAA to stack in an orderly crystalline arrangement, a similar reduction in crystallinity on addition of hydrophobic grafts can be seen in other polymers; such as lactide grafted chitosan (15).

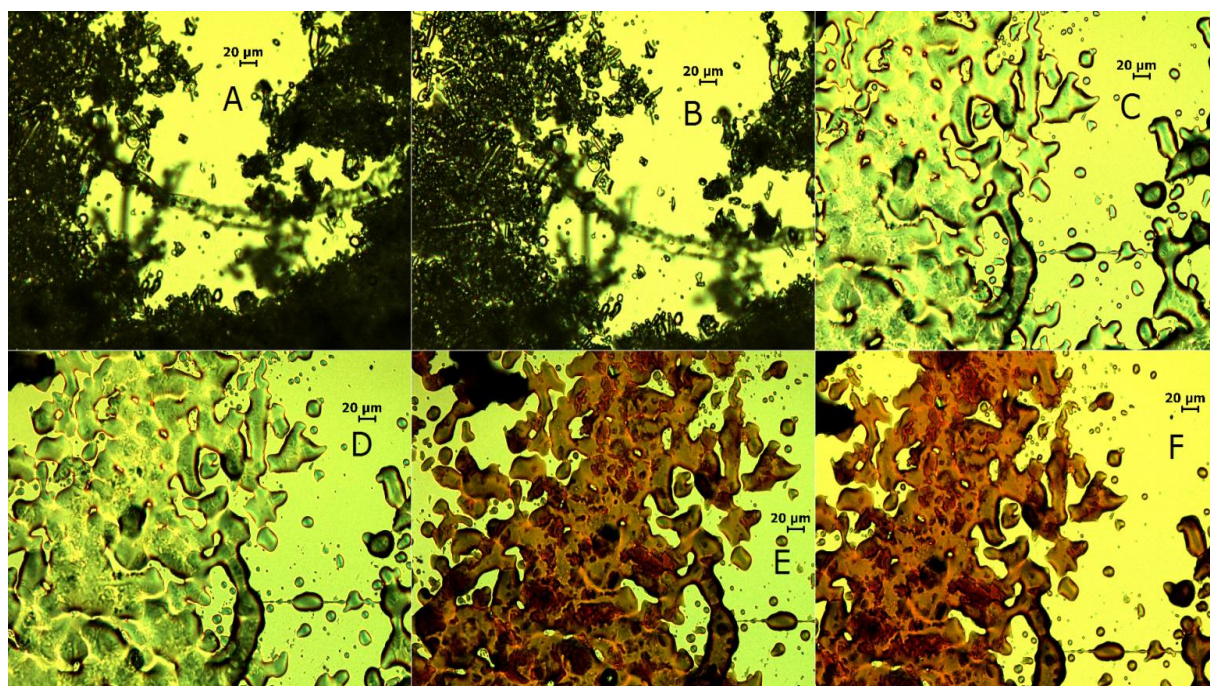


Figure 2.12 Hot-stage images of pa2.5 at magnification x20. (A) Room temperature (B) 100°C (C) 150°C (D) 200°C (E) 300°C (F) Cooled to room temperature.

The second endotherm at 171°C also shows a widening effect. Although, there was no clear correlation with hot-stage images at the same temperature, with no observable change evident until approximately 210°C at which point discolouration of the polymer began, continuing up to 300°C. There may have been a secondary melt/form of crystals that went undetected by hot-stage microscopy. The second

endotherm may also have been due to some type of polymer degradation occurring prior to the observed discolouration at 210°C.

TGA data shows approximately 33% reduction in weight up to 300°C (Figure 2.13), this is approximately double that of PAA. Furthermore, pa2.5 did not revert to original condition on cooling, or show similar DSC peaks during reheating. There appeared to be a permanent change in polymer structure in a result similar to PAA.

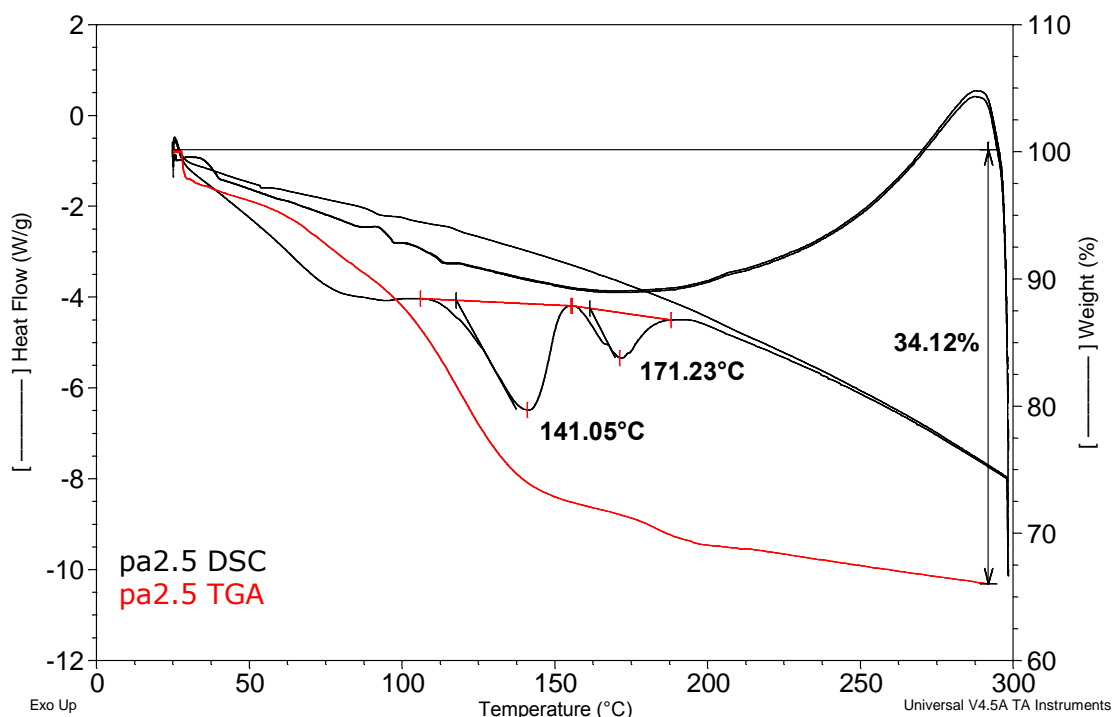


Figure 2.13 Heat/cool/reheat DSC thermogram and TGA for pa2.5.

Results for pa5 showed a wide endotherm at 146°C, attributed to polymer melting, followed by an exotherm at 171°C. On examination by hot stage microscopy (Figure 2.14); pa5 can be seen to begin melting at approximately 100°C, by 140°C the process appears to be complete. This shows some similarity to the wide DSC peak at 146°C (Figure 2.9), as well as having a resemblance to the initial endotherm of pa2.5, which was to be expected, as the difference in hydrophobic grafting is small and the compounds were expected to show relatively similar results.

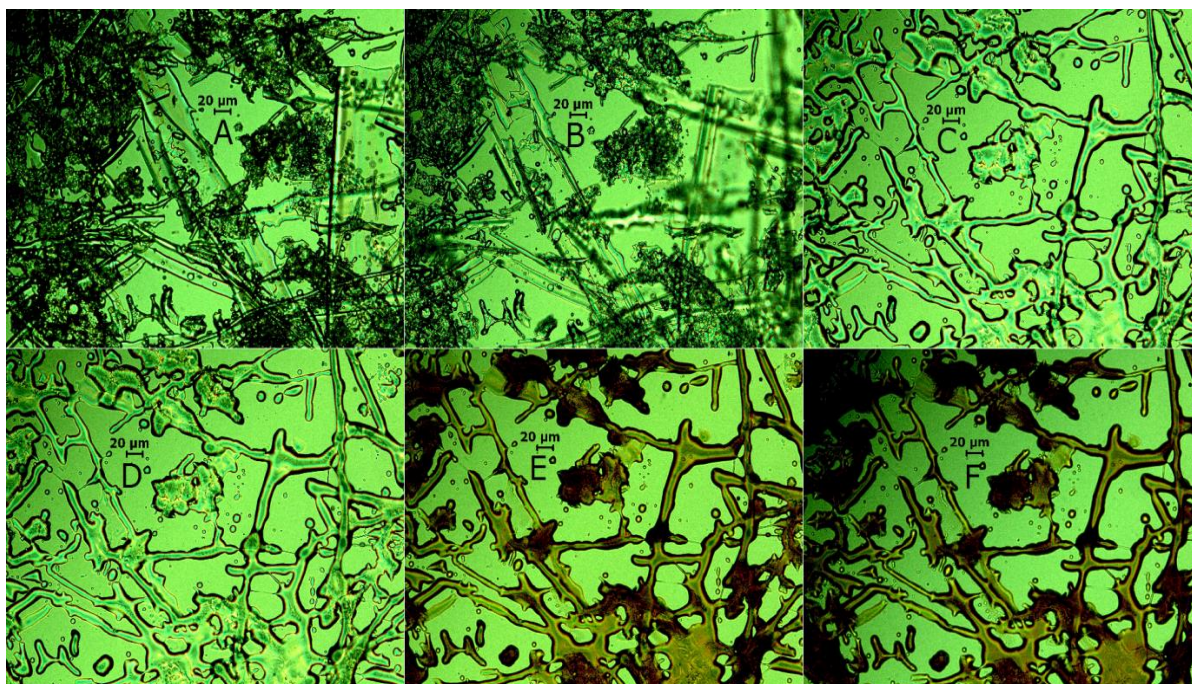


Figure 2.14 Hot-stage images of pa5 at magnification x20. (A) Room temperature (B) 100°C (C) 140°C (D) 210°C (E) 300°C (F) Cooled to room temperature.

Discolouration of the sample began at approximately 200°C, similarly to pa2.5. Data from TGA (Figure 2.15) showed a 35% weight loss measured by 300°C, with DSC cooling and reheating thermograms showing that the polymer did not undergo the same thermal events as the first heating cycle, in a result similar to that of pa2.5, as well as the parent molecule PAA.

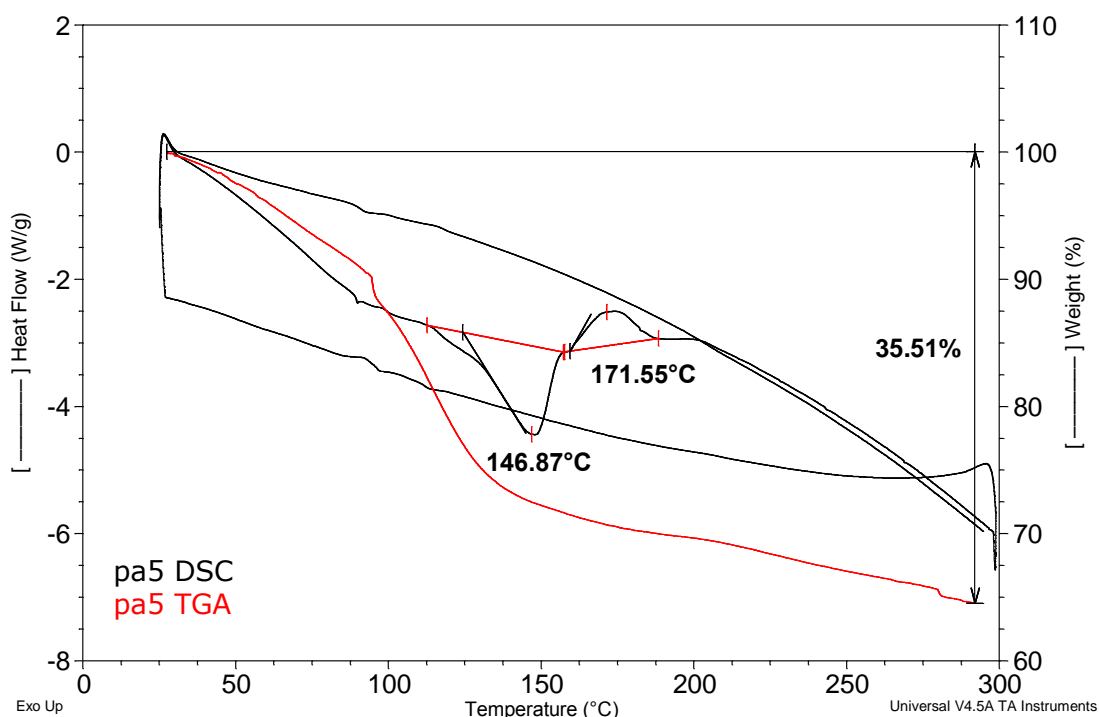


Figure 2.15 Heat/cool/reheat DSC thermogram and TGA for pa5.

The DSC thermogram of pa2.5 presented with two successive endotherms, whereas pa5 showed an endotherm quickly followed by an exotherm. When supplemented with data from hot-stage microscopy and TGA, it appeared that both pa2.5 and pa5 underwent melting followed closely by degradation.

The area under the curve of the first endotherm of pa5 (83.02J/g) was found to be less than that found for the first endotherm of pa2.5 (149.8J/g). This was seen as an indication that pa5 was perhaps less crystalline than pa2.5 which was in turn less crystalline than PAA. When viewed in conjunction with other results, this further supports the successful synthesis of PEs with slight differences in hydrophobic grafting.

Quaternisation of amphiphilic polymers led to a substantial change in DSC thermograms. As shown in figure 2.16, Qpa2.5 failed to exhibit clear thermograms at similar temperatures to those of pa2.5.

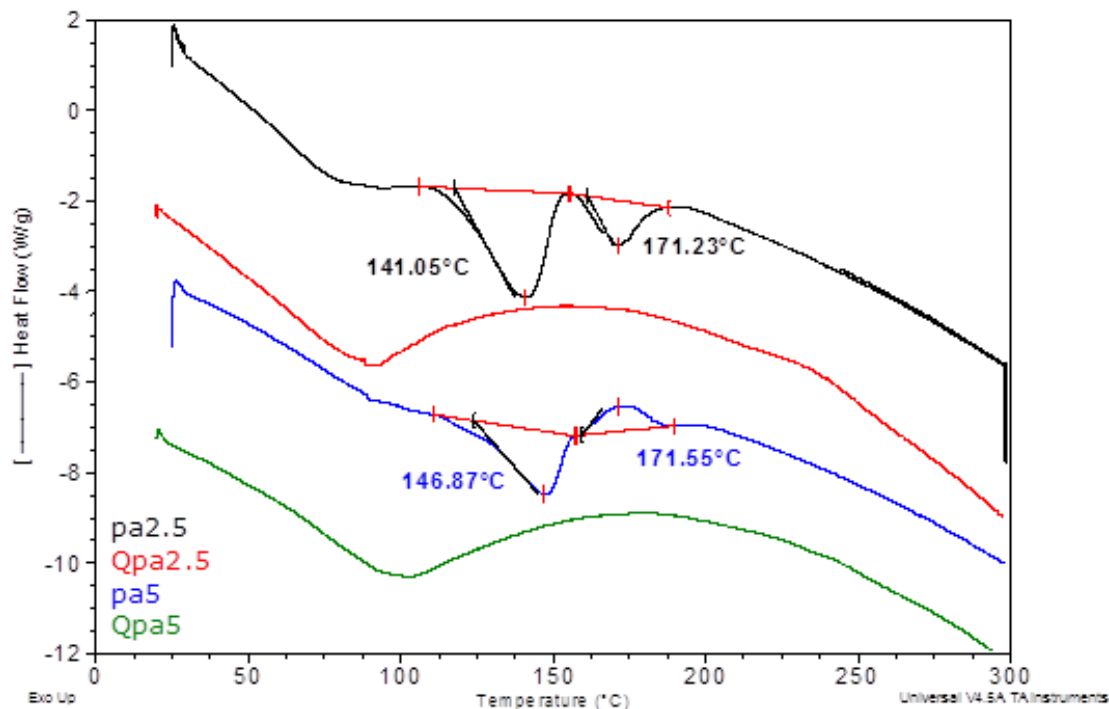


Figure 2.16 DSC thermograms of pa2.5, pa5, Qpa2.5 and Qpa5.

A similar result was found with Qpa5. Both quaternised polymers showed a wide signal around 100°C that was attributed to evaporation of bound water.

On investigation under hot-stage microscopy (Figure 2.17), Qpa2.5 appeared to contract at approximately 200°C. Discolouration began at 255°C and continued up to 300°C. Upon cooling the sample did not return to its original state.

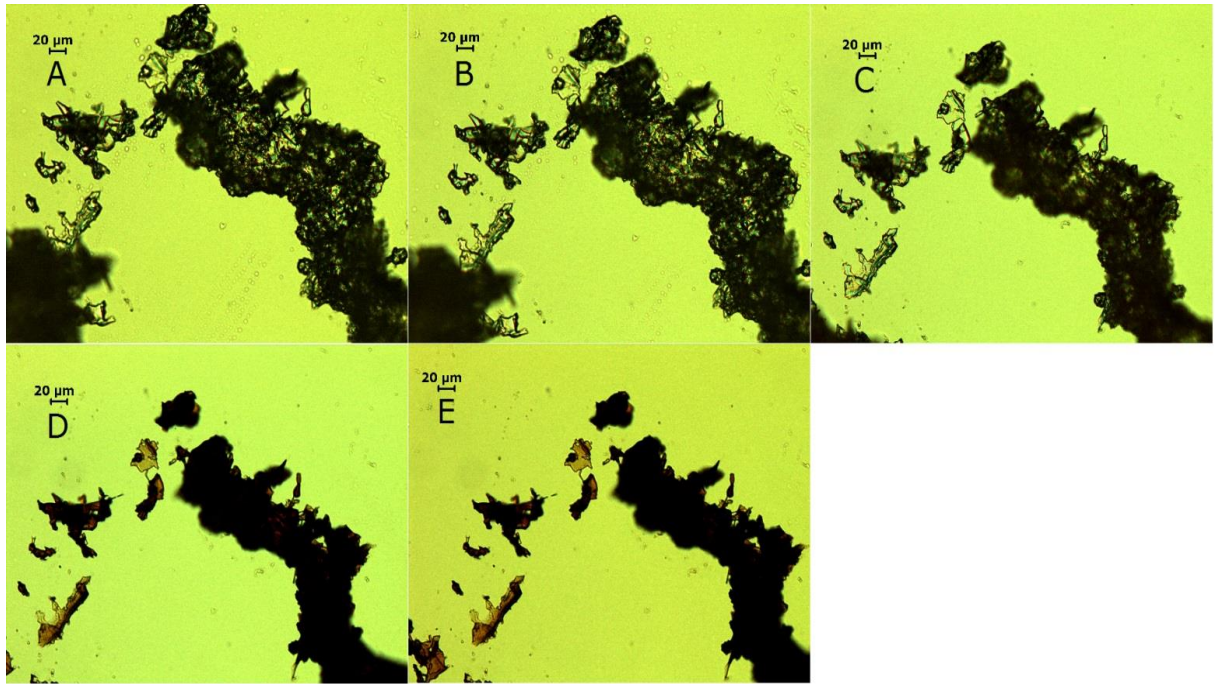


Figure 2.17 Hot-stage images of Qpa2.5 at magnification x20. (A) Room temperature (B) 100°C (C) 225°C (D) 300°C (E) Cooled to room temperature.

In the case of Qpa5 (Figure 2.18), contraction began at approximately 220°C, while discolouration became evident at 240°C. The process again appeared to be irreversible as the sample failed to return to original state upon cooling.

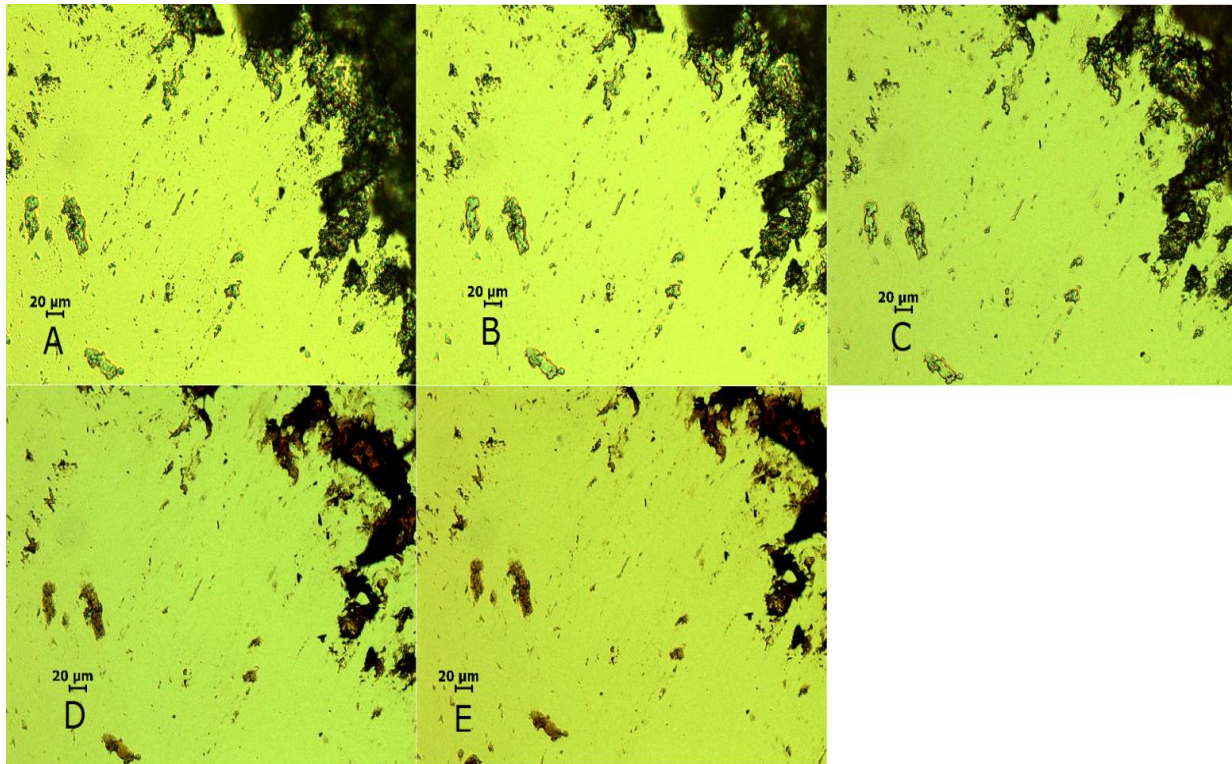


Figure 2.18 Hot-stage images of Qpa5 at x20 magnification. (A) Room temperature (B) 100°C (C) 230°C (D) 300°C (E) Cooled to room temperature.

Both Qpa2.5 and Qpa5 showed no signs of melting at temperatures similar to those of non-quaternised samples, or indeed over the temperature range measured. Quaternisation appeared to have further hindered the crystalline nature of PAA, leading to increased amorphous characteristics, principally the loss of a distinct melting point or melting range.

In general, the thermal analysis of synthesised polymers showed a trend of increasing amorphous character following hydrophobic grafting and quaternisation. This was to be expected, as both processes introduce bulk to the polymers and likely interfered with chain packing leading to reduced crystallinity (1, 15).

2.5. Conclusion

The purpose of this chapter was to investigate the synthesis of polymers used in this study.

From results of elemental analysis and NMR, it was seen that the structure of PAA underwent alteration; this change was attributed to the addition of palmitic acid grafts.

In order to investigate the result of quaternisation; NMR was used qualitatively alongside elemental analysis.

Polymers investigated using TGA showed a degree of weight loss over the measured temperature range. The amount of weight loss was not sufficiently large as to be attributed to complete decomposition. Therefore it was assumed that what took place was an initial loss of adsorbed water, followed by the loss of structural water and some form of polymer degradation, such as random or side group scission (16).

The polymers discussed in this chapter were used in combination with sodium alginate to synthesise polyelectrolyte complexes, the results of these combinations will be covered in chapter 3.

References

1. C. Thompson, C. Ding, X. Qu, Z Yang, I. Uchegbu, L. Tetley, W. Cheng. The effect of polymer architecture on the nano self-assemblies based on novel comb-shaped amphiphilic poly(allylamine). *Colloid polymer science* 286 (2008) 1511-1526.
2. W. Wang, L. Tetley, I. Uchegbu. A New Class of Amphiphilic Poly-L-lysine Based Polymers Forms Nanoparticles on Probe Sonication in Aqueous Media. *Langmuir* 16 (2000) 7859-7866.
3. W. Wang, X. Qu, A. Gray, L. Tetley, I. Uchegbu. Self-Assembly of Cetyl Linear Polyethylenimine To Give Micelles, Vesicles, and Dense Nanoparticles. *Macromolecules* 37 (2004) 9114-9122.
4. Y. Wan, B. Peppley, K. Creber, V. Tam Bui, E. Halliop. Quaternized-chitosan membranes for possible applications in alkaline fuel cells. *Journal of power sources* 185 (2008) 183-187.
5. L. Fan, M. Cao, S. Gao, W. Wang, K. Peng, C. Tan, F. Wen, S. Tao, W. Xie. Preparation and characterization of a quaternary ammonium derivative of pectin. *Carbohydrate polymers* 88 (2012) 707-712.
6. L. Ye, L. Zhai, J. Fang, J. Liu, C. Li, R. Guan. Synthesis and characterization of novel cross-linked quaternized poly(vinyl alcohol) membranes based on morpholine for anion exchange membranes. *Solid state ionics* 240 (2013) 1-9.
7. Y. Frère, P. Gramain. Reaction Kinetics of Polymer Substituents. Macromolecular Steric Hindrance Effect in Quaternization of Poly(vinylpyridines). *Macromolecules* 25 (1992) 3184-3189.
8. G. Jiang, D. Quan, K. Liao, H. Wang. Preparation of polymeric micelles based on chitosan bearing a small amount of highly hydrophobic groups. *Carbohydrate polymers* 66 (2006) 514-520.
9. D. Snyman, T. Govender, A. F. Kotze'. Low molecular weight quaternised chitosan (I): synthesis and characterisation. *Pharmazie* 58 (2003) 705-708.
10. R. Moustafine, A. Bodrov, V. Kemenova, P. Rombaut, G. Van den Mooter. Drug release modification by interpolymer interaction between countercharged types of Eudragit® RL 30D and FS 30D in double-layer films. *International journal of pharmaceutics* 439 (2012) 17-21.

- 11.Y. Xiong, J. Fang, Q. Zeng, Q. Liu. Preparation and characterization of cross-linked quaternized poly(vinyl alcohol) membranes for anion exchange membrane fuel cells. *Journal of Membrane Science* 311 (2008) 319–325.
- 12.I. Yudovin-Farber, J. Golenser, N. Beyth, E. Weiss, A. Domb. Quaternary Ammonium Polyethyleneimine: Antibacterial Activity. *Journal of nanomaterial* 2010 (2010) 1-11.
- 13.N. Beyth, I. Yudovin-Farber, R. Bahir, A. Domb, E. Weiss. Antibacterial activity of dental composites containing quaternary ammonium polyethylenimine nanoparticles against *Streptococcus mutans*. *Biomaterials* 27 (2006) 3995–4002.
- 14.J. Fatou, L. Mandelkern. The Effect of Molecular Weight on the Melting Temperature and fusion of polyethylene. *The Journal of Physical Chemistry* 69 (1965) 417-428.
- 15.G. Luckachan, C. Pillai. Chitosan/oligo L-lactide graft copolymers: Effect of hydrophobic side chains on the physico-chemical properties and biodegradability. *Carbohydrate Polymers* 64 (2006) 254–266.
- 16.L. Manring. Thermal degradation of Poly(methyl methacrylate). 4. Random Side-Group Scission. *Macromolecules* 24 (1991) 3304-3309.

3. Polyelectrolyte complex formation

This chapter focuses on the investigation of the different ratios of poly(allylamine) derivatives and sodium alginate used in the formulation of polyelectrolyte complexes (PECs).

Characterisation and analysis of resulting PECs was used to assist in the selection of the most stable and reproducible combinations. These would then be investigated further with regard to their interaction with insulin, discussed in chapter 4.

Analytical techniques used include dynamic light scattering, which was used to estimate the average particle size of complexes in suspension, as well as the average polydispersity index.

UV-visible spectroscopy together with a visual inspection was used to assess colloidal stability of PECs.

Infra-red and thermal analysis were used to interpret the effect of the electrostatic interaction between the polyelectrolytes (PEs) in the solid state.

3.1 Materials

Sodium alginate (Mw= 120000-190000Da) (Sigma-Aldrich, UK), sodium hydroxide, and hydrochloric acid buffers were sourced from fisher scientific, UK. Synthesised polymers used in polyelectrolyte complex formation include pa2.5, pa5, Qpa2.5, Qpa5.

3.2 Polyelectrolyte complex formation

Polyelectrolyte complex formulation was based on the work of Sarmento et al (1); with a view to preparing the following complexes: alg/pa2.5, alg/pa5, alg/Qpa2.5, and alg/Qpa5 at a number of ratios.

Initially, samples of cationic PEs pa2.5, pa5, Qpa2.5, Qpa5, or anionic sodium alginate were dissolved in distilled water 10mL (all at 0.1% w/v). Sonication for 5 minutes at 20kHz was necessary in the preparation of solutions of cationic PEs. The oppositely charged PEs were then prepared at a concentration corresponding to table 3.1.

Table 3.1 Mass ratios used in the formation of polyelectrolyte complexes, and concentrations of constituent polyelectrolyte solutions.

	Sodium alginate (alg) solution	Cationic polyelectrolyte (PE ⁺) ^{**} solution
*alg/PE ⁺ 4.3:1	0.1% w/v	0.0232% w/v
alg/PE ⁺ 3:1	0.1% w/v	0.0333% w/v
alg/PE ⁺ 1:3	0.0333% w/v	0.1% w/v
*alg/PE ⁺ 1:4.3	0.0232% w/v	0.1% w/v

* The mass ratios of 4.3:1 and 1:4.3 were not prepared for quaternised polyelectrolytes.

** Cationic PEs included pa5, pa2.5, Qpa5 and Qpa2.5.

The alginate and amphiphilic PE solutions were then adjusted using 1M hydrochloric acid and/or sodium hydroxide, to pH 4.9 and 4.6, respectively, in order to achieve ionisation of component PEs. Solutions were then combined by drop-wise addition of the lower concentration PE solution from a burette into the PE solution of higher concentration over 5 minutes, under gentle magnetic stirring. Resulting solutions were characterised in the liquid state or after lyophilisation for 24 hours using a freeze drier (VirTis advantage, Biopharma Process Systems, UK).

3.3 Polyelectrolyte complex characterisation

3.3.1 Dynamic light scattering

Samples of alg/pa2.5, alg/pa5 at mass ratios of 4.3:1, 3:1, 1:3, 1:4.3, and alg/Qpa2.5, alg/Qpa5 at ratios of 3:1 and 1:3, as well as cationic PE controls at equivalent concentrations were analysed for their average hydrodynamic diameter (Hdd), and polydispersity index (pdI) using a Nano ZS Zetasizer (Malvern instruments, UK). Samples were measured using plastic cuvettes, with a measurement temperature of 25°C at 0.25, 0.5, 1, 2, 24, and 48 hours after PEC formation (n=3).

3.3.2 Transmittance studies

As an indicator of colloidal stability, an UV-Vis spectrometer (Thermo scientific, UK) was used to investigate the average %Transmittance for solutions of PECs and equivalent PE controls at a wavelength of 570nm. A similar experiment was performed by Thompson et al. to provide evidence of complex formation and stability (2). Data was collected at time points of 0, 24, and 48 hours after PEC formation (n=3).

3.3.3 Zeta potential

Samples of alg/pa2.5 1:3 and alg/Qpa2.5 1:3, as well as pa2.5 and Qpa2.5 (concentrations equivalent to final concentration in PECs) were analysed using a Nano ZS Zetasizer (Malvern instruments, UK) in folded capillary plastic cuvettes at 25°C (n=1).

3.3.4 Infra-red analysis

Sample solutions of alg/pa2.5, alg/pa5, alg/Qpa2.5, and alg/Qpa5 at ratios of 3:1 and 1:3 were lyophilised using a freeze drier. With the resulting solid used to acquire a spectrum representing PECs. Data was obtained using a Thermo Nicolet IR spectrophotometer (Thermo Fisher Scientific, USA) with diamond tip accessory. Samples were measured at 32 scans per spectrum between 4000-500cm⁻¹. Analysis was performed using OMNIC software.

3.3.5 Thermal analysis

Lyophilised samples of alg/pa2.5, alg/pa5, alg/Qpa2.5, and alg/Qpa5 (1-5mg) were analysed by DSC over a temperature range of 0-300°C at 20°C/minute under nitrogen atmosphere. The instrument was pre-calibrated with an indium standard.

Hot-stage microscopy was used to assist in the investigation of thermal properties of PECs as well as ascertain any changes in thermal properties of individual polyelectrolytes compared to complexes. Samples of alg/pa2.5, alg/pa5, alg/Qpa2.5, and alg/Qpa5 were observed at 20x magnification from 20°C to 300°C heated at a rate of 5-10°C/minute. Images were captured using a LEICA DFC 420 digital microscope (LEIKA, Germany) coupled to the LINKAM LTS 350 hot-stage (Linkam scientific instruments, UK).

3.3.6 Transmission electron microscopy

Solutions of alg/pa2.5 1:3, alg/Qpa2.5 3:1 and alg/Qpa2.5 1:3 were freshly prepared and sent for transmission electron microscopy (TEM) at the electron microscopy research services facility at Newcastle University. Using a Philips CM100 TEM with compustage and high resolution digital image capture, a number of images were procured for each sample.

3.4 Results and Discussion

The use of ratios of 4.3:1, 3:1, 1:3 and 1:4.3 is based on work performed on chitosan and alginate (1). Other ratios such as 1:1 and 2:1 were attempted but were found to result in immediate precipitation, perhaps due to charge neutralisation.

3.4.1 Dynamic light scattering

Dynamic light scattering (DLS), also known as photon correlation spectroscopy is a light scattering technique capable of producing estimates of particle size in a timely and non-invasive manner. Particles in suspension or solution are subjected to a laser, whose light is then scattered. By analysing the intensity of scattered light, the velocity of Brownian motion can be found.

DLS can then be used to determine particle size by relating the diffusion coefficient (the Brownian motion of the measured particle in a specific environment) to hydrodynamic diameter according to the Stokes-Einstein equation (Equation 3.1) (3).

$$D = kT \div 3\pi\eta d$$

Equation 3.1 Stokes-Einstein equation.

Where D is the diffusion coefficient, k is the Boltzmann constant, T is the absolute temperature, η is the viscosity of the suspension liquid, and d is particle hydrodynamic diameter.

The polydispersity of particles in solution was also measured. Polydispersity indices show the distribution of size data acquired by DLS, with greater values indicating a wider distribution of particle sizes and a lack of uniformity.

Using this technique, a study of the different mass ratios of PEs used and the subsequent effect on the interaction between alginate and amphiphilic PEs towards the formation of PECs was carried out with regard to the average Hdd and average pdI.

The amphiphilic poly (allyl amine) derivatives synthesised in chapter 2, self-assemble into nanoaggregates at concentrations above their critical aggregation concentration (4). Furthermore, at the pH conditions used in PEC formation, the anionic carbonyl groups of sodium alginate were expected to interact electrostatically with the protonated and quaternary amines of amphiphilic PEs.

Additionally, Van der Waals forces and hydrophobic interactions were expected to have an effect (Figure 3.1). The combination of amphiphilic polymers based on poly(allyl amine) and alginate by the aforementioned forces was believed to be novel.

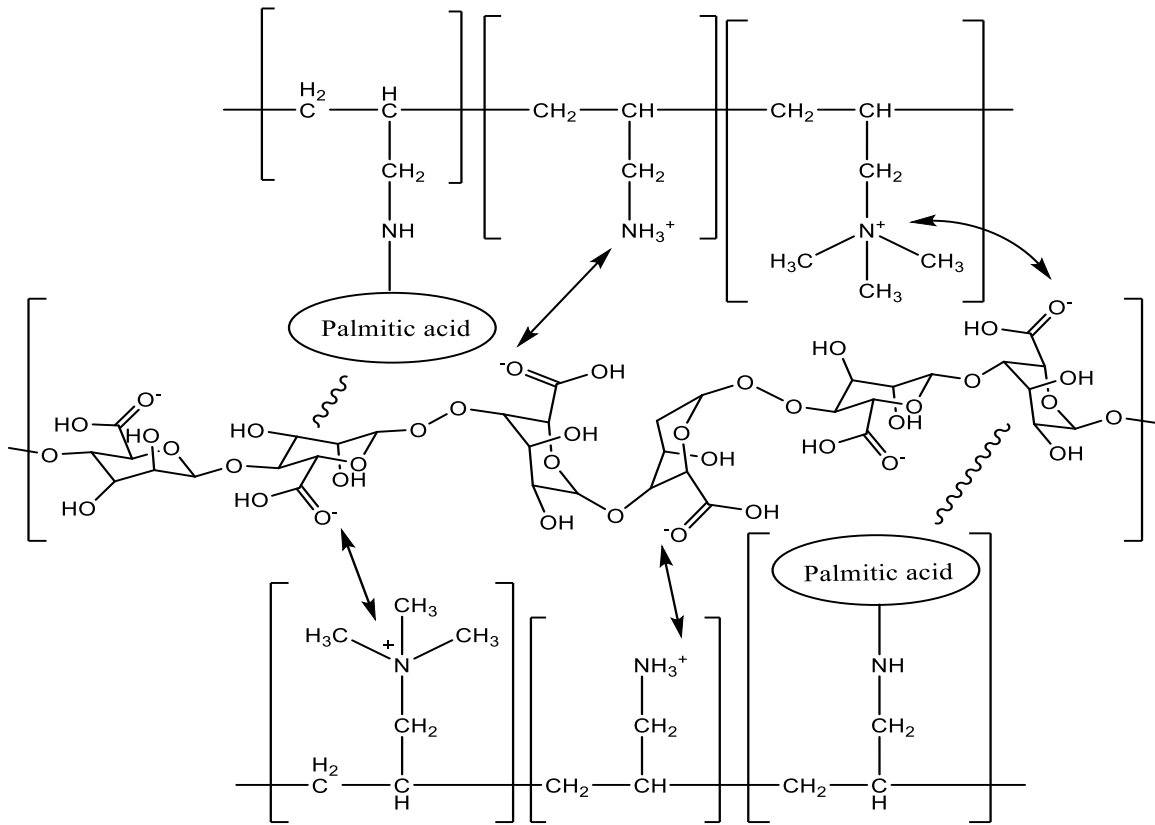


Figure 3.1 Proposed electrostatic interaction between sodium alginate and quaternised amphiphilic poly(allyl amine). The wavy bonds represent the hypothesised hydrophobic and Van der Waals forces between palmitic acid chains and alginate backbone.

Complexes of alg/pa5 4.3:1 were analysed by DLS and compared with the results of a pa5 control (with a concentration equivalent to pa5 in complex). Results showed a reduction in Hdd and pdI for the complex compared to the pa5 alone (Figure 3.2).

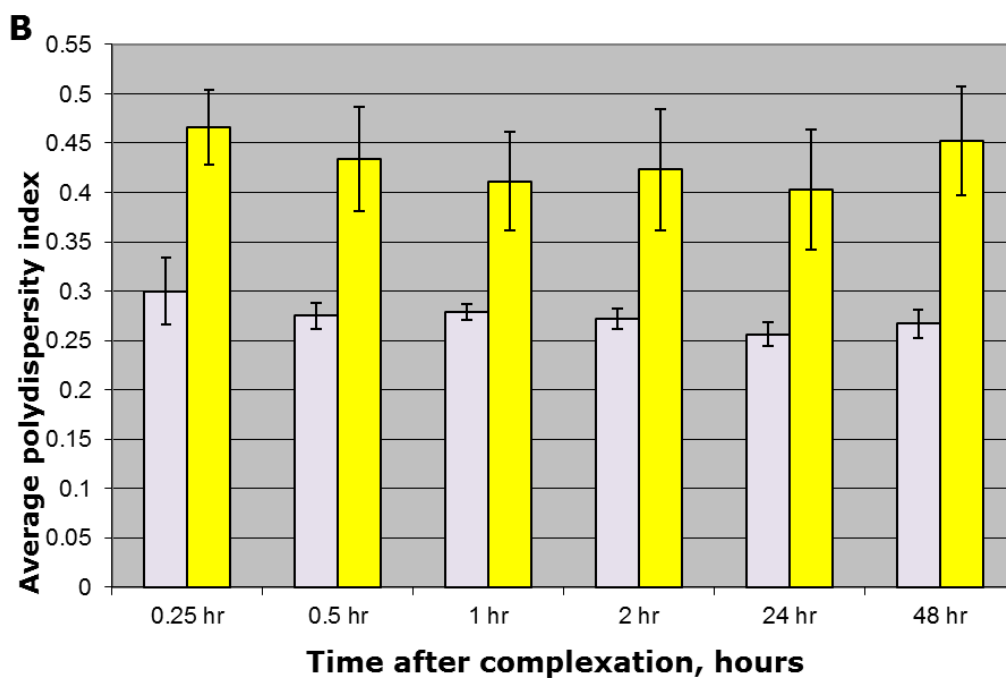
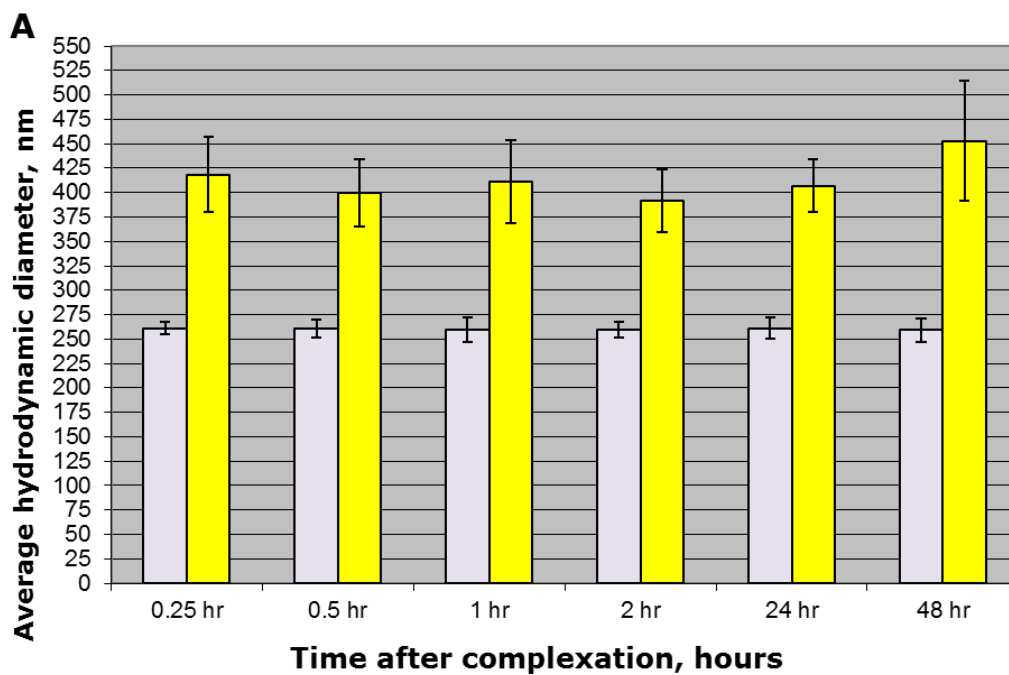


Figure 3.2 Results of DLS for alg/pa5 4.3:1 and pa5 0.116mg/ml. (A) Comparison of average hydrodynamic diameter (B) Comparison of average polydispersity index. alg/pa5 4.3:1 pa5 0.116mg/ml (Mean \pm SD, n=3).

Similar results can be seen with alg/pa5 3:1 relative to a pa5 control (figure 3.3).

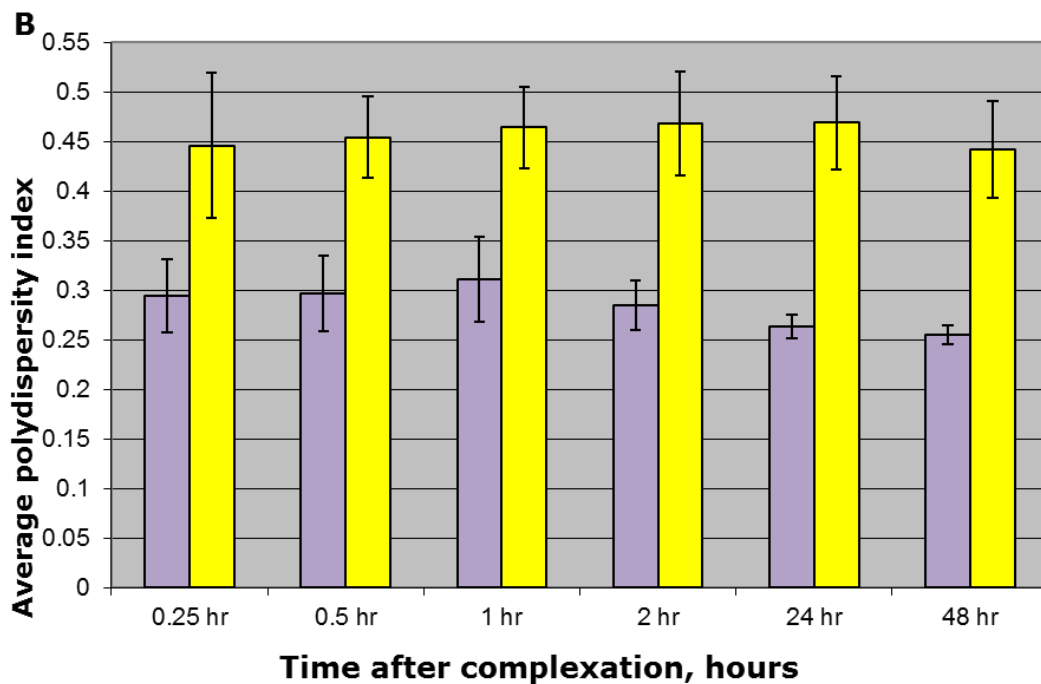
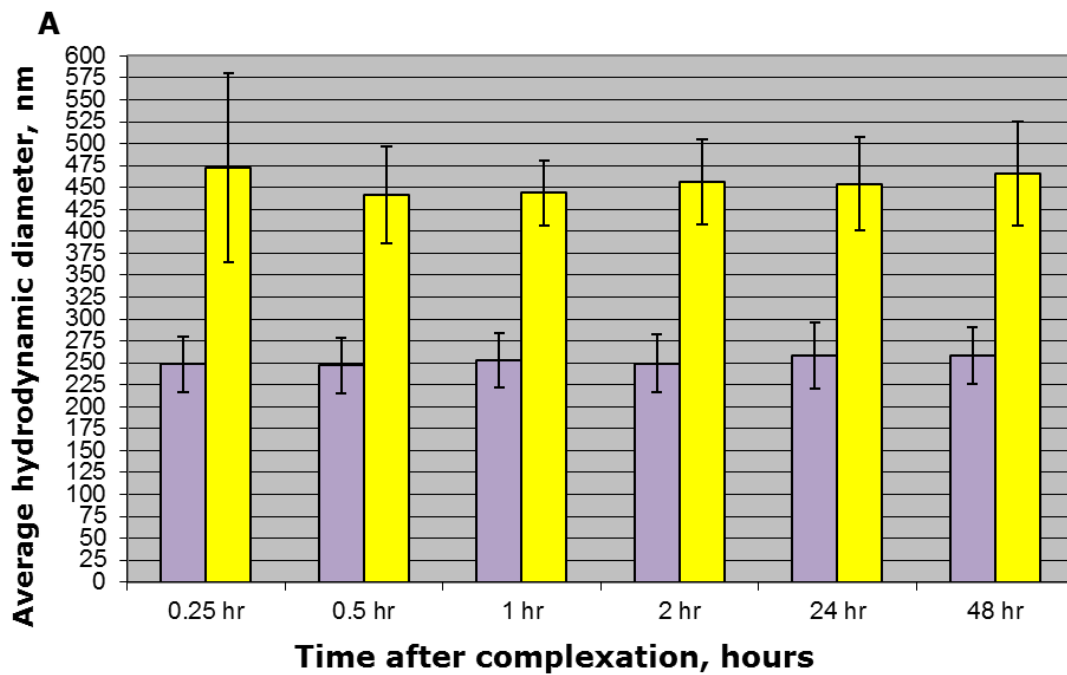


Figure 3.3 Results of DLS for alg/pa5 3:1 and pa5 0.166mg/ml. (A) Comparison of average hydrodynamic diameter (B) Comparison of average polydispersity index. alg/pa5 3:1 pa5 0.166mg/mL (Mean \pm SD, n=3).

Whereas alg/pa5 1:3 and 1:4.3 (0.5mg/mL pa5 control for both) resulted in a reduced Hdd and increased pdI (Figure 3.4).

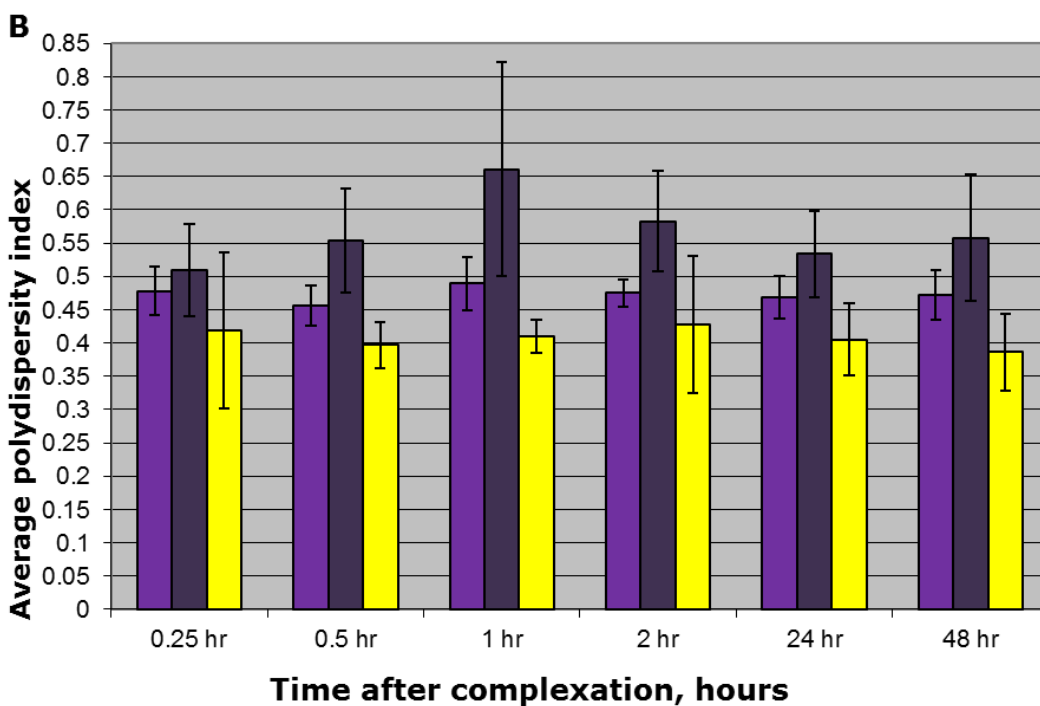
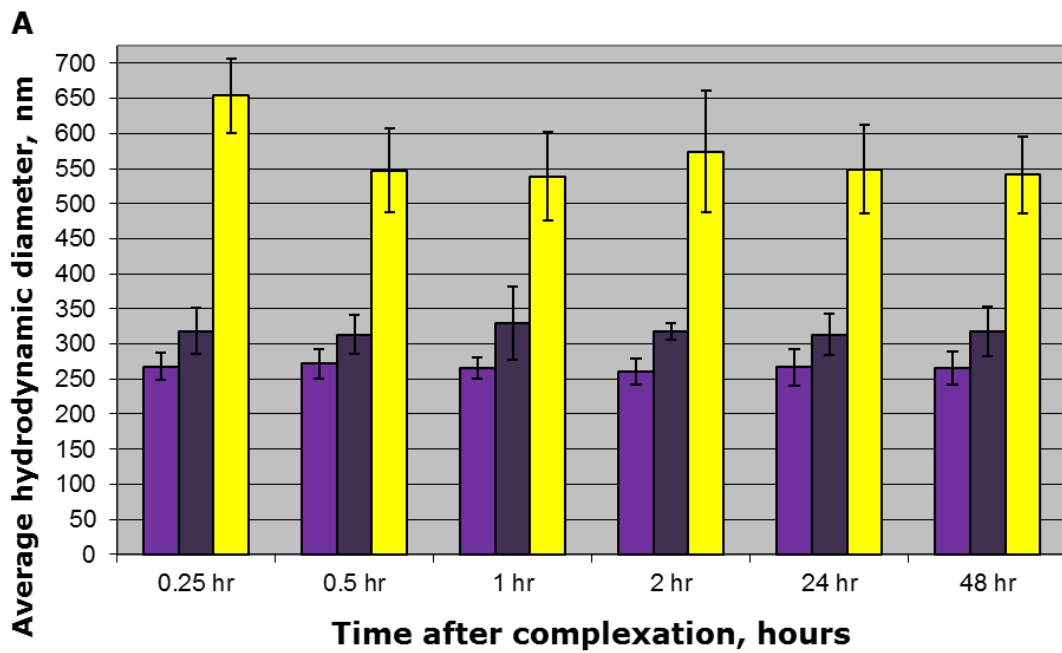
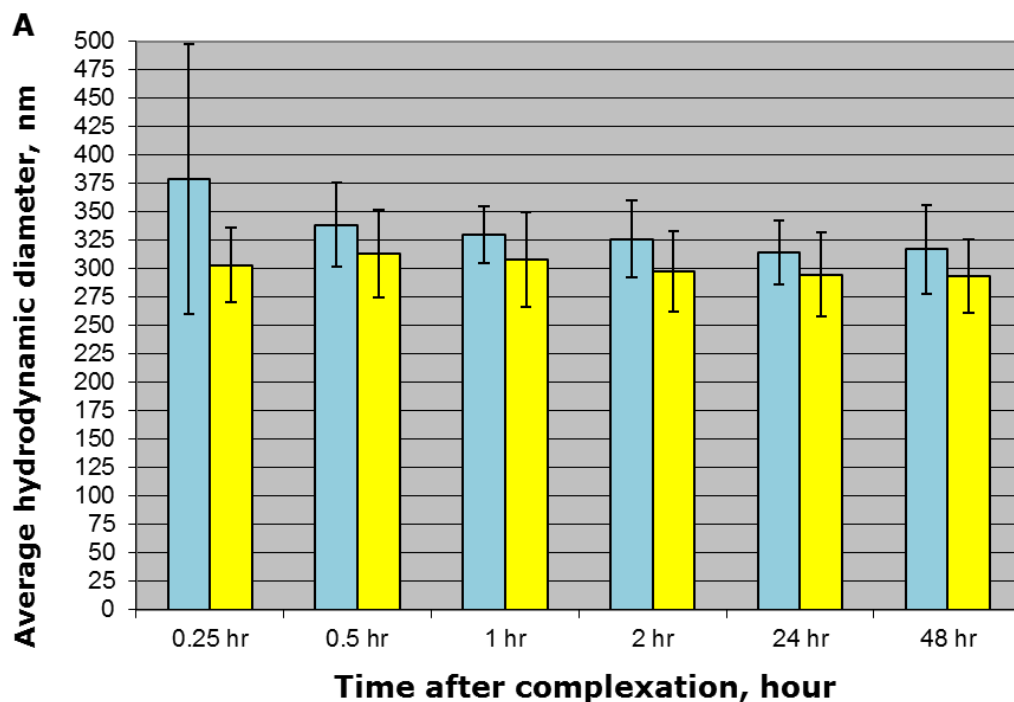


Figure 3.4 Results of DLS for alg/pa5 1:3, 1:4.3 and pa5 0.5mg/ml. (A) Comparison of average hydrodynamic diameter (B) Comparison of average polydispersity index. ■ alg/pa5 1:3 ■ alg/pa5 1:4.3 ■ pa5 0.5mg/mL (Mean \pm SD, n=3).

From the figures above, it appeared that the interaction between pa5 and alginate led to the formation of nano-sized aggregates with reduced Hdd in all ratios investigated, while results seemed to be relatively stable over 48 hours.

It can be seen that regardless of the amount of alginate used in the experiment, the average Hdd of complexes was less than pa5 controls. However, the average pdI showed that the interaction between alginate and pa5 may have been different at each ratio. The average size was found to be in the range of 250-300nm for all pa5 complexes, but the distribution of size data was more disperse in the case of 1:3 and 1:4.3 (0.46-0.66) in comparison to 4.3:1 and 3:1 (0.25-0.31). This may be due to a number of factors, including differences in electrostatic interactions, hydrophobic interactions, as well as the order and rate of addition of PEs in the formation of PECs (5, 6).

Comparisons between complexes of pa2.5 complexes, and equivalent concentration pa2.5 controls produced different results to those found for pa5 complexes (Figures 3.5-3.7).



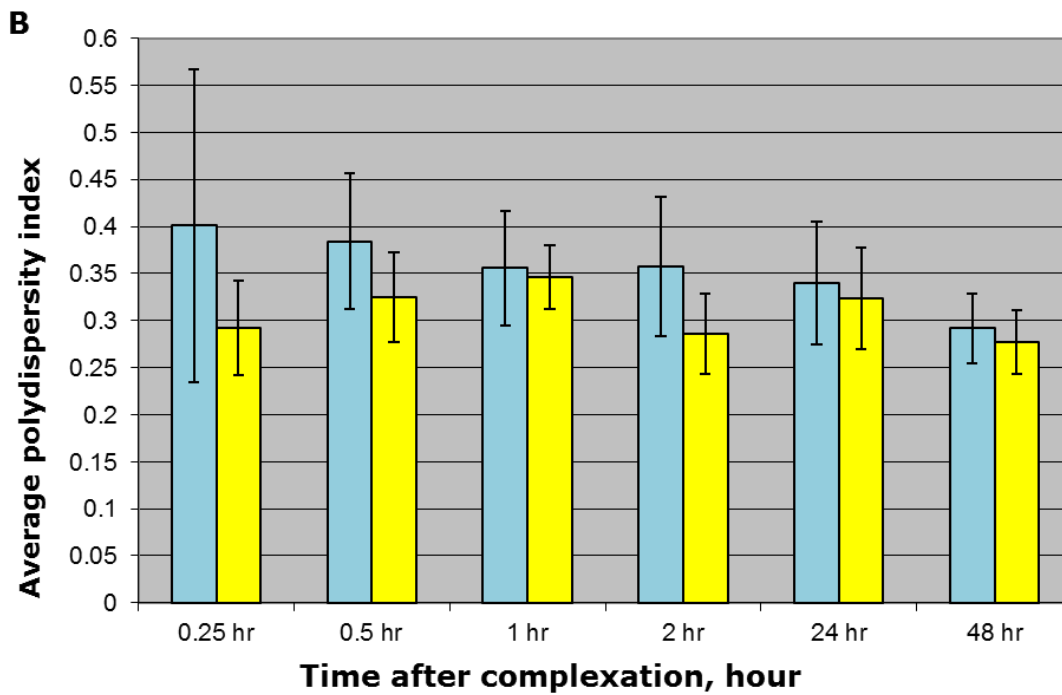
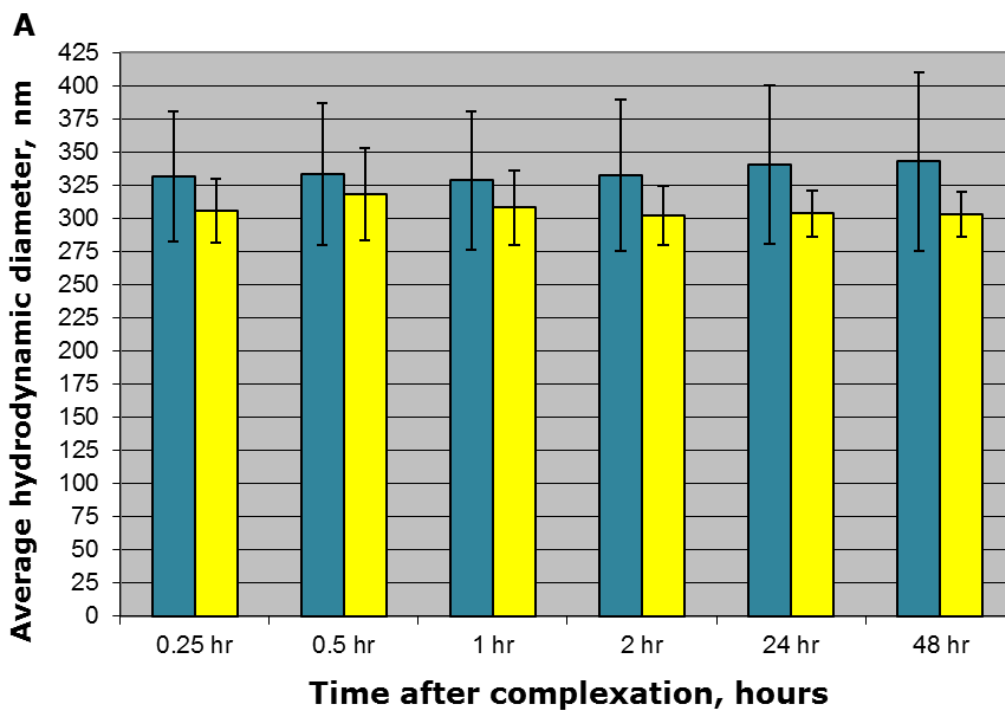


Figure 3.5 Results of DLS for alg/pa2.5 4.3:1 and pa2.5 0.116mg/mL. (A) Comparison of average hydrodynamic diameter (B) Comparison of average polydispersity index. ■ alg/pa2.5 4.3:1 ■ pa2.5 0.116mg/mL (Mean \pm SD, n=3).



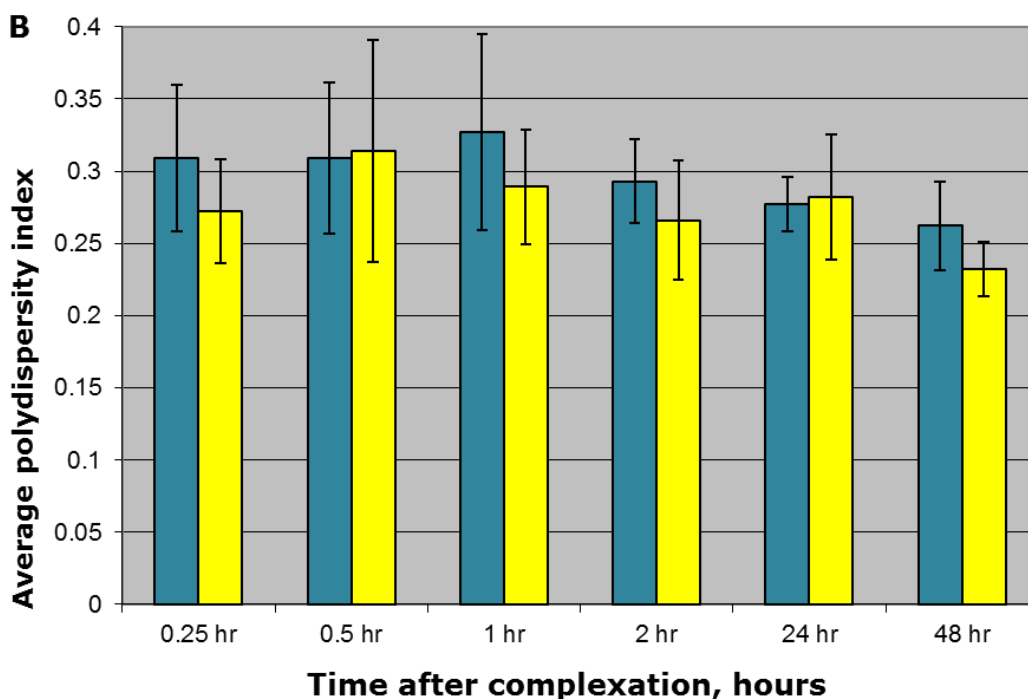
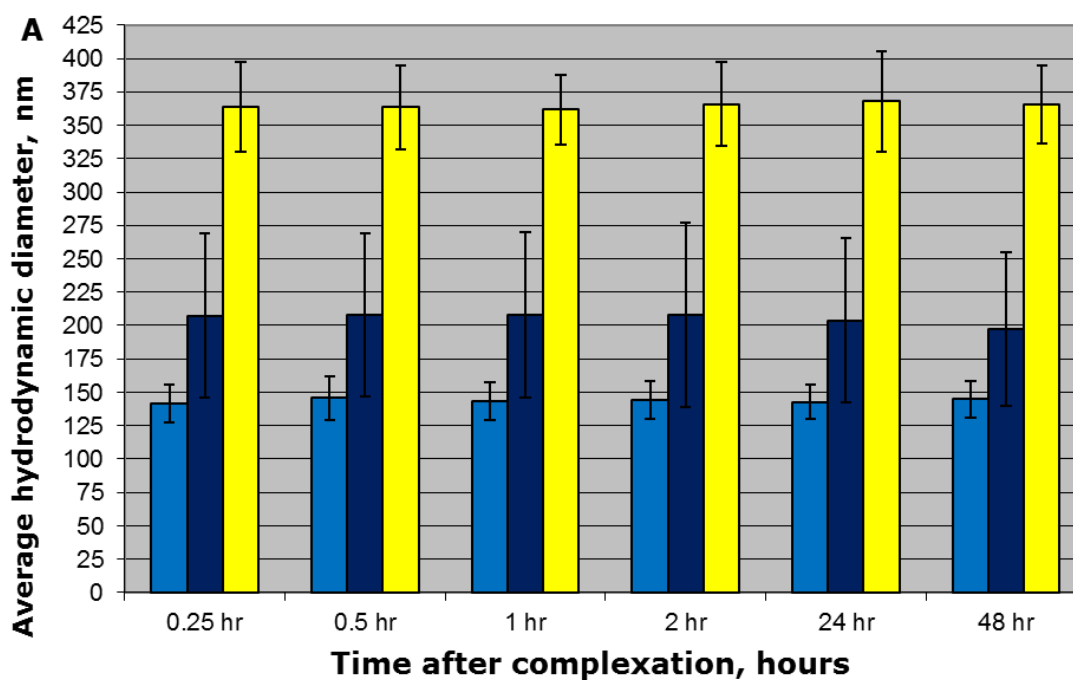


Figure 3.6 Results of DLS for alg/pa2.5 3:1 and pa2.5 0.166mg/mL. (A) Comparison of average hydrodynamic diameter (B) Comparison of average polydispersity index. ■ alg/pa2.5 3:1 ■ pa2.5 0.166mg/mL (Mean \pm SD, n=3).

In the case of alg/pa2.5 4.3:1 and 3:1 there appeared to be a relatively small increase in Hdd and pdI compared to pa2.5 control (Figures 3.5 and 3.6).



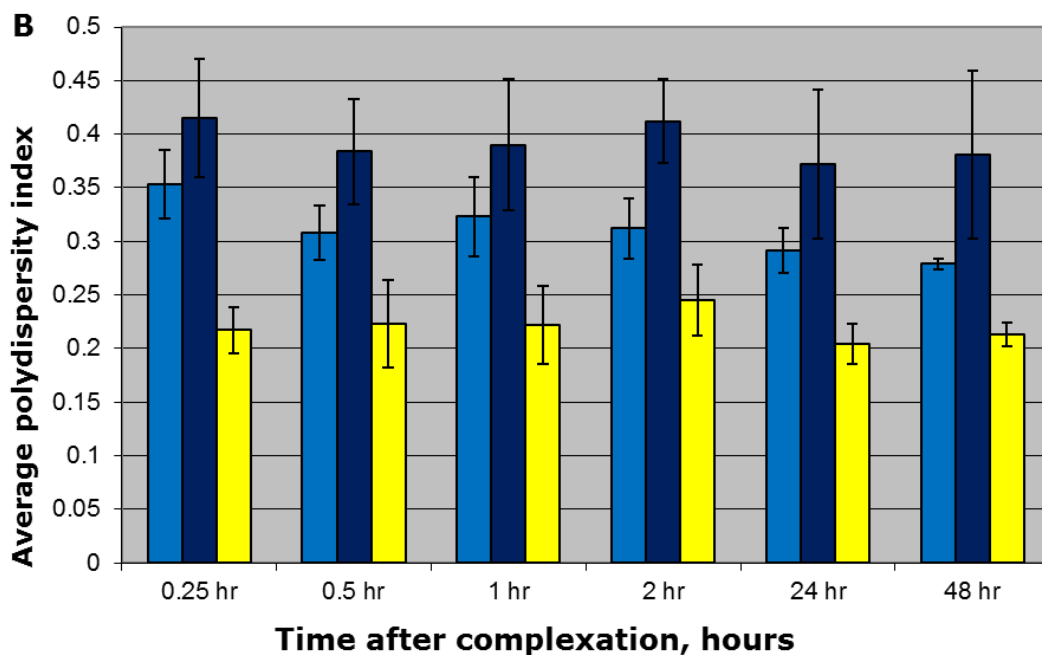


Figure 3.7 Results of DLS for alg/pa2.5 1:3, 1:4.3 and pa2.5 0.5mg/mL. (A) Comparison of average hydrodynamic diameter (B) Comparison of average polydispersity index. ■ alg/pa2.5 1:3 ■ alg/pa2.5 1:4.3 ■ pa2.5 0.5mg/mL (Mean \pm SD, n=3).

Complexes of alg/pa2.5 1:3 and 1:4.3 showed a reduction in Hdd and an increase in pdI compared to pa2.5 alone at equivalent concentrations (figure 3.7).

As with pa5, results for pa2.5 complexes were relatively stable over the 48 hour period of experimentation.

While alg/pa2.5 1:3 and 1:4.3 presented with similar trends in changes in pdI and Hdd compared to their controls as their equivalent pa5 complexes, this was not the case for alg/pa2.5 3:1 and 4.3:1 complexes and their equivalent pa5 complexes. It may be that the small difference in hydrophobic grafting between pa2.5 and pa5 had an effect on the interaction between amphiphilic PEs and alginate; which may be due to differences in Van der Waal forces, hydrophobic, and electrostatic interactions. Differences that may have arisen as a result of the increased number of free amines on pa2.5 compared to the more highly substituted, and therefore more hydrophobic, pa5.

Figure 3.8 shows the Hdd and pdI results of pa5 complexes.

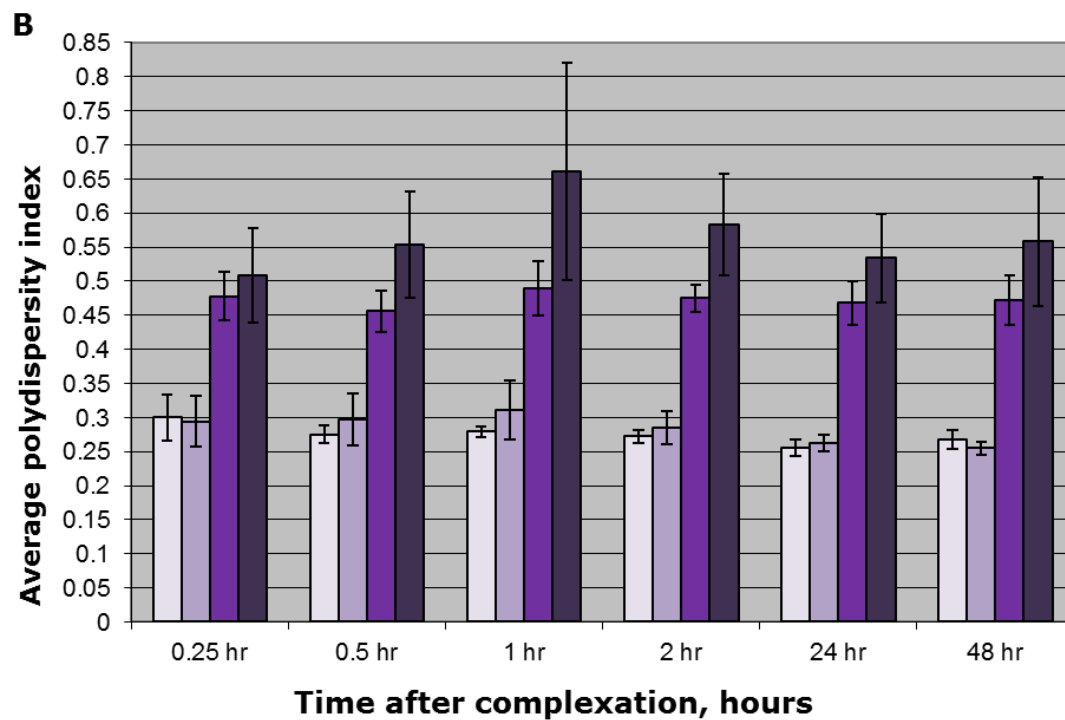
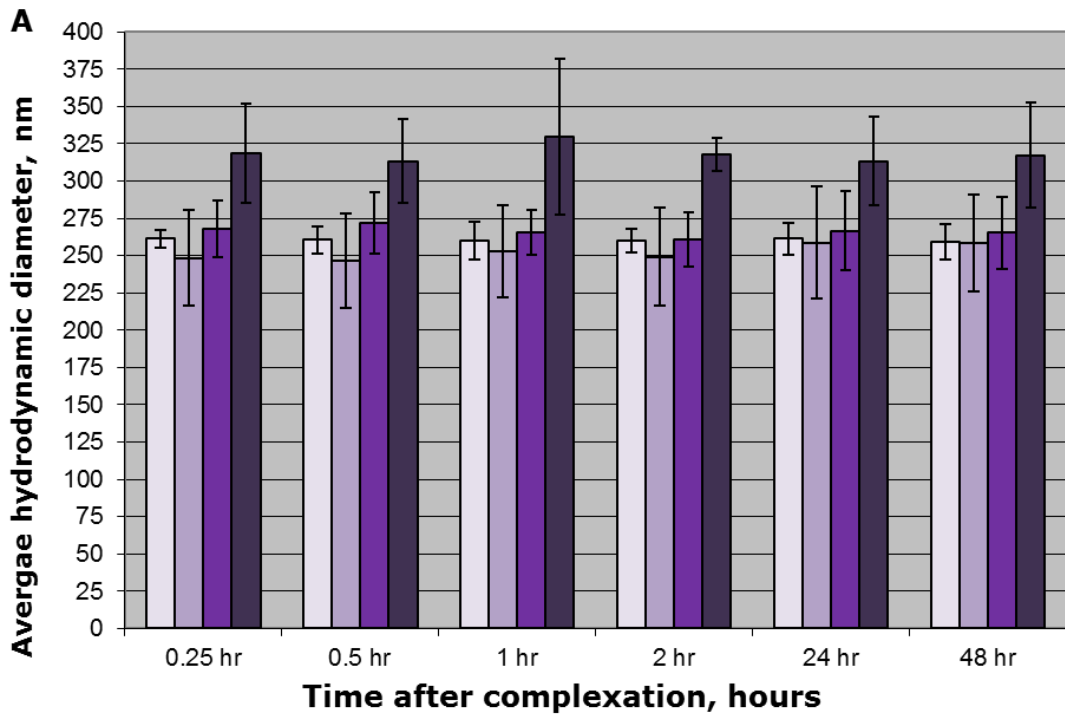
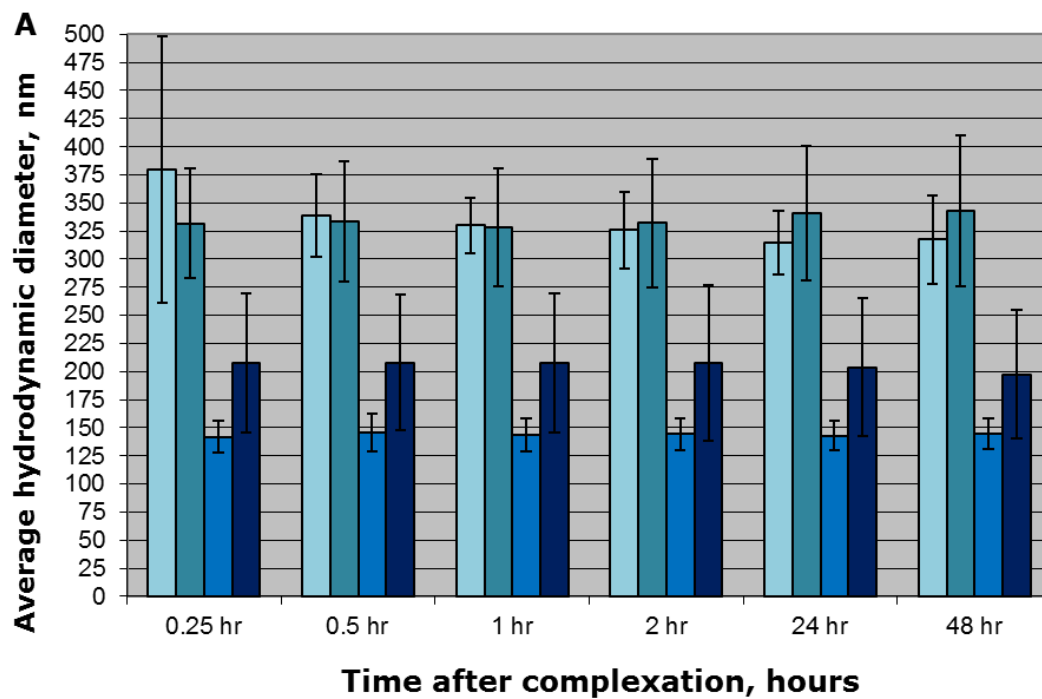


Figure 3.8 Results of DLS for alg/pa5 4.3:1, 3:1, 1:3 and 1:4.3. (A) Comparison of average hydrodynamic diameter (B) Comparison of average polydispersity index. ■ alg/pa5 4.3:1 ■ alg/pa5 3:1 ■ alg/pa5 1:3 ■ alg/pa5 1:4.3 (Mean \pm SD, n=3).

It can be seen that all complexes exhibited similar Hdd results. Whereas the complexes with higher concentrations of alginate (4.3:1 and 3:1), consistently showed smaller pdI values than complexes with higher concentrations of pa5 (1:3 and 1:4.3).

Figure 3.9 shows the Hdd and pdI results of all pa2.5 complexes.



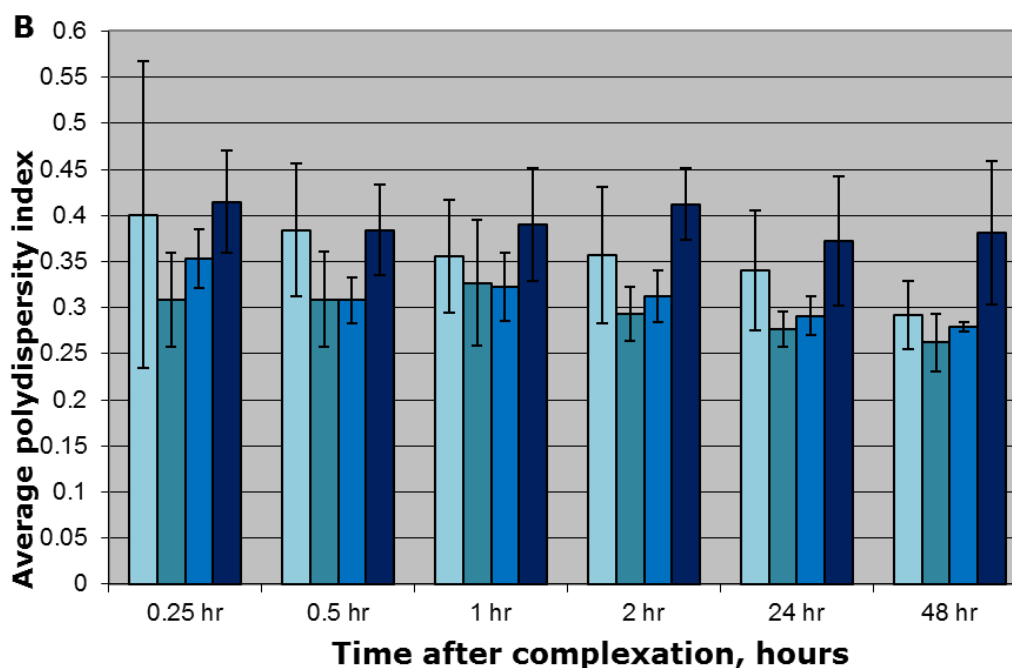


Figure 3.9 Results of DLS for alg/pa2.5 4.3:1, 3:1, 1:3 and 1:4.3. (A) Comparison of average hydrodynamic diameter (B) Comparison of average polydispersity index. ■ alg/pa2.5 4.3:1 ■ alg/pa2.5 3:1 ■ alg/pa2.5 1:3 ■ alg/pa2.5 1:4.3 (Mean \pm SD, n=3).

Results for pdI appeared to be relatively similar. However, there appeared to be a marked difference in Hdd between the opposing ratios; with 1:3 (140nm) and 1:4.3 (200nm) resulting in smaller average values than 4.3:1 (330nm) and 3:1 (335nm) complexes over 48 hours. By comparing figures 3.8 and 3.9, it appeared that pa2.5 based complexes showed similar pdI values while Hdd showed ratio dependent differences. pa5 based combinations however, formed nanosized objects of similar average Hdd, with pdI showing ratio dependence. This may indicate a potential measure of control over particle size and size distribution, through the manipulation of alginate and PE⁺ concentration.

Further investigations were then undertaken with the quaternised PEs, Qpa2.5 and Qpa5. The effect of quaternisation on individual amphiphilic PE self-assemblies with regard to Hdd and pdI can be seen in table 3.2.

Table 3.2 Comparison of average Hdd and pdI values of amphiphilic PEs and quaternised equivalents (Mean \pm SD, n=3).

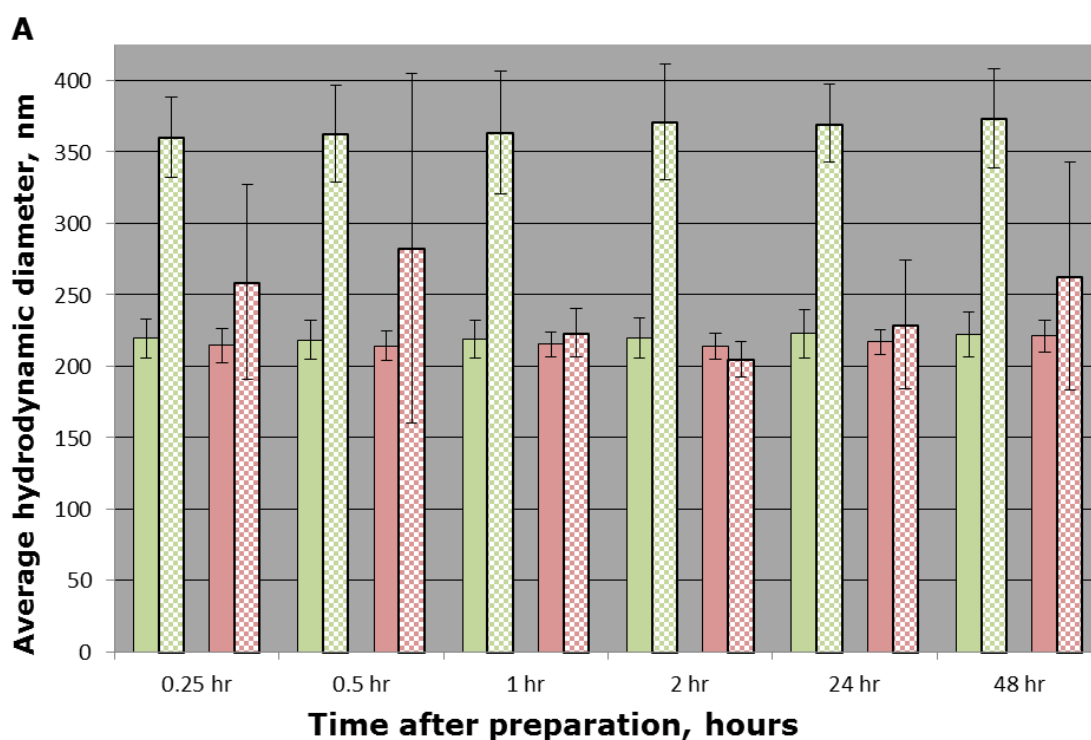
	Average Hdd at 48 hours, nm.	Average pdI at 48 hours.
pa5 0.166mg/mL	466.0 (59.3)	0.442 (0.049)
Qpa5 0.166mg/mL	373.5 (34.4)	0.359 (0.051)
pa2.5 0.166mg/mL	302.8 (17.1)	0.232 (0.019)
Qpa2.5 0.166mg/mL	263.1 (79.6)	0.387 (0.057)
pa5 0.5mg/mL	541.3 (54.6)	0.386 (0.057)
Qpa5 0.5mg/mL	385.3 (19.7)	0.324 (0.031)
pa2.5 0.5mg/mL	365.2 (29.2)	0.213 (0.011)
Qpa2.5 0.5mg/mL	204.7 (16.3)	0.269 (0.045)

With regard to Hdd, Quaternisation appeared to lead to reductions in Hdd data in all cases investigated. The average pdI data showed mixed results, with pa5 0.166mg/mL and 0.5mg/mL showing reductions in average pdI following quaternisation, whereas pa2.5 0.166mg/mL and 0.5mg/mL showed an apparent increase.

The process of quaternisation appears to have altered the state of intermolecular interactions for each amphiphilic PE. The presence of permanent positive charges on the backbone may have led to greater repulsive forces between molecules, leading to increased porosity of the particle structure. This in turn may have led to the constriction of the particle by hydrophobic attraction in order to prevent the penetration of the surrounding water, until a balance between repulsive and attractive forces was achieved. Qpa5, which has an estimated degree of quaternisation of 35% (Chapter 2 section 2.4.1), appeared to have a reduction in Hdd and pdI compared to pa5, whereas Qpa2.5, which has an estimated degree of quaternisation of 18%, presented with reduced average Hdd, but increased pdI.

The effect of quaternisation of amphiphilic poly (allyl amine) on the formation of PECs with alginate was investigated for Qpa5 and Qpa2.5 at ratios of 3:1 and 1:3 only. These combinations were chosen based on the results of dynamic light scattering for non-quaternised PECs, as well as the increased tendency of 4.3:1 complexes to precipitate over time.

Figure 3.10 shows the Hdd and pdI results of quaternised complexes at a ratio of 3:1 along with their equivalent PE⁺ controls.



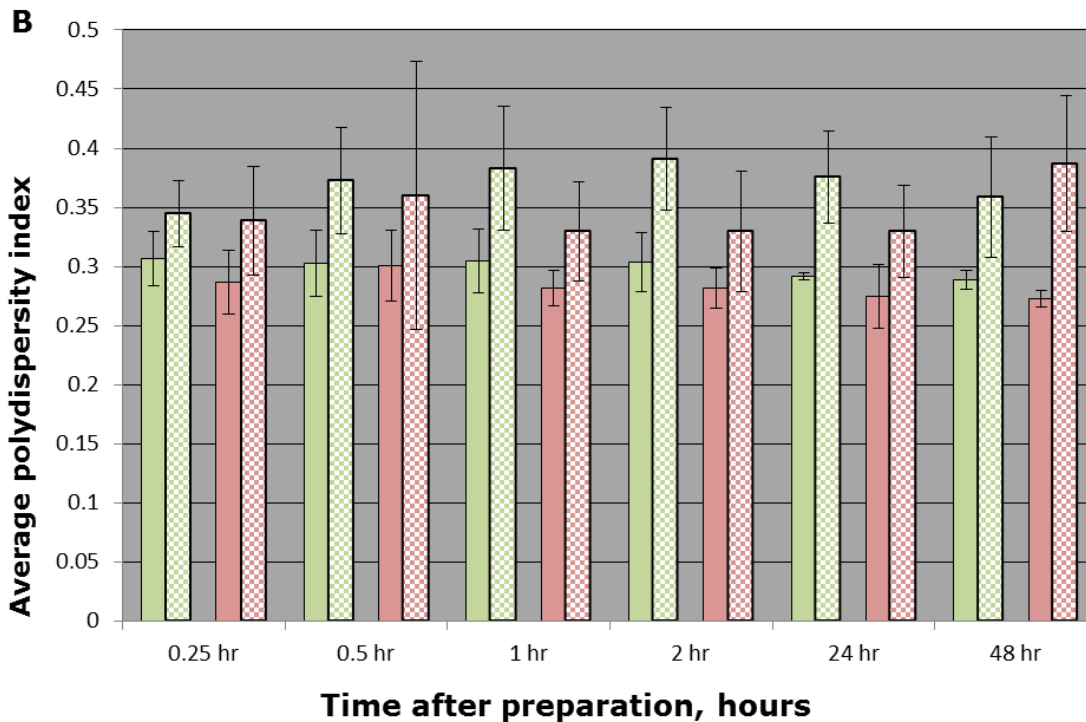


Figure 3.10 Results of DLS for alg/Qpa5 3:1, alg/Qpa2.5 3:1 and equivalent controls. (A) Comparison of average hydrodynamic diameter (B) comparison of average polydispersity index. alg/Qpa5 3:1 Qpa5 0.5mg/mL alg/Qpa2.5 3:1 Qpa2.5 0.5mg/mL (Mean \pm SD, n=3).

From figure 3.10, it would appear that alg/Qpa5 3:1 led to reduction in Hdd compared to Qpa5 0.5mg/mL control, the apparent reduction in size was accompanied by a less clear reduction in pdI. The results for alg/Qpa2.5 3:1 and its control were more similar, showing perhaps that Qpa2.5 interacts with alginate in a different way than Qpa5, possibly due to the difference in hydrophobic grafting. Both sets of data were relatively unchanged over the 48 hour experimentation period, indicating the formation of stable nano-aggregates with reduced size and size dispersity.

Figure 3.11 shows the Hdd and pdI results of quaternised complexes at a ratio of 1:3 alongside their equivalent PE⁺ controls.

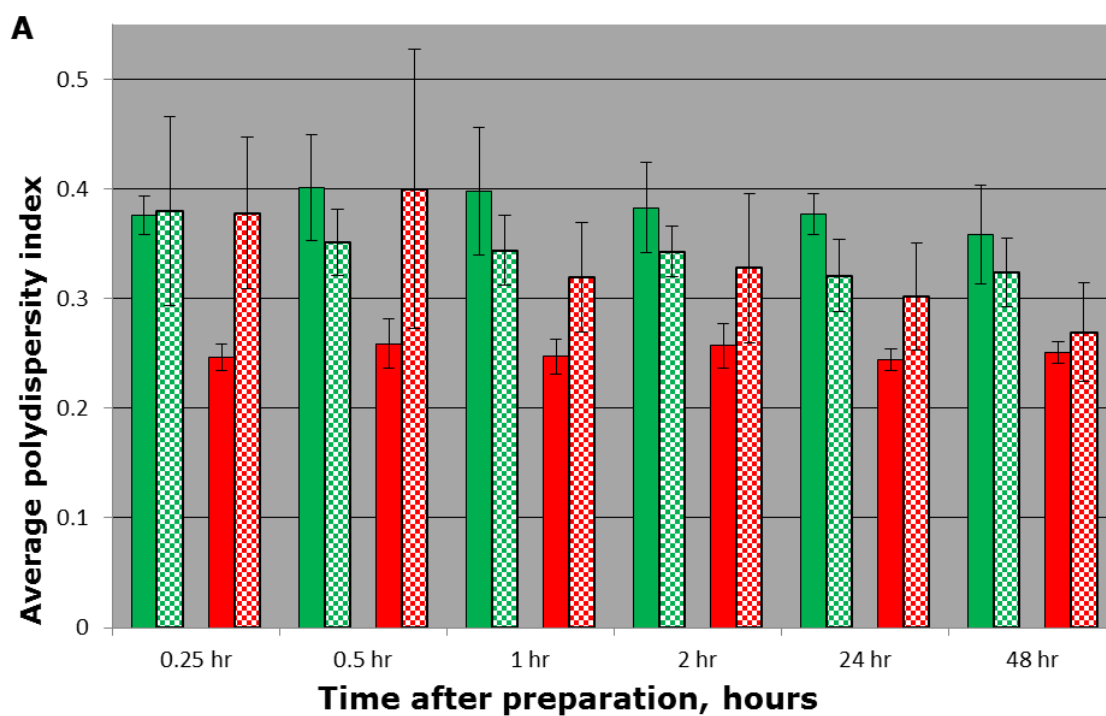
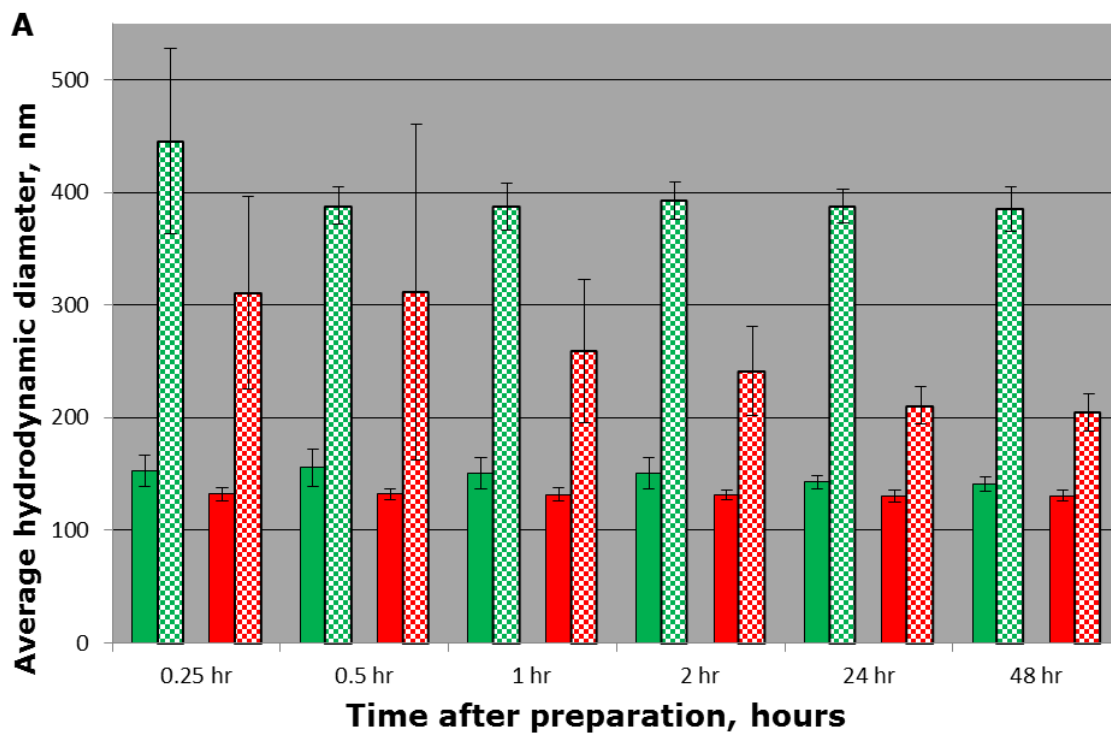


Figure 3.11 Results of DLS for alg/Qpa5 1:3, alg/Qpa2.5 1:3 and equivalent controls. (A) Comparison of average hydrodynamic diameter (B) comparison of average polydispersity index. ■ alg/Qpa5 1:3 ▨ Qpa5 0.5mg/mL ■ alg/Qpa2.5 1:3 ▨ Qpa2.5 0.5mg/mL (Mean \pm SD, n=3).

As with the 3:1 complexes all results in figure 3.11 were relatively stable over 48 hours. However, unlike 3:1 complexes, both alg/Qpa5 1:3 and alg/Qpa2.5 1:3 led to reductions in Hdd compared to their respective controls, while showing moderate changes in pdI. It would seem that the addition of a small amount of alginate led to the formation of nano-sized objects with reduced size, while the moderate changes in pdI indicated that the size reduction was seen in most of the size populations.

Regardless of ratio used, the combination of alginate and Qpa5, or Qpa2.5 led to reductions in Hdd values compared to quaternised controls at equivalent concentrations.

Finally, the differences between quaternised complexes and non-quaternised complexes were examined, with results shown in table 3.3.

Table 3.3 Comparison of average Hdd and pdI values of non-quaternised and quaternised PECs at 3:1 and 1:3 ratios (Mean \pm SD, n=3).

	Average Hdd at 48 hours.	Average pdI at 48 hours.
alg/pa5 3:1	258.5 (32.6)	0.255 (0.010)
alg/Qpa5 3:1	222.3 (15.8)	0.289 (0.008)
alg/pa2.5 3:1	342.8 (67.4)	0.262 (0.031)
alg/Qpa2.5 3:1	221.1 (11.1)	0.273 (0.007)
alg/pa5 1:3	265.4 (24.1)	0.472 (0.037)
alg/Qpa5 1:3	141.2 (6.2)	0.358 (0.045)
alg/pa2.5 1:3	144.8 (13.4)	0.279 (0.005)
alg/Qpa2.5 1:3	130.9 (4.9)	0.251 (0.010)

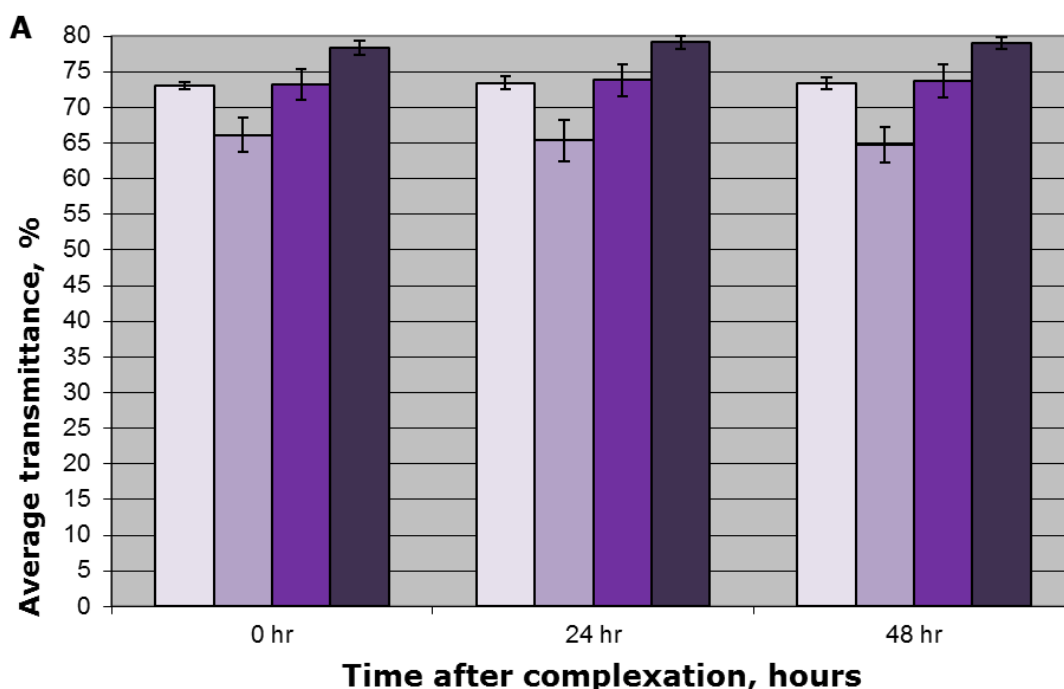
It can be seen that the quaternised complexes resulted in smaller Hdd values than their non-quaternised counterparts regardless of ratio. The reduction in Hdd was attributed to increased electrostatic attraction between quaternised amphiphilic PEs and alginate due to the presence of quaternary nitrogen.

The difference in average pdI between the two types of complexes was less clear, with quaternised 3:1 complexes exhibiting quite similar pdI values to their non-quaternised equivalents, which may indicate that the observed reductions in Hdd were uniform. Quaternised 1:3 complexes showed small reductions in pdI compared to non-quaternised equivalents. When viewed concomitantly with average Hdd data, there appeared to be a trend towards smaller, less polydisperse nano-sized objects.

From the results discussed, it appears that quaternisation may lead to more compact nano-sized PECs than non-quaternised complexes. Furthermore, increasing the degree of quaternisation may lead to still greater reductions in Hdd.

3.4.2 Transmittance studies

The colloidal stability of prepared solutions was assessed using a UV-Vis spectrometer to measure sample solutions %Transmittance of light, alongside a visual inspection. Figure 3.12 shows the average %Transmittance of pa5 and pa2.5 based combinations over a 48 hour period.



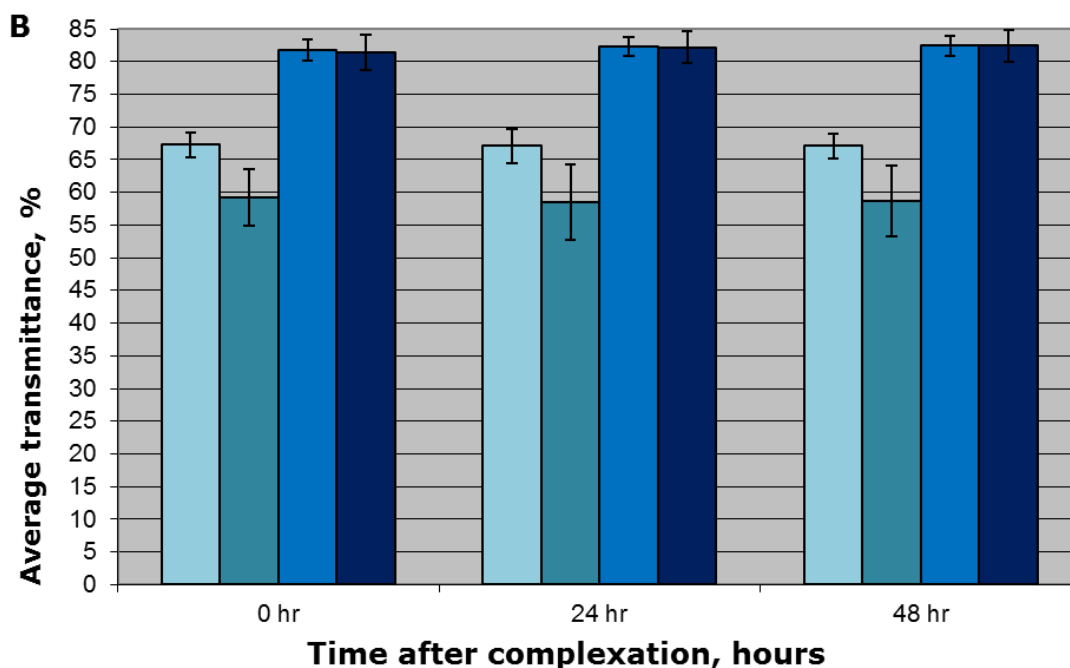


Figure 3.12 Results of %Transmittance studies for pa5 and pa 2.5 based complexes. (A) Comparison of average %Transmittance of alg/pa5 complexes (B) Comparison of average %Transmittance of alg/pa2.5 complexes. ■ alg/pa5 4.3:1 ■ alg/pa5 3:1 ■ alg/pa5 1:3 ■ alg/pa5 1:4.3. ■ alg/pa2.5 4.3:1 ■ alg/pa2.5 3:1 ■ alg/pa2.5 1:3 ■ alg/pa2.5 1:4.3 (Mean \pm SD, n=3).

All samples appeared to show stable results over the 48 hour monitoring period. For pa5 complexes, there may have been a slight trend towards increased turbidity when alginate was the majority component of complexes, despite the fact that %Transmittance values were quite similar, this is due to visual inspections showing that alg/pa5 4.3:1 and 3:1 began to exhibit evidence of precipitation after 24 hours. pa2.5 based complex data showed a clearer contrast, with alg/pa2.5 4.3:1 and 3:1 showing markedly reduced transmittance when compared to 1:3 and 1:4.3, the visual inspections also showed that 4.3:1 and 3:1 began to precipitate after 24 hours, whereas 1:3 and 1:4.3 remained unchanged over 48 hours. Increasing the concentration of alginate in PECs appeared to lead to increased turbidity of solutions and subsequently reduced transmittance of light; this was most clearly seen in 3:1 complexes.

Tables 3.4 and 3.5 show the %Transmittance of PE⁺ complexes with alginate compared to equivalent PE⁺ controls.

Table 3.4 Comparison of average %Transmittance of alg/pa5 complexes and equivalent pa5 controls at 48 hours after preparation (Mean \pm SD, n=3).

Sample	Average %Transmittance at 48 hours, %
alg/pa5 4.3:1	73.4 (0.8)
pa5 0.116mg/mL	84.2 (0.6)
alg/pa5 3:1	64.8 (2.5)
pa5 0.166mg/mL	84.7 (1.1)
alg/pa5 1:3	73.7 (2.4)
alg/pa5 1:4.3	79.0 (0.9)
pa5 0.5mg/mL	76.6 (0.5)

Table 3.5 Comparison of average %Transmittance of alg/pa2.5 complexes and equivalent pa2.5 controls at 48 hours after preparation (Mean \pm SD, n=3).

Sample	Average %Transmittance at 48 hours, %
alg/pa2.5 4.3:1	66.7 (2.1)
pa2.5 0.116mg/mL	86.2 (0.6)
alg/pa2.5 3:1	58.6 (5.4)
pa2.5 0.166mg/mL	86.1 (0.5)
alg/pa2.5 1:3	82.4 (1.6)
alg/pa2.5 1:4.3	82.4 (2.4)
pa2.5 0.5mg/mL	84.2 (0.2)

Controls exhibited greater transmittance of light than complexes in general, except for alg/pa5 1:4.3, which resulted in solutions with greater average %Transmittance than its 0.5mg/mL pa5 controls.

%Transmittance data for all quaternised complexes at ratios of 3:1 and 1:3 can be seen in figure 3.13.

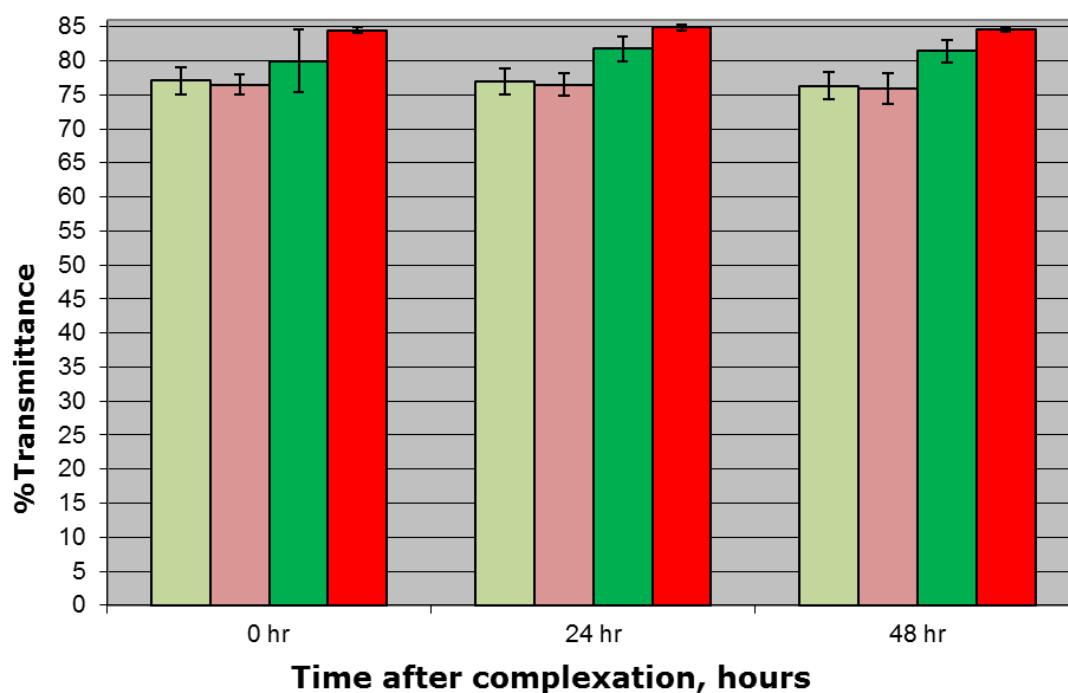


Figure 3.13 Results of %Transmittance studies for quaternised complexes. █ alg/Qpa5 3:1 █ alg/Qpa2.5 3:1 █ alg/Qpa5 1:3 █ alg/Qpa2.5 1:3 (Mean \pm SD, n=3).

In all cases quaternised complexes clearly led to increased %Transmittance when compared to equivalent non-quaternised PECs seen in figure 3.12, which was perhaps due to the increased interaction with alginate, and reduced incidence of precipitation. As with previous results, the %Transmittance data of all quaternised complexes remained stable over 48 hours.

Table 3.6 shows the %Transmittance of alg/QPE⁺ complexes and their equivalent PE⁺ controls.

Table 3.6 Comparison of the average %Transmittance of alg/QPE⁺ complexes and their equivalent PE⁺ controls at 48 hours after sample preparation (Mean± SD, n=3).

Sample	Average %Transmittance at 48 hours, %
alg/Qpa5 3:1	76.3 (2.0)
Qpa5 0.166mg/mL	86.9 (0.0)
alg/Qpa2.5 3:1	75.9 (2.2)
Qpa2.5 0.166mg/mL	87.0 (0.2)
alg/Qpa5 1:3	81.4 (1.6)
Qpa5 0.5mg/mL	85.1 (0.2)
alg/Qpa2.5 1:3	84.6 (0.4)
Qpa2.5 0.5mg/mL	86.2 (0.8)

As with non-quaternised complexes, PE⁺ controls showed greater %Transmittance values than equivalent complexes, which was to be expected due to the absence of alginate and the good solubility of quaternised PEs.

When %Transmittance data is viewed concomitantly with Hdd and pdI data, it may indicate the formation of nanosized objects of stable size, size dispersity, and colloidal stability over at least 48 hours.

3.4.3 Zeta potential

Zeta potential is the measure of the electrical potential at the shear plane between the diffuse ions of the solvent and the condensed ions surrounding the charged surface of particles. Measurement of zeta potential has long been used as an indicator of colloidal stability. Zeta potential values indicating good stability are usually greater than 30mV whether positive or negative, values greater than 60mV are often seen as possessing excellent colloidal stability (7, 8).

Results of zeta potential measurements can be seen in table 3.7. Analysis was performed using solutions of pH 4.6 and 8.0, so as to mimic the conditions used in experiments discussed in chapters 3 and 4, respectively.

Table 3.7 Results of Zeta potential studies of pa2.5, Qpa2.5, alg/pa2.5 1:3 and alg/Qpa2.5 1:3 (n=1).

Sample	pH 4.6	pH 8.0
pa2.5	69.9	63.2
Qpa2.5	60.7	49.3
alg/pa2.5 1:3	63.7	50.2
alg/Qpa2.5 1:3	59.3	54.0

Cationic PEs pa2.5 and Qpa2.5 showed greater positive values at the more acidic pH, Qpa2.5 surprisingly was found to have a lesser positive charge than pa2.5 regardless of pH. Samples of pa2.5 and Qpa2.5 showed increased positive values at pH 4.6, which was to be expected as ionisation of amines would be greater in an acidic environment.

The complexes investigated for zeta potential contained low concentrations of sodium alginate and accordingly resulted in elevated positive charges, even at pH 8.

The results of Zeta potential, when discussed in conjunction with DLS, and %Transmittance studies, support the formation of stable colloidal particles in the nano-size range.

3.4.4 Infra-red analysis

Analysis and comparison of the IR spectra of individual PEs with those of PECs, was used to investigate the anticipated interaction between alginate and amphiphilic PEs. Analysis of individual PEs can be found in chapter 2 (section 2.4.2).

As shown in figure 3.14, sodium alginate exhibits O-H stretching vibrations at 3279cm^{-1} . Carboxylic acid carbonyl shows antisymmetric and symmetric stretching

vibrations at 1596cm^{-1} and 1406cm^{-1} respectively. The signal from $1026\text{--}1080$ represents the antisymmetric stretch of C-O-C bonds (9).

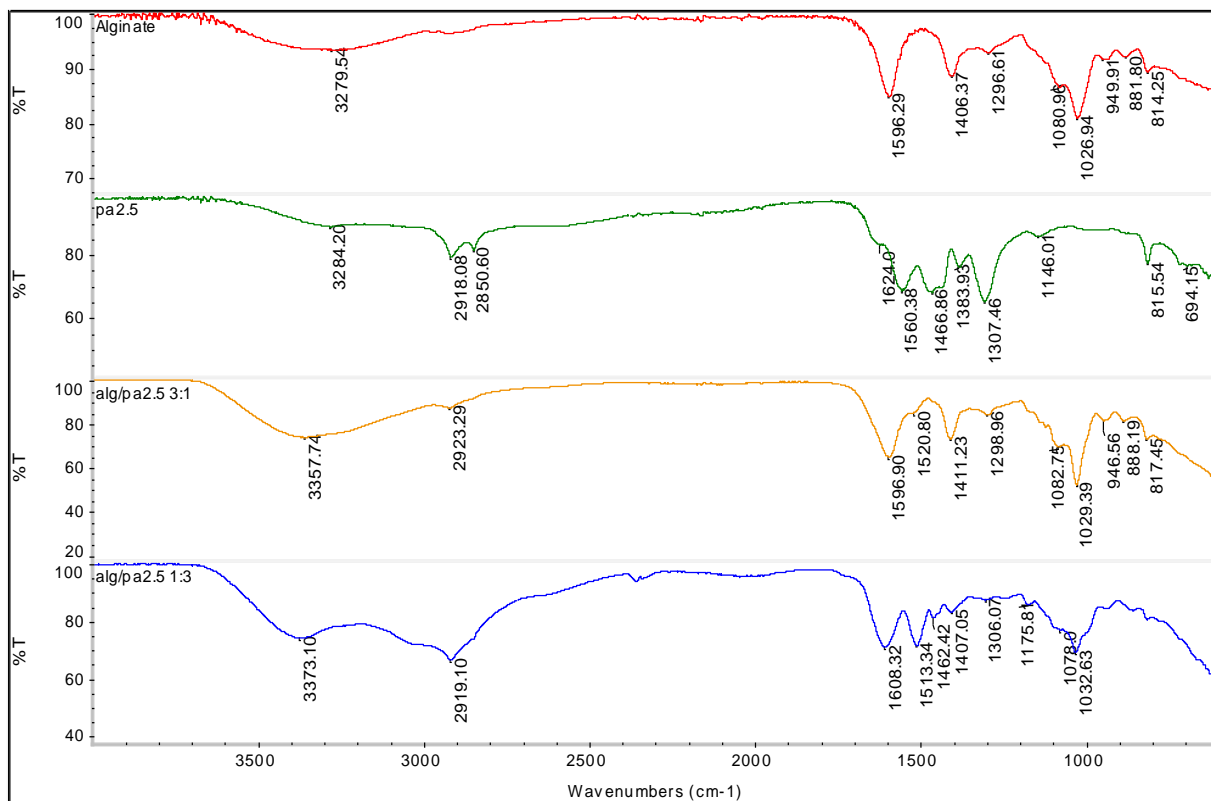


Figure 3.14 IR spectra of sodium alginate and pa2.5 based complexes at 3:1 and 1:3 mass ratios.

Upon investigation of the alg/pa2.5 3:1 combination, alginate was quite clearly the majority given the similarity in spectra to alginate alone. Weak C-H stretch vibrations at 2923cm^{-1} were the only indication of the presence of pa2.5. While a reduction in transmittance at 3357cm^{-1} may be due to an increase in hydrogen bonding in the system, a similar result was found by Fang et al. who synthesised a PEC from poly(L-glutamic acid) and chitosan (10). Furthermore a new signal at 1520cm^{-1} was detected, which may be associated with the protonated amines of pa2.5 and an interaction with alginate.

The 1:3 combination of alg/pa2.5 presented a result more representative of pa2.5. Despite alginate being in the minority, C-O-C stretch vibrations at $1032\text{--}1078\text{cm}^{-1}$ were clearly visible, as well as carbonyl stretching vibrations at 1608cm^{-1} and 1407cm^{-1} . pa2.5 contributed to the spectrum with C-H stretching and bending vibrations at 2919cm^{-1} and 1462cm^{-1} , respectively. As well as C-N stretch

vibrations at 1175cm^{-1} . As with the 3:1 ratio, the vibration at 3373cm^{-1} showed reduced transmittance when compared to PEs alone.

The signal at 1513cm^{-1} is absent from the spectra of alginate and pa2.5, and may be a similar indication of some interaction as with the new signal found at 1520cm^{-1} in alg/pa2.5 3:1.

Complexes based on pa5 (Figure 3.15) showed quite similar results to those of pa2.5.

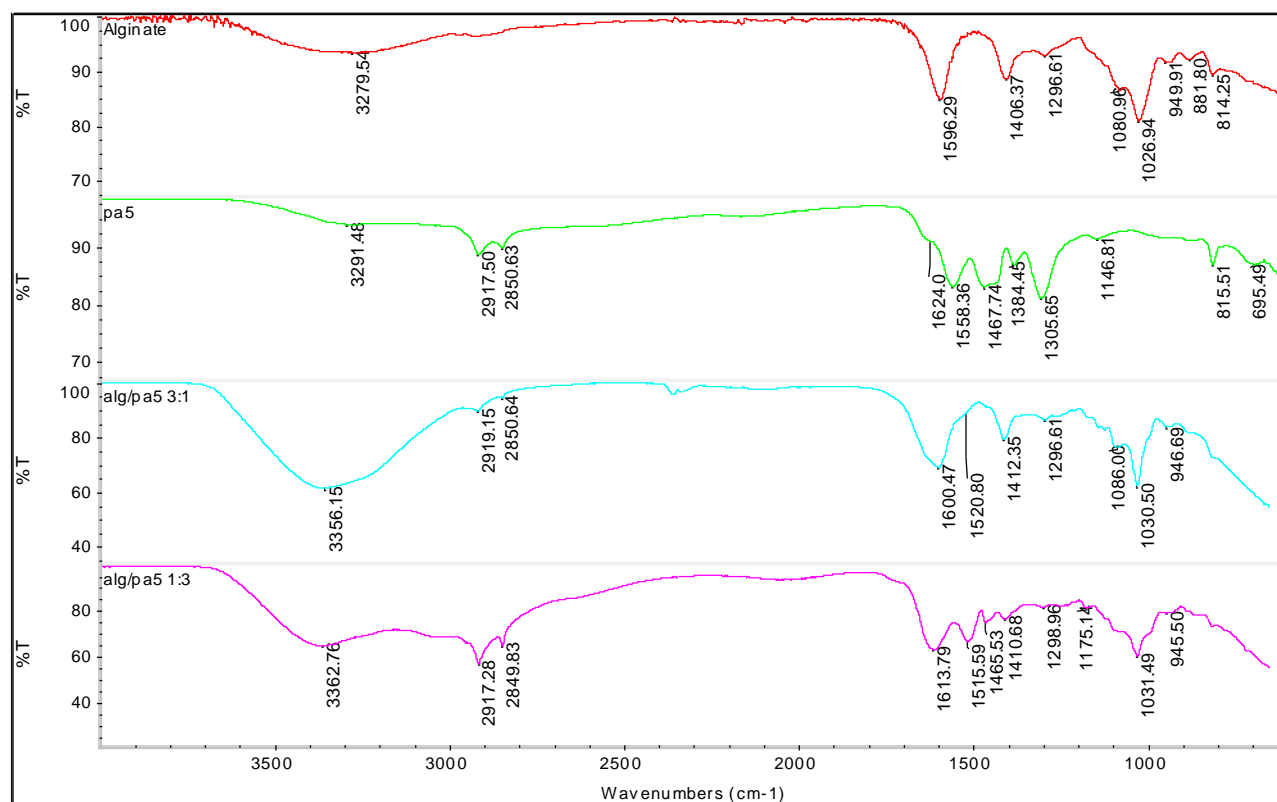


Figure 3.15 IR spectra of sodium alginate and pa5 based complexes at 3:1 and 1:3 mass ratios.

In the case of alg/pa5 3:1 complex, characteristic vibrations of alginate were visibly dominant, while pa5 provided C-H stretching vibrations at 2919cm^{-1} and 2850cm^{-1} . A small shoulder at 1520cm^{-1} may be similar to the new signals detected in pa2.5 complexes. The strong, broad peak at 3356cm^{-1} may be due to stretching vibrations of O-H (present in alginate) and N-H (present in pa5).

The reduction in transmittance in the region from $3200\text{--}3400\text{cm}^{-1}$ of the PECs was attributed to hydrogen bonding. It could simply be evidence of the presence of water in the sample.

The alg/pa5 1:3 complex showed the distinctive peaks of alginate at 1613cm^{-1} , 1410cm^{-1} , and 1031cm^{-1} . Vibrations attributed to pa5 included C-H stretching at 2917cm^{-1} and 2849cm^{-1} , with bending vibrations at 1465cm^{-1} . C-N stretching vibrations were visible at 1175cm^{-1} . A new signal was detected at 1515cm^{-1} in a similar result to previously mentioned complexes.

The new signals detected $\approx 1515\text{cm}^{-1}$ may be the result of electrostatic interaction between PEs. Furthermore there appears to be a slight $5\text{-}10\text{cm}^{-1}$ shift in carbonyl vibration frequency of alginate, which may also indicate an interaction. Li et al. attributed similar shifts in the frequency of carbonyl groups of alginate and amine groups of chitosan to electrostatic interaction, in a study of PEC formation (11).

The IR spectra of Qpa2.5 and its complexes with alginate can be seen in figure 3.16; an IR analysis of Qpa2.5 was discussed in chapter 2. The alg/Qpa2.5 3:1 based complex showed some of the characteristic vibrations of sodium alginate at 1600cm^{-1} , 1411cm^{-1} and $1028\text{-}1080\text{cm}^{-1}$. Vibrations indicative of Qpa2.5 were less obvious. C-H stretching vibrations can be seen at 2924cm^{-1} . A small peak at 1721cm^{-1} was not present in either of the original PEs, and may be previously undetected carbonyl stretch vibrations. There appears to be a slight shoulder at 1514cm^{-1} which may be similar to the signal at 1518cm^{-1} found in Qpa2.5 which was attributed to Quaternary nitrogen in chapter 2. The shift from 1518cm^{-1} to 1514cm^{-1} may indicate some form of interaction, as in the case of the new signals found in non-quaternised complexes.

The use of IR as evidence of electrostatic interaction between PEs has been used previously, as shown by Wang et al. in a study of a chitosan and alginate PEC (12).

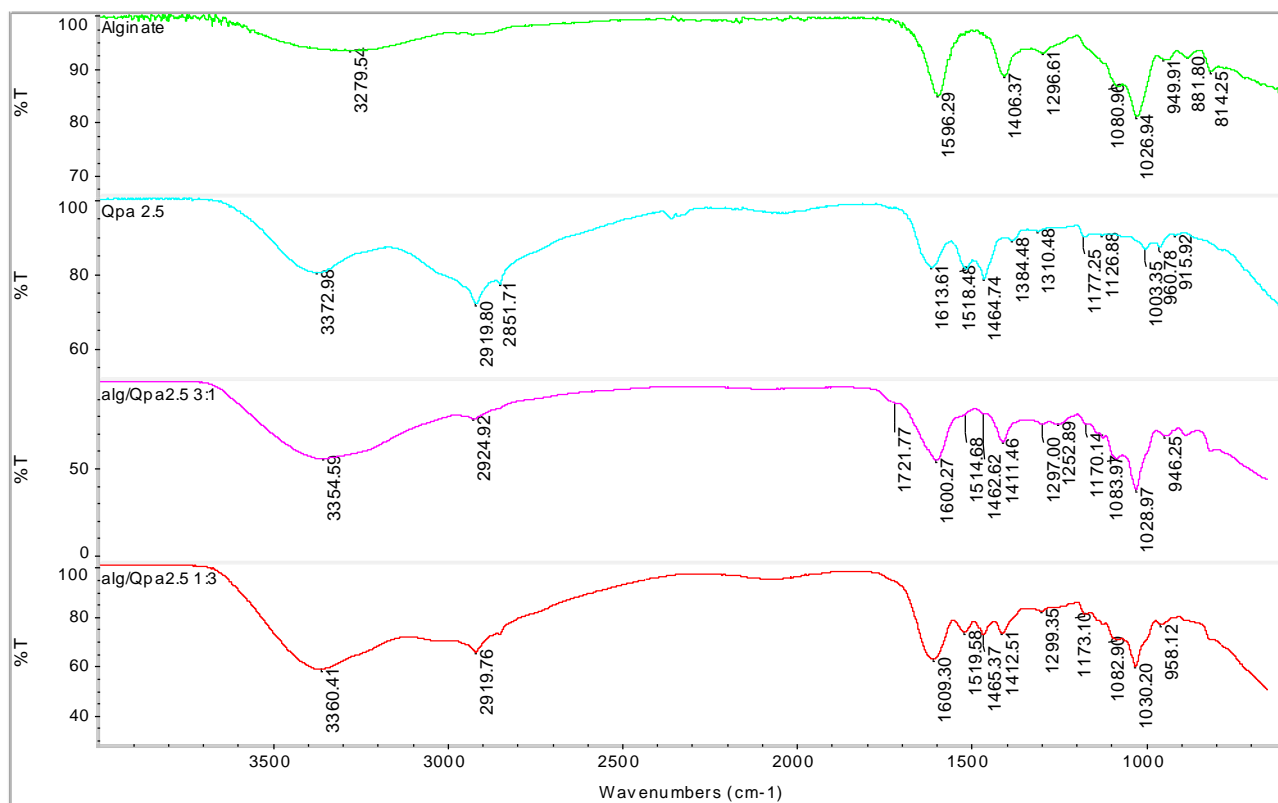


Figure 3.16 IR spectra of sodium alginate and Qpa2.5 based complexes at 3:1 and 1:3 mass ratios.

The alg/Qpa2.5 1:3 complex shows similarities to the 3:1 complex with regard to alginate vibrations. Furthermore, as in the case of alg/pa2.5 and alg/pa5, the 1:3 complex exhibits more signature vibrations of the cationic component, such as sharper signals at 2919 cm^{-1} , 1609 cm^{-1} and 1466 cm^{-1} .

The vibrations at 1519 cm^{-1} and 1412 cm^{-1} were attributed to the electrostatic interaction of PEs in a result similar to those of previously discussed complexes.

The IR spectra of Qpa5 based complexes with alginate are shown in figure 3.17. At a mass ratio of 3:1 the spectrum of alg/Qpa5 is quite similar to that of sodium alginate, with carbonyl stretch vibrations at 1598 cm^{-1} and 1411 cm^{-1} , a weaker signal at 1717 cm^{-1} was detected, despite being absent from alginate and Qpa5.

The vibrations at 1027-1083 cm^{-1} were similarly typical of the anionic PE. Although not detected by the software, there may be a weak signal at approximately 1520 cm^{-1} (denoted by an arrow in figure 3.17), which could be associated with the small peak at 1518 cm^{-1} in Qpa5.

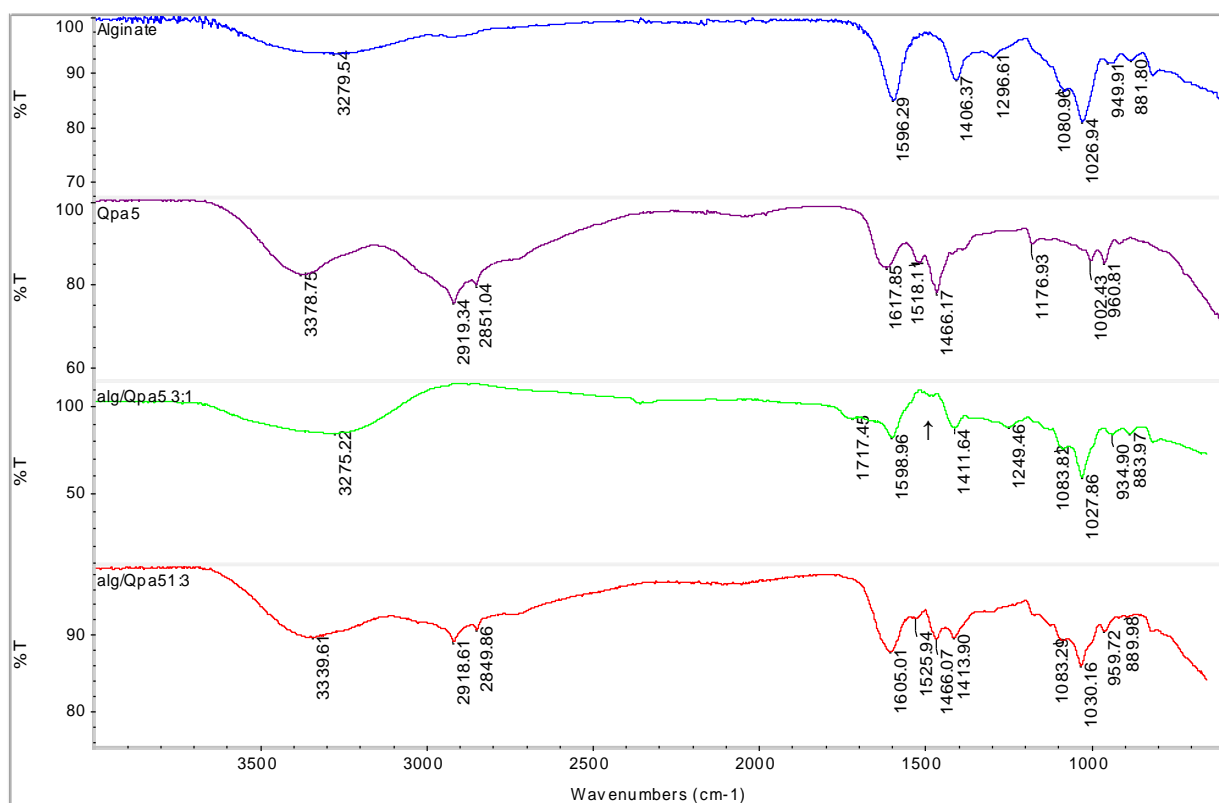


Figure 3.17 IR spectra of sodium alginate and Qpa5 based complexes at 3:1 and 1:3.

As for alg/Qpa5 1:3, the spectrum showed the C-H stretching and bending vibrations of Qpa5 at 2918cm^{-1} , 2849cm^{-1} and 1466cm^{-1} respectively. Results also showed a signal at 959cm^{-1} which appeared to be similar to the signal at 960cm^{-1} found in Qpa5, which was attributed to quaternary ammonium during the discussion of Quaternised PEs in chapter 2.

The alg/Qpa5 1:3 combination also showed some of the characteristic vibrations of alginate at $1030\text{-}1083\text{cm}^{-1}$.

The signals at 1525cm^{-1} and 1413cm^{-1} may have been related to the vibrations at 1518cm^{-1} in Qpa5 and 1406cm^{-1} in alginate. The shift in wave number might have been caused by some form of interaction between the two PEs, in a result similar to Qpa2.5 based complexes.

3.4.5 Thermal analysis

The thermal properties of sodium alginate were investigated using DSC and hot-stage microscopy. Results of DSC analysis are shown in figure 3.18.

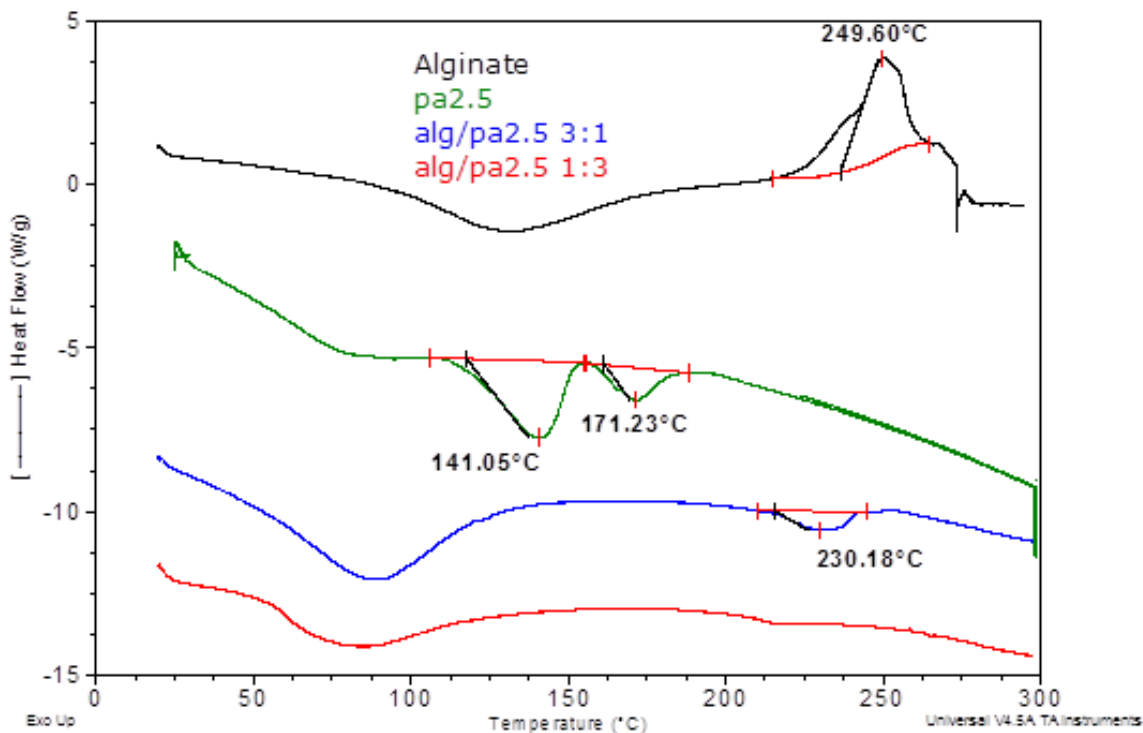


Figure 3.18 DSC thermograms of alginate, pa2.5, alg/pa2.5 3:1 and alg/pa2.5 1:3.

Alginate showed a wide exotherm at 249°C which was attributed to decomposition, similar results were found by Soares et al. in a study of the thermal properties of alginate (13).

Hot-stage microscopy images of alginate (figure 3.19) showed that discolouration of the sample began at approximately 190°C, followed by contraction starting from 230°C up to 260°C; this is in agreement with results of DSC which showed a peak decomposition temperature of 249°C. Upon cooling to room temperature the sample did not return to its original state.

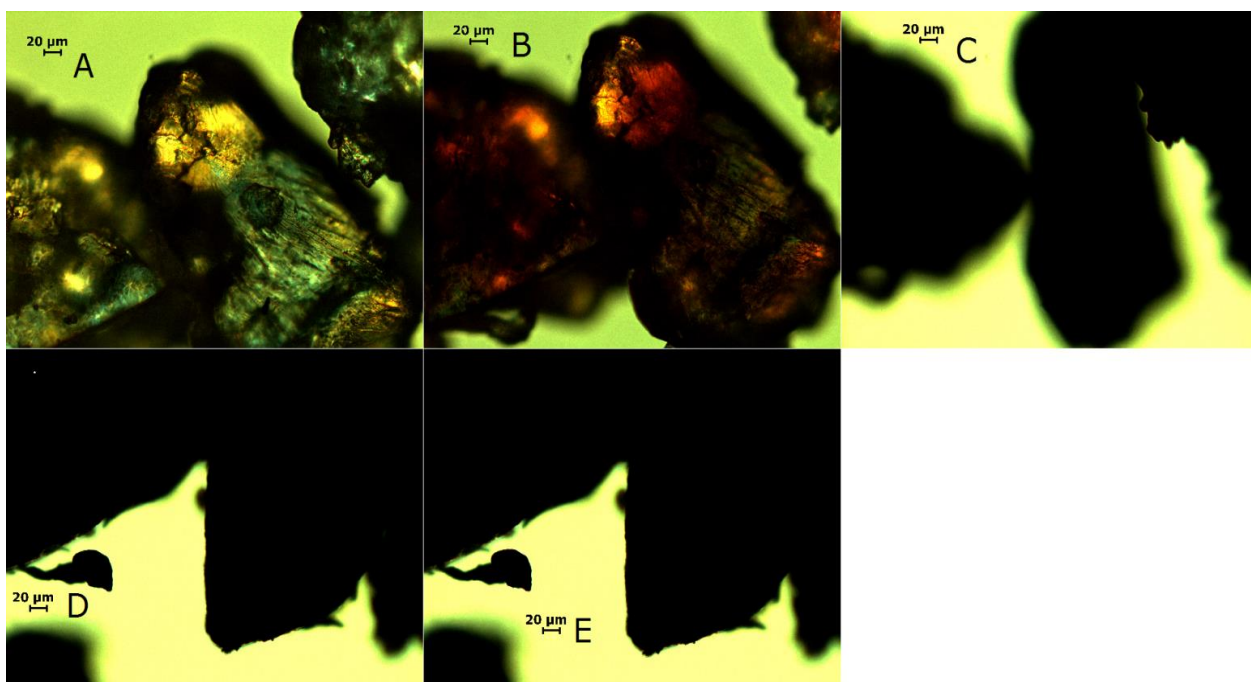


Figure 3.19 Hot-stage images of sodium alginate at magnification x20. (A) Room temperature (B) 200°C (C) 230°C (D) 300° (E) Cooled to room temperature.

The thermogram of alg/pa2.5 3:1 complex (figure 3.18) is distinctly different from the thermogram of pa2.5 and sodium alginate, despite alginate being the major component of the complex. Results showed an endotherm at 230°C, which may be an indicator of decomposition.

Images from hot stage-microscopy (figure 3.20) show that discolouration of the sample began at approximately 170°C which did not show any correlation to DSC data. Furthermore, onset of discolouration at 170°C was found to be less than that found for pa2.5 (210°C) and alginate (190°C). There was also no evidence of melting or changes in shape on further heating/cooling.

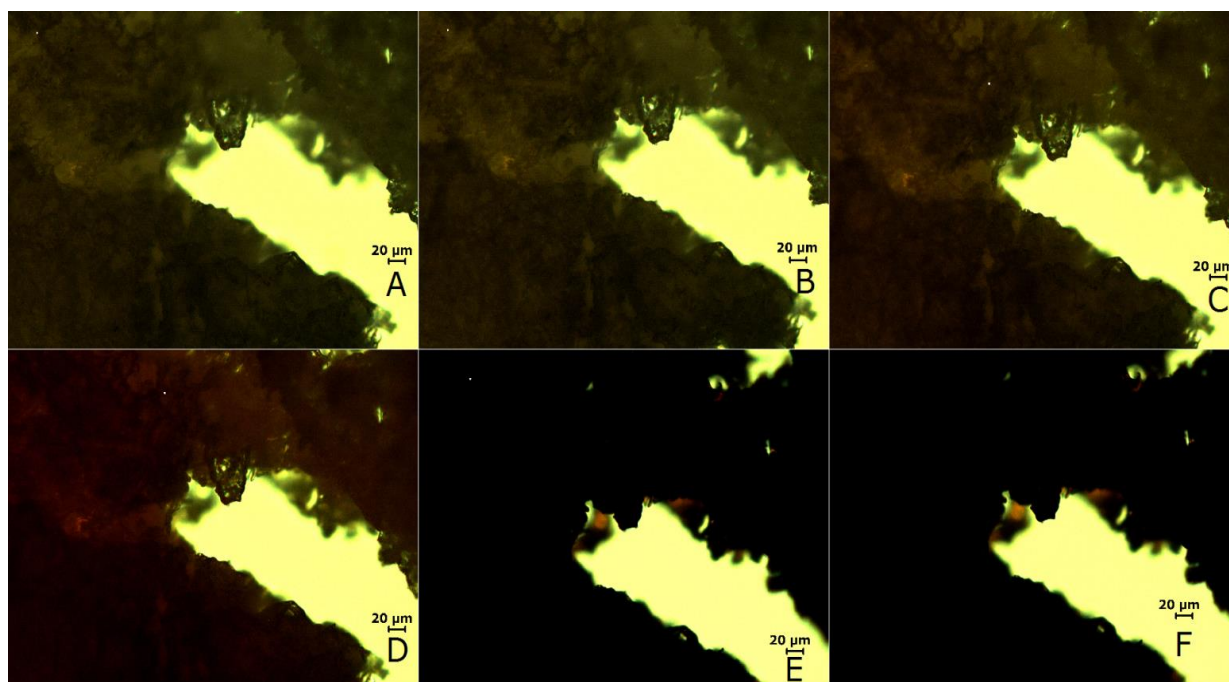


Figure 3.20 Hot-stage images of alg/pa2.5 3:1 complex at magnification x20. (A) Room temperature (B) 100°C (C) 170°C (D) 200°C (E) 300°C (F) Cooled to room temperature.

The DSC thermogram of alg/pa2.5 1:3 complex (figure 3.18) showed no obvious thermal events; whereas, hot-stage images (figure 3.21) showed that the complex began to discolour at 180°C continuing up to 300°C. Upon cooling, the sample did not return to its preheated state, indicating degradation of some or all of the complex components.

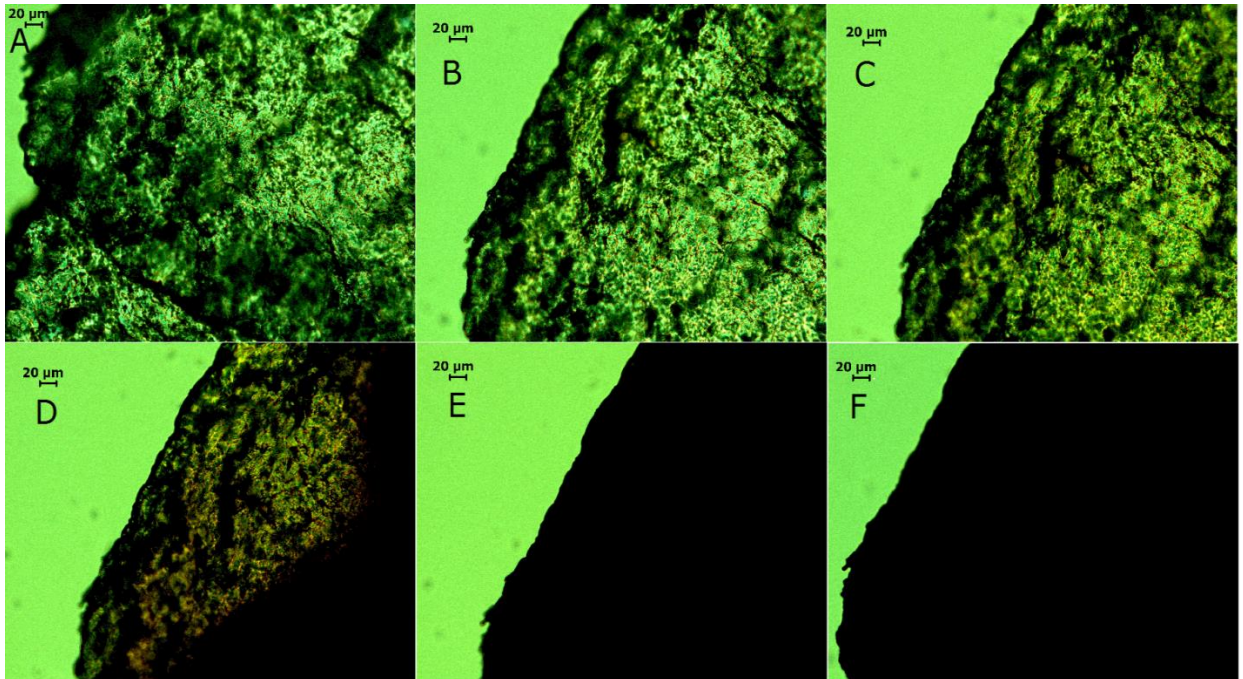


Figure 3.21 Hot-stage images of alg/pa2.5 1:3 complex at magnification x20. (A) Room temperature (B) 100°C (C) 190°C (D) 210°C (E) 300°C (F) Cooled to room temperature.

The major component in the complex was pa2.5, which when investigated in chapter 2 (Section 2.4.3, Figure 12) clearly underwent a melting process at 140°C, however when in complex with alginate there appeared to be no evidence of melting on DSC and hot-stage data. It would appear that the melting point of the complex was increased to a point above decomposition temperature, which was assumed to have taken place upon discolouration.

Figure 3.22 shows the DSC thermograms of pa5 based complexes and alginate.

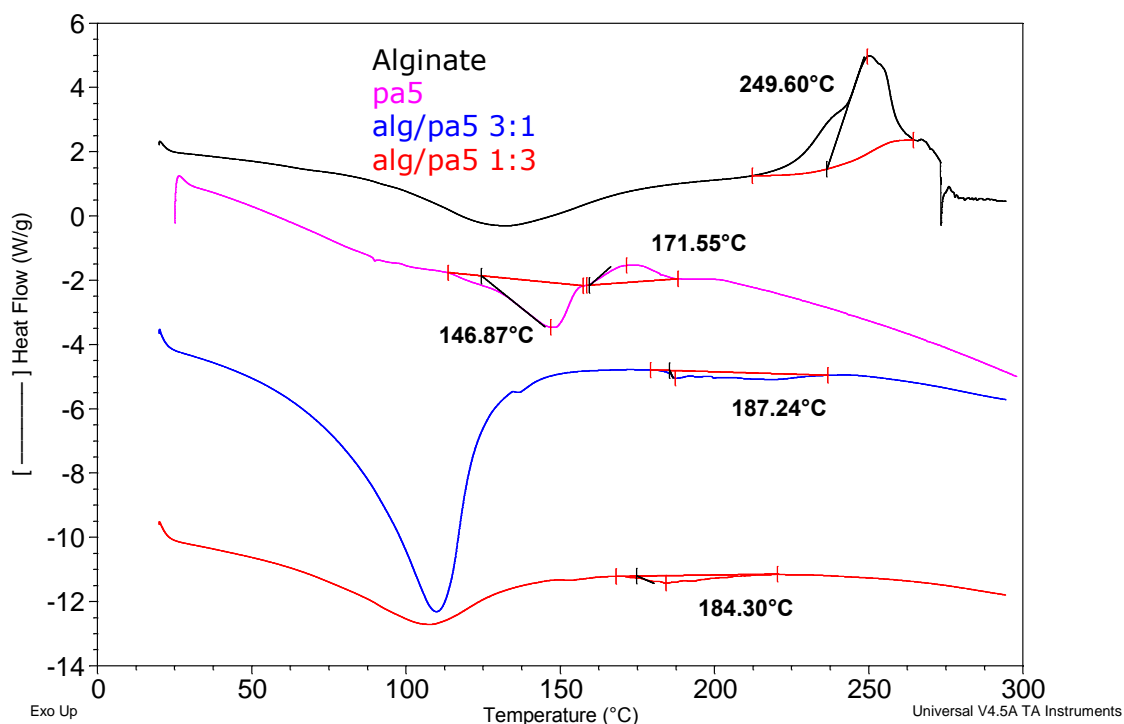


Figure 3.22 DSC thermogram of sodium alginate, pa5, alg/pa5 3:1 and alg/pa5 1:3 (A) sodium alginate and pa5 (B) pa5 based complexes.

According to the DSC thermogram of alg/pa5 3:1 complex (figure 3.22), the complex does not exhibit the same thermal events as either pa5 or alginate alone, it would appear that the resultant complex led to changes in one or both of the constituent PEs. As alginate is the chief component in alg/pa5 3:1, it would be expected to exhibit an exotherm at 249°C, this was however absent, as the only thermal event detected was an indistinct signal at 187°C.

Meanwhile hot-stage images of alg/pa5 3:1 complex (figure 3.23), showed discolouration beginning at 185°C which is similar to alginate alone. Therefore it was unclear whether any changes in thermal properties had occurred.

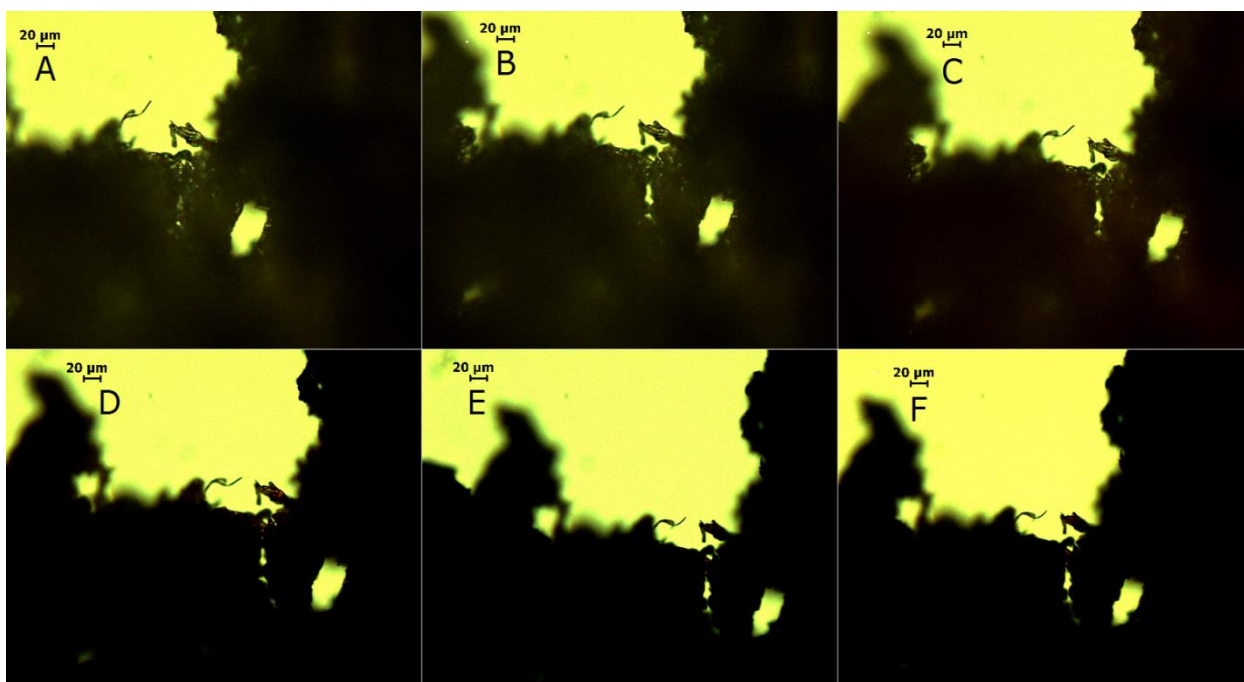


Figure 3.23 Hot-stage images of alg/pa5 3:1 complex at magnification x20. (A) Room temperature (B) 105°C (C) 185°C (D) 225°C (E) 285°C (F) cooled to room temperature.

There appears to be differences between alg/pa5 3:1 and alg/pa2.5 3:1, which as discussed above, resulted in a reduced temperature of onset of discolouration. The difference in hydrophobic grafting between pa2.5 and pa5 may have some role in the observed disparity.

DSC investigation of alg/pa5 1:3 (figure 3.22) complex showed a possible thermal event at 184°C. It may be that the DSC device used in this study did not possess the sensitivity to detect a similar endotherm for alg/pa2.5 1:3, indicating that these thermograms may be associated with the small difference in hydrophobic substitution.

Hot stage images (figure 3.24) showed discolouration of the sample beginning at 170°C, becoming more obvious by 220°C and continuing up to 300°C. There was no evidence of melting, which would be expected around 146°C for a complex with a high concentration of pa5. Furthermore, the process was irreversible and the sample did not revert to original state on cooling.

As with alg/pa2.5 1:3, there appeared to be a reduction in the temperature of onset of discolouration (assumed to be decomposition), coupled with a change melting properties.

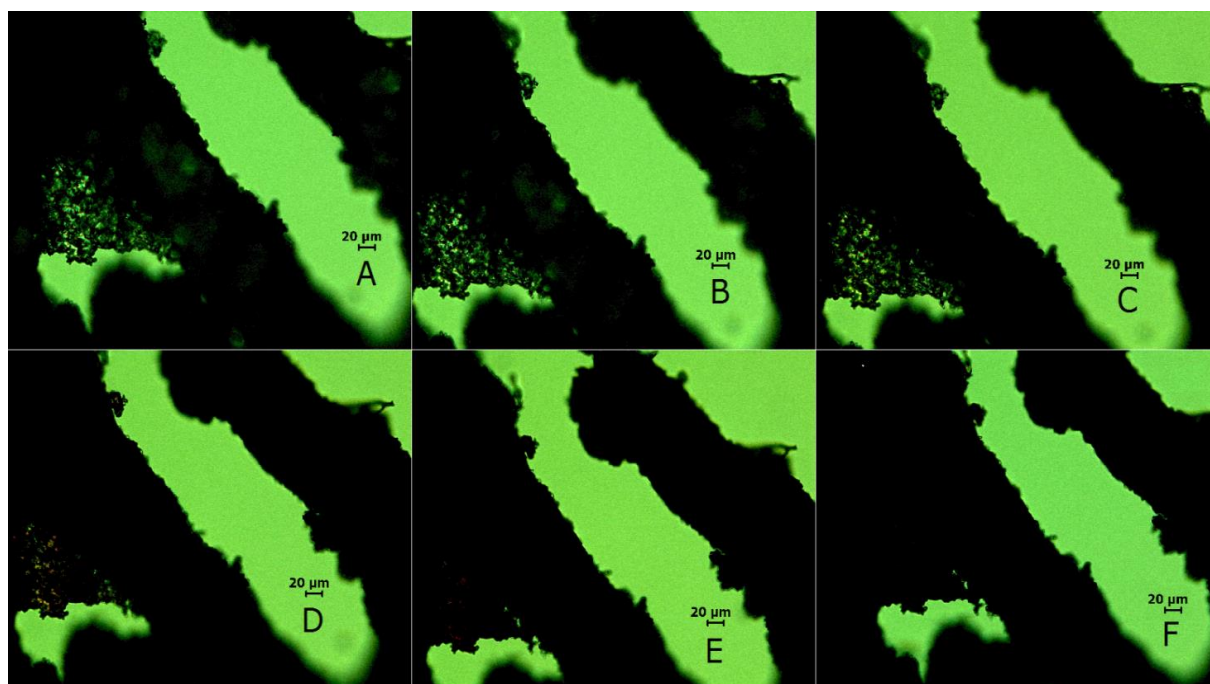


Figure 3.24 Hot-stage images of alg/pa5 1:3 complex at magnification x20. (A) Room temperature (B) 100°C (C) 190°C (D) 240°C (E) 300°C (F) cooled to room temperature.

It appeared that the electrostatic interaction produced a reduction in decomposition temperature, Fang et al found an opposite result using poly(L-glutamic acid) and chitosan to produce PEC microspheres; which showed increased decomposition temperatures compared to individual components (10).

DSC investigations of complexes based on the interaction between Qpa2.5 and alginate can be seen in figure 3.25.

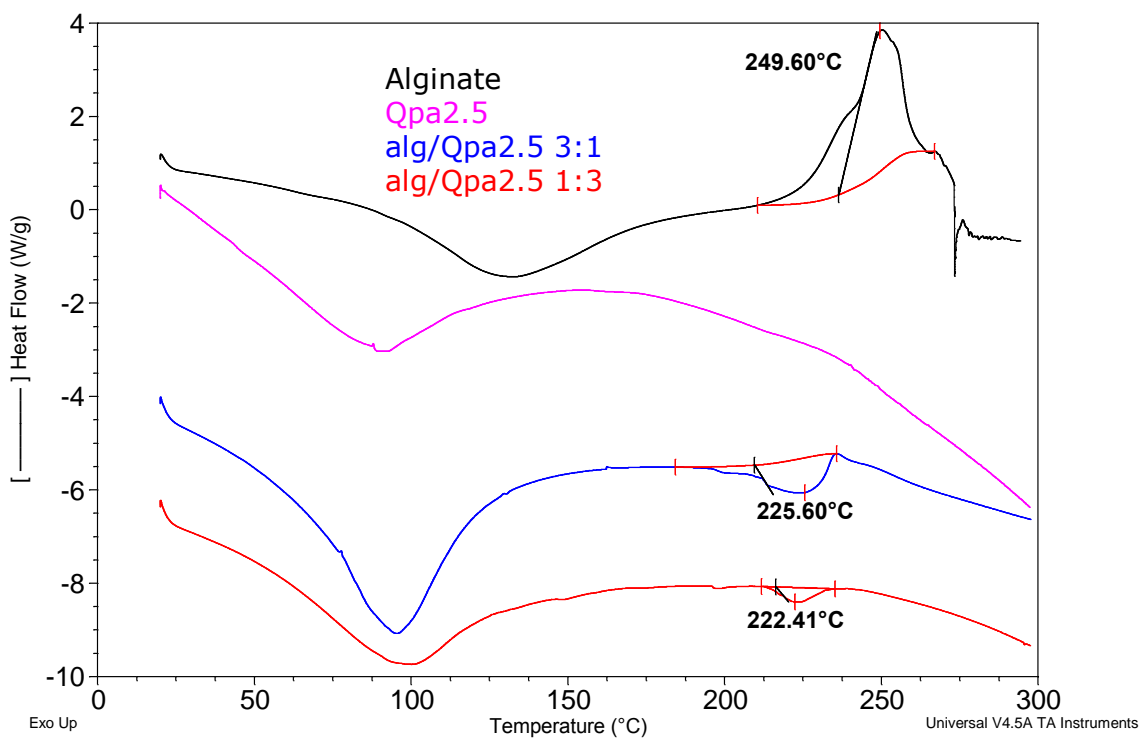


Figure 3.25 DSC thermograms of alginate, Qpa2.5, alg/Qpa2.5 3:1 and alg/Qpa2.5 1:3.

The thermogram of alg/Qpa2.5 3:1 complex showed an endotherm at 225°C, which is distinctly different from individual PEs.

Hot-stage images can be seen in figure 3.26, and showed discolouration of the sample beginning at 195°C, as well as an apparent contraction of the sample. The result appears to indicate the decomposition of the sample in a manner reminiscent of sodium alginate, albeit with an earlier onset of sample contraction, 195°C compared to 230°C for alginate alone.

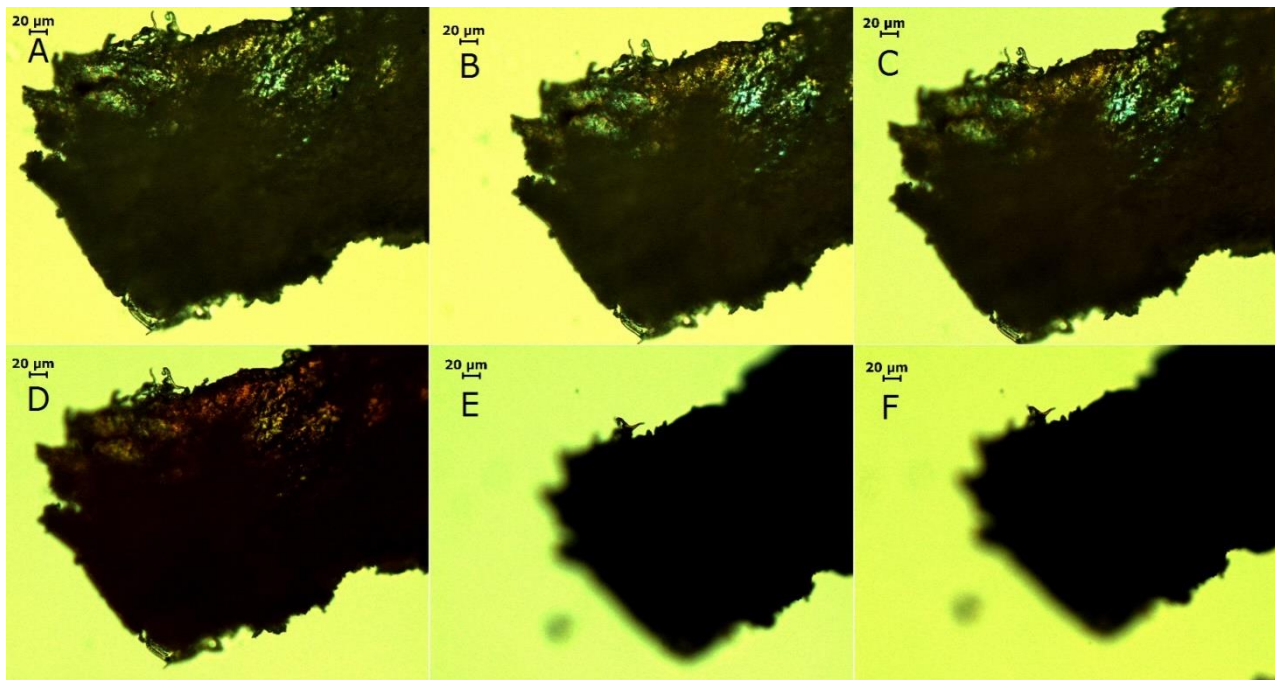


Figure 3.26 Hot-stage images of alg/Qpa2.5 3:1 complex at magnification x20. (A) Room temperature (B) 100°C (C) 170°C (D) 205°C (E) 280°C (F) cooled to room temperature.

DSC results of alg/Qpa2.5 1:3 showed an endotherm at 222°C, which is absent from the thermograms of individual PEs.

Hot-stage images (figure 3.27) showed discolouration of the sample beginning at 200°C and continuing to 270°C. Individual samples of Qpa2.5 did not exhibit discolouration until 255°C. Therefore, it would appear that complexation led to a reduction in what was assumed to be the decomposition temperature of the major constituent of the PEC.

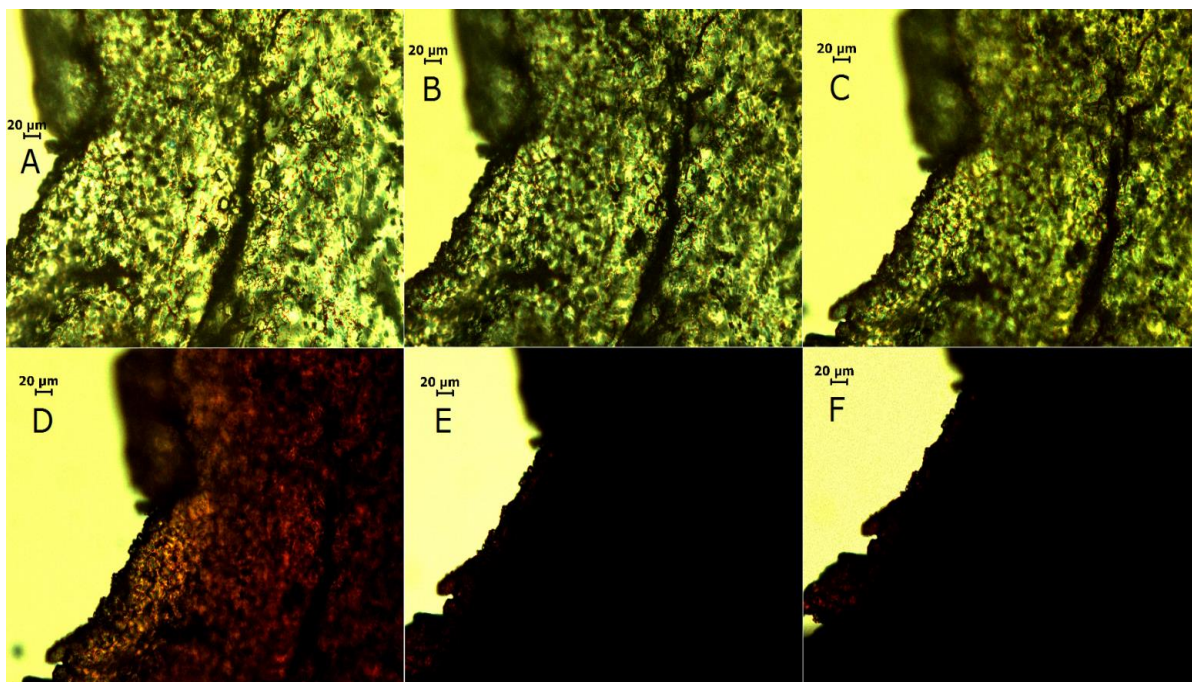


Figure 3.27 Hot-stage images of alg/Qpa2.5 1:3 complex at magnification x20. (A) Room temperature (B) 100°C (C) 200°C (D) 240°C (E) 280°C (F) cooled to room temperature.

Results of DSC for Qpa5 based complexes are shown in figure 3.28.

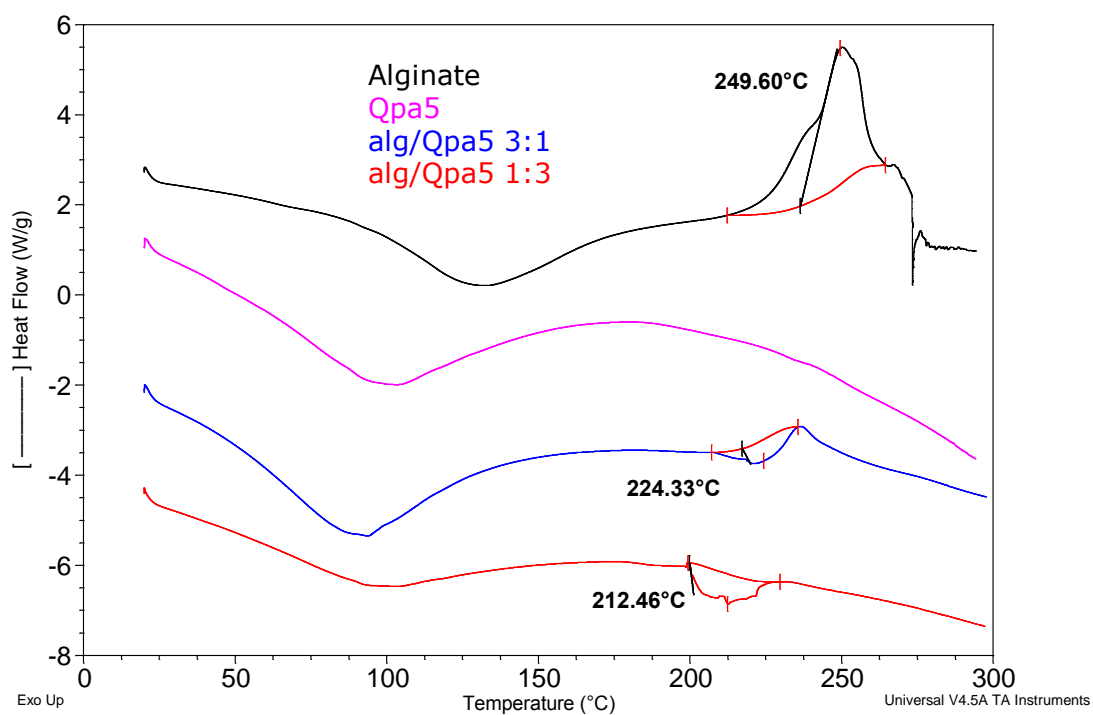


Figure 3.28 DSC thermograms of sodium alginate, Qpa5, alg/Qpa5 3:1 and alg/Qpa5 1:3.

DSC results of alg/Qpa5 3:1 complex showed a thermal event at 224°C, which is distinct from Qpa5 and alginate. The result showed some similarity to that of alg/Qpa2.5 3:1.

Hot stage images (figure 3.29) showed discolouration and contraction beginning at approximately 200°C and continuing to 290°C, which was slightly higher than alginate (190°C). There was no change on cooling to room temperature with discolouration attributed to decomposition.

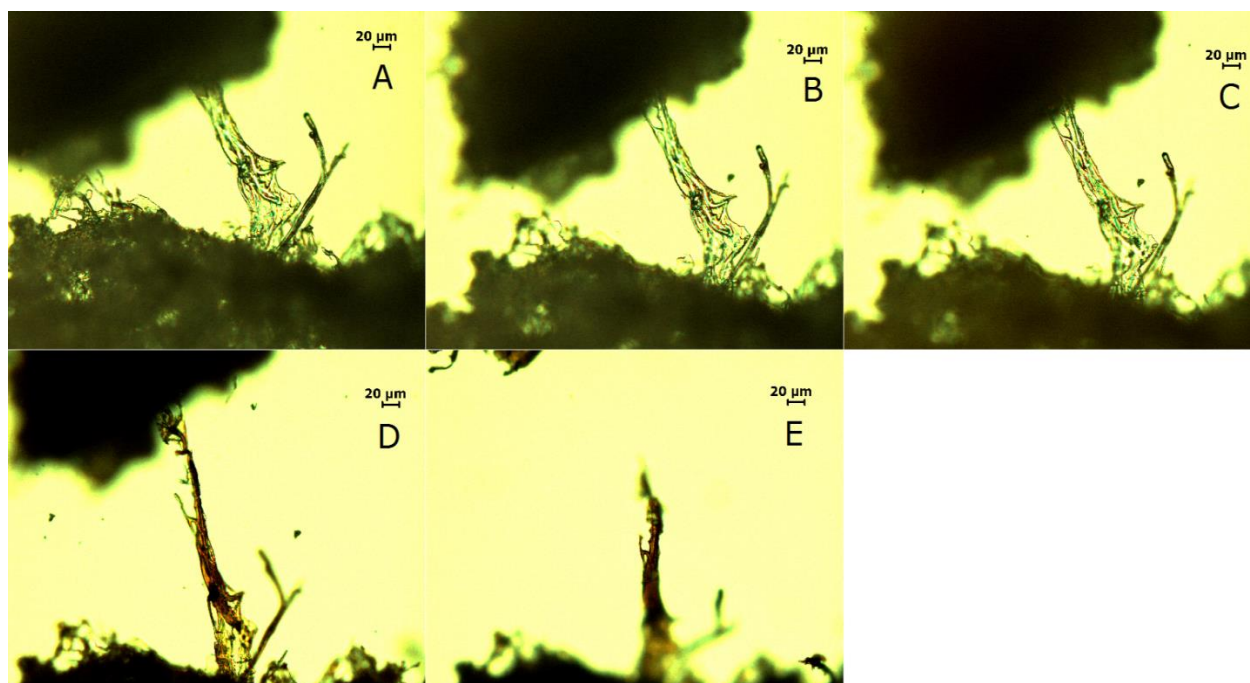


Figure 3.29 Hot-stage images of alg/Qpa5 3:1 complex at magnification x20. (A) Room temperature (B) 100°C (C) 180°C (D) 240°C (E) 290°C.

The DSC results of alg/Qpa5 1:3 complex (figure 3.28), showed an endotherm at 212°C, which was again different from either component. While hot-stage images (figure 3.30) showed discolouration and contraction beginning at 185°C continuing up to 290°C. Qpa5 alone did not show signs of discolouration until 240°C, indicating a possible reduction in temperature of decomposition in a result similar to alg/Qpa2.5 1:3.

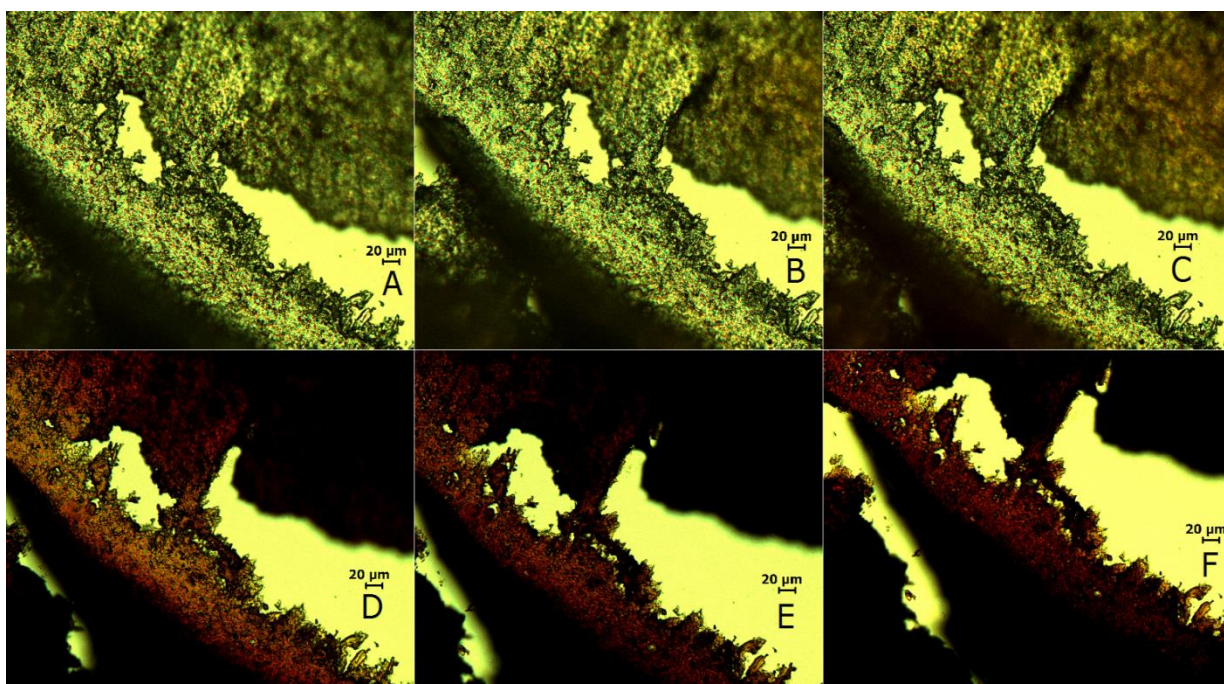


Figure 3.30 Hot-stage images of alg/Qpa5 1:3 complex at magnification x20. (A) Room temperature (B) 100°C (C) 170°C (D) 240°C (E) 290°C (F) cooled to room temperature.

It would appear that the electrostatic interaction between PEs led to the formation of complexes which had different thermal properties than the component PEs alone. In the case of pa2.5, the pair of endotherms discussed in chapter 2 were consistently absent from thermograms of complexes. Furthermore, there was no observable evidence of melting for alg/pa2.5 1:3 even though pa2.5 was in the majority. Additionally, the endotherm and exotherm pairing of pa5 was absent from alg/pa5 complexes, as was any sign of melting. Qpa5 and Qpa2.5 based complexes, which lacked clear individual thermal signs showed a reduction in apparent decomposition temperature, similarly to non-quaternised complexes. The reduction in decomposition temperature appeared to be clearest in 1:3 complexes regardless of quaternisation, indicating that a small amount of alginate may exert more of an effect on the thermal properties of amphiphilic PEs, than the reverse case of 3:1 complexes.

3.4.6 Transmission electron microscopy

Only a select number of samples were sent for TEM analysis due to cost. Therefore alg/pa2.5 1:3, alg/Qpa2.5 3:1, and alg/Qpa2.5 1:3 were chosen based on the stability and size data acquired from DLS, %Transmittance and Zeta potential. Due

to difficulties that arose at the time of preparation, it was not possible to include alg/pa2.5 3:1 to the list of analysed samples.

Figure 3.31 shows the results for alg/pa2.5 1:3.

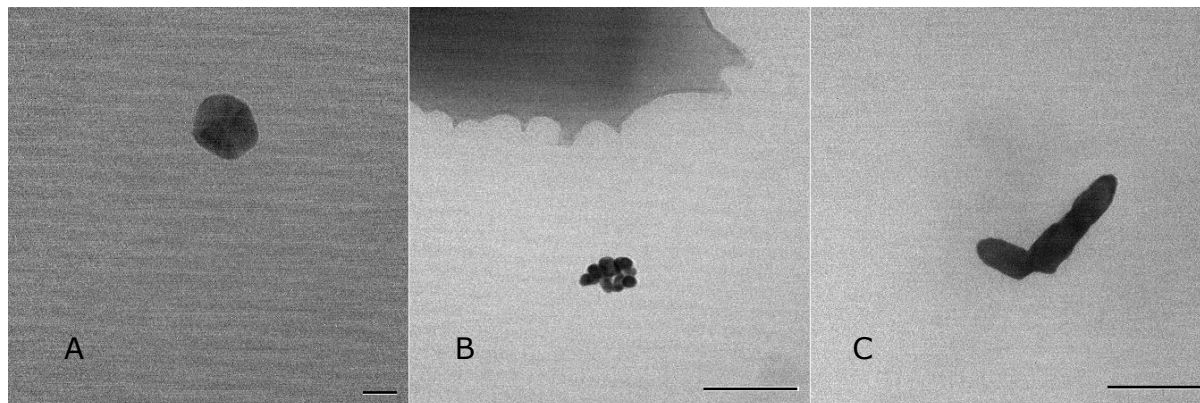


Figure 3.31 TEM images for alg/pa2.5 1:3. (A) 450000x (Bar=20 nm) (B) 245000x (Bar=100 nm) (C) 245000x (Bar =100 nm).

As shown in figure 3.31, alg/pa2.5 1:3 appeared to result in a mixture of spherical, rod shaped, and agglomerated spherical nanoparticles.

Figure 3.32 shows a sample of the TEM results of alg/Qpa2.5 3:1.

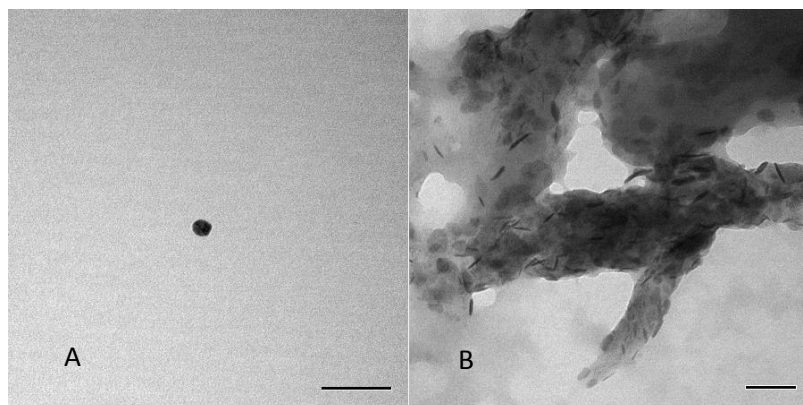


Figure 3.32 TEM images for alg/Qpa2.5 3:1. (A) 180000x (Bar= 100 nm) (B) 130000x (Bar= 100 nm).

Results appeared to show the formation of individual spherical nanoparticles and large agglomerates which may contain spherical and needle shaped structures.

Figure 3.33 shows some of the TEM results of alg/Qpa2.5 1:3.

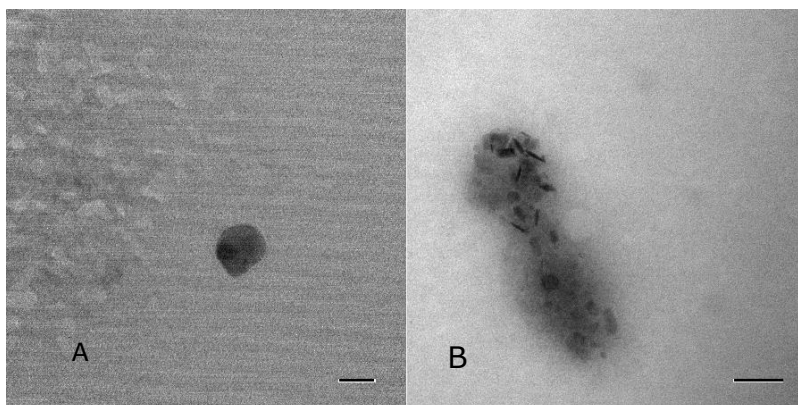


Figure 3.33 TEM images for alg/Qpa2.5 1:3. (A) 450000x (Bar= 20 nm) (B) 130000x (Bar= 100 nm).

The TEM results for alg/Qpa2.5 1:3 indicated the formation of spherical, rod, and needle shaped nanoparticles and were similar to those of alg/Qpa2.5 3:1 (Figure 3.32).

From figures 3.31-3.33, it can be seen that the complexes investigated result in a mixture of different particle morphologies and sizes. The presence of agglomerates in quaternised complex samples may indicate precipitation. However, this was not evident from transmittance or DLS data or visual inspection, and all TEM samples were analysed within 48hr of preparation. Further investigations would be required to ascertain what has caused this apparent agglomeration and if it is possible to separate the individual particles which appeared to be trapped inside this agglomerated structure. Palmitoyl grafted poly (allyl amine) has been shown to form nanoparticles in the literature, Thompson et al. synthesised a 5% palmitoyl grafted poly (allyl amine), which appeared to form discrete nanoparticles with a size range of 80-150nm and was in relatively close agreement with the group's DLS data (4). It was not clear if the smaller individual particles were complexes of alginate and PE⁺ or self-assemblies of PE⁺.

There was quite a discrepancy in size data between DLS and TEM in this experiment, with average Hdd results falling within the range of 150-350nm, while results from TEM showed particles with diameters of much greater range (approximately 25-100nm for discrete particles to several hundred nanometers in the case of agglomerates). This may be due to the dehydration of samples during preparation for electron microscopy which has been found with other polymer nanoparticles in previous studies (14, 15).

3.5 Conclusion

The electrostatic interaction between amphiphilic PEs (quaternised and non-quaternised) and sodium alginate can lead to the formation of nano-sized PECs in the region of 130-400nm. Data from transmittance studies showed some agreement with DLS data.

IR spectroscopy results may have shown some evidence of electrostatic interaction between PEs, with small shifts in the vibrational frequencies of charge carrying sections of PEs, perhaps indicating changes in bond strength.

By investigating the thermal properties of lyophilised samples of PECs and comparing the results with those of individual PEs, it appeared that the electrostatic interaction led to marked changes in the behaviour of samples under investigation, including a change in melting and decomposition temperatures.

Finally, TEM images appear to show PECs resulting in a number of possible conformations including spherical, rod, and needle shaped particles. Whether the aforementioned morphologies are the same in the hydrated state is not known.

Following these findings, a number of the synthesised PECs will be investigated towards further complexation with insulin, discussed in chapter 4.

References

1. B. Sarmiento, S. Martins, A. Ribeiro, F. Veiga, R. Neufeld, D. Ferreira. Development and Comparison of Different Nanoparticulate Polyelectrolyte Complexes as Insulin Carriers. *International Journal of Peptide Research and Therapeutics* 12 (2) (2006) 131-138.
2. C. Thompson, L. Tetley, I. Uchegbu, W. Cheng. The complexation between novel comb shaped amphiphilic polyallylamine and insulin—Towards oral insulin delivery. *International Journal of Pharmaceutics* 376 (2009) 46–55.
3. N. De Jaeger, H. Demeyere, R. Finsy, R. Sneyers, J. Vanderdeelen, P. van der Meeren, M. van Laethem. Part I: Monodisperse Latices: Influences of scattering angle and concentration of dispersed material. *Particle & particle systems characterization* 8 (1991) 179-186.
4. C. Thompson, C. Ding, X. Qu, Z. Yang, I. Uchegbu, L. Tetley, W. Cheng. The effect of polymer architecture on the nano self-assemblies based on novel comb-shaped amphiphilic poly(allylamine). *Colloid and Polymer Science* 286 (2008) 1511-1526.
5. E. Dragan, S. Schwarz. Polyelectrolyte Complexes. VII. Complex Nanoparticles Based on Poly(sodium 2-acrylamido-2-methylpropanesulfonate) Tailored by the Titrant Addition Rate. *Journal of Polymer Science: Part A: Polymer Chemistry* 42 (2004) 5244-5252.
6. C. Schatz, J. Lucas, C. Viton, A. Domard, C. Pichot, T. Delair. Formation and Properties of Positively Charged Colloids Based on Polyelectrolyte Complexes of Biopolymers. *Langmuir* 20 (2004) 7766-7778.
7. J. Koetz, S. Kosmella. *Polyelectrolytes and Nanoparticles*. Berlin : Springer; 2007.
8. S. Honary, F. Zahir. Effect of Zeta Potential on the Properties of Nano-Drug Delivery Systems – A Review (Part 2). *Tropical Journal of Pharmaceutical Research* 12 (2) (2013) 265-273.
9. G. Lawrie, I. Keen, B. Drew, A. Chandler-Temple, L. Rintoul, P. Fredericks, L. Grøndahl. Interactions between Alginate and Chitosan Biopolymers Characterized Using FTIR and XPS. *Biomacromolecules* 8 (2007) 2533-2541.
10. J. Fang, Y. Zhang, S. Yan, Z. Liu, S. He, L. Cui, J. Yin. Poly(L-glutamic acid)/chitosan polyelectrolyte complex porous microspheres as cell microcarriers for cartilage regeneration. *Acta Biomaterialia* 10 (2014) 276-288.

11. P. Li, Y. Dai, J. Zhang, A. Wang, Q. Wei. Chitosan-Alginate Nanoparticles as a Novel Drug Delivery System for Nifedipine. *International journal of Biomedical science* 4 (3) (2008) 221-228.
12. L. Wang, E. Khor, L. Lim. Chitosan-Alginate-CaCl₂ System for Membrane Coat Application. *Journal of Pharmaceutical Sciences* 90 (8) (2001) 1134-1142.
13. J. Soares, J. Santos, G. Chierice, E. Cavalheiro. Thermal behavior of alginic acid and its sodium salt. *Eletica quimica* 29 (2) (2004) 53-56.
14. M. Bodnar, J. Hartmann, J. Borbely. Preparation and Characterization of Chitosan-Based Nanoparticles. *Biomacromolecules* 6 (2005) 2521-2527.
15. K. Douglas, M. Tabrizian. Effect of experimental parameters on the formation of alginate-chitosan nanoparticles and evaluation of their potential application as DNA carrier. *Journal of Biomaterials Science Polymer Edition* 16 (2005) 43-56.

4. Polyelectrolyte interaction with Insulin

Following on from the synthesis of PECs in chapter 3, subsequent work involved the formulation of insulin with selected PECs. Insulin was to be initially mixed with one of the available cationic polyelectrolytes (PE⁺) before the addition of sodium alginate to result in a final alg/PE⁺/insulin polyelectrolyte complex (PEC). The PE⁺ used were either pa2.5 or Qpa2.5 as they were found to form stable PECs (details in chapter 3).

Techniques used in the characterisation of results were similar to those used in chapter 3, and included dynamic light scattering (DLS), infra-red analysis, differential scanning calorimetry (DSC) and hot stage microscopy. Zeta potential and %Transmittance were also used with DLS to achieve a better understanding of the effect of complexation between insulin and the polymers on PEC stability.

The ability of PECs, synthesised from alginate and hydrophobically grafted poly (allyl amine), to protect incorporated insulin from enzymatic degradation by α -chymotrypsin was also investigated by reverse phase high performance liquid chromatography.

4.1 Materials

Recombinant human insulin (Sigma Aldrich), α -chymotrypsin (type II from bovine pancreas, ≥ 40 units/mg protein) (Sigma Aldrich), acetonitrile (HPLC grade) (Fisher Scientific, UK), trifluoroacetic acid (HPLC grade) (Fisher Scientific, UK).

Polyelectrolytes used in the synthesis of PECs included sodium alginate ($M_w = 120000$ - 190000 Da) (Sigma Aldrich, UK), and previously synthesised PE⁺ pa2.5, and Qpa2.5.

4.2 Insulin polyelectrolyte complex formation

Formation of PECs with insulin was based on the work of Thompson et al. (1).

Solutions of alg/PE⁺ 1:3 (where PE⁺ is either pa2.5 or Qpa2.5) with insulin were to be prepared at a mass ratio of 2:1 in a stock of distilled water buffered to a pH of ≈ 8 with 1M hydrochloric acid and 1M sodium hydroxide, henceforth known as solvent.

Insulin (3.3mg) was dissolved in 2.5mL 0.01M hydrochloric acid solution, and PE⁺ (5mg) was sonicated in 2.5mL pH 8 solvent, in separate small vials. The PE⁺ solution was poured by hand into the insulin solution and the pH was adjusted to 8 using 1M hydrochloric acid and/or 1M sodium hydroxide.

Alginate (1.6mg) was dissolved in 5mL pH 8 solvent, and was then added drop-wise to PE⁺/insulin solution from a burette over 5 minutes under gentle magnetic stirring ($n=3$).

Using similar polymer mass ratios, solutions of alg/PE⁺/insulin were prepared at pH 4.6 (for use in Zeta potential; section 4.3.3) using distilled water rather than pH 8 solvent. The final solutions were adjusted to pH 4.6 using 1M hydrochloric acid and/or 1M sodium hydroxide.

4.3 Insulin polyelectrolyte complex characterisation

Characterisation of PEC results was performed in both the liquid state following sample preparation, and in the solid state, following lyophilisation for 24 hours using a freeze drier (VirTis advantage, Biopharma Process Systems, UK).

4.3.1 Dynamic light scattering

Hdd and pdI were determined for samples of alg/pa2.5 and alg/Qpa2.5 (1:3), and alg/pa2.5/insulin and alg/Qpa2.5/insulin. Approximately 1mL of sample was added to disposable plastic cuvettes, which were then analysed using a Nano ZS Zetasizer (Malvern instruments, UK) at a temperature of 25°C. Measurements were taken at time points of 0.25, 0.5, 1, 2, 24, and 48 hours after complexation (n=3).

4.3.2 Transmittance studies

Stability of colloidal solutions of alg/pa2.5 and alg/Qpa2.5 (1:3), and alg/pa2.5/insulin and alg/Qpa2.5/insulin were assessed using an UV/Vis spectrometer (Thermo scientific, UK). Using plastic cuvettes, the %transmittance of samples were analysed at a wavelength of 570nm. Measurements were taken immediately after sample preparation (t = 0 hours), as well as after 24 and 48 hours (n=3).

4.3.3 Zeta potential

Samples of alg/pa2.5/insulin, alg/Qpa2.5/insulin and insulin alone were analysed at pH 4.6 and 8 using a Nano ZS Zetasizer (Malvern instruments, UK) in folded capillary plastic cuvettes at 25°C (n=1).

4.3.4 Thermal analysis

Solutions of insulin, alg/pa2.5/insulin and alg/Qpa2.5/insulin were lyophilised and investigated using differential scanning calorimetry, where 1-5mg samples were run from 0-300°C at a rate of 20°C/minute under nitrogen environment (n=1). The instrument was pre-calibrated with an indium standard.

Hot-stage microscopy was also used in the investigation of thermal properties of the same lyophilised samples. Samples were observed at x20 magnification from 20°C to 300°C heated at a rate of 5-10°C/minute. Images were captured using a LEICA DFC 420 digital microscope (LEIKA, Germany) coupled to the LINKAM LTS 350 hot-stage (Linkam scientific instruments, UK).

4.3.5 Infra-red analysis

Lyophilised samples of alg/pa2.5/insulin and alg/Qpa2.5/insulin were analysed using a Thermo Nicolet IR spectrophotometer (Thermo Fisher Scientific, USA) with diamond tip accessory after an initial background scan. Samples and background were measured at 32 scans per spectrum between 4000-500cm⁻¹, and analysed using accompanying OMNIC software.

4.3.6 Determination of insulin complexation

Insulin standard calibration curve was prepared using dilutions (0.05, 0.1, 0.5, 0.75, 1.0mg/mL) of insulin. Samples were analysed by HPLC using a Perkin Elmer Series 200EP diode array detector ($\lambda_{\text{Max}}=276\text{nm}$), a series 200 pump, with a series 225 autosampler (injection volume= 100 μL) (n=3). The stationary phase was a BEH 130 C₁₈ column (4.6mm \times 150mm; 151 Å) (Waters Corporation, USA), the mobile phase consisted of 0.3% TFA buffered distilled water and 0.3% TFA buffered acetonitrile using a gradient system whereby water:acetonitrile 75:25 was gradually changed to 50:50 over 10 minutes at a flow rate of 1mL/min, followed by column re-equilibration at 75:25 for 5 minutes. The mean area under the insulin peak was used to plot a calibration graph of area against insulin concentration, accompanying data included the coefficient of determination, and the limits of detection and quantification.

Insulin loaded complexes and insulin stock solutions were subsequently analysed for insulin concentration using the above method (n=3).

Insulin loading was estimated using HPLC data (equation 4.1).

$$\text{Complexation efficiency} = \left(\frac{\text{Detected concentration of insulin in PEC}}{\text{Concentration of insulin stock solution}} \right) \times 100$$

Equation 4.1 Estimation of the complexation efficiency of insulin in final polyelectrolyte complex formulation.

4.3.7 α -Chymotrypsin enzyme study

The ability of insulin incorporated PECs to resist enzymatic degradation of α -chymotrypsin was investigated using samples of alg/pa2.5/insulin and alg/Qpa2.5/insulin and an insulin only control.

Solutions of α -chymotrypsin (2mL; 5mg/mL) and insulin PEC solution alg/PE⁺/insulin at a polymer to insulin ratio of 2:1 (4.5mL; PE⁺ 0.5mg/mL, alginate

0.16mg/mL, insulin 0.33mg/mL) were prepared at pH 8 on the day of experimentation. Both solutions were incubated for 1 hour at 37°C using a water bath. Following this, α -chymotrypsin (0.05ml; 5mg/mL) was added to the insulin PEC solution. Aliquots of the enzyme-PEC solution (0.2ml) were withdrawn every 15 minutes for 2 hours and added to ice cold TFA solutions (0.015mL, 0.1% (v/v)) in order to halt all enzymatic activity at the point of withdrawal (n=3).

4.3.8 Transmission electron microscopy

Solutions of alg/pa2.5/insulin, alg/Qpa2.5/insulin were freshly prepared and sent for transmission electron microscopy (TEM) at the electron microscopy research services facility at Newcastle University. Using a Philips CM100 TEM with compustage and high resolution digital image capture, a number of images were procured for each sample.

4.4 Results and discussion

4.4.1 Dynamic light scattering

The results of DLS for alg/PE⁺/Insulin can be seen in figure 4.1. The effect of the addition of insulin to PEC formation appeared to have led to some changes in size data. In the case of alg/pa2.5/Insulin there appeared to be little change with regard to Hdd. However, the complexation of insulin with the quaternised PEC appeared to lead to an increase in Hdd values.

The change in Hdd, or lack thereof, could be due to the way insulin interacts with the other components of the PEC. For alg/pa2.5/insulin, it may be that insulin predominantly interacts with the hydrophobic core of the PEC and so results in similar or slightly more compact complexes. The interaction of insulin with Qpa2.5 may have involved complexation with the charged surface of the polymer due to the presence of quaternary nitrogen. This could have led to insulin coating the outer layer of the polymer, causing a thicker corona to form and so increasing Hdd values. Thompson et al. prepared complexes of a similar amphiphilic poly (allyl amine) with insulin; a quaternised derivative was also used in combination with insulin. In both cases they found that the addition of insulin led to the formation of nano-sized complexes with reduced Hdd and pdI compared to solutions of amphiphilic polymer (or the quaternised derivative) alone (1). The introduction of sodium alginate in this work and the subsequent change in electrostatic interactions e.g. the competition between insulin and alginate for the positive charge on PE⁺, may be responsible for the difference in DLS data compared to the work of Thompson et al. Hydrodynamic size data appeared to be relatively stable over 48 hours for all complexes suggesting these formulations were stable over that time period.

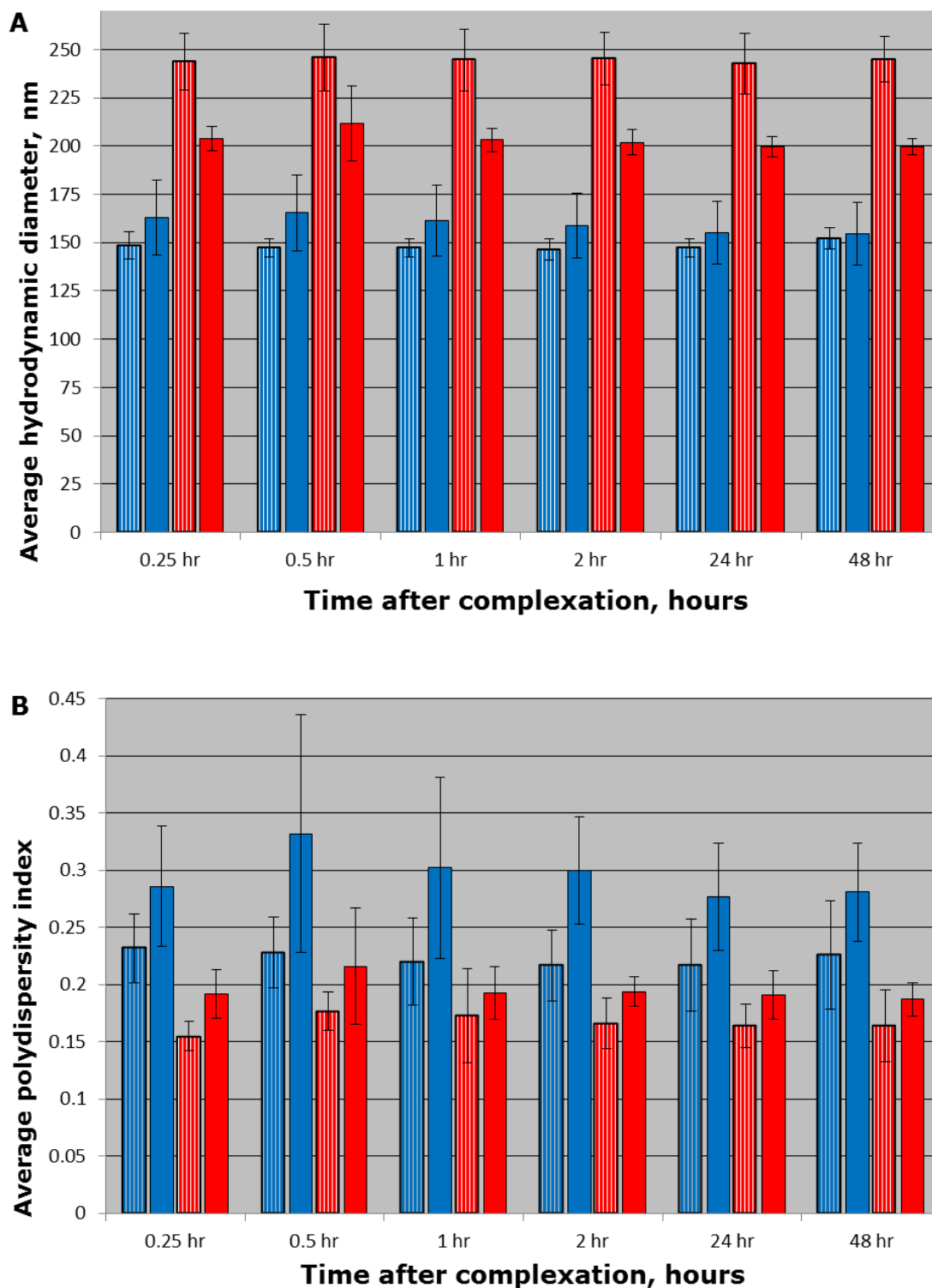


Figure 4.1 Results of DLS for insulin PECs and controls. (A) Comparison of average hydrodynamic diameter (B) Comparison of average polydispersity index. ■■■ alg/pa2.5/Insulin ■ alg/pa2.5 control ■■■ alg/Qpa2.5/Insulin ■ alg/Qpa2.5 control (Mean \pm SD, n=3).

Figure 4.1-B shows the average polydispersity indices over 48 hours. It can be seen that there appeared to be a trend towards a reduction in pdI, which may indicate that the insulin incorporated PECs may lead to the formation of nano-sized aggregates with increased uniformity of size distributions.

4.4.2 Transmittance studies

Figure 4.2 shows the results of transmittance studies for non-quaternised and quaternised PECs with insulin.

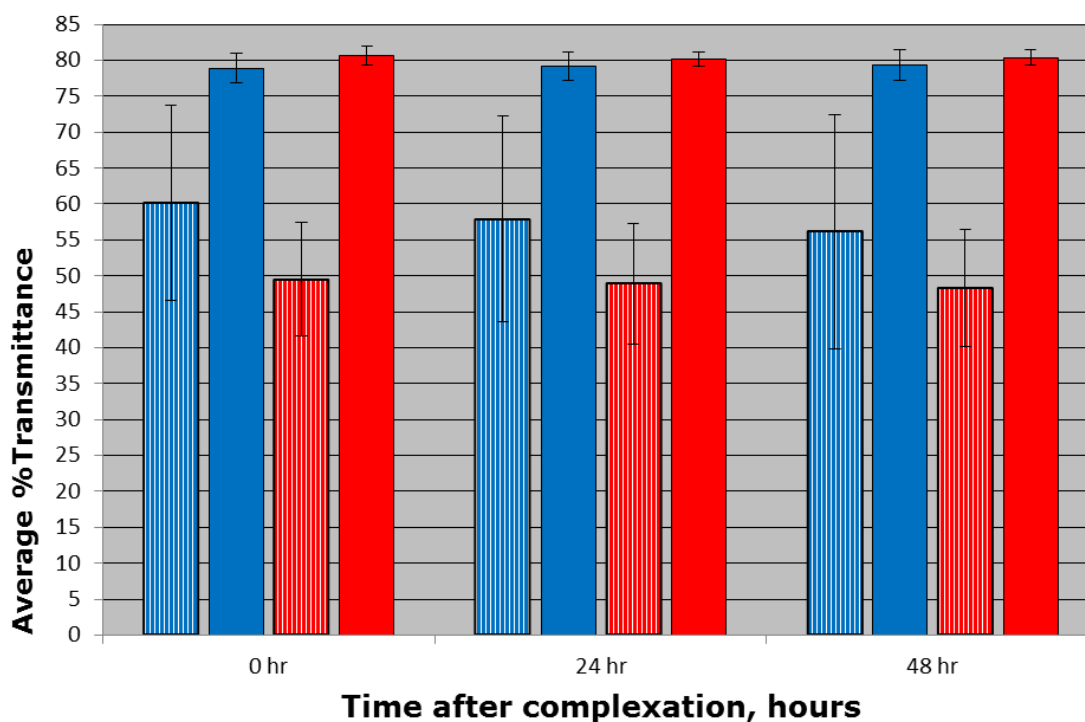


Figure 4.2 Results of %Transmittance studies for insulin PECs and controls.  alg/pa2.5/insulin  alg/pa2.5 control  alg/Qpa2.5/Insulin  alg/Qpa2.5 control (Mean \pm SD, n=3).

The %Transmittance values of insulin PEC sample solutions showed a reduction in transmittance of light for non-quaternised and quaternised samples.

On visual inspection insulin PECs were translucent whereas controls were quite clear. This may indicate a degree of particle aggregation in the system, leading to the reduction in light transmittance. Despite the increase in turbidity all transmittance data appeared to remain stable over 48 hours, and there were no obvious signs of precipitation. Coupled with DLS data, it would appear that the

introduction of insulin did not hinder the formation of stable colloidal nano-sized aggregates.

4.4.3 Zeta potential

According to Langkjær et al. the isoelectric point of human insulin is at pH 5.4, above which it is negatively charged and below which it is positively charged (2). At pH 8, insulin and alginate would be expected to be deprotonated and carry negative charges, while pa2.5 and to a lesser degree Qpa2.5, would be expected to show a reduction in positive charge (Section 3.4.3 table 3.7).

PECs with insulin were prepared at pH 4.6 and 8, which were the conditions used in PEC preparation in chapter 3 and enzymatic studies, respectively. Results of Zeta potential are shown in table 4.1.

Table 4.1 Results of Zeta potential for insulin, alg/pa2.5/insulin, and alg/Qpa2.5/insulin (n = 1); [Zeta potential of PEC control].

	pH 4.6	pH 8.0
Insulin control	26.4	-14.1
alg/pa2.5/insulin	56.5 [63.7]	49.2 [50.2]
alg/Qpa2.5/insulin	52.7 [59.3]	51.5 [54.0]

Insulin control showed a reversal of charge around its isoelectric point as expected.

The zeta potential of formulated complexes was consistently positive. The degree of positive charge appeared to be greater when complexes were formulated at a lower pH. This was expected as amine groups of pa2.5 would be more highly protonated at pH 4.6 than at 8.0, alg/Qpa2.5/insulin was less subject to change, probably due to the presence of quaternary ammonium groups.

As discussed in chapter 3, zeta potential measuring ≥ 30 is indicative of colloidal stability, it would therefore appear that synthesised PECs were relatively stable.

Furthermore, the positive potential value measured for insulin based PECs at pH 8 was found to be less than the values measured for insulin free PEC controls discussed in chapter 3 (section 3.4.3 table 3.7), showing a degree of charge neutralisation possibly due to electrostatic interaction between insulin and PE⁺.

However, an unexpected reduction in Zeta potential was found for insulin complexes prepared at pH 4.6 compared to insulin free PEC controls. At pH 4.6, insulin should be positively charged and no additional charge neutralisations would be expected. This may indicate that alg/PE⁺/insulin might have been accompanied by the formation of alg/PE⁺ and alg/insulin complexes as well, leading to a wider distribution of charges and subsequently less definitive results, although there was no clear sign of extra peaks or widening charge distribution on examining zeta potential graphs.

4.4.4 Transmission electron microscopy

Figure 4.3 shows the results of TEM imaging for alg/pa2.5/insulin.

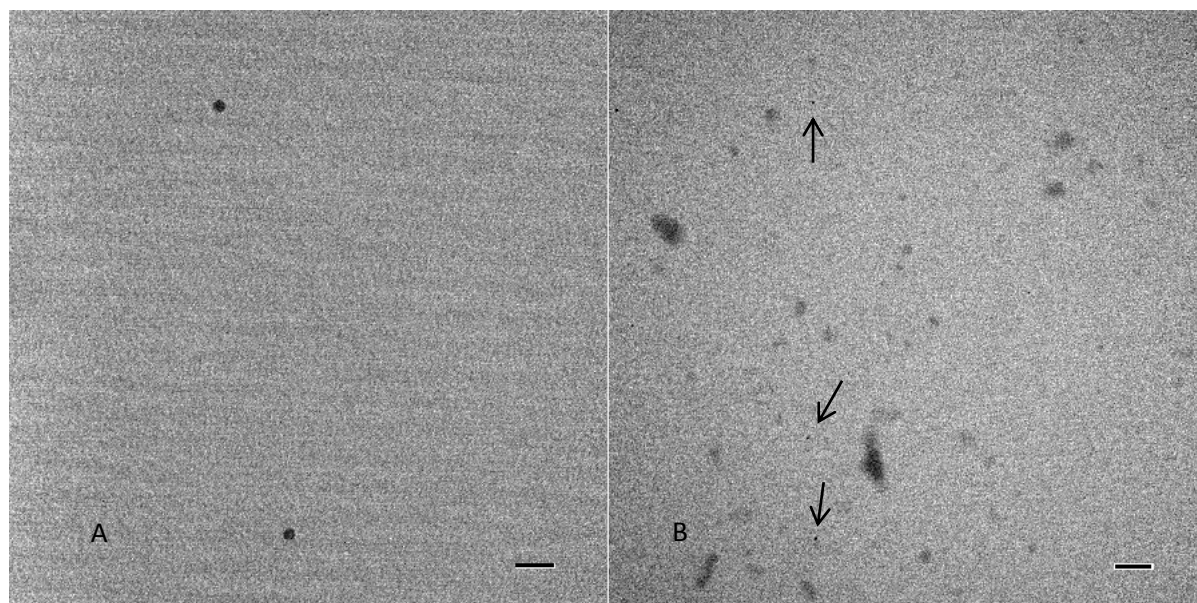


Figure 4.3 TEM images for alg/pa2.5/insulin (A) 340000x (Bar= 20nm) (B) 64000x (Bar =100nm).

It appeared that alg/pa2.5/insulin resulted in small spherical particles less than 10nm in diameter (Figure 4.3-A), and low resolution aggregates that may be accumulated insulin molecules, the arrows in figure 4.3-B indicate the small spherical particles.

Figure 4.4 shows the results of TEM for alg/Qpa2.5/insulin.

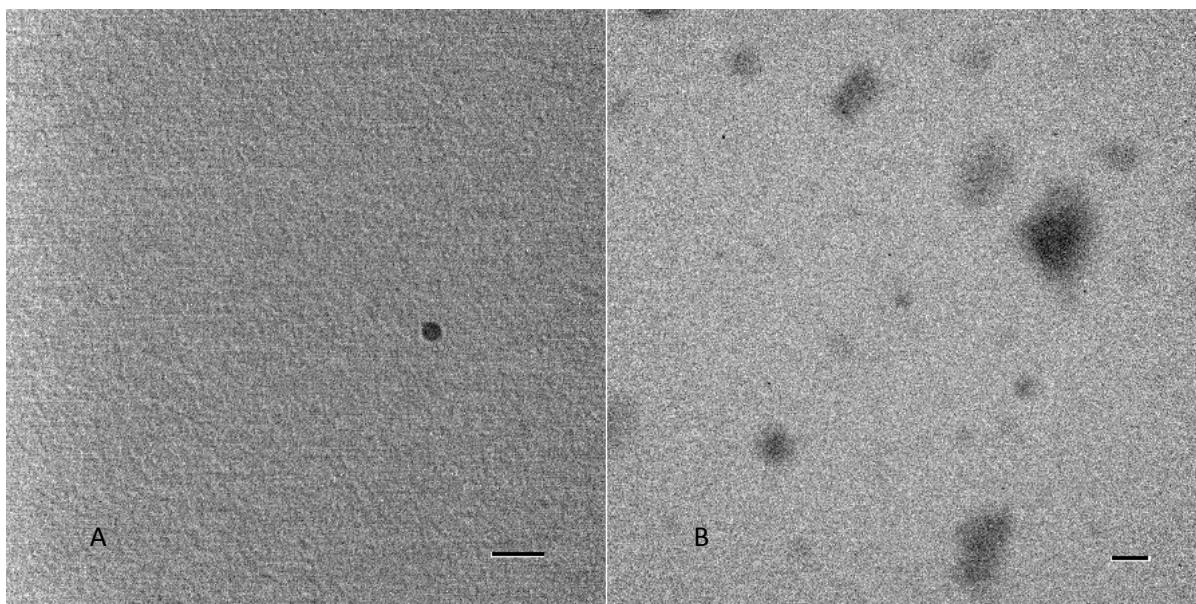


Figure 4.4 TEM images for alg/Qpa2.5/insulin (A) 450000x (Bar= 20 nm) (B) 64000x (Bar= 100 nm).

The results for alg/Qpa2.5/insulin were quite similar to those of alg/pa2.5/insulin, with the appearance of small spherical particles and larger aggregates. As seen in chapter 3 (section 3.4.6), size data from TEM appeared to show smaller particle sizes compared to DLS, which may be due to dehydration of the sample.

The TEM results shown in chapter 3 (section 3.4.6) were based on PECs formed at a pH from 4.6-4.9, whereas those shown in figures 3 and 4 were prepared at pH 8, it would therefore be difficult to compare between the two sets of images with regard to the disappearance of some of the objects seen in chapter 3, such as rod and needle shaped particles, as well as the large 'particle trapping' aggregates.

4.4.5 Thermal analysis

The thermal analysis of insulin and insulin PECs was performed in order to examine the effect of insulin on the thermal properties of the formulations. The thermal properties may also indicate whether an interaction between the polymers and insulin had taken place.

Figure 4.5 shows the results of DSC for insulin and its alg/pa2.5 based complex.

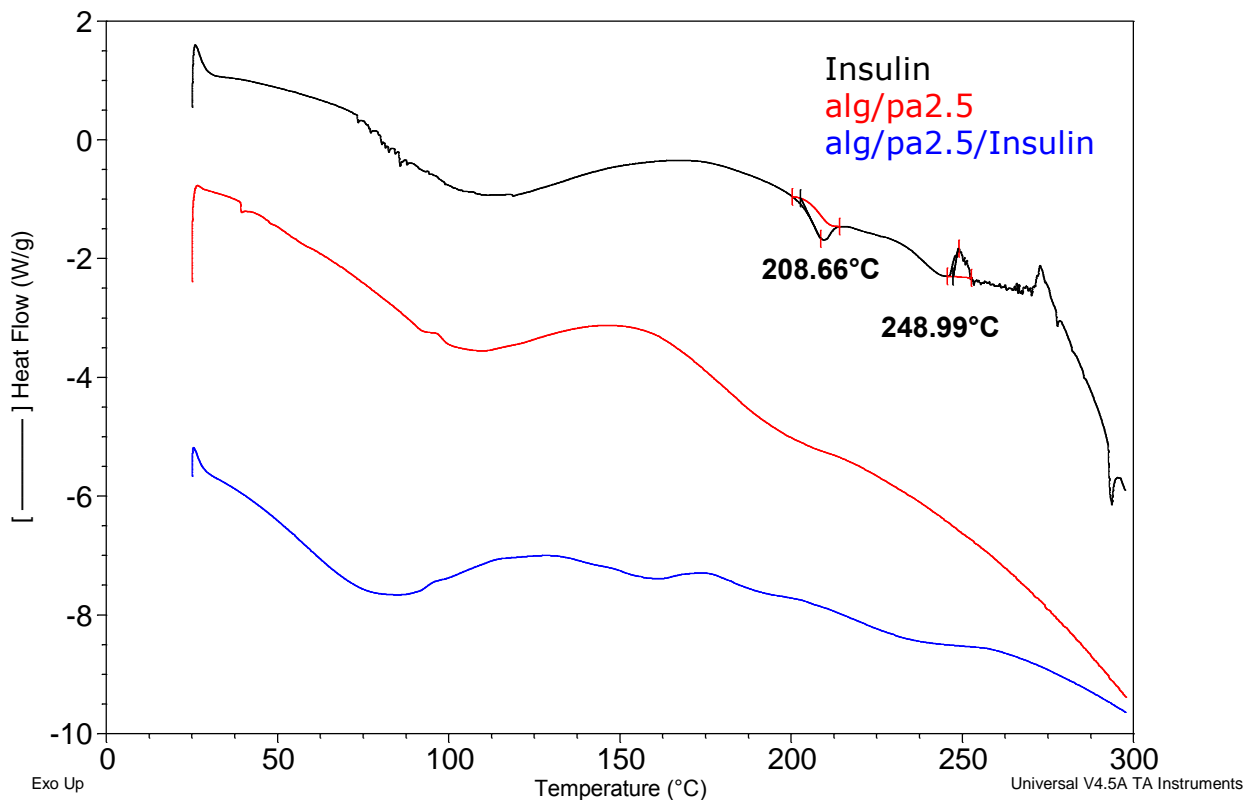


Figure 4.5 DSC thermograms for insulin, alg/pa2.5 and alg/pa2.5/insulin.

Using differential scanning calorimetry and thermogravimetric analysis, Surmacz-Chwedoruk et al. found that insulin appeared to undergo thermal degradation at 269°C with an onset temperature of 208°C (3).

The thermogram for insulin in figure 4.5 shows an endotherm at 208°C, the cause of which is unclear. The exothermic peak at 248°C appears to be indicative of thermal decomposition, especially when viewed in combination with hot-stage images shown in figure 4.6.

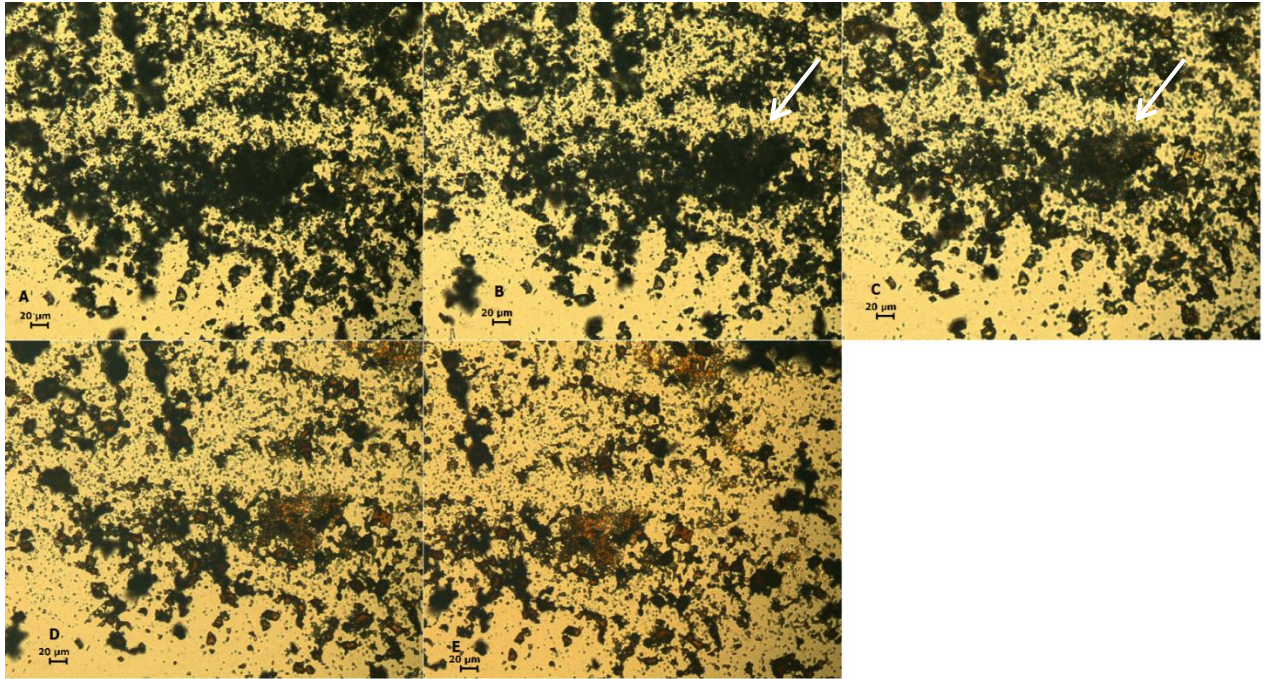


Figure 4.6 Hot stage images of insulin control at magnification x20. (A) Room temperature (B) 100°C (C) 260°C (D) 300°C (E) Cooled to room temperature.

Discolouration of the insulin sample began at 240°C. Insulin is known to denature at temperatures approaching 70°C (4). The degradation assumed to have taken place in figure 4.6 was expected to be degradation at a more fundamental level. The assumption is based on to the observed contraction and discolouration of the sample seen in Figure 4.6, as well as its inability to return to its original state upon cooling. Early signs of discolouration were subtle; the white arrows in panels B and C may help in perceiving the start of discolouration that was more clearly evident in panels D and E.

The complex of alg/pa2.5/insulin did not show any clear thermal events when examined by DSC, indicating a possible change in the thermal properties of insulin towards increased thermal stability, which may have been due to interaction with the polymers.

However, Schmidt et al. found that the thermal stability of soy bean protein was decreased rather than increased in the presence of sodium dodecyl sulphate; this was attributed to changes in protein structure due to electrostatic and hydrophobic interactions (5).

Figure 4.7 shows the hot stage images of alg/pa2.5/insulin.

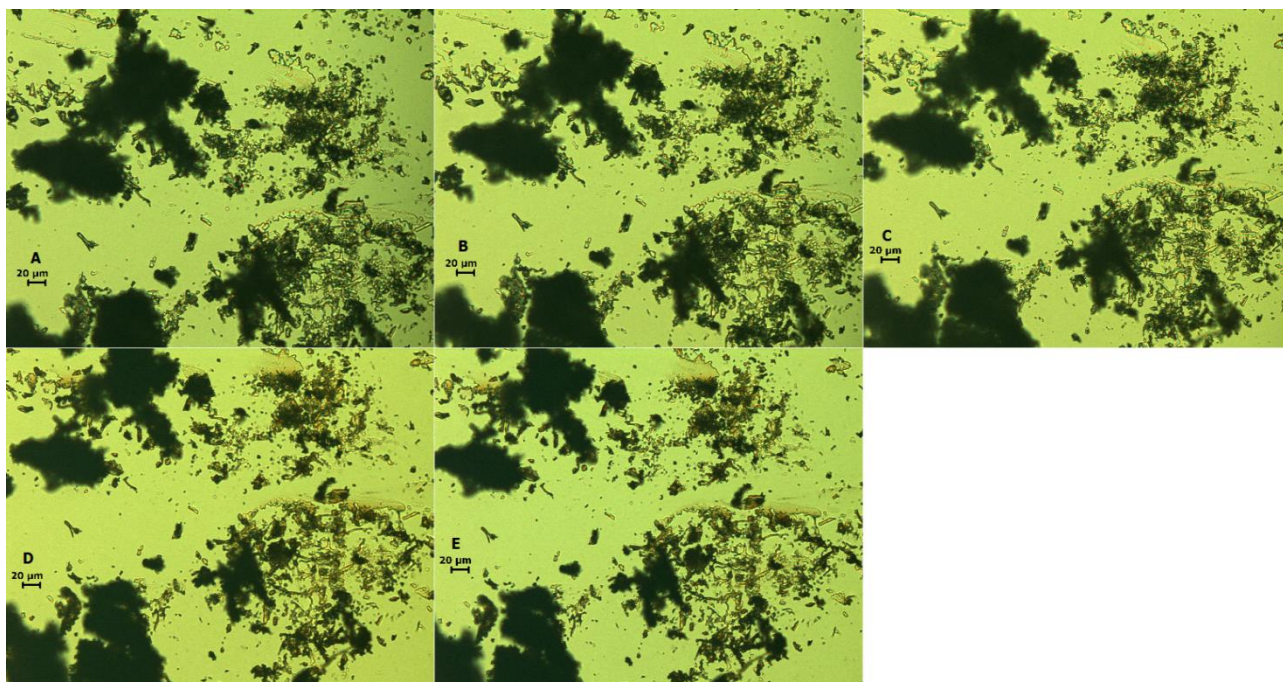


Figure 4.7 Hot stage images of alg/pa2.5/insulin at magnification x20. (A) Room temperature (B) 100°C (C) 190°C (D) 300°C (E) cooled to room temperature.

Lyophilised preparations of alg/pa2.5/insulin began to contract and become irreversibly discoloured at 170°C, which is similar to the hot stage results of alg/pa2.5 1:3 (Section 3.4.5), albeit with a slightly earlier onset of discolouration.

Figure 4.8 shows the DSC results of alg/Qpa2.5/Insulin complex.

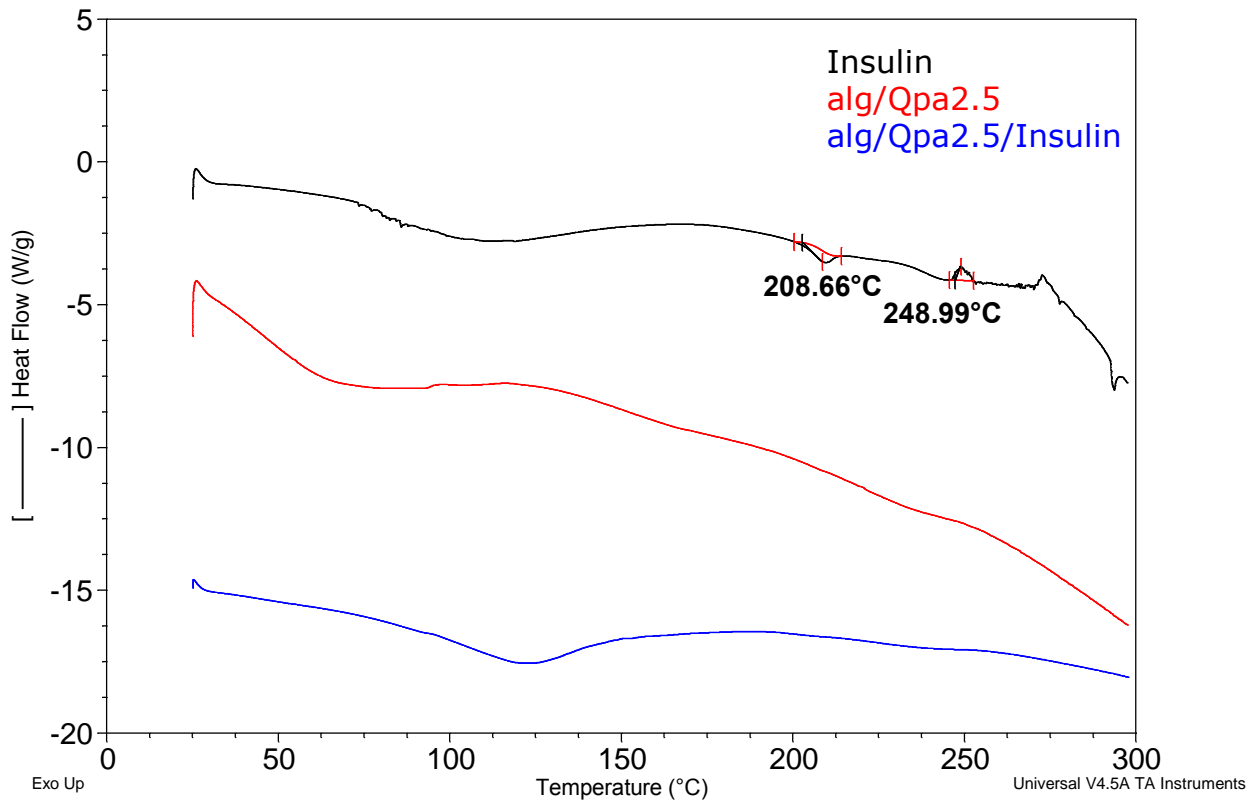


Figure 4.8 DSC thermograms of insulin, alg/Qpa2.5 and alg/Qpa2.5/Insulin.

In a result similar to non-quaternised complexes, alg/Qpa2.5/Insulin did not exhibit any detectable thermal events over the temperature range measured.

It would seem that when used as part of a PEC, the structure of insulin is affected in a way that leads to changes in its thermal properties.

Figure 4.9 shows hot stage images of alg/Qpa2.5/insulin.

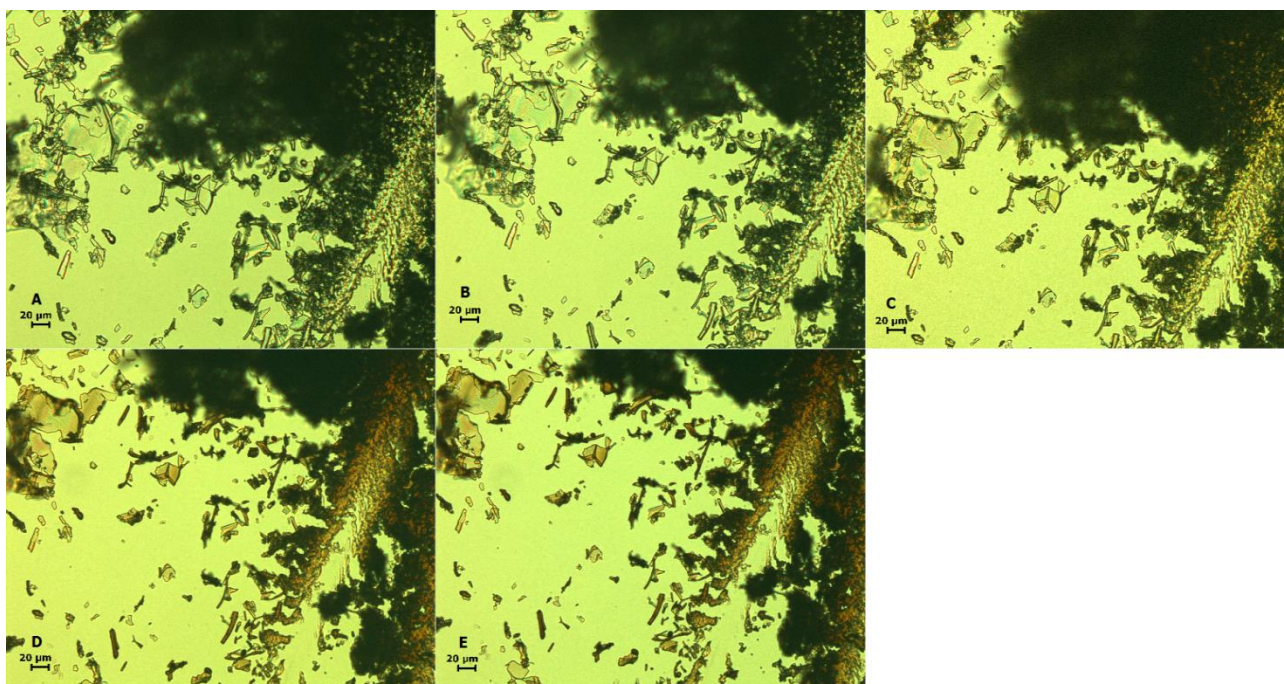


Figure 4.9 Hot stage images of alg/Qpa2.5/insulin at magnification x20. (A) Room temperature (B) 100°C (C) 250°C (D) 300°C (E) Cooled to room temperature.

Figure 4.9 appeared to show sample discolouration beginning at approximately 220°C, while sample contraction began at 280°C. This result was slightly greater than temperatures seen with alg/Qpa2.5 1:3 alone (200°C).

Again it would seem that the only change with the addition of insulin was the appearance of sample contraction and slight changes in temperature of onset of sample discolouration. Sarmiento et al. found that the apparent decomposition temperature of unloaded alginate/chitosan nanoparticle was different from that of equivalent insulin-loaded nanoparticles (6). The changes in apparent decomposition temperatures were different between non-quaternised (earlier onset of discolouration) and quaternised insulin PECs (later onset of discolouration), suggesting a difference in the interaction with insulin of the two types of PECs.

4.4.6 Infra-red analysis.

Lyophilised samples of PECs and insulin control were investigated by IR analysis in order to help understand whether an electrostatic interaction had taken place between the PE components.

Figure 4.10 shows the results of IR analysis for insulin control, and alg/pa2.5 based PECs.

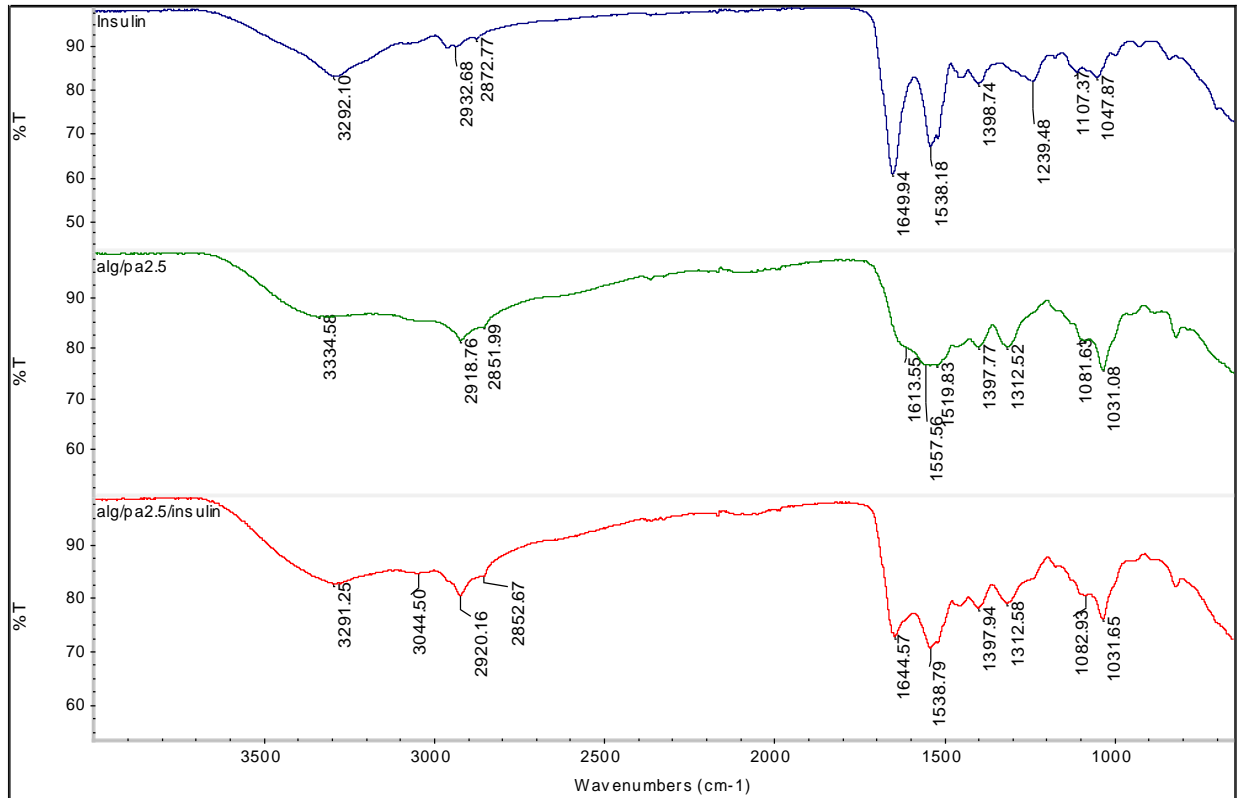


Figure 4.10 IR spectra of insulin alone, alg/pa2.5 PEC, and alg/pa2.5/insulin PEC.

Insulin exhibits amide stretching bands at 1649cm^{-1} and 1538cm^{-1} , a common feature in IR spectra of peptides and proteins (7).

The spectrum of alg/pa2.5/Insulin combines aspects of all three components, alginate is represented by C-O-C stretching bands at $1031\text{--}1082\text{cm}^{-1}$, pa2.5 exhibited C-H stretching vibrations at 2920cm^{-1} and 2852cm^{-1} , while Insulin provided the amide bands at 1644cm^{-1} and 1538cm^{-1} .

The small shift in the amide bands of insulin may indicate some type of interaction with one or both of the components of the PEC. Patil and Devarajan used IR to indicate the association of insulin with alginic acid nanoparticles by the appearance of amide bands associated with peptides (8). While Sarmiento et al. used the same technique albeit using chitosan/alginate/insulin nanoparticles, showing a small shift in the vibrational frequency of an amide band compared to insulin spectrum (6). Both groups attributed small changes in the vibrational frequencies of ionic groups to electrostatic interaction.

Figure 4.11 shows the results of IR analysis for alg/Qpa2.5 based complexes and insulin.

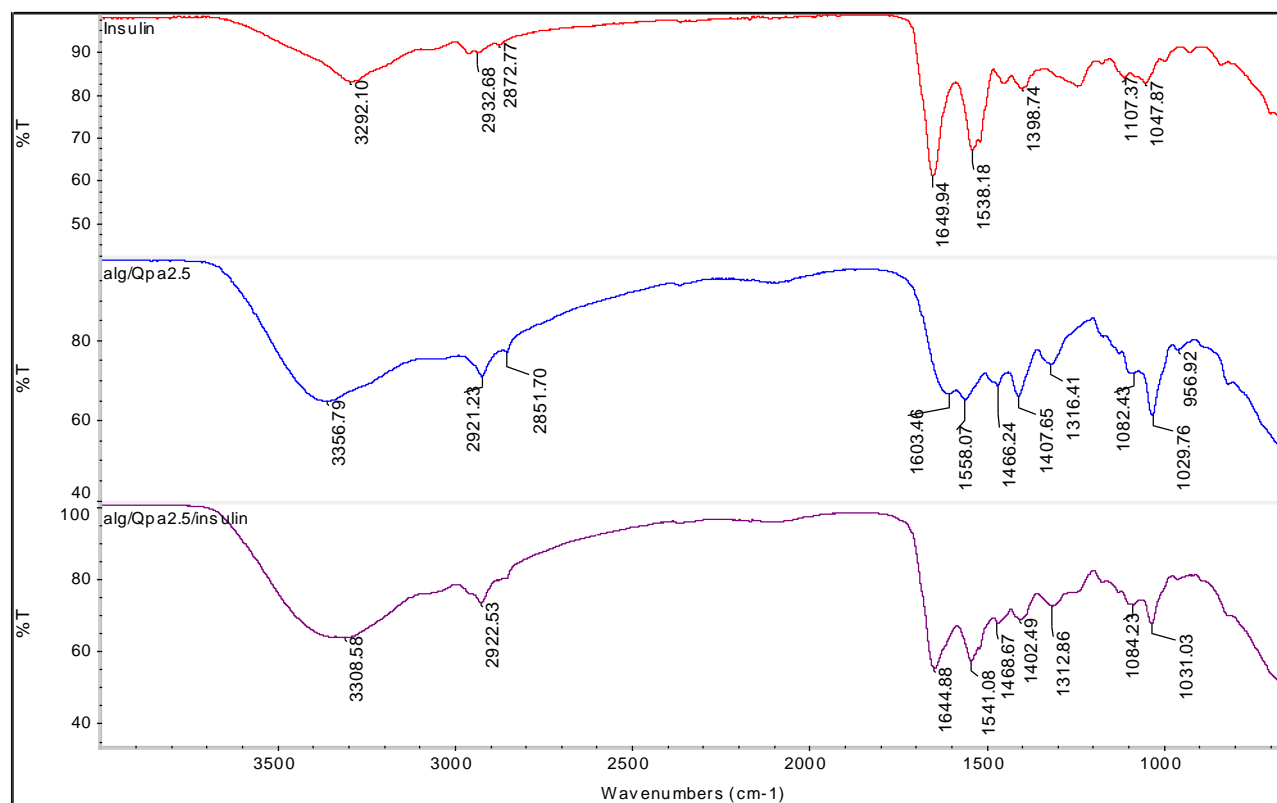


Figure 4.11 IR spectra of insulin alone, alg/Qpa2.5 PEC, and alg/Qpa2.5/Insulin PEC.

The IR spectrum of alg/Qpa2.5/Insulin appeared to show similar results to its non-quaternised equivalent, whereby the amide stretching of insulin appeared to have shifted to 1644cm^{-1} and 1541cm^{-1} . Furthermore, there appeared to be a degree of overlap, leading to the widening of the signal at 1644cm^{-1} compared to 1649cm^{-1} in the insulin spectrum.

4.4.7 Determination of insulin complexation

Figure 4.12 shows the calibration curve prepared from insulin standard solutions using a range of 0.05-1mg/mL dilutions.

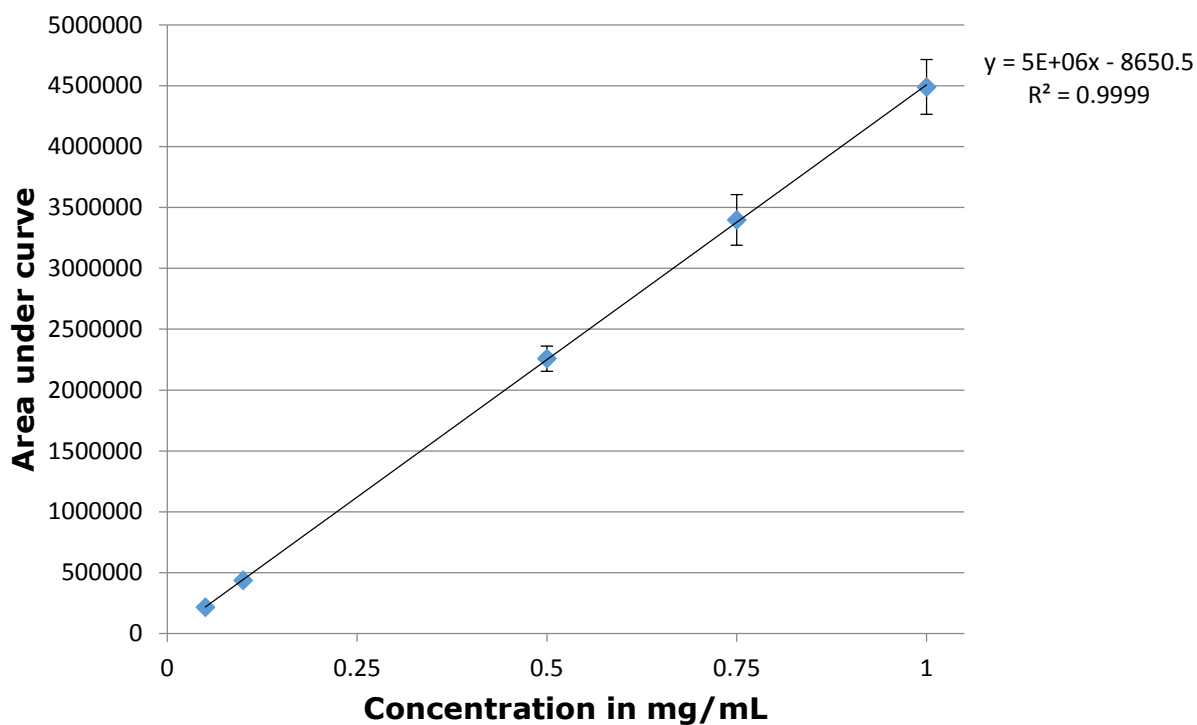


Figure 4.12 Calibration curve of insulin standard solutions (\pm SD, $n=3$).

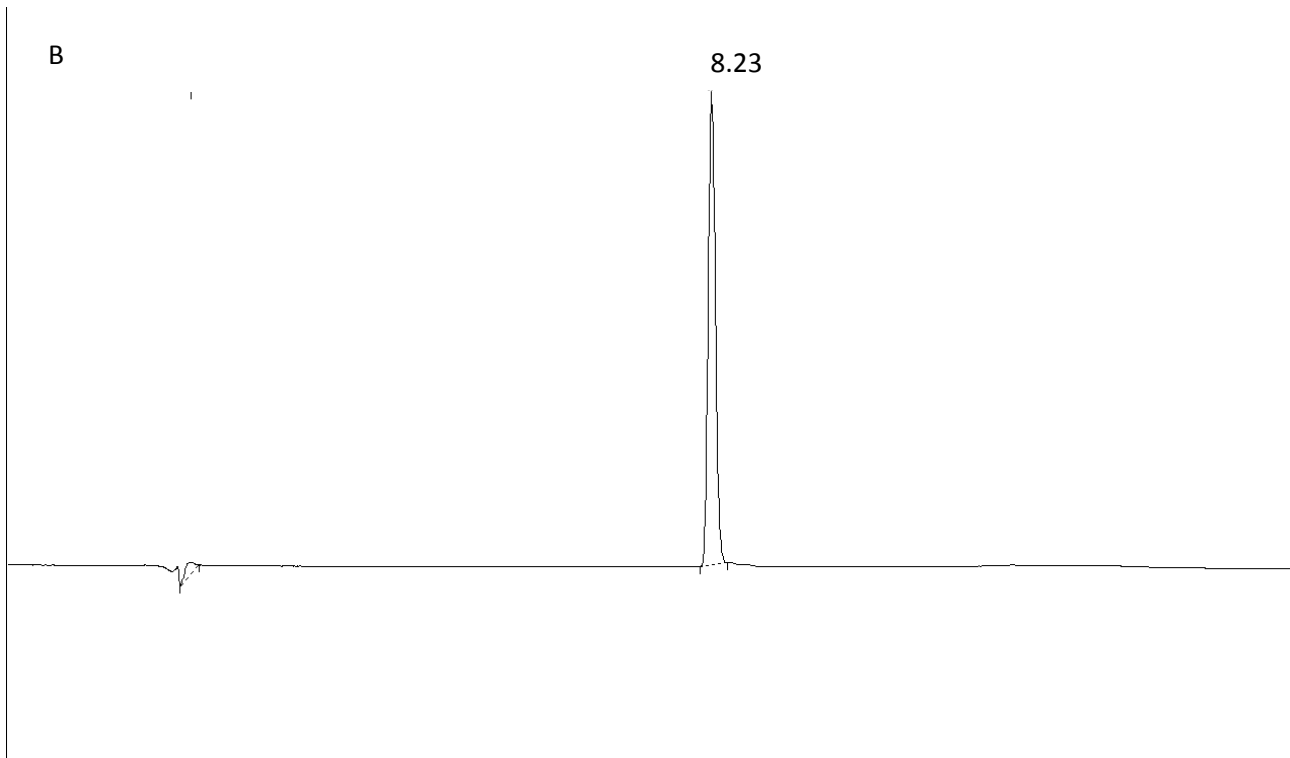
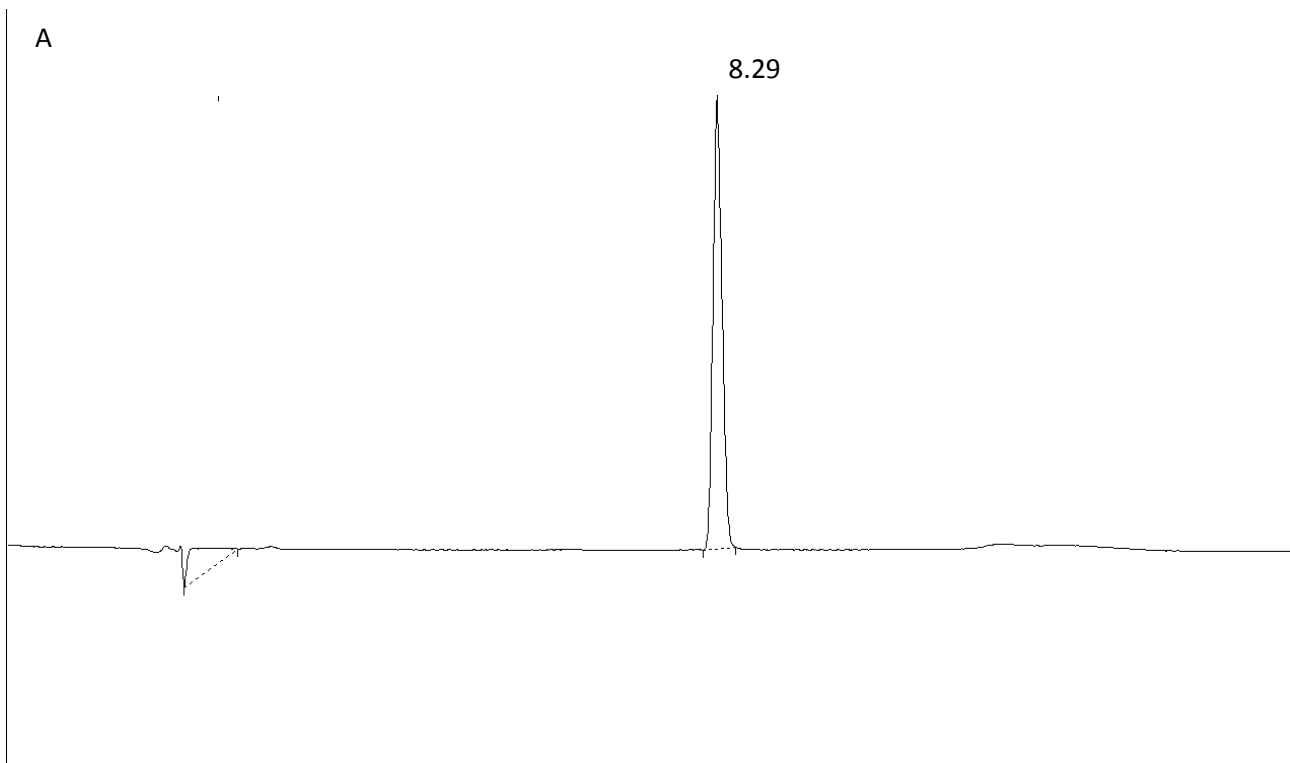
The coefficient of determination (R^2) was found to be 0.9999 while the limit of detection was 0.012mg/mL and limit of quantification was 0.036mg/mL.

Estimations of insulin complexation efficiency can be seen in table 4.2.

Table 4.2 Average estimated complexation efficiency of alg/pa2.5/insulin and alg/Qpa2.5/insulin, ($n=3 \pm$ SD).

Sample	Average complexation efficiency, %
alg/pa2.5/insulin	96.1 (\pm 7.7)
alg/Qpa2.5/insulin	91.4 (\pm 6.1)

Figure 4.13 show the HPLC chromatographs of alg/PE⁺/insulin PECs and insulin control.



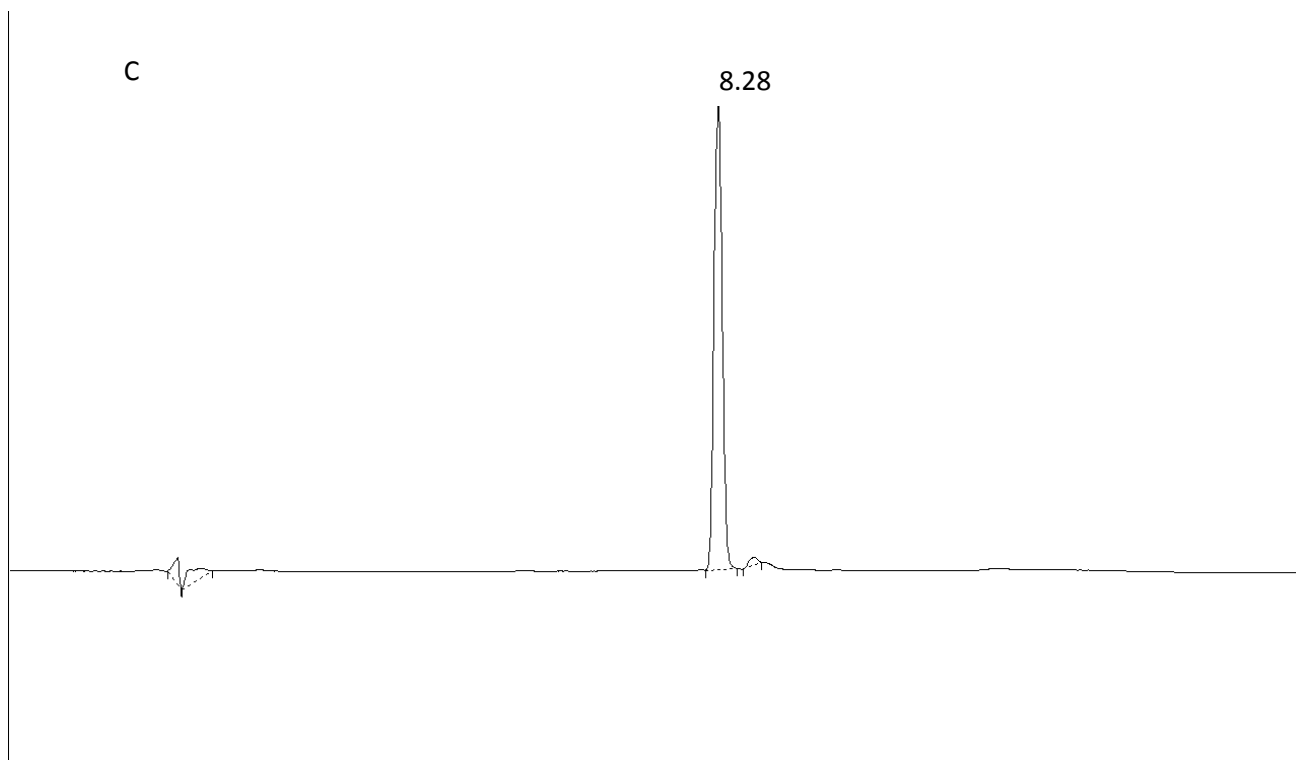


Figure 4.13 HPLC chromatographs with retention times in minutes. (A) Insulin control (B) alg/pa2.5/Insulin (C) alg/Qpa2.5/Insulin.

Results showed that the preparation processes, and assumed complexation appeared to have little to no effect on insulin retention time, with a single peak representing the insulin molecule the only peak detected in all cases. The retention time and area under the curve remained relatively unaffected even after 48 hours.

4.4.8 α -Chymotrypsin enzyme study

Figure 4.14 shows the results of enzymatic studies using PECs with insulin.

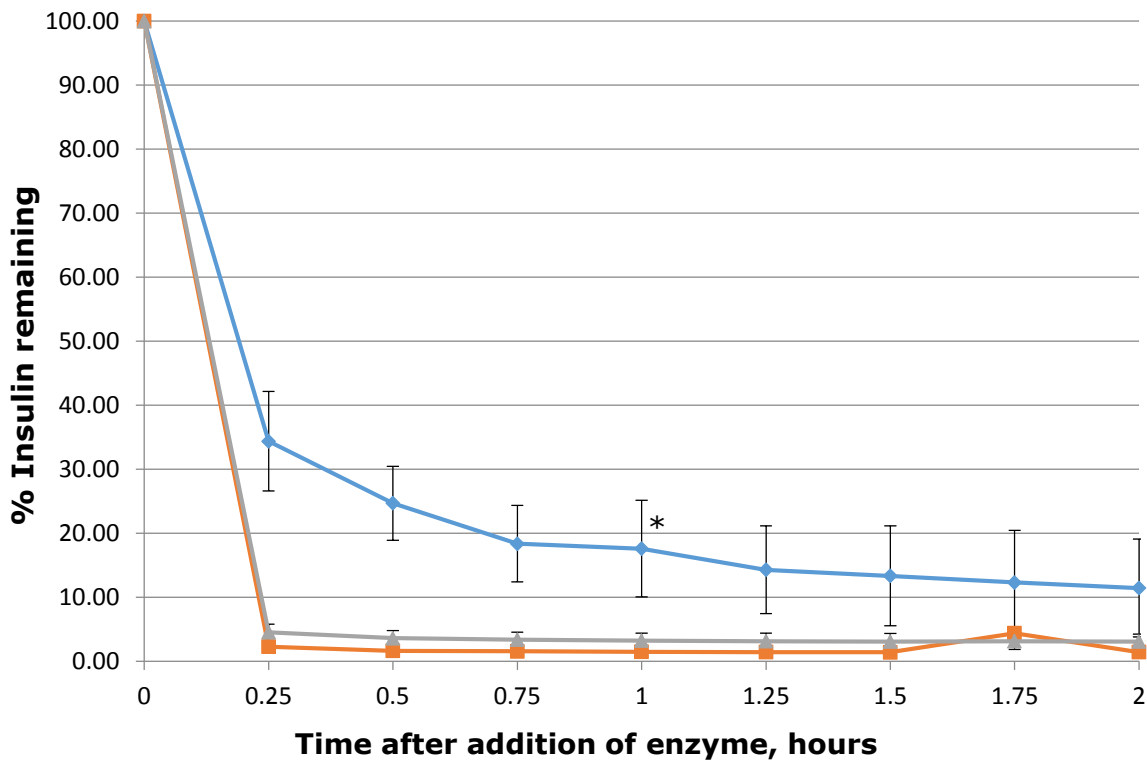


Figure 4.14 Results of α -chymotrypsin enzymatic degradation studies for insulin based PECs. \blacklozenge Insulin control \blacksquare alg/Qpa2.5/insulin \blacktriangle alg/pa2.5/insulin (Mean \pm SD, n=3, * Results at 1 hour mark were based on 2 rather than three data points).

From figure 4.14 it can be seen that approximately 65% of the insulin control sample was degraded within the first 15 minutes. This is similar to the result found by Zhang et al. while studying the stability of insulin in the presence of intestinal proteases (9).

The results showed that complexation with insulin led to an increase in the degradation of insulin incorporated into PECs compared to free insulin control. The reason for this is not known, however it may be the case that the structure of the insulin is altered or uncoiled due to electrostatic interaction and target sites of alpha-chymotrypsin are exposed to the enzyme, leading to the rapid degradation seen over 15 minutes where less than 5% of insulin remained intact. Thompson et al. found a similar result when using PECs of insulin and amphiphilic poly (allyl amine), although their PEC resulted in a smaller increase in insulin degradation in comparison to the findings of this experiment (1).

This may indicate that not only did alginate fail to provide enzyme inhibition by chelation of calcium; it instead may have participated in increasing insulin's

sensitivity to α -chymotrypsin. In comparison, the use of poly (acrylates), polycarbophil and carbomer have been shown to inhibit the activity of α -chymotrypsin in an experiment using solution of poly (acrylates) and N-acetyl-L-tyrosine as enzyme substrate by chelating Ca^{+2} ions which acts as a co-factor in α -chymotrypsin activity (10).

Other PE's have resulted in enhanced enzyme activity, with enzymes such as trypsin and carboxypeptidase B having been shown by Lueßen et al. to have their degradative effects increased in the presence of a chitosan solution in a model using enzyme substrates, no explanation was given as to the cause (11). Kotze et al found that chitosan was not able to protect insulin or buserelin from the enzymatic action of α -chymotrypsin (12).

Despite this result, it was clear that one or both components of the PECs interact with insulin in some way. It may simply be the case of finding the PE, or optimum ratio of PEs, that interact in a manner that leads to the protection rather than the degradation of insulin.

4.5 Conclusion

The results of DLS appeared to show that the Hdd and pdI of resultant PECs was affected by the addition of insulin, the details of this interaction were unclear, but may have been due to a difference in the way insulin interacts with pa2.5 and Qpa2.5. The role of alginate as a competing anionic PE did not appear to be detrimental to PEC formation.

The %Transmittance of light for PECs was less than that for insulin free PECs, regardless of DLS results, although there were no signs of reduced stability over 48 hours.

Zeta potential, as discussed earlier can be used as a measure of stability in colloidal preparations, and appeared to indicate the formation of stable nano-sized colloidal aggregates.

The results of thermal analysis showed that the addition of insulin to PECs appeared to have led to changes in the thermal properties of PEs, which may have been due to changes in interactions and subsequent changes to final PEC structure.

Infra-red analysis, which has been used in the literature to show electrostatic interaction between PEs, appeared to show changes in the vibrational frequencies of charge bearing groups of PEC components, indicating what was presumed to be electrostatic interaction.

Enzymatic degradation studies showed that the prepared PECs were not able to protect insulin from the degradative effects of α -chymotrypsin. Indeed results would show that the interaction between insulin and the polymers used led to more rapid enzymatic cleavage of insulin compared to the peptide alone.

References

1. C. Thompson, L. Tetley, I. Uchegbu, W.P. Cheng. The complexation between novel comb shaped amphiphilic polyallylamine and insulin-Towards oral insulin delivery. *International Journal of Pharmaceutics* 376 (2009) 46-55.
2. L. Langkjær, J. Brange, G. Grodsky, R. Guy. Iontophoresis of monomeric insulin analogues in vitro: effects of insulin charge and skin pretreatment. *Journal of Controlled Release* 51 (1998) 47-56.
3. W. Surmacz-Chwedoruk, I. Malka, Ł. Bozycki, H. Nieznanska, W. Dzwolak. On the Heat Stability of Amyloid-Based Biological Activity: Insights from Thermal Degradation of Insulin Fibrils. *PLoS ONE* 9 (1): e86320. Doi:10.1371/journal.pone.0086320.
4. K. Huus, S. Havelund, H. Olsen, M. van de Weert, S. Frokjaer. Thermal Dissociation and Unfolding of Insulin. *Biochemistry* 44 (2005) 11171-11177.
5. V. Schmidt, C. Giacomelli, V. Soldi. Thermal stability of films formed by soy protein isolate-sodium dodecyl sulphate. *Polymer Degredation and Stability* 87 (2005) 25-31.
6. B. Sarmento, D. Ferreira, F. Veiga, A. Ribeiro. Characterization of insulin-loaded alginate nanoparticles produced by ionotropic pre-gelation through DSC and FTIR studies. *Carbohydrate Polymers* 66 (2006) 1-7.
7. A. Adochitei, G. Drochioiu. Rapid characterization of peptide secondary structure by FT-IR spectroscopy. *Romanian Journal of Chemistry* 56(8) (2011) 783-791.
8. N. Patil, P. Devarajan. Insulin-loaded alginate nanoparticles for sublingual delivery. *Drug Delivery*, Early Online: 1-8. DOI: 10.3109/10717544.2014.916769.
9. L. Zhang, H. Jiang, W. Zhu, L. Wu, L. Song, Q. Wu, Y. Ren. Improving the Stability of Insulin in Solutions Containing Intestinal Proteases *in Vitro*. *International Journal of Molecular Sciences* 9 (2008) 2376-2387.
10. H. Lueßen, B. De Leeuw, D. Perard, C. Lehr, A. De Boer, J. Verhoef, H. Junginger. Mucoadhesive polymers in peroral peptide drug delivery. I. Influence of mucoadhesive excipients on the proteolytic activity of intestinal enzymes. *European Journal of Pharmaceutical Sciences* 4 (1996) 117-128.
11. H. Lueßen, C. Rentel, A. Kotze, C. Lehr, A. De Boer, J. Verhoef, H. Junginger. Mucoadhesive polymers in peroral peptide drug delivery: IV. Polycarbophil and chitosan are potent enhancers of peptide transport across intestinal mucosae *in vitro*. *Journal of Controlled Release* 45 (1997) 15-23.

12. A.F. Kotze, B.J. de Leeuw, H.L. Lueßen, A.G. de Boer, J.C. Verhoef, H.E. Junginger. Chitosans for enhanced delivery of therapeutic peptides across intestinal epithelia: *in vitro* evaluation in Caco-2 cell monolayers. *International Journal of Pharmaceutics* 159 (1997) 243–253.

5. General conclusion

This work showed that amphiphilic poly (allyl amine) and its quaternised derivative were able to form a stable PEC with sodium alginate at investigated mass ratios. Using a simple mixing procedure, solutions of PEs were combined and analysed in the liquid and solid state (following lyophilisation), with results indicating the formation of nano-sized spherical, rod shaped, and aggregated spherical particles. Furthermore, the combination appeared to lead to changes in the physicochemical properties of PEs, such as changes in apparent decomposition temperature. Infra-red analysis was used to show that the electrostatic interaction between charge carrying groups on PEs might be related to shifts in vibrational frequencies of said groups.

The incorporation of insulin into a PEC with alginate and the amphiphilic polymers was undertaken with a view to studying the practicality of these complexes in the enzymatic protection of insulin. Results of DLS analysis suggested the formation of nano-sized aggregates in the range of 150-250nm, while TEM images appeared to show spherical nanoparticles with much smaller dimensions (less than 10nm). The incorporation of insulin into PECs appeared to further alter their thermal properties, leading to additional changes in what was assumed to be the decomposition temperature. As with alg/PE⁺ complexes, changes in IR spectra of alg/PE⁺/insulin complexes were assumed to represent electrostatic interaction between the charged groups of the polymers and insulin. Based on HPLC studies, the process of integrating insulin with the alg/PE⁺ complex was shown to have little to no effect on the insulin molecule, which showed no change in the retention time of the insulin molecule. Furthermore the complexation efficiency of the complexes was found to be greater than 90%.

Finally, the effect of using insulin as part of a PEC with alginate and amphiphilic polymers, in the protection of the insulin molecule from the enzymatic cleavage of α -chymotrypsin was investigated using HPLC. It was found that insulin PECs were not able to protect the peptide from the degradative effects of the enzyme. On the contrary, the incorporation of insulin in the PEC led to acceleration in the breakdown of insulin compared to insulin solution control.

6. Future work

Following on from this work, it would appear that some alterations may be required in order to achieve improved enzymatic protection of insulin. Such future works may include the reduction in level of palmitoylation, while increasing the level of quaternisation. Moreover, the use hydrophobic grafts other than palmitic acid could be investigated.

The use of amphiphilic polymers in combination with an anionic polymer of known enzyme inhibiting characteristics might result in more favourable outcomes. Another possibility is the palmitoylation of the insulin molecule itself rather than just the polymers with a view to enhancing hydrophobic interaction of the peptide with the hydrophobic core of PECs.

Bibliography

- M. Abdel Mouez, N. Zaki, S. Mansour, A. Geneidi. Bioavailability enhancement of verapamil HCl via intranasal chitosan microspheres. *European Journal of Pharmaceutical Sciences* 51 (2014) 59–66.
- A. Adochitei, G. Drochioiu. Rapid characterization of peptide secondary structure by FT-IR spectroscopy. *Romanian Journal of Chemistry* 56(8) (2011) 783-791.
- M. Amidi, E. Mastrobattista, W. Jiskoot, W. E. Hennink. Chitosan-based delivery systems for protein therapeutics and antigens. *Advanced Drug Delivery Reviews* 62 (2010) 59–82.
- J. Anderson, C. Van Itallie. Physiology and Function of the Tight Junction. *Cold Spring Harbor Perspectives in Biology* (2009); 1:a002584.
- T. Aspden, J. Mason, N. Jones, J. Lowe, Ø. Skaugrud, L. Illum. Chitosan as a Nasal Delivery System: The Effect of Chitosan Solutions on in Vitro and in Vivo Mucociliary Transport Rates in Human Turbinates and Volunteers. *Journal of Pharmaceutical Sciences* 86 (1997) 509-513.
- Y. Bai, V. Sachdeva, H. Kim, P. Friden, A. Banga. Transdermal delivery of proteins using a combination of iontophoresis and microporation. *Therapeutic Delivery* 5 (2014) 525-536.
- F. Basmanav, G. Kose, V. Hasirci. Sequential growth factor delivery from complexed microspheres for bone tissue engineering. *Biomaterials* 29 (2008) 4195–4204.
- A. Bernkop-Schnürch, C. Kast, M. Richter. Improvement in the mucoadhesive properties of alginate by the covalent attachment of cysteine. *Journal of Controlled Release* 71 (2001) 277–285.
- A. Bernkop-Schnürch, M. Hornof, T. Zoidl. Thiolated polymers—thiomers: synthesis and in vitro evaluation of chitosan–2-iminothiolane conjugates. *International Journal of Pharmaceutics* 260 (2003) 229–237.
- N. Beyth, I. Yudovin-Farber, R. Bahir, A. Domb, E. Weiss. Antibacterial activity of dental composites containing quaternary ammonium polyethylenimine

nanoparticles against *Streptococcus mutans*. *Biomaterials* 27 (2006) 3995–4002.

M. Bodnar, J. Hartmann, J. Borbely. Preparation and Characterization of Chitosan-Based Nanoparticles. *Biomacromolecules* 6 (2005) 2521-2527.

K. Bowman, K. W. Leong. Chitosan nanoparticles for oral drug and gene delivery. *International Journal of Nanomedicine* 1 (2006) 117–128.

J. Brange, L. Langkjaer, S. Havelund, A. Vølund. Chemical stability of insulin. 1. Hydrolytic degradation during storage of pharmaceutical preparations. *Pharmaceutical Research* 9 (1992) 715-726.

E. Broderick, H. Lyons, T. Pembroke, H. Byrne, B. Murray, M. Hall. The characterisation of a novel, covalently modified, amphiphilic alginate derivative, which retains gelling and non-toxic properties. *Journal of Colloid and Interface Science* 298 (2006) 154–161.

B. Brodin, C. Nielsen, B. Steffansen, S. Frøkjær. Transport of Piptidomimetic Drugs by the Intestinal Di/Tri-peptide Transporter, PepT1. *Pharmacology & Toxicology* 90 (2002) 285–296.

T. Cavaiola, S. Edelman. Inhaled insulin: A breath of fresh air? a review of inhaled insulin. *Clinical Therapeutics* 36 (2014) 1275-1289.

W. Cho, M. Kim, M. Jung, J. Park, K. Cha, J. Kim, H. Park, A. Alhalaweh, S. Velaga, S. Hwang. Design of salmon calcitonin particles for nasal delivery using spray-drying and novel supercritical fluid-assisted spray-drying processes. *International Journal of Pharmaceutics* 478 (2015) 288-296.

B. Choonara, Y. Choonara, P. Kumar, D. Bijukumar, L. du Troit, V. Pillay. A review of advanced oral drug delivery technologies facilitating the protection and absorption of protein and peptide molecules. *Biotechnology advances* 32 (2014) 1269-1282.

F. de Abreu, S. Campana-Filho. Characteristics and properties of carboxymethylchitosan. *Carbohydrate Polymers* 75 (2009) 214–221.

N. De Jaeger, H. Demeyere, R. Finsy, R. Sneyers, J. Vanderdeelen, P. van der Meeren, M. van Laethem. Part I: Monodisperse Latices: Influences of scattering

angle and concentration of dispersed material. *Particle & particle systems characterization* 8 (1991) 179-186.

M. Desai, V. Labhsetwar, E. Walter, R. Levy, G. Amidon. The Mechanism of Uptake of Biodegradable Microparticles in Caco-2 Cells is Size Dependent. *Pharmaceutical Research* 14 (1997) 1568-1573.

J. Doczi. Process for purification of chitosan by means of the salicylic acid salt thereof. US patent: US2795579 A (1953).

V. Dodane, M. A. Khan, J. R. Merwin. Effect of chitosan on epithelial permeability and structure. *International Journal of Pharmaceutics* 182 (1999) 21-32.

Z. Dong, K. Abdul Hamid, Y. Gao, Y. Lin, H. Katsumi, T. Sakane, A. Yamamoto. Polyamidoamine Dendrimers Can Improve the Pulmonary Absorption of Insulin and Calcitonin in Rats. *Journal of Pharmaceutical Sciences* 100 (2011) 1866-1878.

L. Dongwon, Z. Weidong, S. Shirley, K. Xiaoyuan, G. Hellermann, R. Lockey, S. Mohapatra. Thiolated Chitosan/DNA Nanocomplexes Exhibit Enhanced and Sustained Gene Delivery. *Pharmaceutical Research* 24 (2007) 157-167.

K. Douglas, M. Tabrizian. Effect of experimental parameters on the formation of alginate-chitosan nanoparticles and evaluation of their potential application as DNA carrier. *Journal of Biomaterials Science, Polymer Edition* 16 (2005) 43-56.

E. Dragan, S. Schwarz. Polyelectrolyte Complexes. VII. Complex Nanoparticles Based on Poly(sodium 2-acrylamido-2-methylpropanesulfonate) Tailored by the Titrant Addition Rate. *Journal of Polymer Science: Part A: Polymer Chemistry* 42 (2004) 5244-5252.

K. Draget, O. Smidsrød, G. Skjåk-Bræk. 2005. Alginates from Algae. In: A. Steinbüchel, S. Rhee. Eds. *Polysaccharides and polyamides in the food industry. Properties, production and patents*. Weinheim, Germany: Wiley, pp. 1-30.

L. Fan, M. Cao, S. Gao, W. Wang, K. Peng, C. Tan, F. Wen, S. Tao, W. Xie. Preparation and characterization of a quaternary ammonium derivative of pectin. *Carbohydrate polymers* 88 (2012) 707-712.

J. Fang, Y. Zhang, S. Yan, Z. Liu, S. He, L. Cui, J. Yin. Poly(L-glutamic acid)/chitosan polyelectrolyte complex porous microspheres as cell microcarriers for cartilage regeneration. *Acta Biomaterialia* 10 (2014) 276-288.

J. Fatou, L. Mandelkern. The Effect of Molecular Weight on the Melting Temperature and fusion of polyethylene. *The Journal of Physical Chemistry* 69 (1965) 417-428.

U.S Food and Drug Administration. Database of Select Committee on GRAS Substances Reviews. 1973 (24 CFR 184.1724).

Y. Frère, P. Gramain. Reaction Kinetics of Polymer Substituents. Macromolecular Steric Hindrance Effect in Quaternization of Poly(vinylpyridines). *Macromolecules* 25 (1992) 3184-3189.

E. Frömter, J. Diamond. Route of Passive Ion Permeation in Epithelia. *Nature new biology* 235 (1972) 9-13.

Y. Fukui, T. Maruyama, Y. Iwamatsu, A. Fujii, T. Tanaka, Y. Ohmukai, H. Matsuyama. Preparation of monodispersed polyelectrolyte microcapsules with high encapsulation efficiency by an electrospray technique. *Colloids and Surfaces A: Physicochemical and Engineering Aspects* 370 (2010) 28-34.

X. Gao, Y. Cao, X. Song, Z. Zhang, X. Zhuang, C. He, X. Chen. Biodegradable, pH-responsive carboxymethyl cellulose/poly(acrylic acid) hydrogels for oral insulin delivery. *Macromolecular Bioscience* 14 (2014) 565-575.

J. Hamman, M. Stander, A. Kotze. Effect of the degree of quaternisation of N-trimethyl chitosan chloride on absorption enhancement: in vivo evaluation in rat nasal epithelia. *International Journal of Pharmaceutics* 232 (2002) 235-242.

S. Hartig, R. Greene, M. Dikov, A. Prokop, J. Davidson. Multifunctional Nanoparticulate Polyelectrolyte Complexes. *Pharmaceutical Research* 24 (2007) 2353-2369.

A. Haug, B. Larsen, O. Smidsrød. The degradation of Alginates at different pH values. *Acta Chemica Scandinavica* 17 (1963) 1466-1468.

A. Haug. Dissociation of alginic acid. *Acta Chemica Scandinavica* 15 (1961) 950-952.

A. Haug. Ion exchange properties of alginate fractions. *Acta Chemica Scandinavica* 13 (1959) 601-603.

L. Heinemann, Y. Jacques. Oral Insulin and Buccal Insulin: A Critical Reappraisal. *Journal of Diabetes Science and Technology* 3 (2009) 568-584.

A. Herwadkar, A. Banga. 2011. Transdermal Delivery of Peptides and Proteins. In: C. Van der Walle. Ed. *Peptide and Protein Delivery*. London, UK: Elsevier, pp. 69-86.15. F. Yin, S. Guo, Y. Gan, X. Zhang. Preparation of redispersible liposomal dry powder using an ultrasonic spray freeze-drying technique for transdermal delivery of human epithelial growth factor.

M. Hess, R. Jones, J. Kahovec, T. Kitayama, P. Kratochvil, P. Kubisa, W. Mormann, R. Stepto, D. Tabak, J. Vohlidal, E. Wilks. Terminology of polymers containing ionizable or ionic groups and of polymers containing ions (IUPAC Recommendations 2006). *Pure and Applied Chemistry* 78 (2006) 2067-2074.

S. Honary, F. Zahir. Effect of Zeta Potential on the Properties of Nano-Drug Delivery Systems – A Review (Part 2). *Tropical Journal of Pharmaceutical Research* 12 (2) (2013) 265-273.

A. Huang, Z. Su, M. Sun, Y. Xiao, Q. Ping, Y. Deng. Oral absorption enhancement of salmon calcitonin by using both N-trimethyl chitosan chloride and oligoarginine-modified liposomes as the carriers. *Drug Delivery* 21 (2014) 388-396.

Y. Huang, C. Wang. Pulmonary delivery of insulin by liposomal carriers. *Journal of Controlled Release* 113 (2006) 9-14.

K. Huus, S. Havelund, H. Olsen, M. van de Weert, S. Frokjaer. Thermal Dissociation and Unfolding of Insulin. *Biochemistry* 44 (2005) 11171-11177.

C. Ibie, R. Knott, C. Thompson. In-vitro evaluation of the effect of polymer structure on the uptake of novel polymer-insulin polyelectrolyte complexes by human epithelial cells. *International Journal of Pharmaceutics* 479 (2015) 103-117.

G. Jiang, D. Quan, K. Liao, H. Wang. Preparation of polymeric micelles based on chitosan bearing a small amount of highly hydrophobic groups. *Carbohydrate polymers* 66 (2006) 514-520.

A. Jintapattanakit, V. Junyaprasert, S. Maob, J. Sitterberg, U. Bakowsky, T. Kissel. Peroral delivery of insulin using chitosan derivatives: A comparative study of polyelectrolyte nanocomplexes and nanoparticles. *International Journal of Pharmaceutics* 342 (2007) 240–249.

N. Kamei, M. Takeda-Morishita. Brain delivery of insulin boosted by intranasal coadministration with cell-penetrating peptides. *Journal of Controlled Release* 197 (2015) 105-110.

K. Klemmer, L. Waldner, A. Stone, N. Low, M. Nickerson. Complex coacervation of pea protein isolate and alginate polysaccharides. *Food Chemistry* 130 (2012) 710–715.

J. Koetz, S. Kosmella. *Polyelectrolytes and Nanoparticles*. Berlin : Springer; 2007.

A. Kotze, M. Thanou, H. Lueßen, B. de Boer, J. Verhoef, H. Junginger. Effect of the degree of quaternization of N-trimethyl chitosan chloride on the permeability of intestinal epithelial cells (Caco-2). *European Journal of Pharmaceutics and Biopharmaceutics* 47 (1999) 269–274.

A. Kotze, B. de Leeuw, H. Lueßen, A. de Boer, J. Verhoef, H. Junginger. Chitosans for enhanced delivery of therapeutic peptides across intestinal epithelia: in vitro evaluation in Caco-2 cell monolayers. *International Journal of Pharmaceutics* 159 (1997) 243–253.

M. Kumar. A review of chitin and chitosan applications. *Reactive & Functional Polymers* 46 (2000) 1–27.

P. Kwok, H. Chan. 2011. Pulmonary Delivery of Peptides and Proteins. In: C. Van der Walle. Ed. *Peptide and Protein Delivery*. London, UK: Elsevier, pp. 23-46.

L. Langkjær, J. Brange, G. Grodsky, R. Guy. Iontophoresis of monomeric insulin analogues in vitro: effects of insulin charge and skin pretreatment. *Journal of Controlled Release* 51 (1998) 47–56.

S. Lankalapalli, V. R. M. Kolapalli. Polyelectrolyte Complexes: A Review of their Applicability in Drug Delivery Technology. *Indian Journal of Pharmaceutical Sciences* 71 (5) (2009) 481-487.

- G. Lawrie, I. Keen, B. Drew, A. Chandler-Temple, L. Rintoul, P. Fredericks, L. Grøndahl. Interactions between Alginate and Chitosan Biopolymers Characterized Using FTIR and XPS. *Biomacromolecules* 8 (2007) 2533-2541.
- D. Lee, A. Ryle. Pepsin D a minor component of commercial pepsin preparations. *Biochemical Journal* 104 (1967) 742-748.
- K. Lee, D. Mooney. Alginate: Properties and biomedical applications. *Progress in Polymer Science* 37 (2012) 106–126.
- C. Lehr, J. Bouwstra, E. Schacht, H. Junginger. In vitro evaluation of mucoadhesive properties of chitosan and some other natural polymers. *International Journal of Pharmaceutics* 78 (1992) 43-48.
- P. Li, Y. Dai, J. Zhang, A. Wang, Q. Wei. Chitosan-Alginate Nanoparticles as a Novel Drug Delivery System for Nifedipine. *International journal of Biomedical science* 4 (3) (2008) 221-228.
- T. Li, X. Shi, Y. Du, Y. Tang. Quaternized chitosan/alginate nanoparticles for protein delivery. *Journal of biomedical materials research Part A*. 83 (2007) 383-390.
- Y. Liqun, Z. Bifang, W. Liqun, L. Qiuyi, Z. Li-Ming. Amphiphilic cholesteryl grafted sodium alginate derivative: Synthesis and self-assembly in aqueous solution. *Carbohydrate Polymers* 68 (2007) 218-225.
- W. Liu, S. Sun, Z. Cao, X. Zhang, K. Yao, W. Lu, K. Luk. An investigation on the physicochemical properties of chitosan/DNA polyelectrolyte complexes. *Biomaterials* 26 (2005) 2705–2711.
- G. Luckachan, C. Pillai. Chitosan/oligo L-lactide graft copolymers: Effect of hydrophobic side chains on the physico-chemical properties and biodegradability. *Carbohydrate Polymers* 64 (2006) 254–266.
- H. Lueßen, B. De Leeuw, D. Perard, C. Lehr, A. De Boer, J. Verhoef, H. Junginger. Mucoadhesive polymers in peroral peptide drug delivery. I. Influence of mucoadhesive excipients on the proteolytic activity of intestinal enzymes. *European Journal of Pharmaceutical Sciences* 4 (1996) 117-128.
- H. Lueßen, B. de Leeuw, M. Langmeyer, A. De Boer, J. Verhoef, H. Junginger. Mucoadhesive Polymers in Peroral Peptide Drug Delivery. VI. Carbomer and

Chitosan Improve the Intestinal Absorption of the Peptide Drug Buserelin In Vivo. *Pharmaceutical Research* 13 (11) (1996) 1668-1672.

H. Lueßen, C. Rentel, A. Kotze, C. Lehr, A. De Boer, J. Verhoef, H. Junginger. Mucoadhesive polymers in peroral peptide drug delivery: IV. Polycarbophil and chitosan are potent enhancers of peptide transport across intestinal mucosae in vitro. *Journal of Controlled Release* 45 (1997) 15-23.

Shelly, M. Ahuja, A. Kumar. Gum ghatti–chitosan polyelectrolyte nanoparticles: Preparation and characterization. *International Journal of Biological Macromolecules* 61 (2013) 411– 415.

L. Manring. Thermal degradation of poly(methyl methacrylate). 4. Random Side-Group Scission. *Macromolecules* 24 (1991) 3304-3309.

S. Mao, X. Shuai, F. Unger, M. Simona, D. Bi, T. Kissel. The depolymerization of chitosan: effects on physicochemical and biological properties. *International Journal of Pharmaceutics* 281 (2004) 45–54.

D. McHugh. A guide to the seaweed industry FAO Fisheries technical paper No. 441, 2003. Chapter 5, Alginate, 39-49.

C. Mei-Chin, W. Hen-Sheng, L. Kun-Ju, C. Hsin-Lung, W. Shiaw-Pyng, K. Sonaje, L. Yu-Hsin, C. Che-Yi, S. Hsing-Wen. The characteristics, biodistribution and bioavailability of a chitosan-based nanoparticulate system for the oral delivery of heparin. *Biomaterials* 30 (2009) 6629–6637.

M. Mende, S. Schwarz, S. Zschoche, G. Petzold, A. Janke. Influence of the Hydrophobicity of Polyelectrolytes on Polyelectrolyte Complex Formation and Complex Particle Structure and Shape. *Polymers* 3 (2011) 1363-1376.

R. Moustafine, A. Bodrov, V. Kemenova, P. Rombaut, G. Van den Mooter. Drug release modification by interpolymer interaction between countercharged types of Eudragit® RL 30D and FS 30D in double-layer films. *International journal of pharmaceutics* 439 (2012) 17-21.

M. Muller. 2014. Polyelectrolyte Complexes in the Dispersed and Solid State II Application Aspects. Heidelberg, Germany: Springer.

- J. Nam, C. Choi, M. Jang, Y. Jeong, J. Nah. Insulin-incorporated Chitosan Nanoparticles Based on Polyelectrolyte Complex Formation. *Macromolecular Research* 18 (7) (2010) 630-635.
- H. Onishi, Y. Machida. Biodegradation and distribution of water-soluble chitosan in mice. *Biomaterials* 20 (1999) 175-182.
- G. Orive, A. M. Carcaboso, R. M. Hernandez, A. R. Gascon, J. L. Pedraz. Biocompatibility Evaluation of Different Alginates and Alginate-Based Microcapsules. *Biomacromolecules* 6 (2005) 927-931.
- J. Parmentier, G. Hofhaus, S. Thomas, L. Cuesta, F. Gropp, R. Schröder, K. Hartmann, G. Fricker. Improved oral bioavailability of human growth hormone by a combination of liposomes containing bio-enhancers and tetraether lipids and omeprazole. *Journal of Pharmaceutical Sciences* 103 (2014) 3985-3993.
- N. Patil, P. Devarajan. Insulin-loaded alginic acid nanoparticles for sublingual delivery. *Drug Delivery*, Early Online: 1-8. DOI: 10.3109/10717544.2014.916769.
- D. Pillion, J. Bartlett, E. Meezan, M. Yang, R. Crain, W. Grizzle. Systemic absorption of insulin delivered topically to the rat eye. *Investigative Ophthalmology & Visual Science* 32 (1991) 3021-3027.
- A. Rampino, M. Borgogna, P. Blasi, B. Bellich, A. Cesàro. Chitosan nanoparticles: Preparation, size evolution and stability. *International Journal of Pharmaceutics* 455 (2013) 219– 228.
- B. Rehm, S. Valla. Bacterial alginates: biosynthesis and applications. *Applied Microbiology and Biotechnology* 48 (1997) 281-288.
- M. Rekha, C. Sharma. 2010. Nanoparticle Mediated Oral Delivery of Peptides and Proteins: Challenges and Perspectives. In: C. Van der Walle. Ed. *Peptide and Protein Delivery*. Elsevier, pp. 165-195.
- M. Rinaudo, G. Pavlov, J. Desbrières. Influence of acetic acid concentration on the solubilisation of chitosan. *Polymer* 40 (1999) 7029-7032.
- M. Sakkinen, T. Tuononen, H. Jurjenson, P. Veski, M. Marvola. Evaluation of microcrystalline chitosans for gastro-retentive drug delivery. *European Journal of Pharmaceutical Sciences* 19 (2003) 345–353.

M. Sakkinen, J. Marvola, H. Kanerva, K. Lindevall, A. Ahonen, M. Marvola. Are chitosan formulations mucoadhesive in the human small intestine? An evaluation based on gamma scintigraphy. *International Journal of Pharmaceutics* 307 (2006) 285–291.

B. Sarmiento, A. Ribeiro, F. Veiga, P. Sampaio, R. Neufeld, D. Ferreira. Alginate/Chitosan Nanoparticles are Effective for Oral Insulin Delivery. *Pharmaceutical Research* 24 (2007) 2198-2206.

B. Sarmiento, D. Ferreira, F. Veiga, A. Ribeiro. Characterization of insulin-loaded alginate nanoparticles produced by ionotropic pre-gelation through DSC and FTIR studies. *Carbohydrate Polymers* 66 (2006) 1-7.

B. Sarmiento, D. Ferreira, L. Jorgensen, M. van de Weert. Probing insulin's secondary structure after entrapment into alginate/chitosan nanoparticles. *European Journal of Pharmaceutics and Biopharmaceutics* 65 (2007) 10–17.

B. Sarmiento, S. Martins, A. Ribeiro, F. Veiga, R. Neufeld, D. Ferreira. Development and Comparison of Different Nanoparticulate Polyelectrolyte Complexes as Insulin Carriers. *International Journal of Peptide Research and Therapeutics* 12 (2006) 131–138.

F. Sarti, A. Bernkop-Schnürch. Chitosan and Thiolated Chitosan. *Advances in Polymer Science* 243 (2011) 93–110.

C. Schatz, J. Lucas, C. Viton, A. Domard, C. Pichot, T. Delair. Formation and Properties of Positively Charged Colloids Based on Polyelectrolyte Complexes of Biopolymers. *Langmuir* 20 (2004) 7766-7778.

V. Schmidt, C. Giacomelli, V. Soldi. Thermal stability of films formed by soy protein isolate-sodium dodecyl sulphate. *Polymer Degredation and Stability* 87 (2005) 25-31.

F. Shahidi, J. Kamil, V. Arachchi, Y. Jeon. Food applications of chitin and chitosans. *Trends in Food Science & Technology* 10 (1999) 37-51.

A. Sieval, M. Thanou, A. Kotze, J. Verhoef, J. Brussee, H. Junginger. Preparation and NMR characterization of highly substituted IV-trimethyl chitosan chloride. *Carbohydrate Polymers* 36 (1998) 157-165.

M. Simon, I. Behrens, L. Dailey, M. Wittmar, T. Kissel. Nanosized insulin-complexes based on biodegradable amine-modified graft polyesters poly[vinyl-3-(diethylamino)-propylcarbamate-co-(vinyl acetate)-co-(vinyl alcohol)]-graft-poly-(L-lactic acid): Protection against enzymatic degradation, interaction with Caco-2 cell monolayers, peptide transport and cytotoxicity. *European Journal of Pharmaceutics and Biopharmaceutics* 66 (2007) 165–172.

M. Simon, M. Wittmar, T. Kissel, T. Linn. Insulin Containing Nanocomplexes Formed by Self-Assembly from Biodegradable Amine-Modified Poly(Vinyl Alcohol)-Graft-Poly(L-Lactide): Bioavailability and Nasal Tolerability in Rats. *Pharmaceutical Research* 22 (2005) 1879-1886.

M. Simon, M. Wittmar, U. Bakowsky, T. Kissel. Self-Assembling Nanocomplexes from Insulin and Water-Soluble Branched Polyesters, Poly[(vinyl-3-(diethylamino)-propylcarbamate-co-(vinyl acetate)-co-(vinyl alcohol)]-graftpoly(L-lactic acid): A Novel Carrier for Transmucosal Delivery of Peptides. *Bioconjugate Chemistry* 15 (2004) 841-849.

O. Smidsrød, A. Haug. Properties of poly (1,4-heuronates) in the gel state, comparison of gels of different chemical composition. *Acta Chemica Scandinavica* 26 (1972) 79-88.

D. Snyman, T. Govender, A. F. Kotze'. Low molecular weight quaternised chitosan (I): synthesis and characterisation. *Pharmazie* 58 (2003) 705–708.

J. Soares, J. Santos, G. Chierice, E. Cavalheiro. Thermal behavior of alginic acid and its sodium salt. *Eletica quimica* 29 (2) (2004) 53-56.

W. Surmacz-Chwedoruk, I. Malka, Ł. Bozycki, H. Nieznanska, W. Dzwolak. On the Heat Stability of Amyloid-Based Biological Activity: Insights from Thermal Degradation of Insulin Fibrils. *PLoS ONE* 9 (1): e86320. Doi:10.1371/journal.pone.0086320.

M. Thanou, A. Kotze, T. Scharringhausen, H. Lueßen, A. de Boer, J. Verhoef, H. Junginger. Effect of degree of quaternization of N-trimethyl chitosan chloride for enhanced transport of hydrophilic compounds across intestinal Caco-2 cell monolayers. *Journal of Controlled Release* 64 (2000) 15–25.

M. Thanou, M. Nihot, M. Jansen, J. Verhoef, H. Junginger. Mono-N-Carboxymethyl Chitosan (MCC), a Polyampholytic Chitosan Derivative,

Enhances the Intestinal Absorption of Low Molecular Weight Heparin Across Intestinal Epithelia In Vitro and In Vivo. *Journal of pharmaceutical sciences* 90 (2001) 38-46.

C. Thompson, C. Ding, X. Qu, Z Yang, I. Uchegbu, L. Tetley, W. Cheng. The effect of polymer architecture on the nano self-assemblies based on novel comb-shaped amphiphilic poly(allylamine). *Colloid polymer science* 286 (2008) 1511-1526.

C. Thompson, L. Tetley, I. Uchegbu, W. Cheng. The complexation between novel comb shaped amphiphilic polyallylamine and insulin—Towards oral insulin delivery. *International Journal of Pharmaceutics* 376 (2009) 46–55.

C. Thompson, W. Cheng, P. Gadad, K. Skene, M. Smith, G. Smith, A. McKinnon, R. Knott. Uptake and Transport of Novel Amphiphilic Polyelectrolyte-Insulin Nanocomplexes by Caco-2 Cells—Towards Oral Insulin. *Pharmaceutical Research* 28 (2011) 886–896.

C. Tsao, C. Chang, Y. Lin, M. Wu, J. Wang, J. Han, K. Hsieh. Antibacterial activity and biocompatibility of a chitosan–c-poly(glutamic acid) polyelectrolyte complex hydrogel. *Carbohydrate Research* 345 (2010) 1774-1780.

C. van der Walle. 2011. Peptide and protein delivery. London, UK: Elsevier.

J. van der Gucht, E. Spruijt, M. Lemmers, M. Cohen Stuart. Polyelectrolyte complexes: Bulk phases and colloidal systems. *Journal of Colloid and Interface Science* 361 (2011) 407-422.

S. Wadhwa, R. Paliwal, S. Paliwal, S. Vyas. Nanocarriers in ocular drug delivery: an update review. *Current Pharmaceutical Design* 15 (2009) 2724-2750.

Y. Wan, B. Peppley, K. Creber, V. Tam Bui, E. Halliop. Quaternized-chitosan membranes for possible applications in alkaline fuel cells. *Journal of power sources* 185 (2008) 183-187.

W. Wang, L. Tetley, I. Uchegbu. A New Class of Amphiphilic Poly-L-lysine Based Polymers Forms Nanoparticles on Probe Sonication in Aqueous Media. *Langmuir* 16 (2000) 7859-7866.

- J. Wang, Y. Tabata, K. Morimoto. Aminated gelatin microspheres as a nasal delivery system for peptide drugs: Evaluation of in vitro release and in vivo insulin absorption in rats. *Journal of Controlled Release* 113 (2006) 31-37.
- L. Wang, E. Khor, L. Lim. Chitosan-Alginate-CaCl₂ System for Membrane Coat Application. *Journal of Pharmaceutical Sciences* 90 (8) (2001) 1134-1142.
- L. Wang, L. Li, Y. Sun, Y. Tian, Y. Li, C. Li, V. Junyaprasert, S. Mao. Exploration of hydrophobic modification degree of chitosan-based nanocomplexes on the oral delivery of enoxaparin. *European Journal of Pharmaceutical Sciences* 50 (2013) 263–271.
- W. Wang, X. Qu, A. Gray, L. Tetley, I. Uchegbu. Self-Assembly of Cetyl Linear Polyethylenimine To Give Micelles, Vesicles, and Dense Nanoparticles, and Dense Nanoparticles. *Macromolecules* 37 (2004) 9114-9122.
- W. Wang, Y. Dua, Y. Qiu, X. Wang, Y. Hu, J. Yang, J. Cai, J. F. Kennedy. A new green technology for direct production of low molecular weight chitosan. *Carbohydrate Polymers* 74 (2008) 127–132.
- M. Werle, H. Takeuchi, A. Bernkop-schnurch. Modified Chitosans for Oral Drug Delivery. *Journal of Pharmaceutical Sciences* 98 (2009) 1643–1656.
- Y. Xiong, J. Fang, Q. Zeng, Q. Liu. Preparation and characterization of cross-linked quaternized poly(vinyl alcohol) membranes for anion exchange membrane fuel cells. *Journal of Membrane Science* 311 (2008) 319–325.
- A. Yamamoto, A. Luo, S. Dodda-Kashi, V. Lee. The ocular route for systemic insulin delivery in the albino rabbit. *The Journal of Pharmacology and Experimental Therapeutics* 249 (1989) 249-255.
- L. Ye, L. Zhai, J. Fang, J. Liu, C. Li, R. Guan. Synthesis and characterization of novel cross-linked quaternized poly(vinyl alcohol) membranes based on morpholine for anion exchange membranes. *Solid state ionics* 240 (2013) 1-9.
- K. Yerramsetty, V. Rachakonda, B. Neely, S. Madihally, K. Gasem. Effect of different enhancers on the transdermal permeation of insulin analog. *International Journal of Pharmaceutics* 398 (2010) 83-92.

I. Yudovin-Farber, J. Golenser, N. Beyth, E. Weiss, A. Domb. Quaternary Ammonium Polyethyleneimine: Antibacterial Activity. *Journal of nanomaterial* 2010 (2010) 1-11.

L. Zhang, H. Jiang, W. Zhu, L. Wu, L. Song, Q. Wu, Y. Ren. Improving the stability of insulin in solutions containing intestinal proteases in vitro. *International Journal of Molecular Sciences* 9 (2008) 2376-2387.

